

**APPLICATION OF ANGLES-WITH-PLATE RETROFIT IN REPAIRING
DISTORTION-INDUCED FATIGUE DAMAGES IN STRINGER TO FLOORBEAM
CONNECTIONS AND SKEWED GIRDER TO CROSS-FRAME CONNECTIONS**

BY

Danqing Yu

Submitted to the graduate degree program in Civil, Architectural, and Environmental Engineering and the Graduate Faculty of the University of Kansas in partial fulfillment of the requirements for the degree of Master of Science.

Committee members:

Chairperson Dr. Caroline Bennett

Dr. Adolfo Matamoros

Dr. Jian Li

Dr. Matthew Floyd Fadden

Dr. William Norfleet Collins

Date defended: Feb. 27, 2018

The Thesis Committee for Danqing Yu
certifies that this is the approved version of the following thesis:

**APPLICATION OF ANGLES-WITH-PLATE RETROFIT IN REPAIRING
DISTORTION-INDUCED FATIGUE DAMAGES IN STRINGER TO FLOORBEAM
CONNECTIONS AND SKEWED GIRDER TO CROSS-FRAME CONNECTIONS**

Chairperson Dr. Caroline Bennett

Dr. Adolfo Matamoros

Dr. Jian Li

Dr. Matthew Floyd Fadden

Dr. William Norfleet Collins

Date approved: _____

Executive Summary

Distortion-induced fatigue is a serious problem faced by many aging bridges. When live loads produce relative displacement between adjacent members, fatigue moments are generated and produce secondary stresses at connections. Usually, the moments are not large-magnitude, but for fatigue-sensitive details such as web-gap regions, even small stress ranges may lead to cracking. It is thought that approximately 90% of fatigue damage in steel bridges is caused by secondary stresses (Connor and Fisher 2005). The angles-with-plates retrofit developed at the University of Kansas has shown its potential to effectively and cost-efficiently repair distortion-induced fatigue damage in straight girder to cross-frame connections (Bennett et al. 2014). The performance of the retrofit in this application motivated the researchers to investigate its performance in other types of connections susceptible to distortion-induced fatigue.

This thesis consists of two parts. Each part includes a description of two physical tests and a series of computer simulations. Part I describes an investigation on single-plate and double-angle stringer to floorbeam connection subassemblies. Part II describes a study conducted on 20-degree and 40-degree skewed girder to cross-frame connection subassemblies. Both studies were aimed at evaluating the efficacy of the angles-with-plate retrofit in repairing distortion-induced fatigue damage, as well as developing an improved understanding of the fatigue performance of these connections.

The efficacy of the angles-with-plate retrofit in stopping fatigue crack propagation was evaluated through physical tests. Cyclic loads were applied on the connection subassemblies to initiate and propagate fatigue cracks. The angles-with-plate retrofit was then applied to repair the damaged connections. The retrofit was removed at regular intervals during the tests to measure crack growth. Computer simulations of the tested specimens were used to quantitatively analyze effectiveness of

the retrofit in reducing stress demands at damaged regions. Computer simulation results were compared with physical test results.

The results indicated that the angles-with-plate retrofit can efficiently mitigate distortion-induced fatigue damage in these connections. In the tests of the single-plate connection and the skewed girder to cross-frame connections, the retrofit successfully stopped the development of fatigue cracks. The computer simulation results indicated that in the single-plate connection subassembly, the retrofit was able to reduce the peak stress at cracks in the floorbeam web by 80% and by 90% for cracks at the floorbeam web-to-flange weld; in the skewed girder to cross-frame connection subassemblies, the retrofit reduced the peak stress in the 20-degree connection and 40-degree connection by 56% and 66%, respectively (Chen 2015). The double-angle connection subassembly did not show any sign of fatigue damage, therefore, the retrofit was not tested on it.

Acknowledgements

I wish to express my deepest gratitude to my advisors Dr. Caroline Bennett and Dr. Adolfo Matamoros, who played key roles in these projects, for their wisdom, knowledge and experience that always guide me forward, and their patience and kindness that help me out of all the hardships and frustrations. I am highly indebted to my senior fellow graduate student Eric Bonet, who taught me to use software and equipment, and the most important, inspired me about how to be a valuable graduate student. I am grateful to Dr. Jian Li, Dr. William Collins, Dr. Matthew Fadden, Dr. Elaina Sutley, Dr. Stan Rolfe, and Dr. Ronald Barrett, for them provided crucial guidance during the research and also inspired me through the enlightening discussions with them.

The completion of these studies would not be possible without the help of our lab Technologists. My sincere gratitude to David Woody, who helped me fabricate and erect specimens, taught me operate tools and equipment, and also provided many critical suggestions. I am also thankful to Matt Maksimowicz, Eric Nicholson, and Kent Dye, who played important roles in fabricating specimens and maintaining equipment. Further, I would like to thank my fellow graduate students Cheng Chen, Xiangxiong Kong, James Zhou, Hao Liu, Kien Quang Nguyen, and Hayder Ibrahim Al-Salih for their supports and friendships. I also admire the help of our undergraduate assistants Duncan MacLachlan and Heelai Ahmadullah for their supports and strong work ethic.

Finally, I would like to express my appreciation to my parents Penglei Yu and Zhongling Li for their unconditional love and supports. To my husband Xunzhao Yin, for his love, understanding, and patience of my occasional bad temper. And to my fluffy friend Doodle, for her warm snuggling that always makes me smile.

Contents

PART I:

APPLICATION OF ANGLES-WITH-PLATE RETROFIT FOR REPAIRING DISTORTION-INDUCED FATIGUE DAMAGE IN STRINGER TO FLOORBEAM CONNECTIONS

1. Background and Literature Review	2
1.1 Problem Statement	2
1.2 Distortion-Induced Fatigue Cracks in Single-Plate and Double-Angle Connections.....	4
1.2.1 Fatigue Cracks at Cope Area	4
1.2.2 Fatigue Cracks in the Web-Gap Region of a Single-Plate Connection	4
1.2.3 Fatigue Cracks in Connecting Elements of Double-Angle Connections.....	6
1.2.4 Fatigue Cracks in Rivets in Double-Angle Connections	6
1.3 Repair and Retrofitting of Distortion-Induced Fatigue Cracks.....	6
1.3.1 Grinding and Re-Welding.....	7
1.3.2 Bolted Doubler Plates	7
1.3.3 Crack-Arrest Holes	7
1.3.4 Connection Softening.....	8
1.3.5 Connection Stiffening	10
1.4 Summary of Relevant Previous Research.....	12
1.4.1 Work at the University of Kansas – Fatigue Properties and Retrofits of Web-Gap	12
1.4.2 Research at the University of Washington – Fatigue Properties and Retrofit of Stringer Cope Area	15
1.4.3 Research at Chalmers University of Technology – Fatigue of Riveted Double-Angle Connection	18
2. Objective and Scope	20
3. Physical Test of Single-Plate Connection (Specimen FS1) – Test Introduction	21
3.1 Description of Floorbeam-Stringer Specimen FS1.....	21
3.2 Instrumentation	24
3.3 Test Procedure	26
4. Physical Test of Single-Plate Connection (FS1) – Results and Discussion.....	27
4.1 Crack Initiation and Propagation	28
4.1.1 General Description of Crack Initiation and Propagation.....	28
4.1.2 Crack Initiation and Propagation in Each Trial	30
4.1.4 Crack Propagation Behavior for Test 1	40
4.2 Actuator Displacement.....	42

4.3 Stress	43
4.3.1 Floorbeam Stresses	43
4.3.2 Stringer Flange Stresses	48
4.3.3 Stresses at the Stringer Cope.....	48
5. Computer Simulation of Single-Plate Connection (FS1).....	50
5.1 General Introduction	50
5.2 Simulation Results for Specimen FS1	56
5.2.1 Early-Stage Fatigue Damage - Model 1, Model 2, and Model 3.....	56
5.2.2 Middle-Stage Fatigue Damage – Model 4 and Model 5.....	60
5.2.3 Late-Stage Fatigue Damage – Model 6 and Model 7	62
6. Comparison between Computer Simulation and Physical Test Results of Single-Plate Connection (FS1)	68
7. Physical Test of Double-Angle Connection (FS2)	77
7.1 Test Introduction.....	77
7.1.1 Specimen Dimensions.....	77
7.1.2 Instrumentation	78
7.1.3 Test Procedure	79
7.2 Test Result	81
7.2.1 Actuator Displacement.....	81
7.2.2 Stress	84
8. Computer Simulation of Double-Angle Connection (FS2)	88
8.1 Model for Physical Test FS2 Configuration 1	88
8.1.1 Introduction.....	88
8.1.2 Simulation Results	90
8.2 Model for Physical Test FS2 Configuration 3	95
8.2.1 Introduction.....	95
8.2.2 Simulation Results	96
8.3 Model for Virtual Specimen with Shorter Floorbeam Web.....	98
8.3.1 Introduction.....	98
8.3.2 Simulation Results	99
9. Comparison between Computer Simulation and Physical Test Results for Double-Angle Connection (FS2)	102
9.1 Configuration 1	102
9.2 Configuration 3	103
10. Discussion and Conclusion.....	106

10.1 Comparison between Single-Plate Connection (FS1) and Double-Angle Connection (FS2)	106
10.2 The Mechanism of Fatigue in Web-Gap Region and Stringer Cope Area	107
10.3 Suggestions for Using the Angles-with-Plate Retrofit to Repair Stringer to Floorbeam Connections	108
10.4 Conclusion	109
10.4.1 Single-Plate Connection (FS1)	109
10.4.2 Double-Angle Connection (FS2)	111
10.5 Suggestions for Future Research	112
References	113

PART II:

APPLICATION OF ANGLES-WITH-PLATE RETROFIT FOR REPAIRING DISTORTION-INDUCED FATIGUE DAMAGE IN SKEWED GIRDER TO CROSS-FRAME CONNECTIONS

1. Introduction	116
1.1 Background	116
1.2 Objectives and Scope	119
2. Physical Test of the 20-Degree Skewed Girder to Cross-Frame Connection – Test Introduction	120
2.1 Description of the 20-Degree Skewed Girder to Cross-Frame Specimen	120
2.2 Instrumentation	124
2.3 Test Procedure	126
3. Physical Test of 20-Degree Skewed Girder to Cross-Frame Connection – Test Results	127
3.1 Crack Initiation and Propagation	127
3.1.1 Cracks at Girder Bottom Web-Gap	127
3.1.2 Cracks on Cross-Frame	128
3.1.3 Bottom Web-Gap Crack Growth	130
3.2 Actuator Displacement	132
3.3 Stress	133
3.4 LVDT	135
3.5 Mirror Array Measurements	136
3.5.1 Girder Web Rotation	136
3.5.2 Approximated Stress Calculated from Girder Web Rotation	138
4. Physical Test of the 40-Degree Skewed Girder to Cross-Frame Connection –Introduction	143
4.1 Description of the 40-Degree Skewed Girder to Cross-Frame Specimen	143

4.2 Instrumentation	145
4.3 Test Procedure	147
5. Physical Test of 40-Degree Skewed Girder to Cross-Frame Connection –Result	149
5.1 Crack Initiation and Propagation	149
5.2 Actuator Displacement.....	153
5.3 Stress	154
5.4 LVDT	157
5.5 Mirror Array Measurements	158
5.5.1 Girder Web Rotation.....	158
5.5.2 Approximated Stresses Calculated from Girder Web Rotation.....	161
5.5.3 Influence of the Center Mirror Column on the Rotation and Approximated Stress Contour Plots	163
6. Comparison of Physical Tests and Computer Simulations.....	166
6.1 Stresses Computed from Strain Gages.....	167
6.1.1 20-Degree Skewed Girder to Cross-Frame Specimen	167
6.1.2 40-Degree Skewed Girder to Cross-Frame Specimen	170
6.2 Stresses Approximated from Girder Web Rotations	172
6.2.1 20-Degree Skewed Girder to Cross-Frame Specimen	172
6.2.2 40-Degree Skewed Girder to Cross-Frame Specimen	175
7. Influence of Angles-with-Plate Retrofit on Cross-Frame Gusset Plate Stresses	177
8. Conclusions.....	179
Reference	182

List of Figures

PART I: APPLICATION OF ANGLES-WITH-PLATE RETROFIT IN REPAIRING DISTORTION-INDUCED FATIGUE DAMAGES IN STRINGER TO FLOORBEAM CONNECTIONS

Figure 1-1: Double-angle and single-plate connections	2
Figure 1-2: Distortion caused by relative displacement of adjacent members	3
Figure 1-3: Stringer with cracked cope area	4
Figure 1-4: Fatigue problems in floorbeam web-gap region and stringer cope area	5
Figure 1-5: Typical crack in clip angle	6
Figure 1-6: Location of crack-arrest holes	8
Figure 1-7: Angles-with-plate retrofit	12
Figure 3-1: Specimen dimension and layout of single-plate connection specimen (Test FS1)....	23
Figure 3-2: Dimensions of angles-with-plate retrofit	24
Figure 3-3: Photos of single-plate connection specimen (FS1)	24
Figure 3-4: Strain gage placements on single-plate connection specimen (FS1)	25
Figure 3-5: AASHTO S-N curves.....	26
Figure 4-1: Cracks on single-plate connection specimen (FS1)	31
Figure 4-2: Cracks on connection plate side in Trial 1	32
Figure 4-3: Cracks located on the floorbeam fascia side in Trial 3	33
Figure 4-4: Photograph of cracks on the floorbeam web fascia side 1,200,000 cycles into Trial 3	34
Figure 4-5: Cracks on connection plate side in Trial 3	34
Figure 4-6: Photograph of cracks on floorbeam web fascia side 1,200,000 cycles into Trial 3....	35
Figure 4-7: Crack on floorbeam web fascia side 400,000 cycles into Trial 5	36
Figure 4-8: Crack on connection plate side in Trial 5	37
Figure 4-9: Cracks on floorbeam fascia side in Trial 8	38
Figure 4-10: Photographs of cracks on floorbeam web fascia side 85,000 cycles into Trial 8	39
Figure 4-11: Cracks on connection plate side 85,000 cycles into Trial 8.....	39
Figure 4-12: Photographs of cracks on connection plate side 85,000 cycles into Trial 8	39
Figure 4-13: Connection plate side: crack propagation behavior	40
Figure 4-14: Floorbeam web fascia side: crack propagation behavior	41
Figure 4-15: Actuator displacement at 6 kip actuator forces for single-plate connection specimen FS1	43
Figure 4-16: Floorbeam stresses at 6 kip actuator force for single-plate connection specimen FS1	44
Figure 4-17: Floorbeam stresses in Trial 1 at 6 kip actuator force for single-plate connection specimen FS1	45
Figure 4-18: Stresses computed using strain gages 6 and 7 vs. actuator force in Trials 3, 5, and 8	46
Figure 4-19: Rate of stress decrease (for 6 kip of applied actuator force) vs. number of unretrofitted cycles in single-plate connection test FS1	47
Figure 4-20: Stresses computed using strain gage 6 and 7 vs. actuator force in retrofitted trials	47
Figure 4-21: Stringer flange stresses at 6 kip applied forces for single-plate connection test FS1	48
Figure 4-22: Stringer cope area stresses at 6 kip applied forces for single-plate connection test FS1	49

Figure 5-1: Finite element model for single-plate connection specimen FS1 without retrofit.....	50
Figure 5-2: Finite element model for single-plate connection specimen FS1 with retrofit	50
Figure 5-3: Path 1 (Path 1(a), Path 1(b), and Path 1(c)) and Path 2 in FEM models	55
Figure 5-4: Simulation results for single-plate connection specimen FS1, Model 1	56
Figure 5-5: Simulation results for single-plate connection specimen FS1 Model 2.....	57
Figure 5-6: Simulation results for single-plate specimen FS1 Model 3	58
Figure 5-7: Stresses along Path 1(a) for single-plate connection FS1: Model 1, Model 2, and Model 3.....	59
Figure 5-8: Stresses along Path 2 for single-plate connection FS1: Model 1, Model 2, and Model 3	59
Figure 5-9: Simulation results for single-plate connection Specimen FS1: Model 4.....	60
Figure 5-10: Simulation results for single-plate connection specimen FS1: Model 5.....	61
Figure 5-11: Stresses along Path 1(b) for single-plate connection specimen FS1 Model 4 and Model 5	62
Figure 5-12: Stresses along Path 2 for single-plate connection specimen FS1 Model 4 and Model 5.....	62
Figure 5-13: Simulation results for single-plate connection specimen FS1: Model 6.....	63
Figure 5-14: Simulation results for single-plate connection specimen FS1: Model 7.....	64
Figure 5-15: Stresses along Path 1(c) for single-plate connection specimen FS1 Model 6 and Model 7.....	64
Figure 5-16: Stresses along Path 2 for single-plate connection specimen FS1 Model 6 and Model 7.....	65
Figure 5-17: Comparison of stresses along Path 2 in Model 1, Model 2, and Model 4	66
Figure 5-18: Deformation of the stringer web in single-plate connection models	67
Figure 6-1: Comparison of stresses between FEA results and physical test measurements:.....	68
Figure 6-2: Comparison of stresses between FEA results and physical test measurements:.....	69
Figure 6-3: Comparison of stresses between FEA results and physical test measurements:.....	70
Figure 6-4: Comparison of stresses between FEA results and physical test measurements:.....	71
Figure 6-5: Comparison of stresses between FEA results and physical test measurements:.....	72
Figure 6-6: Comparison of stresses between FEA results and physical test measurements:.....	73
Figure 6-7: Comparison of stresses between FEA results and physical test measurements:.....	74
Figure 6-8: Stresses extracted along the paths defined in the web-gap regions	75
Figure 7-1: Photograph of the double-angle connection	77
Figure 7-2: East connection angle dimensions in specimen FS2.....	77
Figure 7-3: Stringer dimensions for the specimen utilizing a double-angle connection	78
Figure 7-4: Strain gage placements of double-angle connection (specimen FS2) at stringer cope	79
Figure 7-5: Strain gage placements of double-angle connection (specimen FS2) at floorbeam web	79
Figure 7-6: Actuator displacement vs. actuator force in Configuration 1	82
Figure 7-7: Actuator displacement at 6 kip actuator force for Configuration 1	82
Figure 7-8: Actuator displacement in Configuration 2	83
Figure 7-9: Actuator displacement in Configuration 3	84
Figure 7-10: Stresses at 0 Cycle of Configuration 1	85
Figure 7-11: Stresses at 800,000 cycles of Configuration 1	86
Figure 7-12: Stress at 200,000 cycles of Configuration 2	87

Figure 7-13: Stress at 100,000 cycles of Configuration 3	87
Figure 8-1: Finite element model for double-angle connection test FS2.....	88
Figure 8-2: Computed model for double-angle connection test FS2, Configuration 1	90
Figure 8-3: Maximum principal stresses of bolts connecting angle and floorbeam web for the model of double-angle connection test FS2, Configuration 1	91
Figure 8-4: Max principal stresses in bolts connecting angle and stringer for the model of double-angle connection Test FS2, Configuration 1.....	92
Figure 8-5: Maximum principal stresses of west connection angle for the model of double-angle connection Test FS2, Configuration 1	93
Figure 8-6: Floorbeam web and connection angle deformation for the model of double-angle connection Test FS2, Configuration 1 (Deformation is magnified 3.5 times.).....	93
Figure 8-7: Maximum principal stresses of floorbeam web for the model of double-angle connection Test FS2, Configuration 1	94
Figure 8-8: Maximum principal stresses of stringer cope for the model of double-angle connection Test FS2, Configuration 1.....	95
Figure 8-9: Finite element model for double-angle connection, Specimen FS2, Configuration 3.....	96
Figure 8-10: Maximum principal stresses of bolts connecting angle and floorbeam web for the model of double-angle connection test FS2, Configuration 3	96
Figure 8-11: Maximum principal stresses of bolts connecting angle and stringer web for the model of double-angle connection test, Specimen FS2, Configuration 3.....	97
Figure 8-12: Maximum principal stresses of west connection angle for the model of double-angle connection test, Specimen FS2, Configuration 3.....	97
Figure 8-13: Maximum principal stresses of stringer cope for the model of double-angle connection test, Specimen FS2, Configuration 3.....	97
Figure 8-14: Maximum principal stresses of floorbeam web for the model of double-angle connection test, Specimen FS2, Configuration 3.....	98
Figure 8-15: Finite element model for double-angle connection with shorter floorbeam web	99
Figure 8-16: Maximum principal stresses of top west bolt connecting angle and floorbeam web for model of double-angle connection with shorter floorbeam web	99
Figure 8-17: Maximum principal stresses of top bolt connecting angle and stringer web for model of double-angle connection with shorter floorbeam web	100
Figure 8-18: Maximum principal stresses of west connection angle for model of double-angle connection with shorter floorbeam web.....	100
Figure 8-19: Maximum principal stresses of floorbeam web for model of double-angle connection with shorter floorbeam web	100
Figure 8-20: Maximum principal stresses of stringer cope for model of double-angle connection with shorter floorbeam web	101
Figure 9-1: Comparison of computer simulation results and physical test results for double-angle connection, Specimen FS2 Configuration 1	102
Figure 9-2: Comparison of computer simulation results and physical test results for double-angle connection, Specimen FS2, Configuration 1	103
Figure 9-3: Comparison of computer simulation results and physical test results for double-angle connection Specimen FS2, Configuration 3	104
Figure 9-4: Comparison of computer simulation results and physical test results for double-angle connection Specimen FS2, Configuration 3	104
Figure 10-1: Comparison between stringer cope of an existing bridge and the lab specimen ...	108

PART II: APPLICATION OF ANGLES-WITH-PLATE RETROFIT IN REPAIRING DISTORTION-INDUCED FATIGUE DAMAGES IN SKEWED GIRDER TO CROSS-FRAME CONNECTIONS

Figure 1-1: Out-of-plane deformation induced by relative displacement between adjacent members caused by living load (Hartman and Hassel, 2010) 116

Figure 1-2: Distortion in a web-gap region..... 117

Figure 1-3: Angles-with-plate retrofit (Alemdar et al. 2014a; 2014b) 118

Figure 2-1: Specimen layout..... 121

Figure 2-2: Dimensions of the 20-degree skewed cross-frame 122

Figure 2-3: Angles-with-plate retrofit dimensions 123

Figure 2-4: Photographs of 20-degree skewed specimen and retrofit 123

Figure 2-5: Strain gage and LVDT placements for 20-degree skewed specimen 125

Figure 2-6: Mirror array for the 20-degree skewed specimen 125

Figure 2-7: Girder web rotation computations, using measured displacement of reflected laser light 126

Figure 3-1: Cracks at bottom web-gap for 20-degree skewed specimen 1,200,000 cycles into Trial 20-2 128

Figure 3-2: Crack on 20-degree skewed cross-frame 697,000 cycles into Trial 20-2 and the steel angle bolted to repair it 129

Figure 3-3: Cracks on 20-degree skewed cross-frame 775,000 cycles into Trial 2..... 129

Figure 3-4: Shear failure of the bolt connecting the steel angle and cross-frame..... 130

Figure 3-5: Cross-frame after re-welding and repair 130

Figure 3-6: Crack propagation vs. number of applied cycles for 20-degree skewed specimen . 131

Figure 3-7: Actuator displacement at 6 kip of actuator force for the 20-degree skewed specimen 132

Figure 3-8: Stresses computed from strain gages placed on girder web at 6 kip actuator force for 20-degree skewed specimen 134

Figure 3-9: Stresses measured by strain gages placed on cross-frame at 6 kip actuator force for 20-degree skewed specimen..... 135

Figure 3-10: LVDT readings for 6 kip of actuator force for 20-degree skewed specimen 136

Figure 3-11: Y-axis rotations (degree) of the girder web for 20-degree skewed specimen under 6 kip of actuator force, computed from the mirror array measurements 137

Figure 3-12: X-axis rotations (degree) of the girder web for 20-degree skewed specimen under 6 kip of actuator force, computed from the mirror array measurements 138

Figure 3-13: Calculate approximated girder web stresses from girder web rotation..... 139

Figure 3-14: Specimen coordinate system..... 140

Figure 3-15: Approximated stress (ksi) in the girder web in X direction for 20-degree skewed specimen under 6 kip of actuator force, computed from the mirror array measurements 141

Figure 3-16: Approximated stress (ksi) in Y direction of the girder web for 20-degree skewed specimen under 6 kip of actuator force, computed from the mirror array measurements 142

Figure 4-1: Dimensions of 40-degree skewed cross-frame 144

Figure 4-2: Photographs of 40-degree skewed specimen with angles-with-plate retrofit installed 145

Figure 4-3: Instrumentation of the 40-degree skewed specimen 146

Figure 4-4: Mirror placements for 40-degree skewed specimen 147

Figure 4-5: Actuator displacement vs. actuator force before specimen cracking for 20-degree specimen and 40-degree specimen..... 148

Figure 5-1: Cracks present in 40-degree skewed specimen 313,000 cycles into Trial 40-1 (schematic).....	150
Figure 5-2: Cracks of 40-degree skewed specimen 1,150,000 cycles into Trial 40-3 (schematic drawing).....	151
Figure 5-3: Cracks of 40-degree skewed specimen 1,150,000 cycles into Trial 40-3.....	152
Figure 5-4: Crack propagation vs. number of applied cycles for 40-degree skewed specimen .	153
Figure 5-5: Actuator displacement vs. number of applied cycles at 2.5 kip of actuator force for the 40-degree skewed specimen	154
Figure 5-6: Stresses computed from strain gages 1 to 5 at the beginning of Trial 40-1 for the 40-degree skewed specimen under 2.5 kip of actuator force	154
Figure 5-7: Stresses measured by strain gages 17 and 18 placed on the bottom gusset plate for the 40-degree skewed specimen	155
Figure 5-8: Stresses computed from strain gages 10, 11, 12, 13 vs. number of applied cycles for the 40-degree skewed specimen under 2.5 kip of acutator force	156
Figure 5-9: Stresses measured by strain gage 9, 10, 11 vs. number of applied cycles for the 40-degree skewed specimen under 2.5 kip of actuator force	157
Figure 5-10: LVDT measurements for 2.5 kip of actuator force for the 40-degree skewed specimen	158
Figure 5-11: Y-axis rotations (degree) of the girder web computed from mirror array measurements for 40-degree skewed specimen under 2.5 kip of actuator force	159
Figure 5-12: X-axis rotations (degree) of the girder web computed from mirror array measurements for 40-degree skewed specimen under 2.5 kip actuator force	160
Figure 5-13: Approximated stress (ksi) in X direction of the girder web for 40-degree skewed specimen under 2.5 kip of actuator force from mirror array measurements.....	161
Figure 5-14: Approximated stress (ksi) in Y direction in the girder web for 40-degree skewed specimen under 2.5 kip of actuator force from mirror array measurements.....	162
Figure 5-15: Mirror array configurations for 20-degree and 40-degree skewed specimens.....	163
Figure 5-16: Influence of center mirror column on rotation plots for 40-degree skewed specimen	164
Figure 5-17: Influence of center mirror column on plots of approximated stresses for 40-degree skewed specimen	165
Figure 6-1: Comparison between FE results and physical test results for 20-degree skewed specimen without retrofit installed, under 6 kip of actuator force	168
Figure 6-2: Comparison between FE results and physical test results for 20-degree skewed specimen with retrofit installed, under 6 kip of actuator force	169
Figure 6-3: Comparison between FE results and physical test results for the 40-degree skewed specimen without retrofit installed under 2.5 kip of actuator force	171
Figure 6-4: Comparison between stresses in Y direction calculated from girder web rotations and obtained from computer simulations for 20-degree skewed specimen.....	173
Figure 6-5: Comparison between stresses in X direction calculated from girder web rotations and obtained from computer simulations for 20-degree skewed specimen.....	174
Figure 6-6: Comparison between stresses calculated from girder web rotations and streses obtained from computer simulations for 40-degree skewed specimen without retrofit installed.....	176
Figure 7-1: Comparison of gusset plate stresses with and without angles-with-plate retrofit installed.....	178

List of Tables

Part I: Application of Angles-with-Plate Retrofit in Repairing Distortion-Induced Fatigue Damages in Stringer to Floorbeam Connections

Table 3-1: Single-plate connection FS1 physical test trials introduction	27
Table 4-1: Brief introduction of single-plate connection test process	28
Table 4-2: Crack initiation and propagation on connection plate side in Trial 1	31
Table 4-3: Crack initiation and propagation on floorbeam web fascia side in Trial 3	33
Table 4-4: Cracks initiation and propagation on connection plate side in Trial 3	34
Table 4-5: Crack initiation and propagation on floorbeam web fascia side in Trial 5	35
Table 4-6: Crack initiation and propagation on connection plate side in Trial 5	36
Table 4-7: Crack initiation and propagation at floorbeam web fascia side in Trial 8	38
Table 4-8: Connection plate side: average crack growth rate	41
Table 4-9: Floorbeam web fascia side - average crack growth rate	42
Table 5-1: Element size and mesh technique for important model parts in single-plate connection models	51
Table 5-2: Introduction of finite element models for single-plate connection specimen FS1	54
Table 5-3: Summary of the efficacy of the angles-with-plate retrofit in the computer simulations for specimen FS1	65
Table 7-1: Three configurations used in double-angle connection test (FS2)	80
Table 8-1: Element size and mesh technique for important parts in double-angle connection models	89

Part II: Application of Angles-with-Plate Retrofit in Repairing Distortion-Induced Fatigue Damages in Skewed Girder to Cross-Frame Connections

Table 2-1: Test summary of 20-degree skewed specimen	126
Table 4-1: Test summary of 40-degree skewed specimen	148

PART I:

**APPLICATION OF ANGLES-WITH-PLATE RETROFIT FOR REPAIRING
DISTORTION-INDUCED FATIGUE DAMAGE IN STRINGER TO
FLOORBEAM CONNECTIONS**

1. Background and Literature Review

This chapter introduces the background of this study, which includes discussions of the following:

- Problem statement
- Distortion-induced fatigue cracks observed in previous tests and field examinations
- Currently used methods for repairing and retrofitting details susceptible to distortion-induced fatigue
- Current fatigue analysis methods
- Three previous studies that examined the fatigue properties of single-plate and double-angle connections.

1.1 Problem Statement

Shown in Figure 1-1, single-plate and double-angle connections are two typical methods used to connect transverse and longitudinal members in bridges. Connections such as these can be susceptible to distortion-induced fatigue cracking. While the title of this Part refers to floorbeam-to-stringer connections, similar connection types are also used on girder-to-floorbeam connections, which have also been known to exhibit fatigue problems (Haghani 2012). Therefore, this research is not limited to stringer to floorbeam connections.

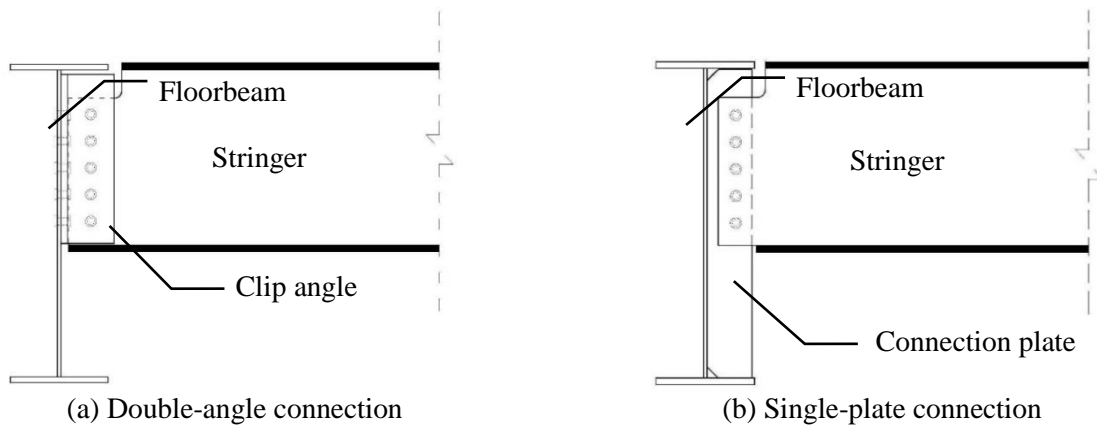


Figure 1-1: Double-angle and single-plate connections

Distortion-induced fatigue is caused by secondary stresses induced by out-of-plane deformation. For many aging bridges, these stresses were not accounted for when the structure was designed. Single-plate and double-angle connections are commonly referred as “shear connections”. In another words, they are intended to act as pinned connections, which implies that they are not intended to transfer moment. However, in reality, these connections are not completely free to rotate (Dexter and Ocel 2013). As shown in Figure 1-2, when live loads produce relative displacement between adjacent members, rotations occur between longitudinal and transverse members and generate moments at the connections. Normally, the moments are not large-magnitude, but connections are usually the place where stresses concentrate due to abrupt changes in dimensions and stiffness. The ignored forces can result in highly localized deformations and stresses, and can make the connections very sensitive to fatigue. There is limited literature regarding how to effectively repair fatigue cracking in connections such as these. Therefore, solutions are needed to repair distortion-induced fatigue cracking in floorbeam-to-stringer connections and connections in similar systems. Additionally, there is not a well-developed understanding of which connection geometries are most susceptible to distortion-induced fatigue in these kinds of connections.

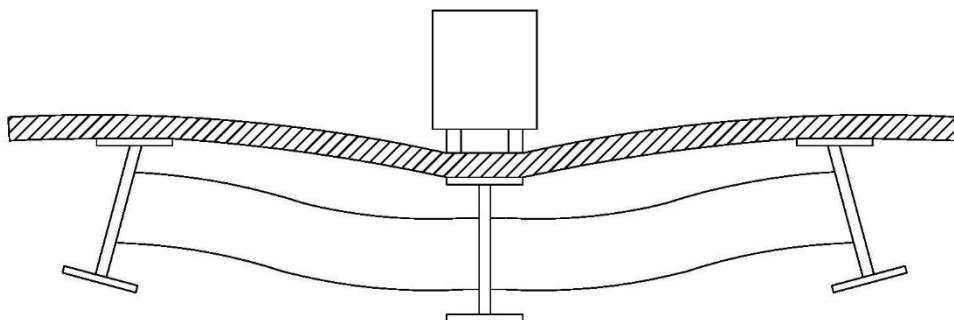


Figure 1-2: Distortion caused by relative displacement of adjacent members

1.2 Distortion-Induced Fatigue Cracks in Single-Plate and Double-Angle Connections

1.2.1 Fatigue Cracks at Cope Area

Figure 1-3 presents a cracked stringer cope. A cope is designed to accommodate the intersection of two members, but coped regions in bridge members have been shown to be susceptible to fatigue cracking (Haghani 2012; Roeder 2001). A coped area experiences a stress concentration due to the change of geometry, and for poorly-fabricated members the situation is worsened. It is reported that workmanship of flame-cut cope regions is often unsatisfactory (Mertz 2012).

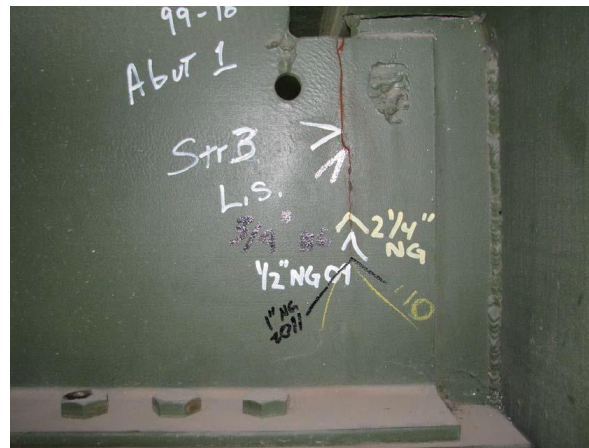


Figure 1-3: Stringer with cracked cope area

1.2.2 Fatigue Cracks in the Web-Gap Region of a Single-Plate Connection

In single-plate connections, the stringer is bolted to a connection plate which is in turn connected to the floorbeam web, typically through welding. For many bridges, the connection plate also functions as a web stiffener. In many cases, the connection plate has cropped ends, which were detailed to avoid introducing welds at the flanges. As shown in Figure 1-4, the cropped end of the connection plate forms a web-gap region with the floorbeam web and the flange. For many bridges built prior to 1985, there is no connection provided between the connection plates and the floorbeam flanges. Engineers at that time believed this to be a good practice to avoid fatigue cracking in flanges, but it resulted in introducing very flexible web-gap regions, which are highly

fatigue-sensitive details. As the stringer rotates, highly localized bending can occur at the web-gap. It is thought that most fatigue cracks found in bridges are caused by distortion-induced fatigue, due to out-of-plane deformations at web-gaps (Fisher et al. 1990). Exterior members tend to undergo greater out-of-plane deformations than interior members (Wipf et al. 1998), which helps explain why cracks in web-gap regions are frequently found in exterior member connections.

Web-gap cracking can be divided into two types. The first type is cracks that initiate at the end of welds connecting the floorbeam or girder web and connection plate, and grow vertically along the weld (Mertz 2012). These are sometimes referred as horseshoe-shaped cracks when they grow horizontally into the web. Another type is cracks that developed horizontally on the web-to-flange weld (Mertz 2012).

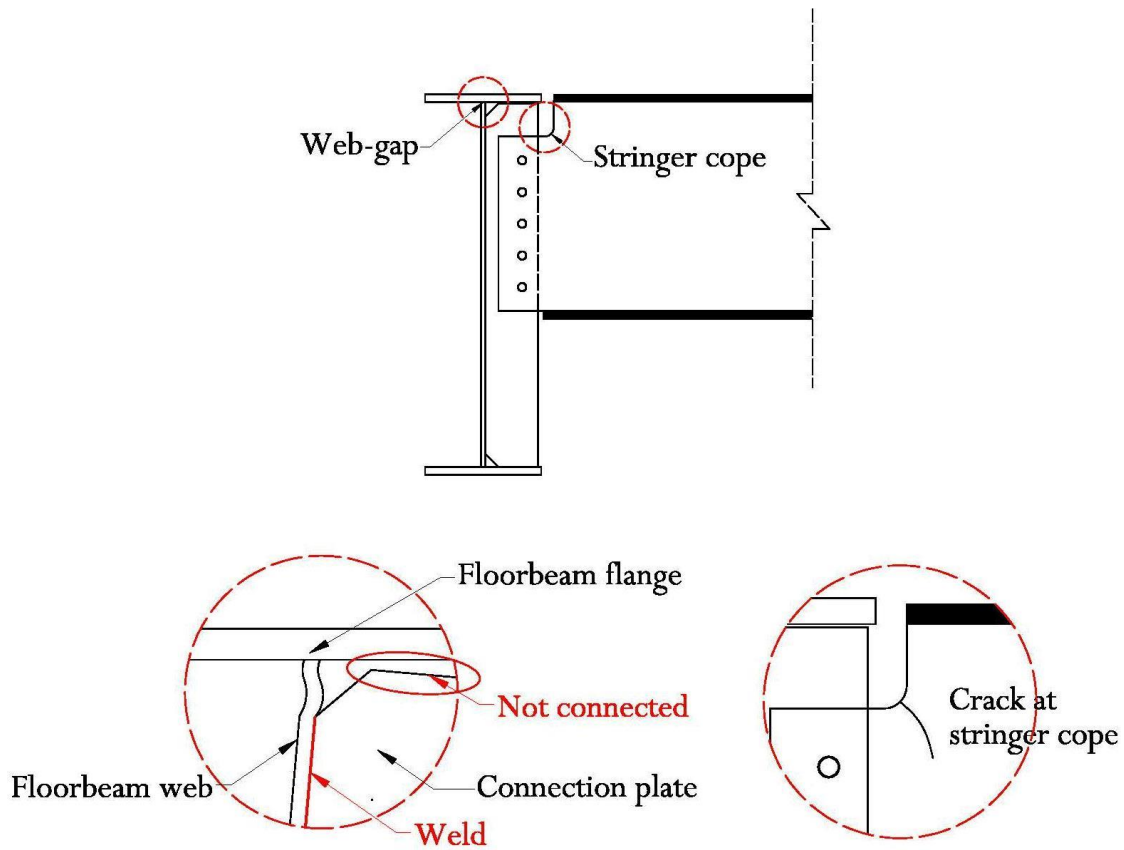


Figure 1-4: Fatigue problems in floorbeam web-gap region and stringer cope area

1.2.3 Fatigue Cracks in Connecting Elements of Double-Angle Connections

As presented in Figure 1-5, for double-angle connections, cracks may occur at the top part of the connection angle near the angle fillet and grow vertically along the corner (Al-Emrani 2005; Haghani 2012).

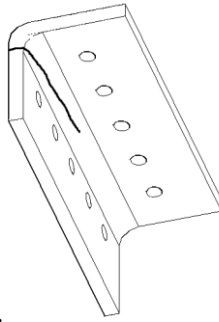


Figure 1-5: Typical crack in clip angle

1.2.4 Fatigue Cracks in Rivets in Double-Angle Connections

Rivets were widely used in steel bridges before welding and bolting were common, and cracking has been found to occur at rivets connecting angles to floorbeam webs (Al-Emrani 2005). In a fatigue test conducted on stringer-to-floorbeam components taken from an old riveted bridge, failures occurred at the junction of rivet shank and head. After microscopic examination, evidence of pre-existing fatigue cracks were found (Al-Emrani 2005). The rivets were designed to transfer shear forces, however, moments were also sustained in practice. Therefore, the rivets had to carry additional bending which was not considered in design.

1.3 Repair and Retrofitting of Distortion-Induced Fatigue Cracks

The *Manual for Repair and Retrofit of Fatigue Crack in Steel Bridges* (Dexter and Ocel 2013) is an excellent reference when studying the various fatigue issues steel bridges may encounter and methods for repairing and retrofitting them. This section will briefly introduce some retrofit methods in repairing distortion-induced fatigue. Readers can refer to the manual for more details.

1.3.1 Grinding and Re-Welding

Grinding and re-welding can be useful in repairing a cracked weld, however, if the crack is on the base metal, the crack should be expected to reinitiate after repairing. Moreover, when the repair is used for cracked weld metal, the best outcome that can be expected is to restore the fatigue strength of the weld to its initial fatigue strength. This is why when welding is used in repairing cracks, it is recommended to be implemented with other repair and retrofit methods, such as bolted doubler plates.

1.3.2 Bolted Doubler Plates

Adding doubler plates is a commonly-used method for repairing cracked members. Doubler plates can be added using either welding or bolting, but bolting is often preferred since a bolted detail tends to perform better than a welded detail in fatigue.

Adding doubler plates locally increases the cross-sectional area and provides an alternate load path so that the stress range is reduced at the crack tips. Plates should be added over both crack faces. In designing plates for load-induced fatigue damage, one should assume the original cracked steel does not contribute in bearing the load. In another word, the doubler plates should be able to sustain the fatigue load independently. Bolted doubler plates can be used with grinding and re-welding or drilling crack-arrest holes to achieve better results.

1.3.3 Crack-Arrest Holes

Drilling crack-arrest holes at the tip(s) of a crack is a commonly-used method to reduce the stress concentration and reduce the driving force behind crack propagation. However, in repairing distortion-induced fatigue damage this method is usually ineffective if it not combined with other techniques. The following are several reasons:

- Crack tips need to be carefully located to effectively reduce the stress concentration, as shown in Figure 1-6. This is not an easy task since the crack tip may be difficult to locate with precision. Furthermore, in some cases there may not be enough space to drill a hole at the center of the crack tip.



Figure 1-6: Location of crack-arrest holes

- Recent research has identified that even when there is ample space to drill a crack-arrest hole, hole-drilling may be ineffective for certain crack placements and geometries under distortion-induced fatigue (Liu 2015).

Hole drilling can only be expected to temporarily pause the growth of cracks under distortion-induced fatigue loading. It is recommended that if hole drilling is used, it should be used in combination with other repair and retrofit techniques.

1.3.4 Connection Softening

The purpose of softening connections susceptible to distortion-induced fatigue is to reduce the stiffness of a connection such that less moment is generated in the web-gap region. Commonly-used softening techniques include:

- **Diaphragm or Cross-Frame Removal**

Removing diaphragms or cross-frames can eliminate the driving force causing distortion-induced fatigue. This method is applicable because lateral bracing does not play a large stability role in positive bending regions after a bridge is constructed. In this scenario, the

compression flanges of the positive bending region are restrained by the concrete deck such that lateral bracing is unnecessary for the purpose of preventing lateral torsional buckling. However, distortion-induced fatigue problems can still occur in negative bending regions where the bottom flange is in compression, and lateral bracing cannot be removed in this situation. Also, the concrete deck may need to be replaced in the service life of a bridge. If there is no lateral bracing during re-decking, then temporary bracing must be provided; this often serves as a disincentive to remove lateral bracing after bridges are constructed.

- **Bolt/Rivet Removal**

A connection may not rely on all bolts/rivets present to develop its full shear capacity. In some cases, a number of fasteners can be eliminated by replacing rivets and lower strength bolts with high strength bolts. Reducing the number of fasteners can make the connection more flexible.

- **Bolt Loosening**

Bolt holes are slightly larger than the bolt shanks. Field tests have shown that the relative displacement between girder flange and connection plate is usually very small. Bolt loosening can be a useful method in providing additional space for the lateral bracing member to move such that less moment is generated at the connection.

Tests have shown that these softening methods have the ability to reduce connection stiffness (Wipf et al. 1998; Wipf et al. 2003), but the effectiveness of these methods is variable.

Iowa State University performed investigations (Wipf et al. 1998) in which the effectiveness of bolt loosening was examined for various types of bracing. The percentage of stress range reduction at the web-gap region was found to vary from 30% to 80%, and the stress range at the web-gap of K-type bracing in some cases even increased after bolt loosening.

In practice, due to fabrication tolerances and erection misalignment, the effect of bolt loosening cannot be guaranteed because a bolt may have already been in bearing with the hole, which makes bolt loosening ineffective (Dexter and Ocel 2013).

Other softening methods include:

- **Connection Plate Shortening**

Shortening the connection plate increases the length of the web-gap, reducing the severity of the localized bending. It also lowers the stiffness of the connection such that less moment is generated. This method has been recommended for deep floorbeams (Dexter and Ocel 2013). The remaining portion of the connection plate must be ground flush with the web, otherwise cracks may initiate again due to the presence of the flaw.

- **Large Hole Retrofit**

Drilling large holes has been suggested as another way to soften a web-gap (Dexter and Ocel 2013). However, other researchers have found that this approach has limited effectiveness, and may raise stresses elsewhere in the web gap region (Liu 2015).

1.3.5 Connection Stiffening

In contrast to softening methods, stiffening methods increase connection stiffness by providing positive attachment between the connection plate and an adjacent element. Stiffening methods work by reducing localized deformations at the web-gap. They also provide an alternative load path so that stresses at the cracked portion of the girder are relieved. The following describes two approaches to stiffening a web-gap region.

- **Providing Attachment between Connection Plate and Girder/Floorbeam Flange**

Since fatigue problems at web-gap regions are caused by not connecting the connection plate to the flange, an obvious thought to solve this issue is to provide attachment between them.

There are multiple ways to provide the attachment, but so far bolting is still viewed as the best method to guarantee effectiveness of the retrofit. However, if bolting is used to provide the attachment, the concrete deck must be removed when cracking is in the top web-gap, to install bolt holes through the steel flanges. The difficulty of removing the concrete deck gives rise to the need to develop an alternative method discussed in the following section (Bennett et al. 2014).

- **Providing Attachment between Connection Plate and Girder/Floorbeam Web – Angles-with-Plate Retrofit**

Instead of connecting the flange and the connection plate, in this method, attachments are installed between the connection plate and the web.

Developed at the University of Kansas (Alemdar et al. 2014a; 2014b), the angles-with-plate retrofit has shown its potential in stopping crack growth in web-gap region without requiring deck removal. The angles-with-plate retrofit includes two angles and a backing plate for an exterior connection, as shown in Figure 1-7; for an interior connection, four angles may be used.

The angles are used to connect the connection plate to the girder/floorbeam web, while the backing plate distributes stresses over a larger region on the reverse side of the web. Although there is no connection between the connection plate and the flange, the applied

attachments distribute the load across a broad area of the web, such that stresses do not concentrate in a small region.

The main benefit of this method is it does not disturb the concrete deck. Tests at the University of Kansas (Alemdar et al. 2014a, 2014b; Bennett et al. 2014) have shown for straight girder to cross-frame connection, the angles-with-plate retrofit can effectively stop the growth of distortion-induced fatigue cracks.



(a) Angle



(b) Backing plate

Figure 1-7: Angles-with-plate retrofit

1.4 Summary of Relevant Previous Research

Three studies pertinent to fatigue tests on single-plate and double-angle connections and the proposed repair technique are summarized in this section.

1.4.1 Work at the University of Kansas – Fatigue Properties and Retrofits of Web-Gap

A series of investigations have been performed at the University of Kansas studying the performance of the angles-with-plates retrofit and the effectiveness of crack-arrest holes in repairing distortion-induced fatigue (Alemdar et al. 2014a, 2014b; Hartman et al. 2013; Bennett et al. 2014)

This work consisted of physical tests performed on a 30 ft scaled bridge system and three 36 in. deep girder-to-cross-frame connection subassemblies component tests, as well as a series of

computer simulations augmenting both physical test series. The effectiveness of undersized crack-arrest holes in distortion-induced fatigue applications was also examined.

1.4.1.1 Physical Test Program

Component Tests

Three component-level specimens were tested at the University of Kansas to study distortion-induced fatigue and the effectiveness of the angles-with-plate retrofit. The effectiveness of undersized crack-arrest holes was also studied in the tests. Each specimen was comprised of a 36 in. deep, 9 ft long girder, a cropped connection plate, and an X-type cross-frame. The cross-frame was bolted to the connection plate which was in turn welded to the centerline of the girder web. Cyclic loads were applied via an actuator connected to the far end of the cross-frame. The bottom flange of the girder was bolted to the lab floor to simulate the effect of a bridge deck.

Cracks were observed along the connection plate-to-web weld (horseshoe-shaped cracks) and along the web-to-flange weld in the tests. After initiation, cracks continued growing in the unretrofitted trials (Alemdar et al. 2014a). The results also indicated that crack-arrest holes were not effective in stopping crack propagation.

Test Bridge System

The test bridge consisted of three 30 ft long girders spaced at 5 ft, with X-type cross-frames installed at mid-span and supports. The top flanges of the girders were restrained by a concrete deck fabricated in the lab. An actuator was used to apply cyclic loads at midspan centered above the interior girder.

Crack growth rates were significantly slowed when the angles-with-plate retrofit was installed. When the crack tip was removed by drilling small diameter crack-arrest holes, crack growth was halted after angles-with-plate retrofit installation.

1.4.1.2 Computer Simulation

A series of computer models were created using the commercially-available finite element analysis software, Abaqus V6.10 (Alemdar et al. 2014b). The models were configured to represent the physical specimens for both the component tests and the 30 ft scaled bridge as faithfully as possible. The computer simulations were primarily aimed at studying the effectiveness of the angles-with-plate retrofit.

The hot spot stress (HSS) technique was used to compare computed stresses between simulations. Stresses were extracted along a path located at 0.2 in. away from the weld toe. Two HSS paths were defined in the models. They corresponded to the crack patterns along the connection plate-to-web weld and along the girder web-to-flange weld. In addition to computing HSS, the J -integral was computed at the tip of the simulated cracks to examine crack growth propensity. A parametric analysis was performed to determine the optimal plate and angle dimensions.

Comparing the computed results and the physical test results, the researchers found that the locations in the physical specimens that experienced fatigue cracks corresponded very well with locations in the finite element models exhibiting the greatest maximum principal stresses.

In the FE models of the test bridge system, results showed that the angles-with-plate retrofit significantly reduced stress demands in the web-gap region. The simulations also showed that the stress distribution in the web-gap of the scaled bridge model was similar to that of the web-gap in the component model.

For all of the different retrofit configurations examined in the analyses, the models indicated that peak stresses in the unretrofitted models were reduced 93% - 98% with respect to peak stresses in the retrofitted models. The lowest average stress demand occurred when the thickness of the angles and plate was 2.7 times the web thickness.

The simulations showed that the angles-with-plate retrofit can be an effective technique for repairing distortion-induced fatigue damage at web-gap regions. The researchers recommended using angle and plate elements with a thickness of at least 2.5 times the girder web thickness. The length of the back plate should be at least 1.5 times the length of the horizontal girder web to flange weld crack, and the back plate should extend beyond the legs of the angles.

The results also showed that the crack-arrest holes only had a slight effect in reducing stresses around crack tips.

1.4.1.3 Conclusions from Prior Angles-with-Plate Research Performed at the University of Kansas

Research performed at the University of Kansas showed that the angles-with-plate retrofit can be an effective and attractive method for repairing distortion-induced fatigue damage in web-gap regions. Computer simulations indicated that stress demand in the web-gap region was significantly reduced after retrofitting. The physical tests verified this finding. When crack tips remained sharp, the angles-with-plate retrofit stopped the growth of the cracks in the component tests, and in the test bridge system, it significantly reduced the crack propagation rate. After crack tips were removed by drilling small crack-arrest holes, crack propagation rates in the test bridge system were slowed even further.

1.4.2 Research at the University of Washington – Fatigue Properties and Retrofit of Stringer Cope Area

The Report *Fatigue Cracking of Riveted, Coped Stringer to Floorbeam Connections* (Roeder 2001) contains a summary of work performed at the University of Washington aimed at studying the fatigue properties of coped stringers and the performance of three repair and retrofit methods. These methods were referred to as damage limitation methods (DLM) in the report.

Sixteen specimens made with W21x16 sections were tested in this research program. A single span configuration was used, wherein one end of the stringer was bolted to a reaction wall and the other end was supported by a roller. A fatigue load was applied at a distance equal to 47.7% of the span length from the reaction wall. The specimens had three different types of copes: square cut, 22 mm flame-cut, and 22 mm flame-cut with notches.

Three DLMs were studied to determine their relative effectiveness in slowing growth of the cracks. They were hole-drilling, hole-drilling with an inserted bolt, and bolt removal. The influence of spring stiffness at the end of the stringer on the fatigue properties of the cope area was also studied in the tests.

Although the flame-cut specimens were intended to simulate actual details, the tests indicated that it was difficult to initiate cracks at flame-cut copes. There was considerable scatter in the test results, which is commonly seen in fatigue tests, but the specimens with the smooth flame-cut cope generally took a long time to initiate cracks, and for one of the specimens there was no crack initiation at all. This finding did not match what was observed in the prototype bridges, in which the stringer copes were more sensitive to fatigue.

The test results showed that the surface condition of the cope area is an important factor influencing crack initiation life. A stringer with a rough or notched cope initiated cracks much faster than a smooth flame-cut cope. The rough or notched cope area resulted in fatigue performance well below the AASHTO category E' curve. The researchers stated that the behavior of a stringer cope in an existing bridge is more similar to a notched specimen than to a smooth flame-cut specimen.

Connection spring stiffness was found to have a significant effect on stringer cope stress and crack growth rate. High magnitude connection stiffness led to higher stringer end moments, which resulted in higher cope stresses, earlier crack initiation, and faster crack growth.

Crack-arrest holes only extended fatigue life for a short time. It was found that a drilled hole with an inserted bolt was much more effective than an empty hole in stopping crack growth. The problem associated with this method is it does not change the stiffness of the connection and does not provide an alternative load path to reduce the stress. One crack may be stopped, but other cracks may initiate elsewhere. Furthermore, once the crack reinitiated at the hole with an inserted bolt, it usually grew faster than before. The bolt removal method was found to effectively stop crack growth when the spring stiffness of the connection was able to be reduced to a sufficiently low level. To achieve a better result, it was recommended to reduce stresses at the coped region to zero or to cause a reversal of the moment so that one could ensure that the crack will stop growing. If the stiffness could not be reduced enough, crack growth can be expected to slow but should not be expected to stop.

Existing linear crack propagation models were used to analyze the crack growth, but the results did not match test observations. The theories did not describe the behavior of the specimen because they did not consider all of the complexities of the connection.

The researchers proposed a procedure for evaluating a retrofit method and developed expressions to estimate remaining fatigue life of a connection.

The researchers also provided some recommendations for future research works:

- Crack growth predicted using existing linear crack propagation model did not match test observations because they did not consider the complexities of the connection. Future research is needed to improve these models.
- More field tests on existing bridges are needed to develop a load spectrum and to understand the actual behavior of the stringer cope on existing bridges.

- The rotational spring stiffness is an important factor in evaluating the coped stringer connection. Research on this topic is limited. Future work is needed to better understand the effect of connection spring stiffness and the use of it in fatigue evaluation processes.

1.4.3 Research at Chalmers University of Technology – Fatigue of Riveted Double-Angle Connection

AI-Emrani (2005) described a study conducted on three full-scale riveted double-angle connection specimens. The specimens were real components taken from an old railway bridge, with each specimen consisting of three floorbeams and four stringers. The floorbeam-stringer specimens were each supported with a pair of rollers underneath the ends of the floorbeams. The loads were applied as two points load through a spreader beam at the center line of each stringer.

The researchers used α to represent the degree of continuity of a connection,

$$\alpha = \frac{M_p}{M_f} = \frac{1}{1+R} \quad \text{Equation 1-1}$$

M_p : Moment at central support of partially-continuous two-span girder

M_f : Moment at central support of fully-continuous two-span girder

$$R = \frac{(3EI/L)_{\text{Stringer}}}{K_{\text{rot}}} \quad \text{Equation 1-2}$$

K_{rot} : Rotational stiffness of each double-angle stringer-to-floorbeam connection

The computed result indicated that those connections were able to develop up to 67% of the moment of a fully continuous beam.

Two modes of fatigue damage were observed in the tests: fatigue cracking of the connection angles and fatigue cracking of the rivets connecting the legs of the connection angles to the floorbeam web. Driven by out-of-plane distortion of the angle legs, new cracks on the connection angles always initiated near the angle fillet at the same height as the upper row of the rivets, and then grew along the height of the angle. The development of cracks in the connection angles led to a gradual reduction of the connection stiffness. The growth rate of the cracks slowed as the cracks grew longer, until the cracks eventually arrested. Fatigue cracking in rivets occurred in all three specimens, with cracks initiating at the junction of the rivet shank and head. The bending moment caused by rotation of the stringer and the stress concentration at the junction was the major mechanism leading to rivet cracking. The rivets exhibited a kind of plastic behavior at failure; when damage was observed, the rivet head and shank did not totally separate, and thus the broken rivet was able to still sustain some portion of the shear load. Rivet failure resulted in significant rotational stiffness reduction. Fracture of two rivets in the upper row was enough to stop further cracking or rivet failure.

For both failure modes, the rate of fatigue damage was fairly slow, and the load-carrying capacity of the connection was not reduced immediately by the damage. Furthermore, the fatigue damage tended to self-arrest as the fatigue cracks grew. However, in some cases the double-angle stringer-to-floorbeam connections resulted in a fracture. This reinforced the philosophy that a repair should be implemented as soon as possible when damage is detected.

2. Objective and Scope

The angles-with-plate retrofit has shown to be an effective method for repairing damaged web-gap regions in cross-frame to girder connections. The objective of this study was to evaluate the effectiveness of the bolted angles-with-plate retrofit for mitigating distortion-induced fatigue cracking in single-plate and double-angle stringer-to-floorbeam connections, as well as to develop a more thorough characterization of the fatigue performance of these connections.

The efficacy of the angles-with-plate retrofit in stopping fatigue crack propagation was evaluated through physical tests. Cyclic loads were applied on the connection subassemblies to initiate and propagate fatigue cracks. The angles-with-plate retrofit was then applied to repair the damaged connections. The retrofit was removed at regular intervals during the tests to measure crack growth. Computer simulations of the tested specimens were used to quantitatively analyze effectiveness of the retrofit in reducing stress demands at damaged regions. Computer simulation results were compared with physical test results.

Chapter 1 presented the background of distortion-induced fatigue and a literature review of relevant topics. Descriptions of the physical tests and computer simulations for the single-plate connection and the double-angle connection are presented in Chapters 3-6 and Chapters 7-9 respectively. Conclusions are provided in Chapter 10.

3. Physical Test of Single-Plate Connection (Specimen FS1) – Test Introduction

3.1 Description of Floorbeam-Stringer Specimen FS1

A floorbeam-stringer test specimen with a single-plate connection (FS1) is described in this section. The specimen consisted of a built-up steel floorbeam and a coped stringer. Steel used in the test was Grade A992.

As shown in Figure 3-1, the built-up floorbeam was 9 ft long, 36 in. tall, with a 34-1/2 in. \times 3/8 in. web, a 11 in. \times 1 in. top flange and a 11 in. \times 5/8 in. bottom flange. The specimen included a 34-3/8 in. \times 5 in. \times 3/8 in. transverse connection plate with 1-1/4 in. cropped ends. The transverse connection plate was welded to the centerline of the floorbeam web, but no connection was provided between the connection plate and the floorbeam flanges.

The cropped end formed a web-gap region with the floorbeam web and the flanges, which was expected to be sensitive to distortion-induced fatigue. The floorbeam was stiffened at its ends, and these stiffeners were welded to both flanges and the web. Both ends of the floorbeam were restrained from lateral movement by steel angles bolted between the top flange and the testing frame. The bottom flange of the floorbeam was fixed to the laboratory strong floor by bolting to a pair of 6 \times 6 \times 1/2 HSS, which were in turn attached to the concrete floor through a series of post-tensioned C5 \times 9 and C10 \times 30 channels. Therefore, the specimen was tested upside-down, with the flange attached to the laboratory floor simulating a top flange connected to a laterally-stiff bridge deck.

In a real bridge system, the top flange of a floorbeam is restrained by a bridge deck, but this situation is difficult to establish in a component test. By fixing the bottom flange of the floorbeam, the displacement of the bottom flange was fully restrained and the influence of in-plane bending

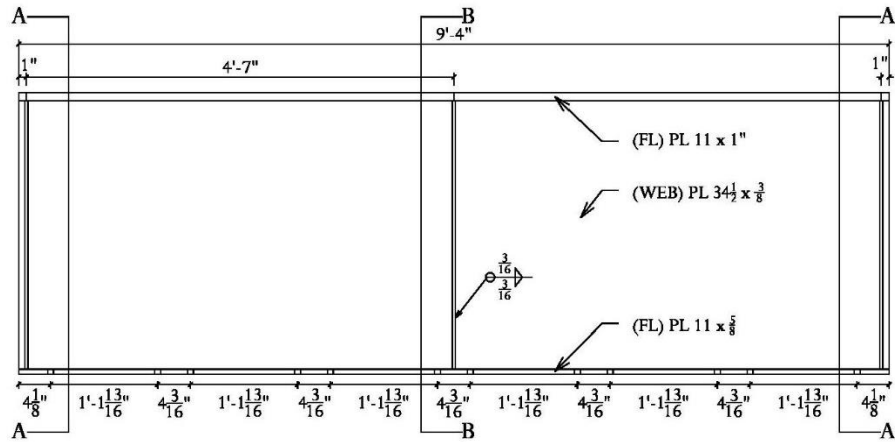
was eliminated. Computer simulations associated with the previous girder to cross-frame tests at the University of Kansas showed that the stress distribution in the component test was similar to that of a real bridge (Alemdar et al. 2014a, 2014b).

A W 21×62 coped stringer was bolted to the transverse connection plate at the mid-length point of the floorbeam. The far end of stringer was bolted to a WT section which was then connected to a servo-hydraulic actuator. In the test, the actuator applied upwards cyclical loading to simulate the effect of passing traffic.

$\frac{3}{4}$ in. A325-SC bolts were used in the tests with hole diameters of $\frac{13}{16}$ in. All welds in the specimens were $\frac{3}{16}$ in. fillet weld.

Figure 3-2 presents the dimensions of the angles-with-plate retrofit. The retrofit was applied to the specimen when cracks grew to $\frac{3}{4}$ in. Photographs of the specimen and retrofit are shown in Figure 3-3.

ELEVATION



SECTION A-A

SECTION B-B

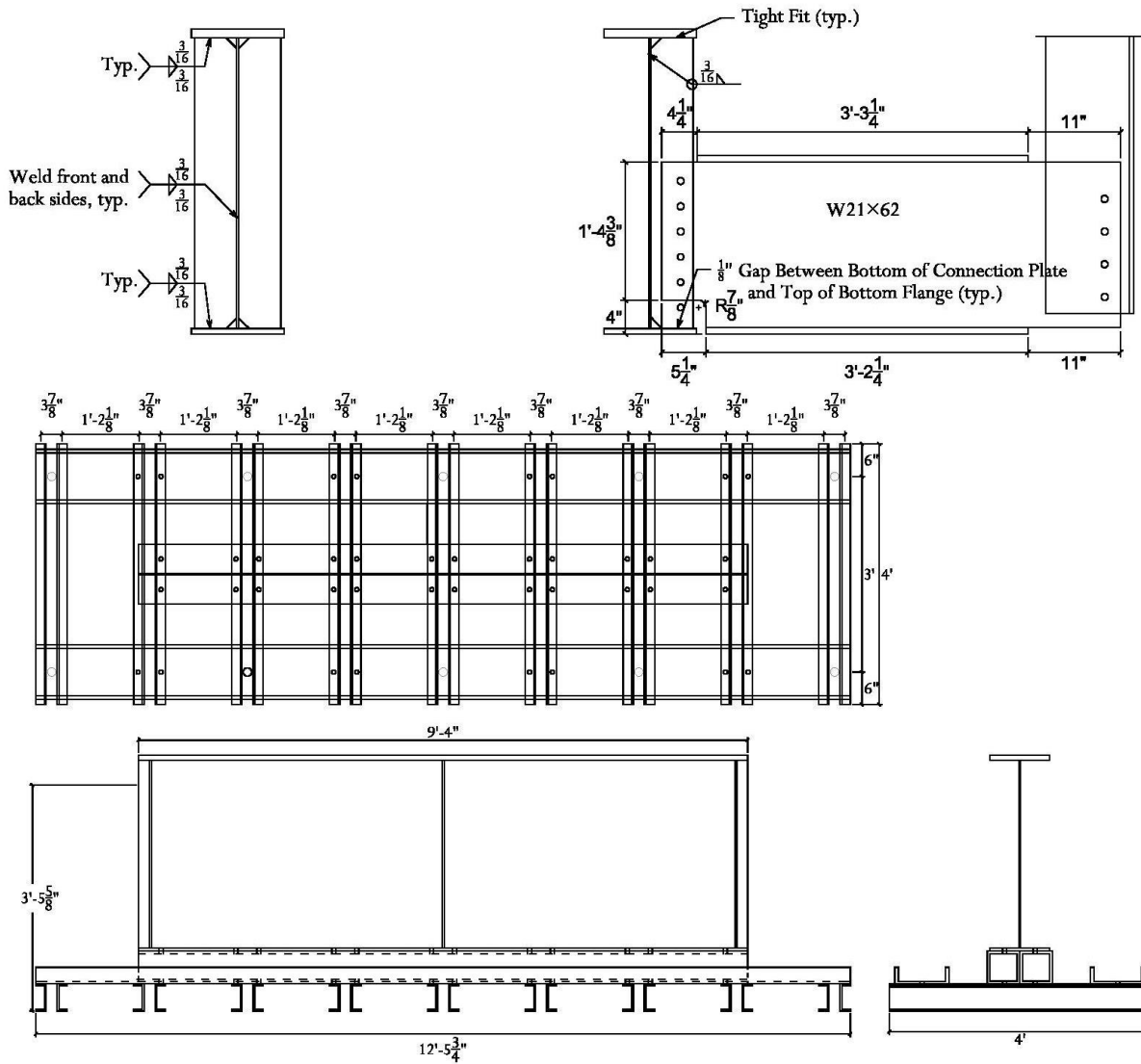


Figure 3-1: Specimen dimension and layout of single-plate connection specimen (Test FS1)

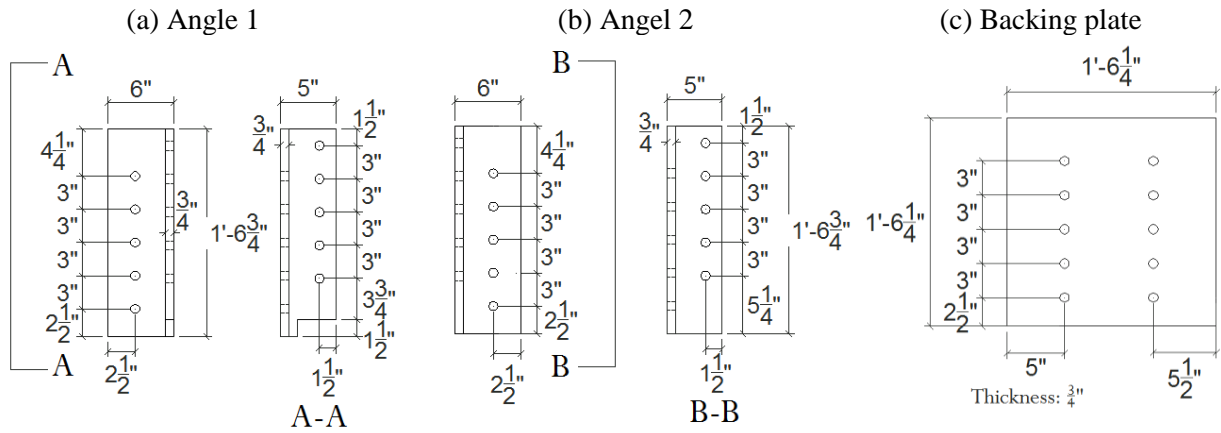


Figure 3-2: Dimensions of angles-with-plate retrofit

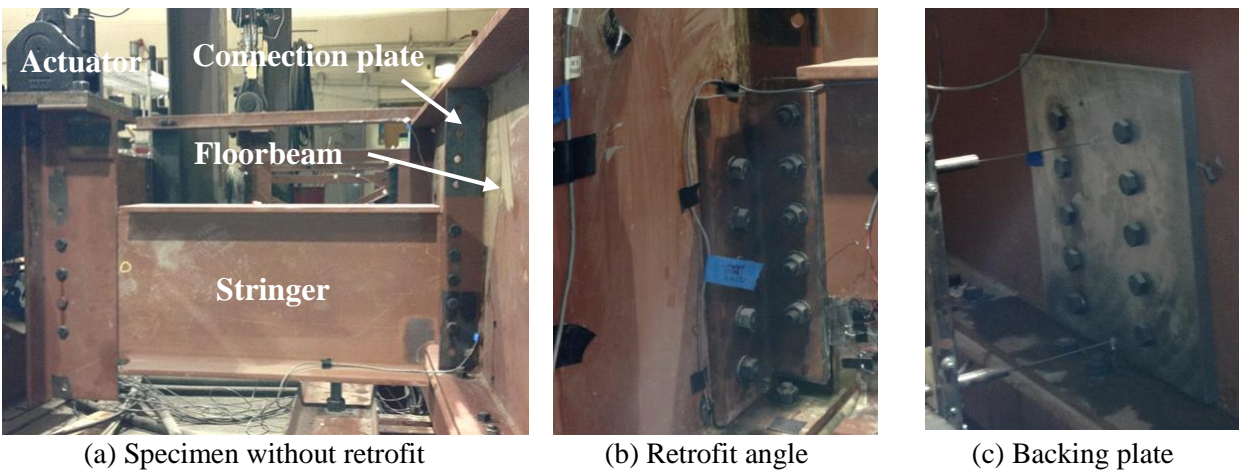


Figure 3-3: Photos of single-plate connection specimen (FS1)

3.2 Instrumentation

Actuator displacement was measured using a string potentiometer and actuator force data was recorded simultaneously via a load cell. Strain gages were attached to the floorbeam and stringer at regions susceptible to fatigue problems as predicted through FE analyses and the existing literature. For this test, the susceptible regions were identified as the bottom web-gap region (formed by the cropped end of the stiffener, the floorbeam web, and the bottom flange) and the coped portion of the stringer.

Figure 3-4 includes a schematic drawing showing the strain gage placements:

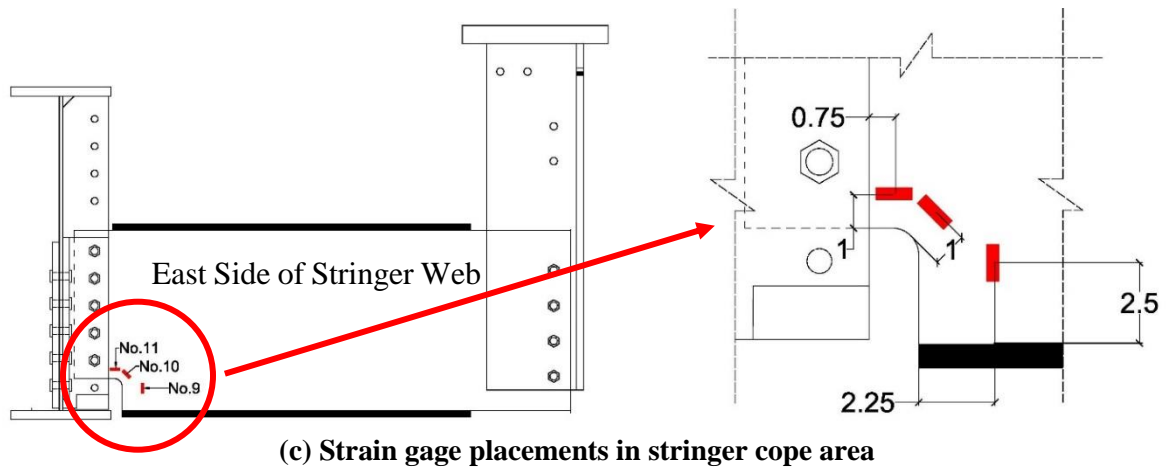
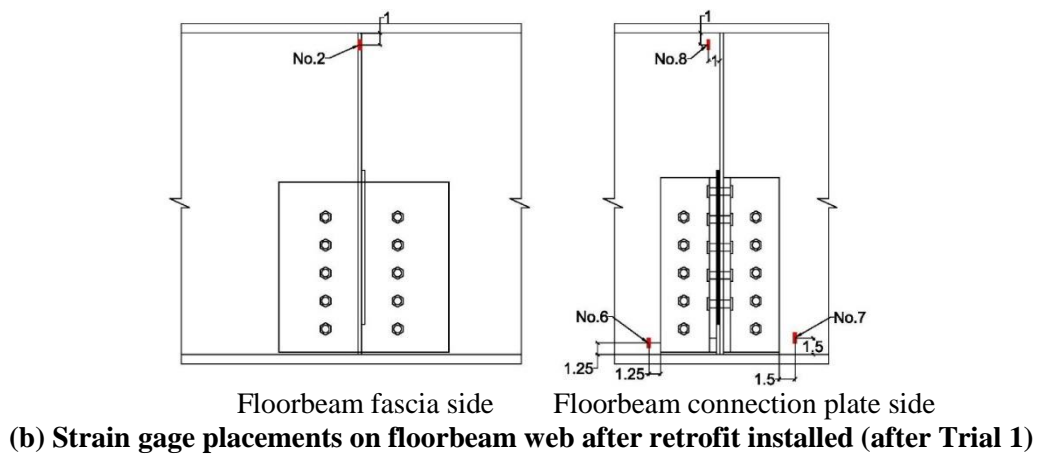
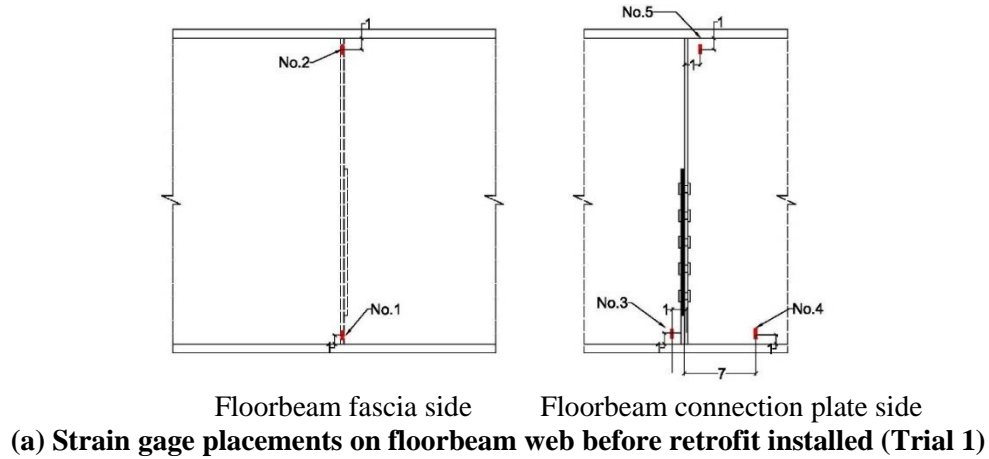


Figure 3-4: Strain gage placements on single-plate connection specimen (FS1)

Besides the strain gages presented in Figure 3-4, there were two additional strain gages [No.12 and No.13] placed at the center of the top surface of the stringer bottom flange, at both sides of the stringer.

3.3 Test Procedure

A summary of the various test trials performed on the single-plate connection floorbeam-stringer specimen FS1 is presented in Table 3-1. The actuator applied upwards cyclic loading for a load range of 1-5 kip at a frequency of 2 Hz. Monotonic tests were conducted at regular intervals by slowly increasing the actuator load from 0-6 kip while recording the actuator force, actuator displacement, and strain gage data. The specimen was regularly inspected for cracking using dye penetrant.

At the beginning of the test, the specimen was loaded under fatigue to initiate cracks. The angles-with-plate retrofit was installed once the cracks had grown to $\frac{3}{4}$ in. along the floorbeam web to connection plate weld.

To determine the efficacy of the retrofit for different crack lengths, the retrofit was removed in unretrofitted trials to propagate the cracks. 1.2 million cycles were applied in each of the retrofitted trials. This threshold was chosen for run-out to allow for possible performance of the detail to exceed category A performance level, since the strain gage No.1 reading at the web-gap region indicated a stress range of approximately 30 ksi for the applied load range of 1-5 kip. The number of cycles applied in unretrofitted trials was determined by the specimen performance.

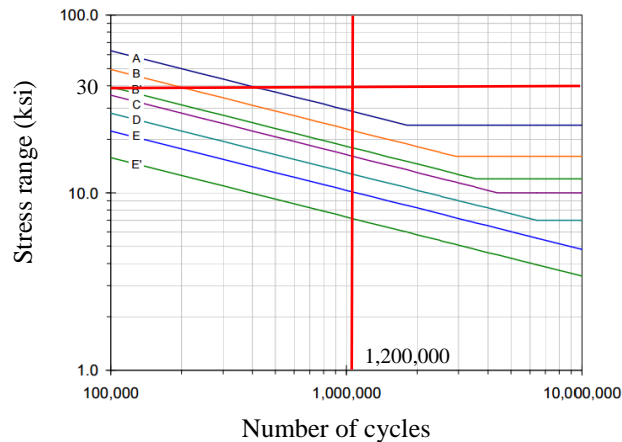


Figure 3-5: AASHTO S-N curves

In Trial 7, the load range was increased to 1.34-6.72 kip to match the displacement of the unretrofitted specimen. In a bridge with floorbeam to stringer connections, the relative displacement between two floorbeams was governed by the deformation of main girders. Therefore, retrofitting a connection may not significantly affect the relative displacement between two floorbeams, implying that the displacement might be invariant. The actuator displacement for the retrofitted connection at an actuator force of 6.72 kip actuator force corresponded to the actuator displacement of the unretrofitted connection at 5 kip actuator force. The load range was selected to match the R-ratio of the original load range. The load range was then reduced to the previous 1-5 kip in Trial 8.

Table 3-1: Single-plate connection FS1 physical test trials introduction

Trial	Retrofit Status	Number of Cycles	Total Cycles
Trial 1	Unretrofitted	90,000	90,000
Trial 2	Retrofitted	1,200,000	1,290,000
Trial 3	Unretrofitted	1,200,000	2,490,000
Trial 4	Retrofitted	1,200,000	3,690,000
Trial 5	Unretrofitted	450,000	4,140,000
Trial 6	Retrofitted	1,200,000	5,340,000
Trial 7*	Retrofitted	1,200,000	6,540,000
Trial 8	Unretrofitted	85,000	6,625,000

Load Range: 1-5 kip

Increased Load Range: 1.34-6.72 kip

Load Frequency: 2 Hz

* Trial 7 is cycled under increased load range

4. Physical Test of Single-Plate Connection (FS1) – Results and Discussion

Eight trials, with a total of 6,625,000 cycles, were applied on the single-plate connection specimen in Test FS1. Results for crack initiation and propagation, actuator displacement, and stresses measured by strain gages are presented in the following. Table 4-1 provides a brief introduction to each test trial.

Table 4-1: Brief introduction of single-plate connection test process

Test	Trial	Number of cycles	Total number of cycles	Retrofit (Y/N)	Introduction
FS1	1	90,000	90,000	N	The specimen was cycled to initiate cracks. Cracks at both sides of the connection plate grew to ¾ in. at 90,000 cycles. Then the retrofit was installed and Trial 2 started.
FS1	2	1,200,000	1,290,000	Y	1,200,000 cycles were applied with the angle-with-plate retrofit in place. No visible crack growth was observed.
FS1	3	1,200,000	2,490,000	N	The specimen was cycled without the retrofit. Cracks grew slowly and steadily. 1,200,000 cycles were applied.
FS1	4	1,200,000	3,690,000	Y	Cycled with the retrofit in place. After 1,200,000 cycles, the retrofit was removed to examine the cracks. No visible crack growth was observed.
FS1	5	450,000	4,140,000	N	A 3 in. crack was observed on the floorbeam bottom flange to web weld at the web fascia side 400,000 cycles into Trial 5.
FS1	6	1,200,000	5,340,000	Y	1,200,000 cycles were applied with the angles-with-plate retrofit in place. No visible crack growth was observed.
FS1	7	1,200,000	6,540,000	Y	The load range was increased to 1.34-6.72 kip. No visible crack growth was observed after 1,200,000 cycles with the retrofit in place.
FS1	8	85,000	6,625,000	N	The results of the previous trials were enough to show the efficacy of the retrofit. The researchers were interested in the performance of the specimen without retrofit applied. The specimen was cycled without retrofit at the original load range (1-5 kip). Only 85,000 cycles were applied because the floorbeam web to bottom flange crack grew so fast that the specimen quickly reached a critical level.

4.1 Crack Initiation and Propagation

4.1.1 General Description of Crack Initiation and Propagation

It was found that cracks initiated and grew only in unretrofitted trials. The angles-with-plate retrofit successfully halted all the crack initiation and propagation in the single-plate floorbeam to stringer specimen FS1.

During the eight test trials, cracks developed on the connection plate-to-floorbeam web weld, the floorbeam web, and the floorbeam web-to-bottom flange weld. Although cracking was anticipated to develop on the stringer cope (cracks have been observed there in existing bridges), no crack was detected at the cope throughout the test.

Cracks were very thin when they first observed, but they quickly extended through the thickness. Cracks first appeared on the connection plate side of the floorbeam 5,000 cycles into Trial 1; they initiated at the bottom of connection plate-to-floorbeam web weld. Then, they grew upward vertically along the weld and propagated outwards into the floorbeam web. After propagating into the web, the cracks grew almost horizontally. Two additional cracks appeared on the floorbeam web-to-connection plate weld 400,000 cycles into Trial 5. They initiated separately from the existing cracks. One propagated vertically along the weld and eventually connected with the existing cracks. The other propagated into the floorbeam web and grew horizontally.

525,000 cycles into Trial 3, cracks on the connection plate side propagated through the thickness and were observed on the fascia side of the floorbeam web. A horizontal crack was first observed, and then branches appeared. Usually, the branches did not originate from the existing cracks. They generated individually, then propagated and connected with the existing cracks.

A crack on the fascia side of the floorbeam web to bottom flange weld was observed 400,000 cycles into Trial 5. It was a long crack when it was first observed, but the crack was still very thin, and difficult to detect. Since the crack was not observed at its initiation, it was unclear when it initiated. It is possible that it initiated between 350,000 to 400,000 cycles into Trial 5 since an inspection was performed at 350,000 cycles, but this crack was not detected. However, it is also possible that it initiated in Trial 4, in which the retrofit was applied, but the researchers failed to detect it. If this were the case, it would imply the retrofit was ineffective in preventing the initiation

of the web-to-bottom flange weld crack. The retrofit was then applied in Trial 6 and Trial 7. Cracks did not initiate or propagate in these two trials. Therefore, the crack on the fascia side floorbeam web-to-bottom flange weld most likely initiated in the unretrofitted Trial 5 rather than the retrofitted Trial 4.

In Trial 8, when the specimen was cycled without the retrofit in place, the crack on the fascia side floorbeam web to flange weld became wider and deeper and grew from 3 in. to 6¼ in. in just 85,000 cycles. The crack started to appear on the connection plate side floorbeam web to flange weld at the end of Trial 8.

Further details regarding crack initiation and propagation are provided in the following sections.

4.1.2 Crack Initiation and Propagation in Each Trial

Figure 4-1 presents a photo of the crack pattern 85,000 cycles into Trial 8, with assigned labels for each crack that developed. Cracks 1-4 initiated on the connection plate side. Cracks 5-8 were on the floorbeam web fascia side. Crack 9 propagated along the fascia side floorbeam web-to-bottom flange weld. Each labeled crack indicated that the crack initiated at a point and propagated without breaking. Two cracks were treated as different if one crack initiated separately and joined an existing crack later.

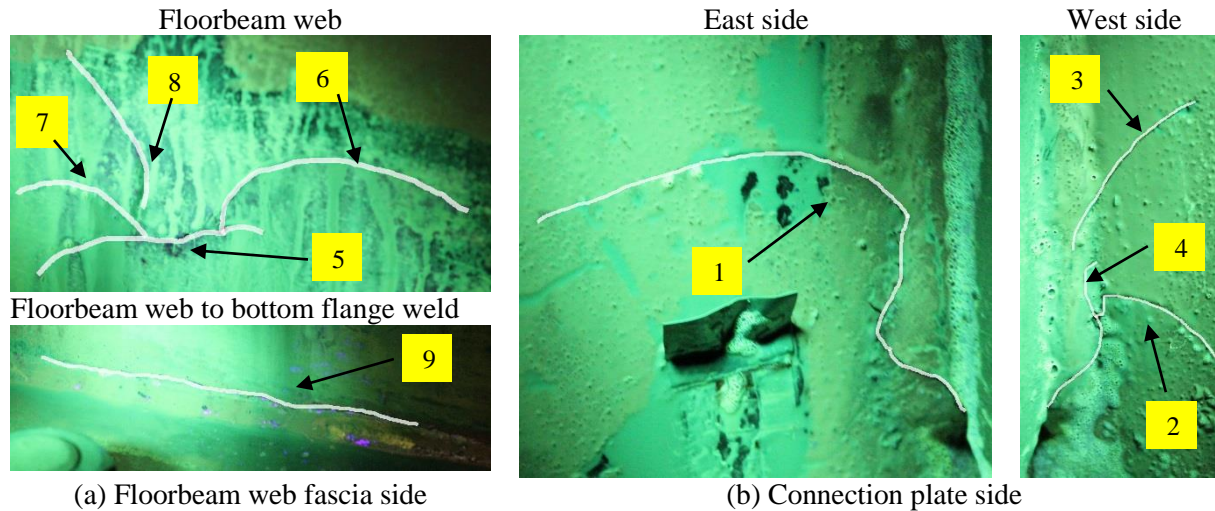


Figure 4-1: Cracks on single-plate connection specimen (FS1)

4.1.2.1 Trial 1 – Unretrofitted

In Trial 1, the specimen was cycled in the unretrofitted condition to initiate cracks.

Floorbeam Web Fascia Side

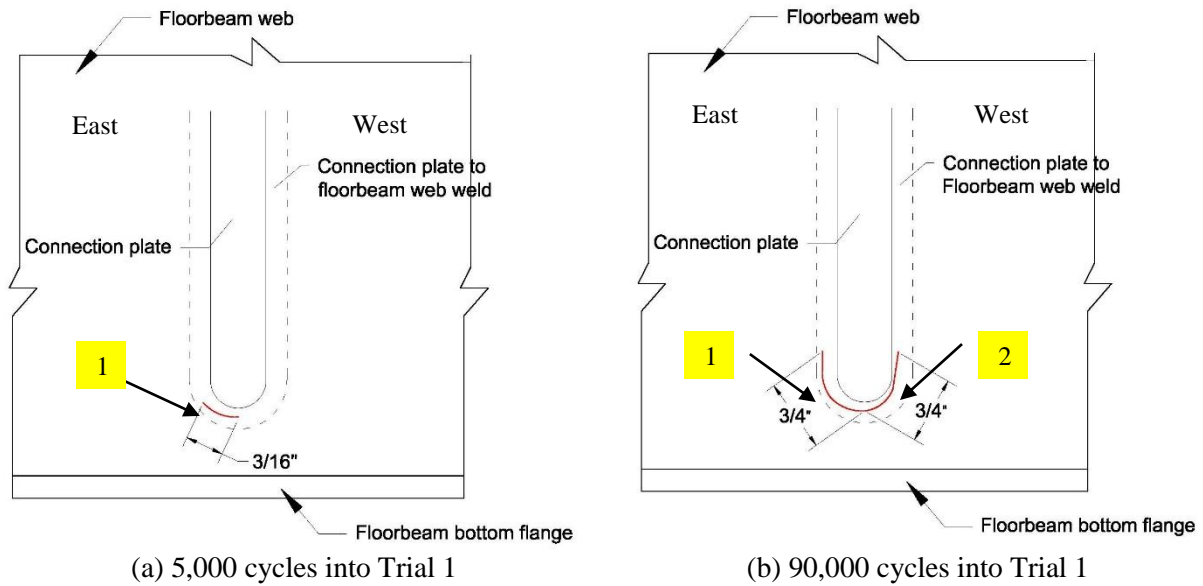
No cracking was observed.

Connection Plate Side:

Crack initiation and propagation behavior on the connection plate side of the specimen in Trial 1 are depicted in Table 4-2 and Figure 4-2. Cracks initiated at the end of the weld connecting the floorbeam web and the connection plate in the bottom web-gap. Trial 1 was ended after 90,000 cycles when cracks on both sides of the connection plate reached $\frac{3}{4}$ in.

Table 4-2: Crack initiation and propagation on connection plate side in Trial 1

Trial 1 cycles	Total cycles	Crack initiation and propagation
5,000	5,000	A $\frac{3}{16}$ in. crack (Crack 1) was observed on the east connection plate-to-floorbeam web weld
13,000	13,000	A $\frac{1}{8}$ in. crack (Crack 2) was observed at the west connection plate-to-floorbeam web weld
90,000	90,000	Both cracks reached $\frac{3}{4}$ in. 90,000 cycles into Trial 1, then the angles-with-plate retrofit was installed.



(a) 5,000 cycles into Trial 1
 (b) 90,000 cycles into Trial 1
Figure 4-2: Cracks on connection plate side in Trial 1

4.1.3.2 Trial 2 – Retrofitted

The angles-with-plate retrofit was installed at the outset of Trial 2. 1,200,000 cycles were applied on the specimen in the retrofitted condition. At the end of Trial 2, the angles-with-plate retrofit was removed, and no visible crack growth was observed.

4.1.3.3 Trial 3 – Unretrofitted

In Trial 3, the specimen was cycled without the retrofit in place, and cracks were allowed to propagate freely.

Floorbeam Web Fascia Side

Cracks first initiated at the connection plate side in Trial 1, and then propagated through the thickness of the girder web, appearing on the web fascia side in Trial 3. At the centerline of the fascia side, a 1 in. horizontal crack was observed 2¼ in. above the bottom flange 525,000 cycles into Trial 3. More crack branches appeared as additional cycles were applied. They joined the existing cracks, and formed spider-shaped cracks. Table 4-3 and Figure 4-3 present crack initiation

and propagation behavior for the floorbeam web fascia side in this trial. A photograph of cracks located on the web fascia side 1,200,000 cycles into Trial 3 is provided in Figure 4-4.

Table 4-3: Crack initiation and propagation on floorbeam web fascia side in Trial 3

Trial 3 cycles	Total cycles	Crack initiation
525,000	1,815,000	A 1 in horizontal crack (Crack 5) was observed 2¼ in. above the floorbeam bottom flange
675,000	1,965,000	A ¼ in branch crack (Crack 6) was observed. The small branch crack quickly connected with the horizontal crack
1,200,000	2,490,000	A ⅜ in branch crack (Crack 7) was observed

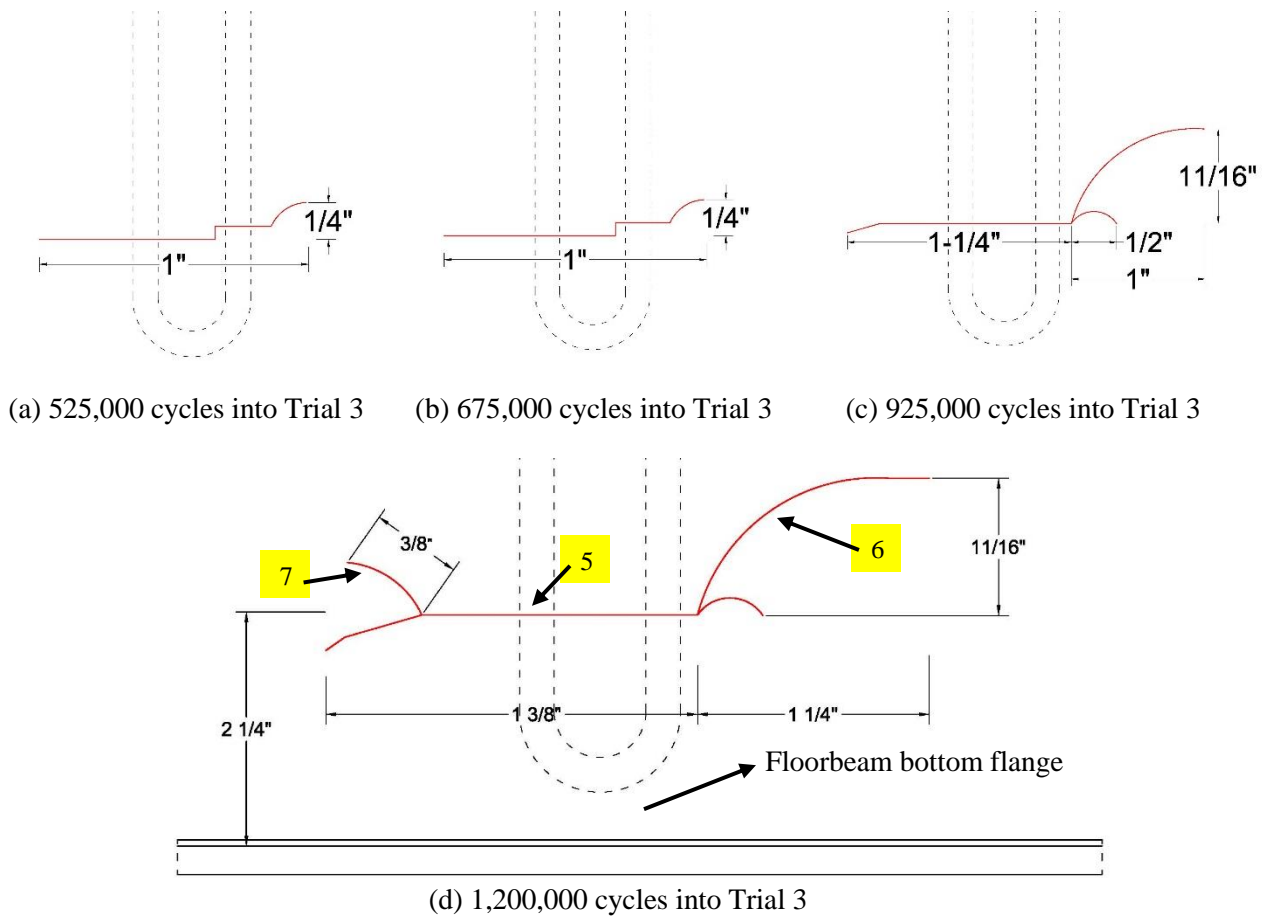
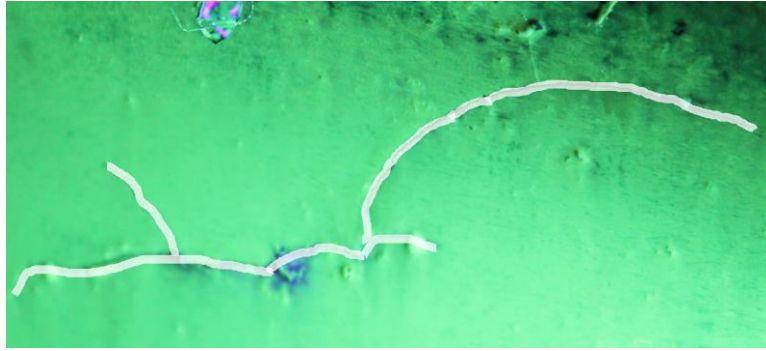


Figure 4-3: Cracks located on the floorbeam fascia side in Trial 3



*Cracks are shown with white lines

Figure 4-4: Photograph of cracks on the floorbeam web fascia side 1,200,000 cycles into Trial 3

Connection Plate Side

The cracks initiated in Trial 1 propagated vertically along the weld connecting the floorbeam web and the connection plate, then grew horizontally after propagating into the web. Crack initiation and propagation behavior on the connection plate side are presented in Table 4-4 and Figure 4-5. Figure 4-6 provides photographs of the cracks on the connection plate side 1,200,000 cycles into Trial 3.

Table 4-4: Cracks initiation and propagation on connection plate side in Trial 3

Trial 3 cycles	Total cycles	Crack initiation and propagation
500,000	1,790,000	Crack 2 grew into the web
1,200,000	2,490,000	A 5/8 in. crack (Crack 3) was observed on the west floorbeam web-to-connection plate weld. The crack had penetrated a little into the web.

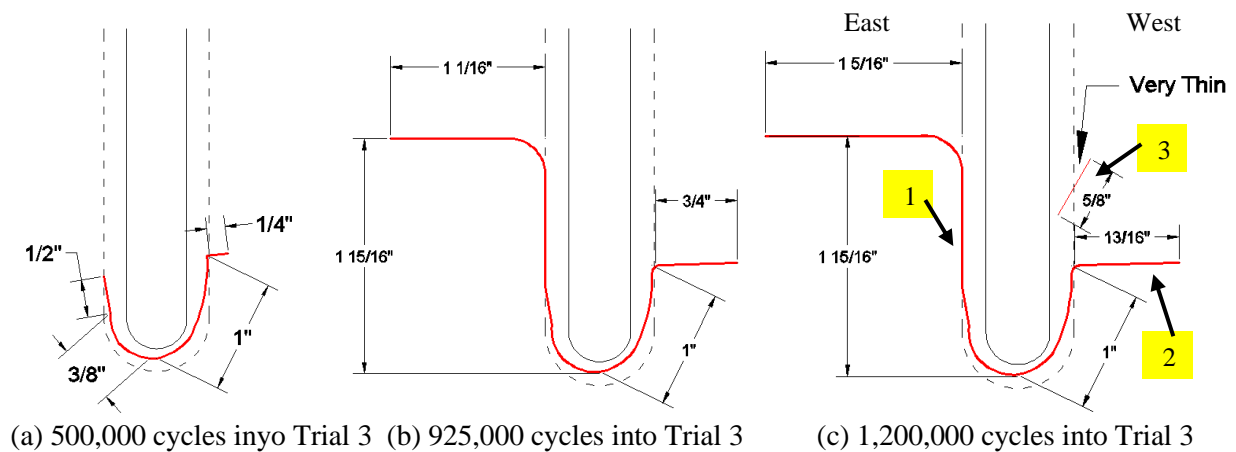
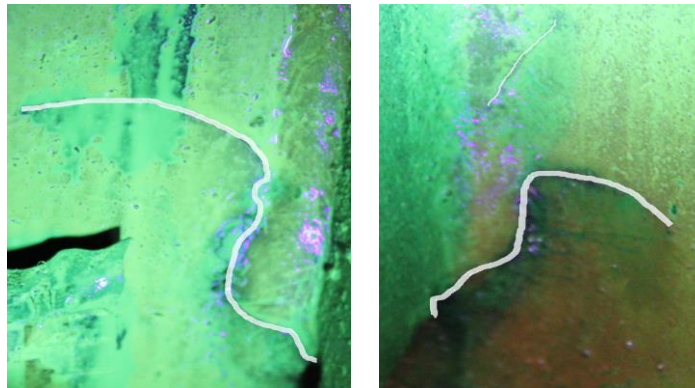


Figure 4-5: Cracks on connection plate side in Trial 3



(a) East side of stiffener

(b) West side of stiffener

* Cracks are shown with white lines

Figure 4-6: Photograph of cracks on floorbeam web fascia side 1,200,000 cycles into Trial 3

4.1.3.4 Trial 4 – Retrofitted

The angles-with-plate retrofit was installed after Trial 3 was completed. 1,200,000 cycles were completed in the retrofitted condition in Trial 4, and no crack growth was observed after the retrofit was removed and the specimen inspected for crack growth.

4.1.3.5 Trial 5 – Unretrofitted

Trial 5 was conducted in the unretrofitted condition, and cracks were allowed to grow freely.

Floorbeam Web Fascia Side

As depicted in Table 4-5 and Figure 4-7, a crack approximately 3 in. long was observed on the weld connecting the floorbeam web and the bottom flange 400,000 cycles into Trial 5. Although the crack was already long, it was extremely thin and the crack was nearly invisible.

Trial 5 was halted after 450,000 cycles, due to observation of the long crack located on the floorbeam web-to-bottom flange weld.

Table 4-5: Crack initiation and propagation on floorbeam web fascia side in Trial 5

Trial 5 Cycles	Total cycles	Crack initiation and propagation
400,000	4,090,000	A 3 in. crack (Crack 9) was observed on the weld connecting the floorbeam web and the bottom flange

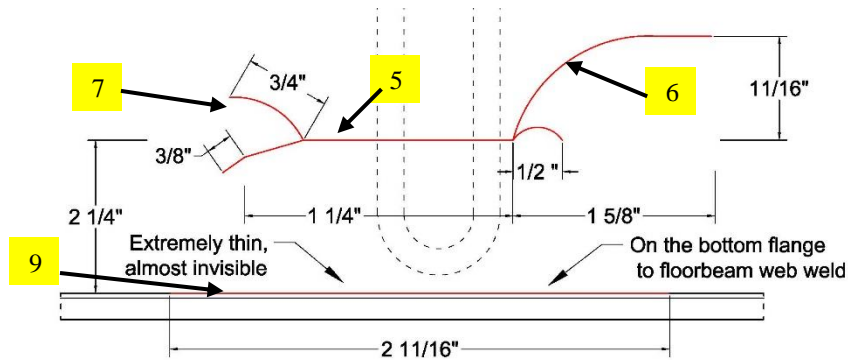


Figure 4-7: Crack on floorbeam web fascia side 400,000 cycles into Trial 5

Connection Plate Side

The existing cracks continued propagating on the connection plate side during Trial 5. A new crack initiated at the weld connecting the floorbeam web and the connection plate 25,000 cycles into Trial 5, and connected with the existing cracks later, as depicted in Table 4-6 and Figure 4-8.

Table 4-6: Crack initiation and propagation on connection plate side in Trial 5

Trial 5 Cycles	Total cycles	Crack initiation and propagation
25,000	3,715,000	A 1/16 in. crack (Crack 4) was observed on the west floorbeam web – connection plate weld. This crack continued growing and eventually connected with the Crack 2.

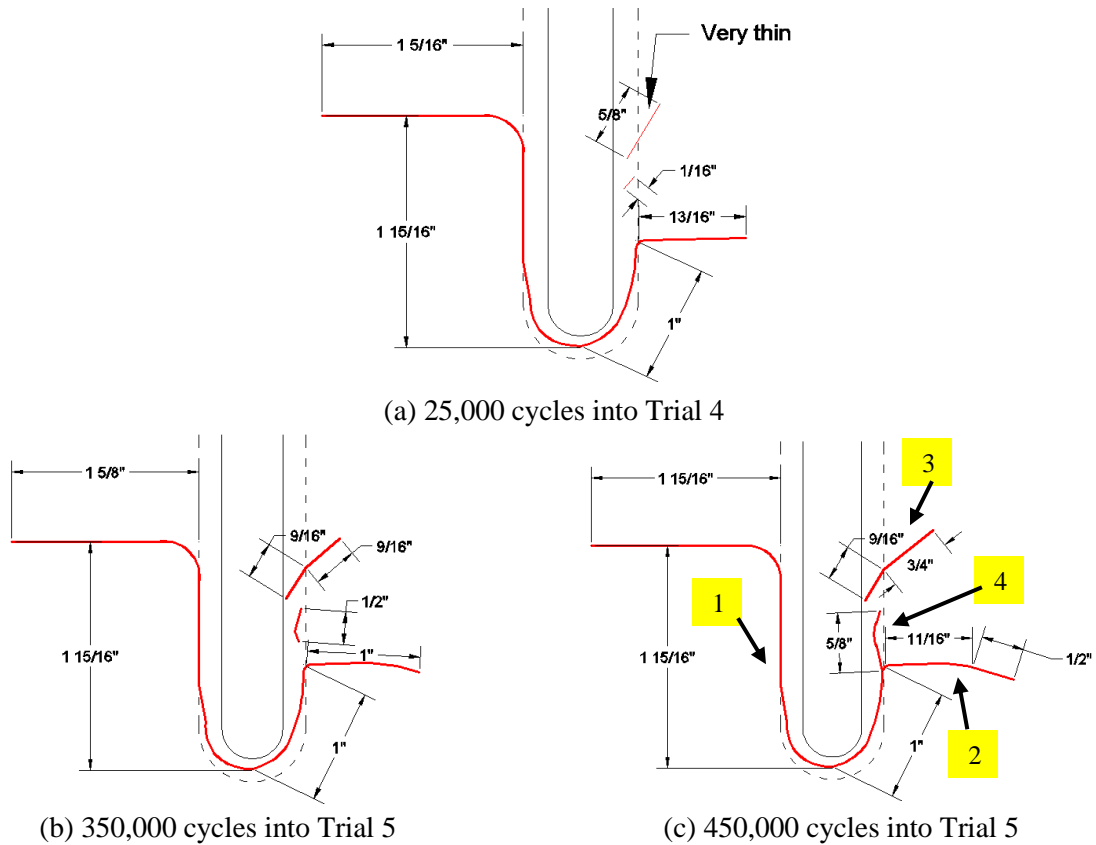


Figure 4-8: Crack on connection plate side in Trial 5

4.1.3.6 Trial 6 – Retrofitted

The angles-with-plate retrofit was installed at the outset of Trial 6 (at a total cycle count of 4,140,000 cycles). 1,200,000 cycles were completed in the retrofitted state, and no visible crack growth was observed during Trial 6.

4.1.3.7 Trial 7 – Retrofitted (Increased Load Range: 1.34-6.72 kip)

1,200,000 cycles were completed in the retrofitted state, and no visible crack growth was observed when the retrofit was removed for inspection.

4.1.3.8 Trial 8 – Unretrofitted

In Trial 8, testing was conducted with the retrofit removed, and cracks were allowed to grow freely.

Floorbeam Web Fascia Side

A new branch crack (Crack 8) was observed 25,000 cycles into Trial 8 on the floorbeam web, as presented in Table 4-7 and Figure 4-9. It grew faster than previous existing cracks. The crack on the floorbeam web-to-bottom flange weld (Crack 9) propagated much faster than the others: the length of the crack increased approximately 3 in. in 85,000 cycles. The test was halted 85,000 cycles into Trial 8, because the specimen had reached a critical state.

Photographs of the cracks 85,000 cycles into Trial 8 are presented in Figure 4-10.

Table 4-7: Crack initiation and propagation at floorbeam web fascia side in Trial 8

Trial8 cycles	Total cycles	Crack initiation and propagation
25,000	6,565,000	A 3/8 in. crack (Crack 8) was observed
85,000	6,625,000	The crack on the floorbeam bottom flange to web weld (Crack 9) grew to 6¼ in.

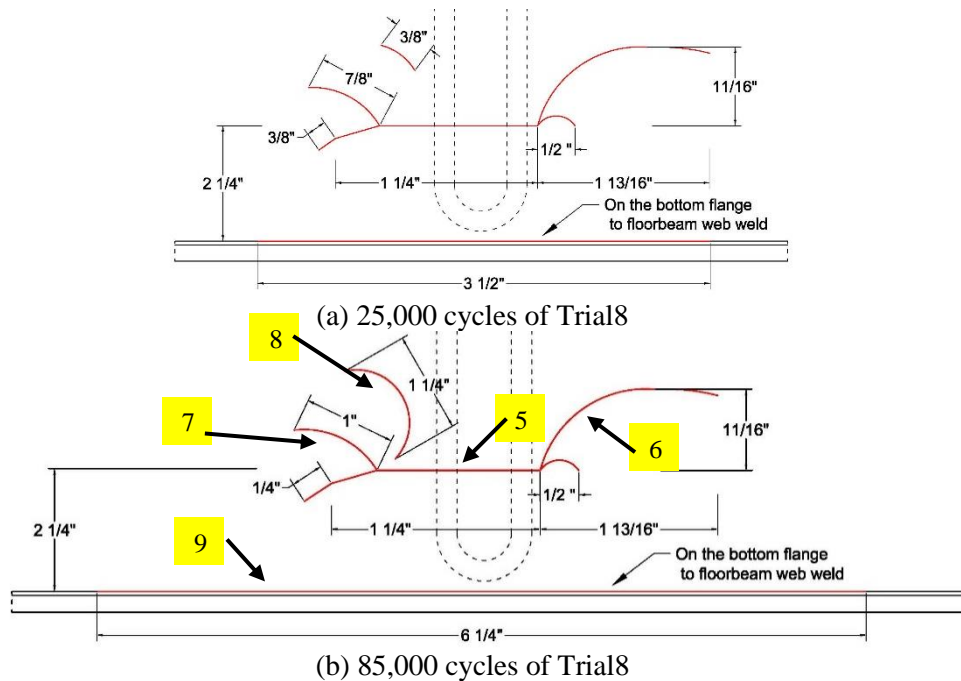
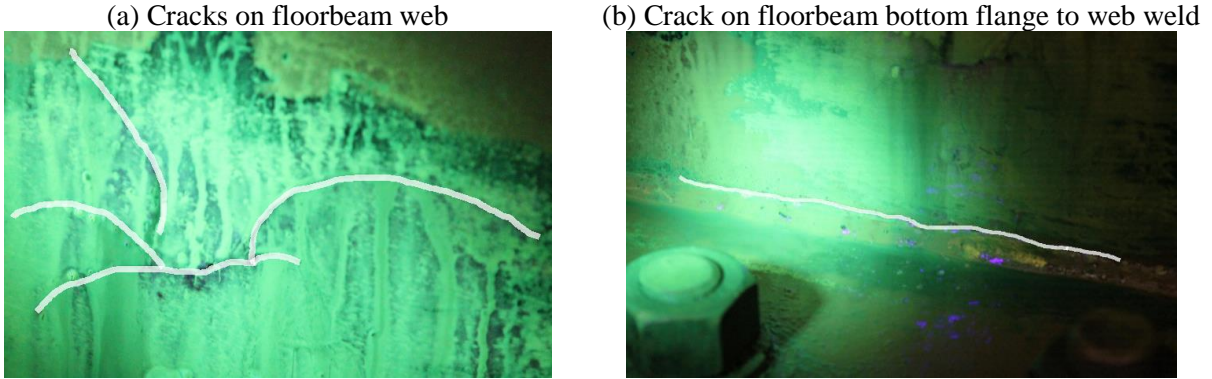


Figure 4-9: Cracks on floorbeam fascia side in Trial 8



* Cracks are shown with white lines

Figure 4-10: Photographs of cracks on floorbeam web fascia side 85,000 cycles into Trial 8

Connection Plate Side

Cracks continued growing on the connection plate side of the specimen throughout Trial 8, as shown in Figure 4-11 and Figure 4-12.

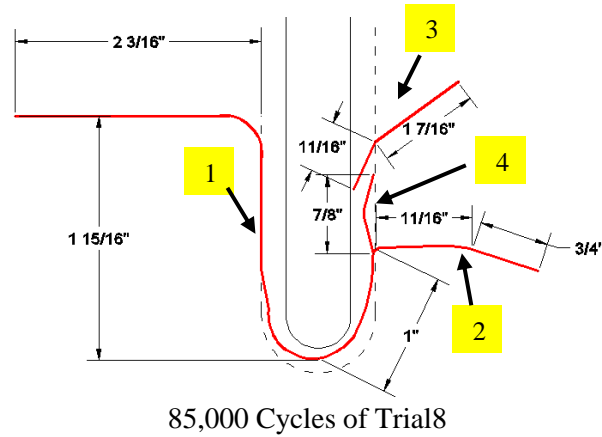
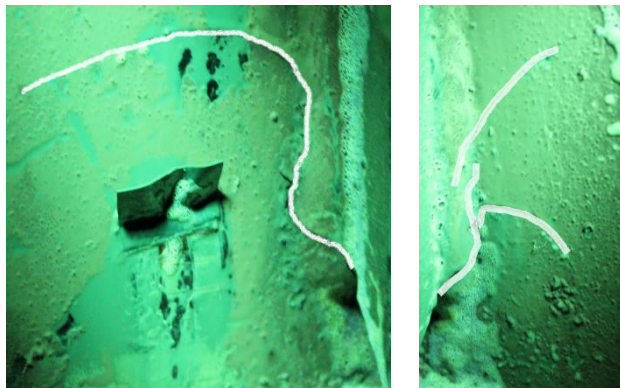


Figure 4-11: Cracks on connection plate side 85,000 cycles into Trial 8



* Cracks are shown with white lines

Figure 4-12: Photographs of cracks on connection plate side 85,000 cycles into Trial 8

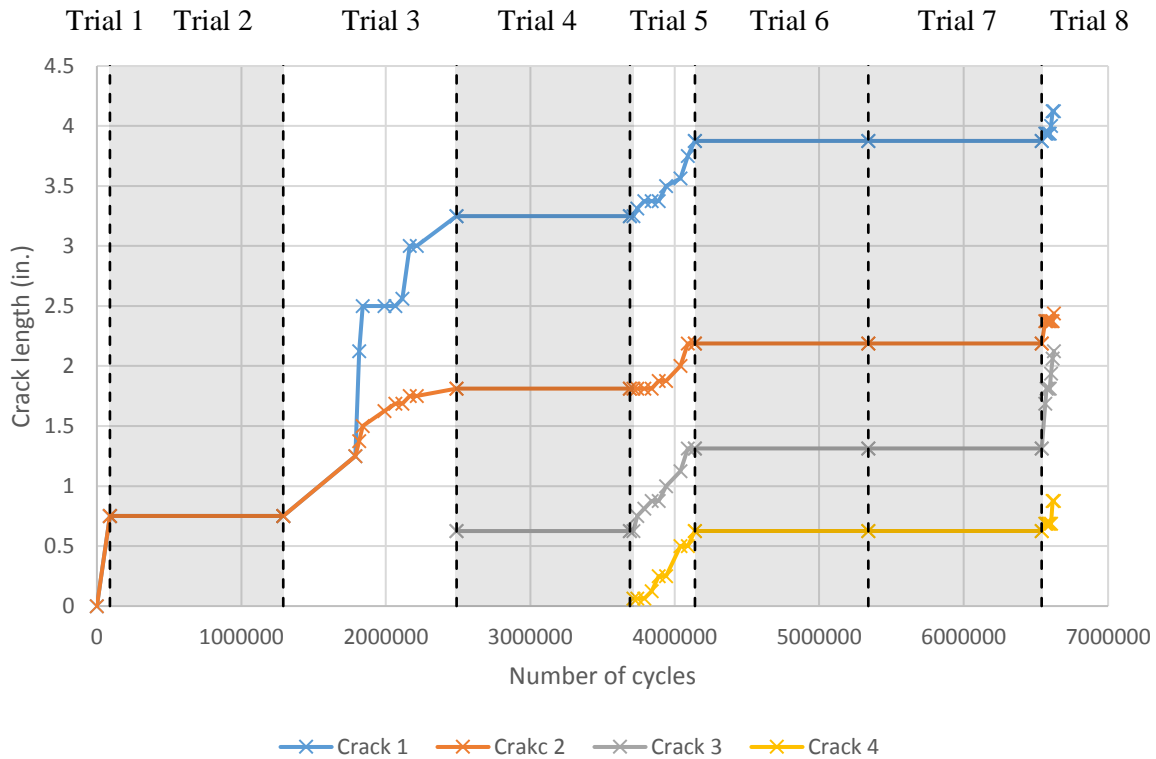
4.1.4 Crack Propagation Behavior for Test 1

Figure 4-13 and Figure 4-14 present the crack length for the single-plate specimen used in Test 1 with respect to the number of cycles applied. Crack propagation was halted in retrofitted trials, which are shown in the shaded areas of the diagrams.

The crack on the floorbeam web-to-bottom flange weld (Crack 9), which initiated in Trial 5, propagated very quickly when the retrofit was not installed. The test showed that the angles-with-plate retrofit was able to stop propagation of a crack approximately 3 in. long on the floorbeam web-to-bottom flange weld.

The crack growth rates are presented in Table 4-8 and Table 4-9.

Connection Plate Side



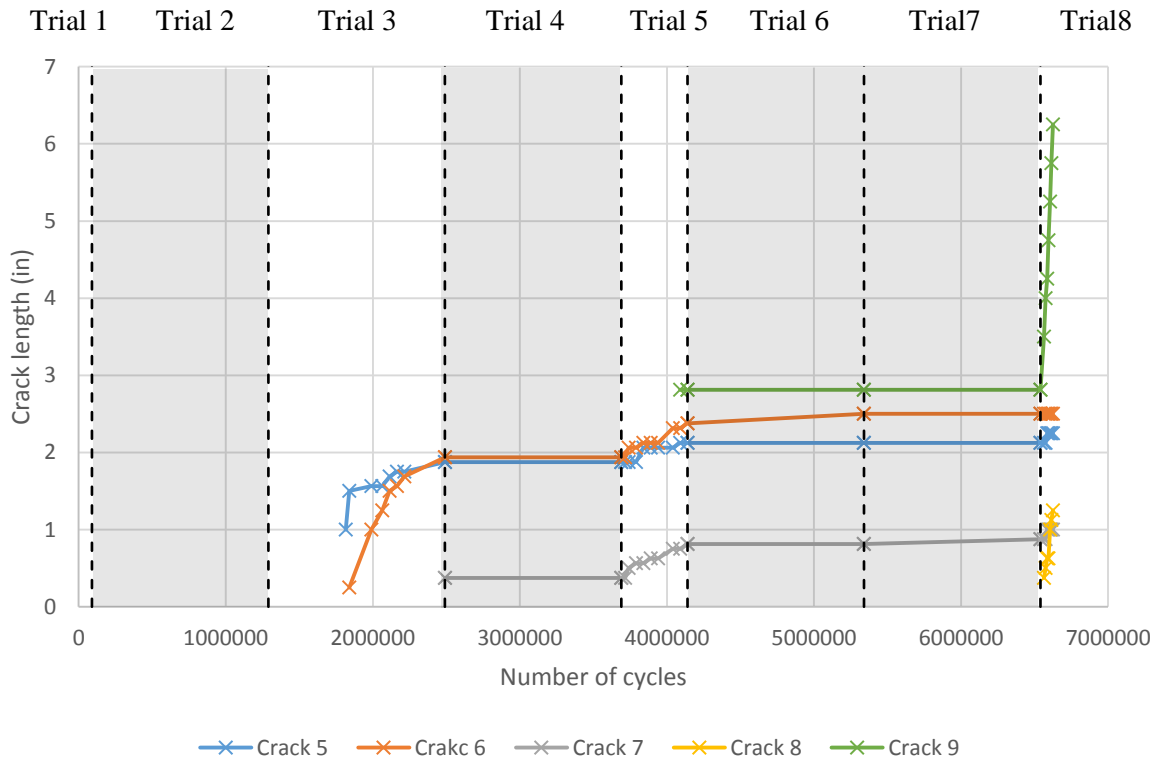
*Trials are separated by dashed lines, and the shaded areas indicate that the trial was retrofitted.

Figure 4-13: Connection plate side: crack propagation behavior

Table 4-8: Connection plate side: average crack growth rate

	Retrofit (Y/N)	Crack 1 (1 in./million cycles)	Crack 2 (1 in./million cycles)	Crack 3 (1 in./million cycles)	Crack 4 (1 in./million cycles)
Trial 1	N	8.3	8.3		
Trial 2	Y	0	0		
Trial 3	N	2.1	0.9		
Trial 4	Y	0	0	0	
Trial 5	N	1.4	0.8	1.5	1.3
Trial 6	Y	0	0	0	0
Trial 7	Y	0	0	0	0
Trial 8	N	2.9	2.9	9.6	2.9

Floorbeam Web Fascia Side



*Trials are separated by dashed lines, and the shaded areas indicate that the trial was retrofitted.

Figure 4-14: Floorbeam web fascia side: crack propagation behavior

Table 4-9: Floorbeam web fascia side - average crack growth rate

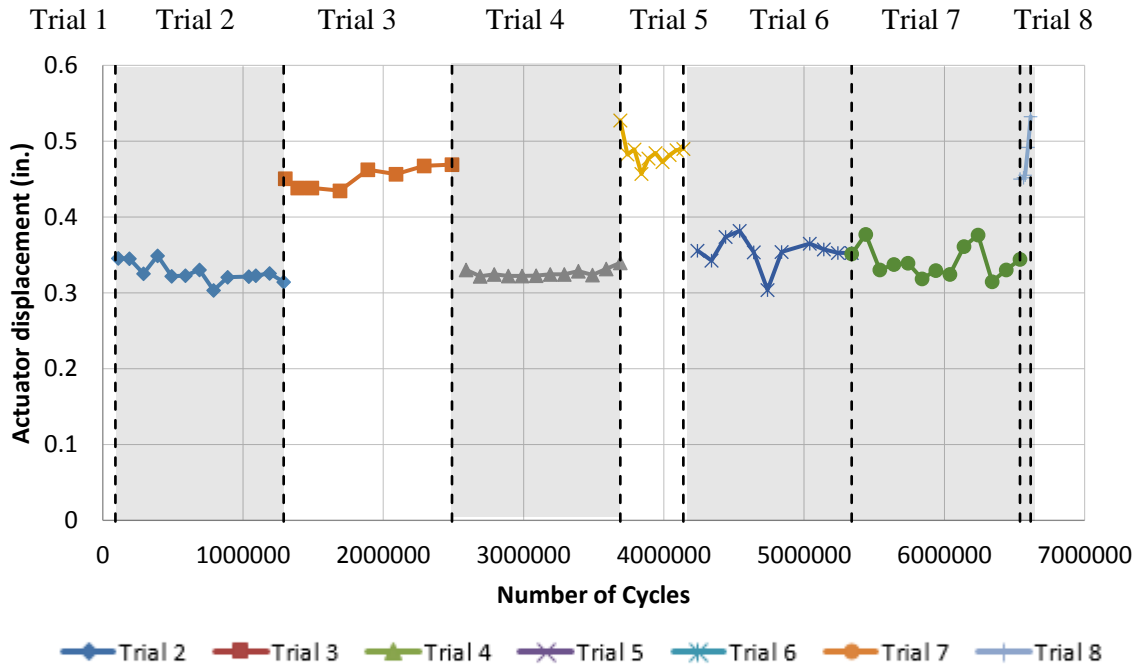
	Retrofit (Y/N)	Crack 5 (1 in./million cycles)	Crack 6 (1 in./million cycles)	Crack 7 (1 in./million cycles)	Crack 8 (1 in./million cycles)	Crack 9 (1 in./million cycles)
Trial 1	N					
Trial 2	Y					
Trial 3	N	1.3	2.6			
Trial 4	Y	0	0			
Trial 5	N	0.6	1.0	1.0		
Trial 6	Y	0	0	0		0
Trial 7	Y	0	0	0		0
Trial 8	N	1.4	0	1.4	14.6	40.6

4.2 Actuator Displacement

Actuator displacement was recorded starting 20,000 cycles into Trial 2. Displacement was examined because it may provide insight into the relative flexibility of the specimen with and without the angles-with-plate retrofit being in place. Additionally, displacement data may indicate any softening of the connection over time as cracks initiate and propagate.

At a load of 6 kip, the actuator displacement was approximately ½ in. without the retrofit and was approximately 0.35 in. with the retrofit in place. The connection stiffness increased 43.4% after retrofitting.

In some cases, it has been observed that the distortion-induced fatigue cracks can self-arrest. A connection can become more flexible as cracks propagate so that less moment is generated. Eventually the moment is reduced to a level such that cracks stop propagating. However, distortion-induced fatigue cracks still need to be treated in time. In this test, with a crack more than 6 in. long at the end of Trial 8, the connection stiffness only decreased approximately 18.2% compared with the beginning of Trial 1. The flexibility of the connection did not significantly increase, even with long cracks present in the floorbeam. In this case, cracks can be expected to continue growing, placing the integrity of the connection in danger.



*Trials are separated by dashed lines, and the shaded areas indicate that the trial was retrofitted.

Figure 4-15: Actuator displacement at 6 kip actuator forces for single-plate connection specimen FS1

4.3 Stress

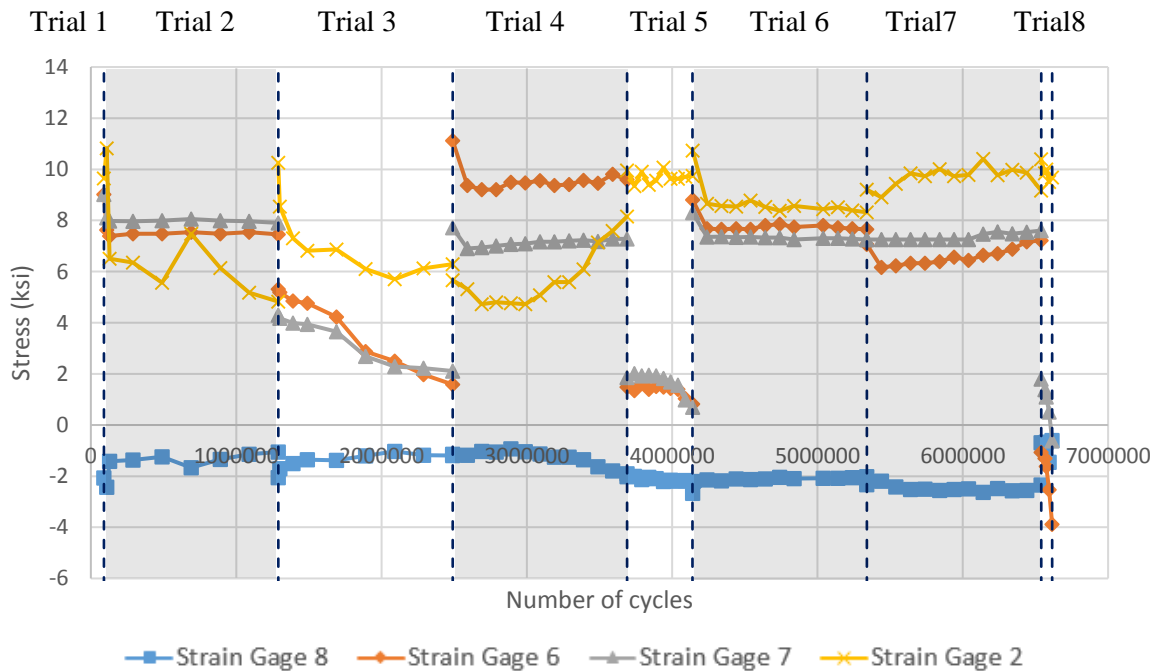
Strain gage measurements have been converted to stresses herein, utilizing Hooke's linear-elastic material relationship, and are discussed in the following sections.

4.3.1 Floorbeam Stresses

Figure 4-16 presents the floorbeam stresses computed using strain gage measurements for 6 kip of actuator force with respect to the number of cycles applied on the specimen from Trial 2 to Trial 8. The stresses obtained during Trial 1 are presented in Figure 4-17 separately because strain gages were removed and reattached at different locations when installing the angles-with-plate retrofit. Stresses in the bottom web-gap region, as indicated by strain gages 6 and 7, were clearly sensitive to the propagation of cracks and to the presence of the retrofit. Stresses in the upper web-gap, as indicated by strain gages 1 and 8, did not seem to be affected by retrofit status and the growing of cracks. This is understandable since these latter locations were far from the area where cracks

developed. In unretrofitted test trials, stresses in the bottom web-gap (strain gages 6 and 7) continued decreasing with increasing crack growth. In Trial 8, these stresses decreased more quickly than in the other trials. This corresponded to high rates of crack propagation in this test trial. During trials in which the retrofit was in place, stresses measured by strain gages 6 and 7 were nearly constant during these trials. This finding makes sense, since the regions around bottom web-gap regained their ability to carry the load with the retrofit in place.

The angles-with-plate retrofit was removed between trials for crack inspections, and this action sometimes broke the strain gages attached around the bottom web-gap. When new strain gages were installed, efforts were made to place them in locations identical to those used previously, however, slight changes in readings were observed between trials.



*Trials are separated by dashed lines, and the shaded areas indicate that the trial was retrofitted.

Figure 4-16: Floorbeam stresses at 6 kip actuator force for single-plate connection specimen FS1

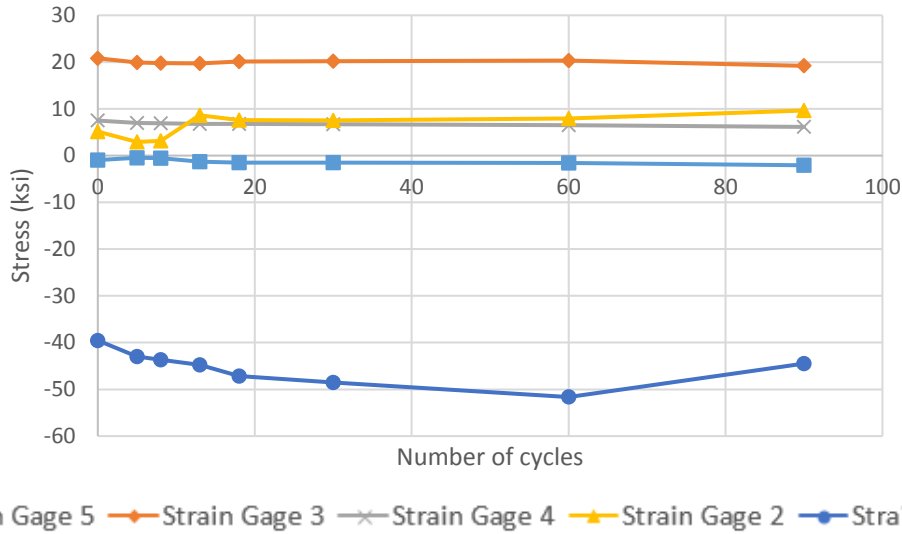
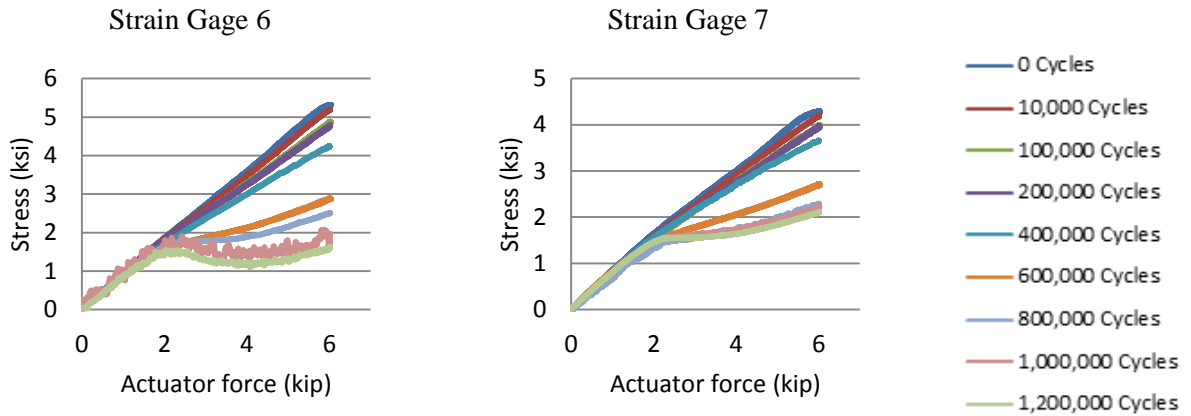


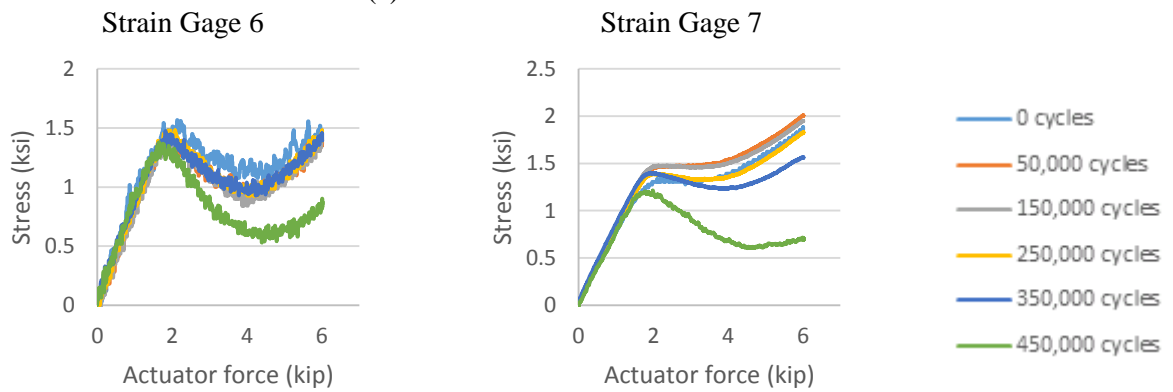
Figure 4-17: Floorbeam stresses in Trial 1 at 6 kip actuator force for single-plate connection specimen FS1

Figure 4-18 presents the relationships between the stresses near the bottom web-gap (strain gages 6 and 7) and the applied actuator force for various numbers of cycles in Trials 3, 5, and 8. These figures illustrate an interesting result.

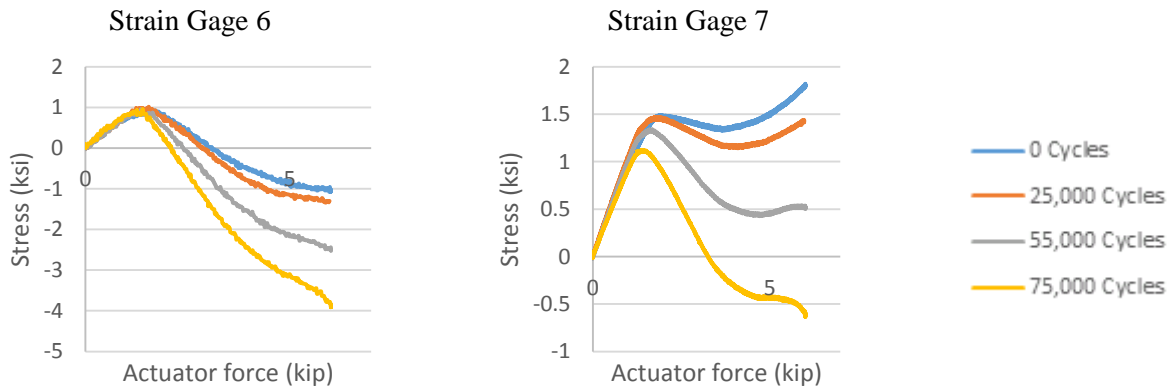
Trials 3, 5, and 8 are the three trials that were performed without the retrofit in place. As discussed in Section 4.1.2, at the beginning of Trial 3, there were only two $\frac{3}{4}$ in. cracks propagating along the connection plate-to-floorbeam web weld. Cracks had not yet propagated into the floorbeam web, and had not grown through to the floorbeam fascia side. The relationship between stresses and applied force were still linear at the beginning of Trial 3. As the cracks grew, a nonlinear relationship became more evident. Under lower load, the stress-applied force relationship was linear, but the linear behavior stopped after a threshold. As stresses increased, the graphs started to curve, and they became more curvilinear as the cracks became longer.



(a) Trial 3



(b) Trial 5



(c) Trial 8

Figure 4-18: Stresses computed using strain gages 6 and 7 vs. actuator force in Trials 3, 5, and 8

As shown in Figure 4-19, the stresses that developed under the action of 6 kip of actuator force dropped at a steady rate until the end of Trial 5, after which the stresses decreased rapidly. This corresponded with detection of the horizontal bottom flange-to-web crack, and its rapid growth in Trial 8.

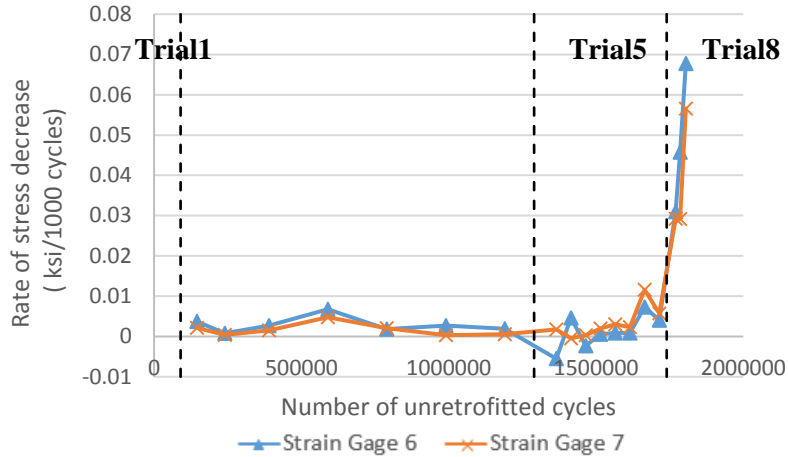


Figure 4-19: Rate of stress decrease (for 6 kip of applied actuator force) vs. number of unretrofitted cycles in single-plate connection test FS1

In trials in which the retrofit was applied (Trials 2, 4, 6, and 7), the region near the bottom web-gap regained its ability to carry load, as shown in Figure 4-20.

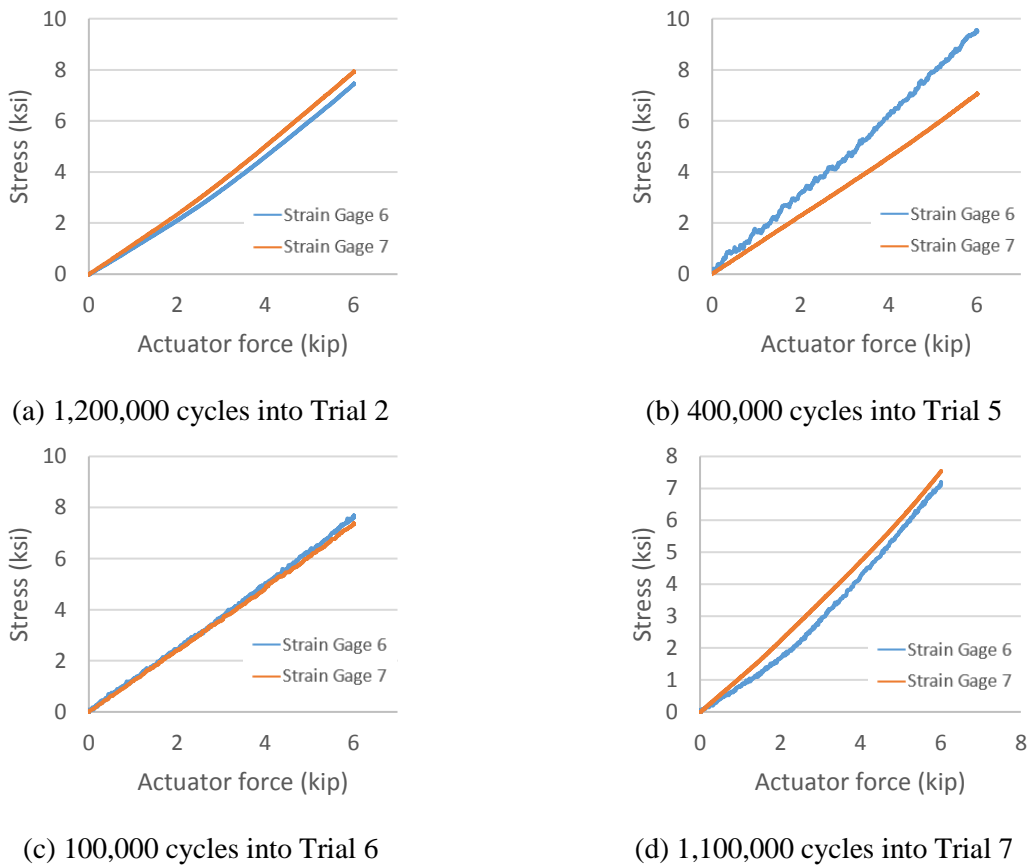
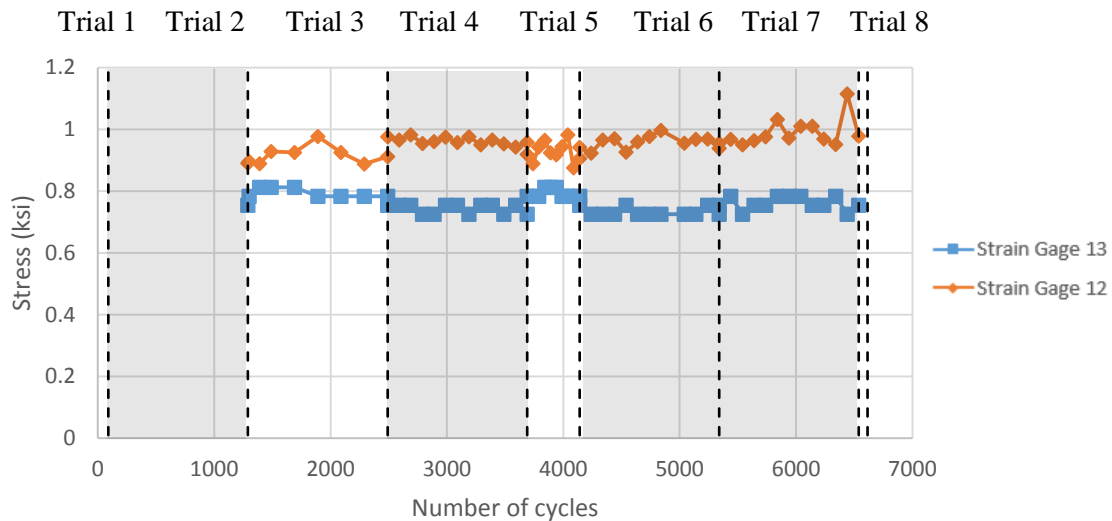


Figure 4-20: Stresses computed using strain gage 6 and 7 vs. actuator force in retrofitted trials

4.3.2 Stringer Flange Stresses

Two strain gages (12 and 13) were located at the center of the stringer on the top of the bottom flange. The test results showed that stresses at these two locations remained fairly constant during the test, regardless of whether the retrofit was installed or not, as presented in Figure 4-21. This is easy to understand, since in this test set-up the stringer can be considered as a cantilever beam if it is examined separately. Retrofit status would not affect the force analysis of the stringer.



*Trials are separated by dashed lines, and the shaded areas indicate the trial was retrofitted.

Figure 4-21: Stringer flange stresses at 6 kip applied forces for single-plate connection test FS1

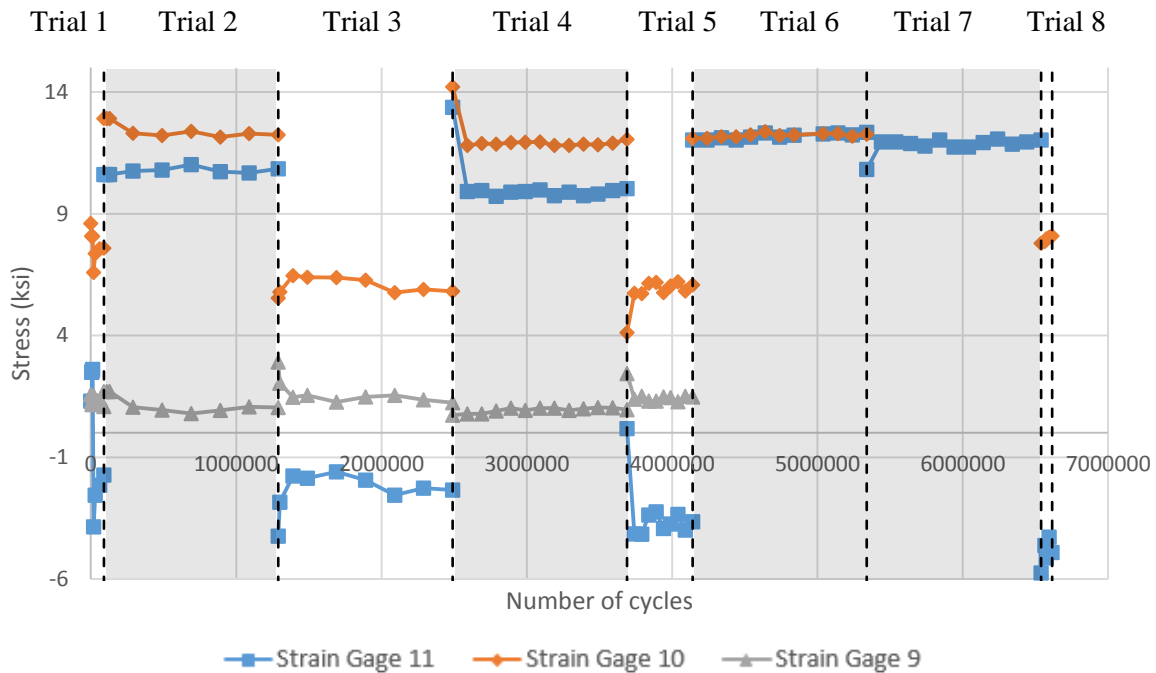
4.3.3 Stresses at the Stringer Cope

There were three strain gages installed around the stringer cope area (strain gages 9, 10, and 11). The researchers were interested in this area because cracking has been observed in stringer copes in the field (Haghani 2012, Al-Emrani 2005). The cope area was expected to crack, so it had been carefully instrumented and observed. However, as discussed, no crack initiation was observed in this area. The stresses around the cope were found to be fairly low, as shown in Figure 4-22.

Although it was not a region that suffered fatigue cracking during the test, the stresses there still caught the researchers' attention. As mentioned, the stringer element in this test set up was

essentially functioning as a cantilevered beam. It seems common sense that a horizontally-oriented strain gage installed on the lower portion of the stringer web should be in tension, since the loads were applied vertically upward at the cantilever's end. However, strain gage 11, which was located just above the stringer cope and was oriented horizontally, recorded negative values in the unretrofitted trials starting 13,000 cycles into Trial 1, indicating compressive stresses. Moreover, it is interesting that strain gages 11 and 10 regularly changed sign and magnitude with the retrofit state.

It should be realized that near a connection where the geometry of a structure changes severely, the stress is very complex. Advanced experimental techniques can be used to determine stresses at a connection but they are costly and time consuming. Using computer software to perform a numerical analysis is a good alternative, and is discussed in the following section.



*Trials are separated by dashed lines, and the shaded areas indicates the trial was retrofitted.

Figure 4-22: Stringer cope area stresses at 6 kip applied forces for single-plate connection test FS1

5. Computer Simulation of Single-Plate Connection (FS1)

5.1 General Introduction

Seven finite element models were created using the commercially-available finite element software, Abaqus V6.12. They corresponded to the different crack propagation and retrofit statuses for the physical test described in the previous sections.

As presented in Figure 5-1 and Figure 5-2, the computer models were created to resemble the physical test setup as faithfully as possible. It included all parts of the specimen, as well as the channels used to restrain the specimen to the laboratory floor.



Figure 5-1: Finite element model for single-plate connection specimen FS1 without retrofit

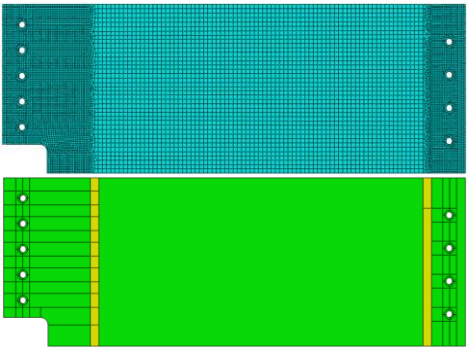
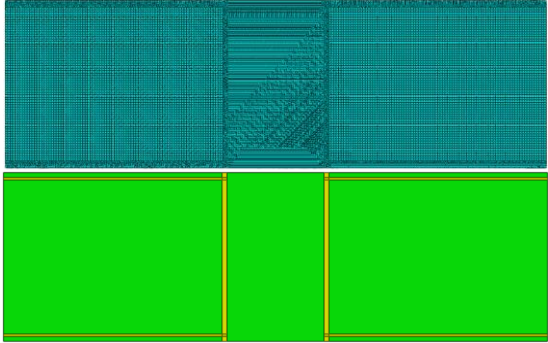
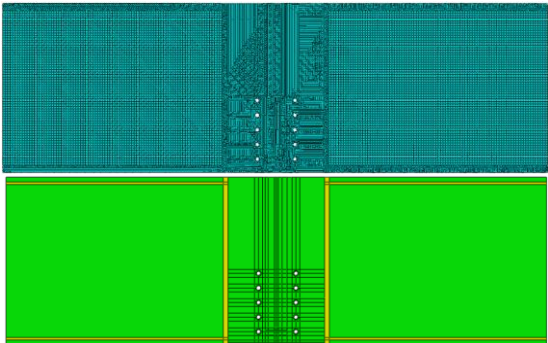


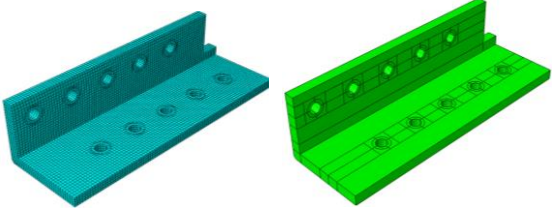
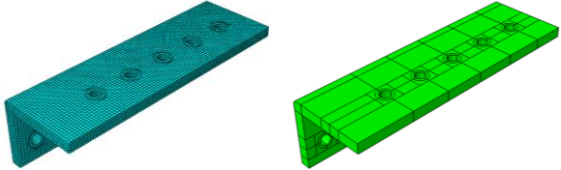
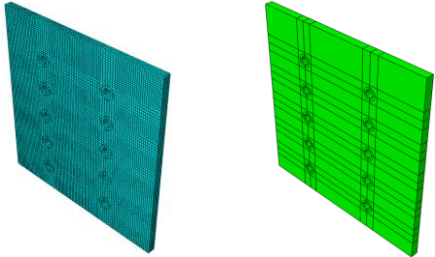

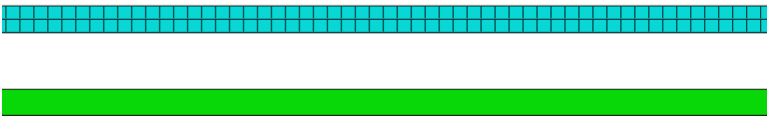
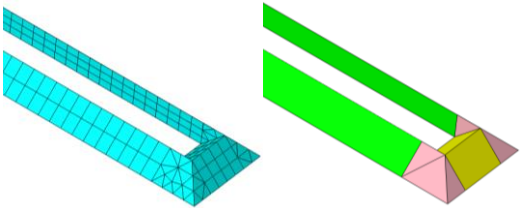

Figure 5-2: Finite element model for single-plate connection specimen FS1 with retrofit

The laboratory floor was modeled as a 192 in. \times 96 in. \times 44 in. concrete block. The bottom flange of the floorbeam was bolted to the channels of the floor tie-down system, which were then constrained to the concrete floor through a series of post-tensioned all-thread rods. The units used in the models were kips and inches. Poisson's ratio and Young's modulus for steel were taken as 0.3 and 29,000 ksi, and for were taken to be 0.2 and 4030 ksi, respectively, for concrete.

The element sizes and the partitioning technique used for the model parts are listed in Table 5-2. The elements shown in the green regions were generated using a structured meshing technique and were assigned a hexagonal shape. The element type used was C3D8R, an 8-node linear brick element. Other types of elements were used in transition regions and regions where structured mesh could not be used.

Table 5-1: Element size and mesh technique for important model parts in single-plate connection models

Part	Element size	Meshed part and partitioning technique
Stringer web	0.2 in. for the region near stringer cope and the connection region with the WT section 0.5 in. for the other region	
Floorbeam web	0.1 in. for the region near the center line and the connection region with the web to flange weld	<p style="text-align: center;">Before retrofitting</p> 
	0.5 in. for the other region	<p style="text-align: center;">After retrofitting</p> 

Retrofit-east angle	0.2 in.	
Retrofit-west angle	0.2 in.	
Retrofit-backing plate	0.2 in.	
Bolt	0.1 in. Except the super bolts used to connect the specimen to the floor. 0.5 in. for the bolts connecting the floor	
Floorbeam web to bottom flange weld	0.1 in.	
Connection plate to floorbeam web weld	0.1 in.	
Connection plate	0.1 in. for the connection region with the Floor-Beam Web 0.2 in. for the other region	

The interaction behavior in the normal direction between steel to steel was set as hard contact. The tangential interaction behavior was modeled using isotropic friction with a friction coefficient of 0.35. Welds were modeled using triangular cross-sections, and were tied to the parts they connected. The two inside faces of the bolts were tied to the surface of the connected parts and modeled with a pretension of 28 ksi to simulate a slip-critical bolted connection. The lab floor and the ends of the bracing angles were fixed by restraining all degrees of freedom. A 6 kip upward force was applied as a uniformly distributed surface load on the actuator plate. The pretension load for the all-thread rods used to restrain the specimen to the laboratory floor was 50 ksi, and was 28 ksi for the A325 bolts used in the connection of the specimen.

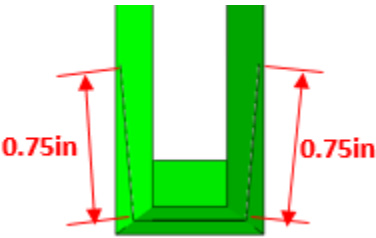
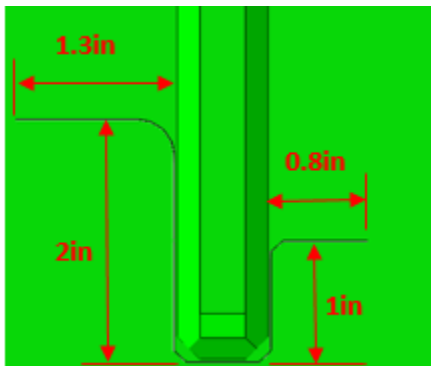
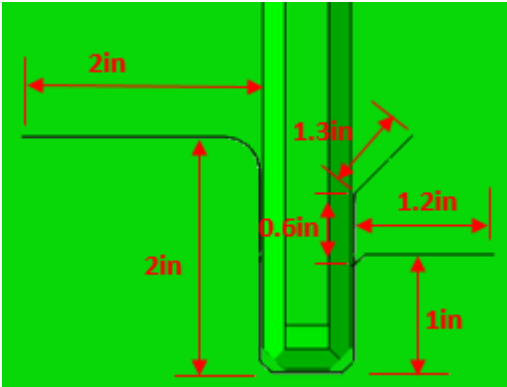
The cracks observed at the end of Trial 1 in the physical test were modeled explicitly by removing a small amount of material from the weld connecting the floorbeam web and the connection plate. The simulated cracks did not cut into the floorbeam web.

The Extended Finite Element Method (XFEM) method was used to simulate the cracks observed at the end of Trial 3 and Trial 5. In those models, the cracks were simulated as zero-width through-thickness cracks on the floorbeam web.

All the models created in this study are linear elastic.

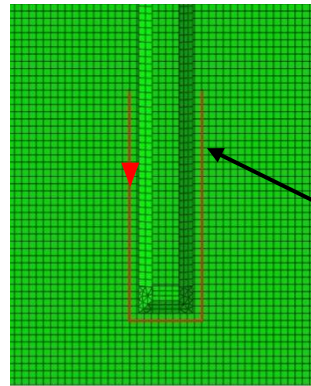
An introduction to the seven finite element models is provided in Table 5-2.

Table 5-2: Introduction of finite element models for single-plate connection specimen FS1

Model	Corresponding physical test status	Crack status		Retrofit status
		Web-to-flange weld crack	Connection plate-to-web weld crack	
1	The beginning of Trial 1	No	No	Without retrofit
2	The end of Trial 1	No		Without retrofit
3	Trial 2			With retrofit
4	The end of Trial 3	No		Without retrofit
5	Trial 4			With retrofit
6	The end of Trial 5	2.7 in.		Without retrofit
7	Trial 6			With retrofit

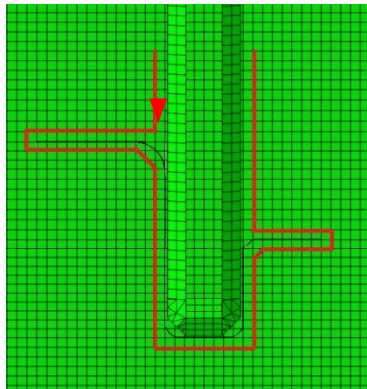
Computed stresses at weld toes and crack tips can be extremely high due to severe stress concentrations at these locations. Using these stresses as a computed measure should not necessarily be expected to provide a reasonable understanding of retrofit performance. To deal with this, stresses were extracted along two paths located at a distance approximately 0.4 times the thickness of the floorbeam web away from weld toes and cracks, as shown in Figure 5-3.

**Floorbeam web
connection plate side**

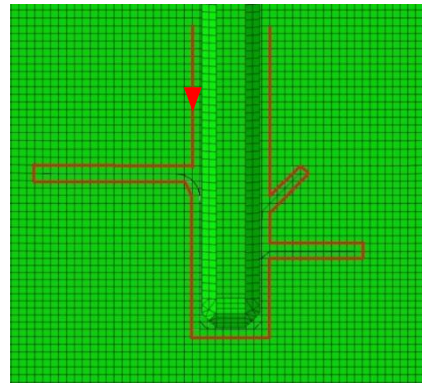


Connection plate to
Floorbeam web weld

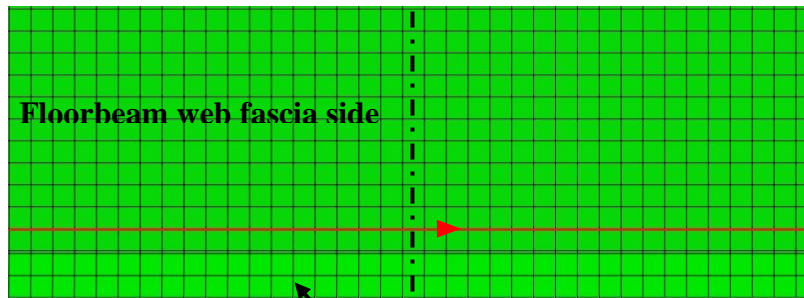
(a) Path 1(a) for Model 1, Model 2, and Model 3



(b) Path 1(b) for Model 4 and Model 5



(c) Path 1(c) for Model 6 and Model 7



Floorbeam web fascia side

Floorbeam web centerline

Floorbeam web to bottom flange weld

(d) Path 2 for all the seven models

Figure 5-3: Path 1 (Path 1(a), Path 1(b), and Path 1(c)) and Path 2 in FEM models

Paths were created by defining node lists. Path 1(a), 1(b), and 1(c) were defined on the surface of the connection plate side. Path 2 was defined on the surface of the web fascia side.

5.2 Simulation Results for Specimen FS1

5.2.1 Early-Stage Fatigue Damage - Model 1, Model 2, and Model 3

An introduction to Model 1, Model 2, and Model 3 is given in Table 5-1. The results of the three models are presented together in this section because they simulated the connection with early-stage fatigue damage.

Model 1 – The Beginning of Trial 1 (Uncracked Geometry)

Model 1 corresponds to Specimen FS1 at the beginning of Trial 1, at which point cracking had not yet initiated. Results for Model 1 are presented in Figure 5-4.

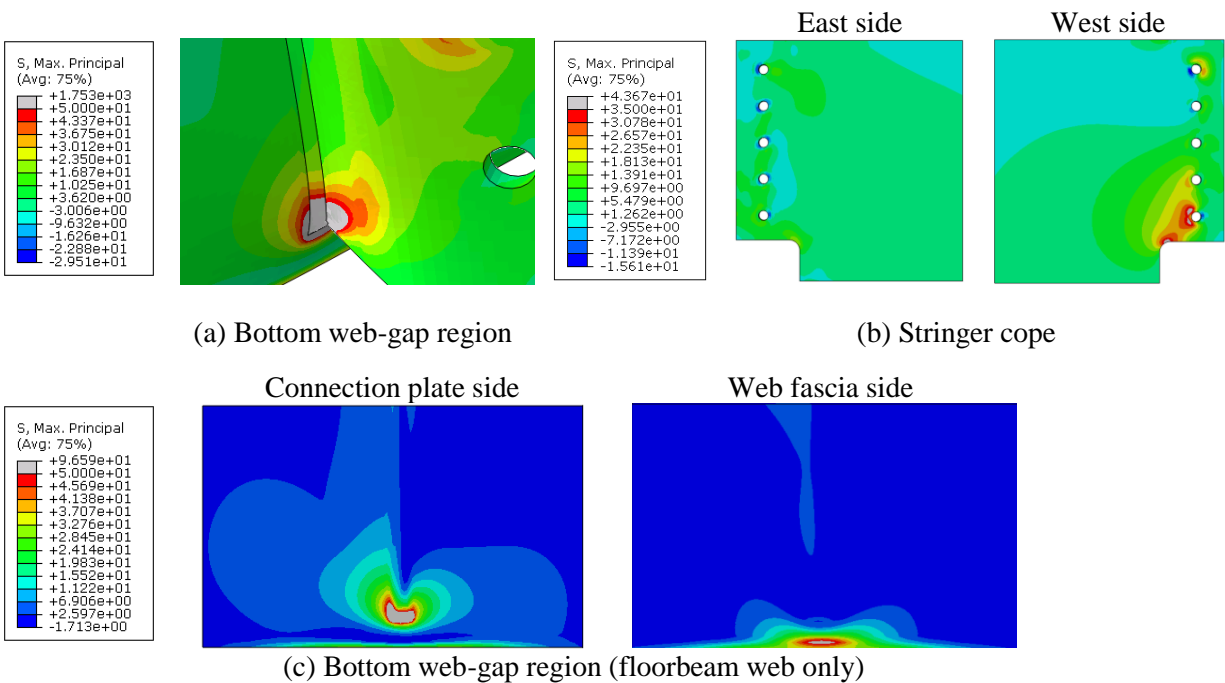


Figure 5-4: Simulation results for single-plate connection specimen FS1, Model 1

As expected, stresses were concentrated in the bottom web-gap region. On the connection plate side, large-magnitude stresses occurred at the bottom of the floorbeam web to connection plate junction. On the fascia side of the web, stresses were concentrated near the bottom flange.

For the stringer, the cope was the location where relatively larger stresses occurred, but the magnitude of the stresses was much lower than those observed in the web-gap region. The distribution of stresses on the two sides of the stringer cope were different. The stresses on the west side were larger than on the east.

Model 2 – The End of Trial 1 (Cracked, without Retrofit)

Model 2 was created to simulate the physical test specimen FS1 at the end of Trial 1. As shown in Table 5-1, two 3/4 in. cracks were created explicitly to simulate the actual crack geometries. The computed stress results are presented in Figure 5-5.

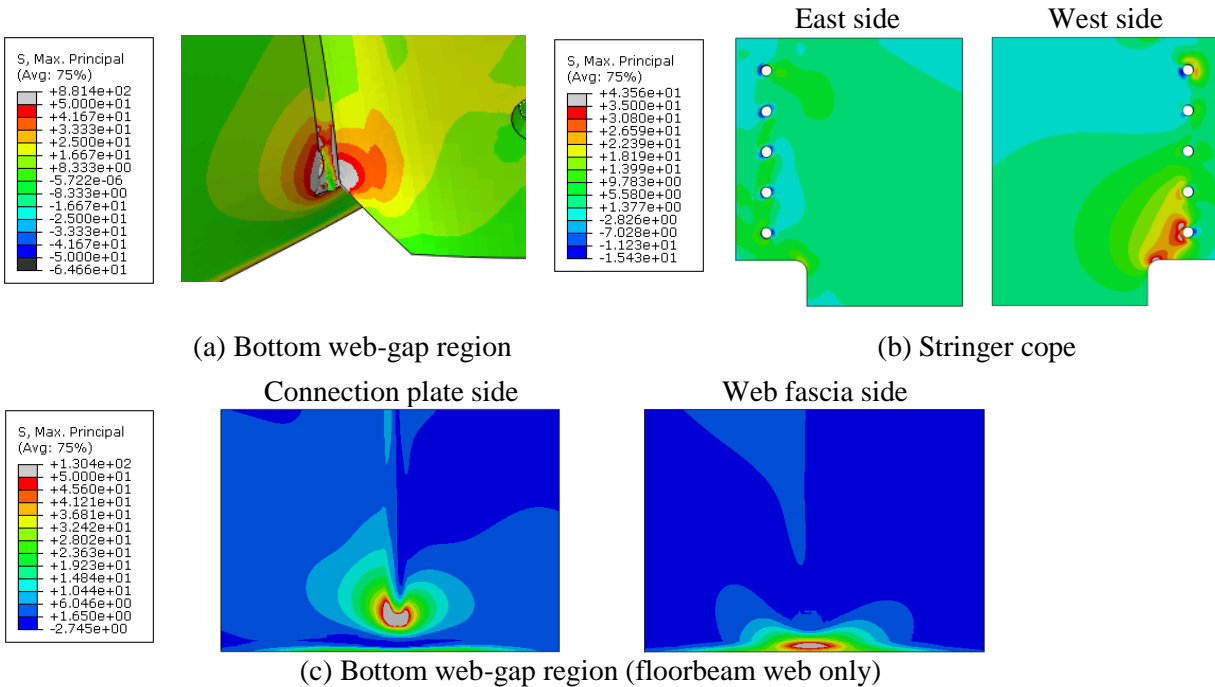
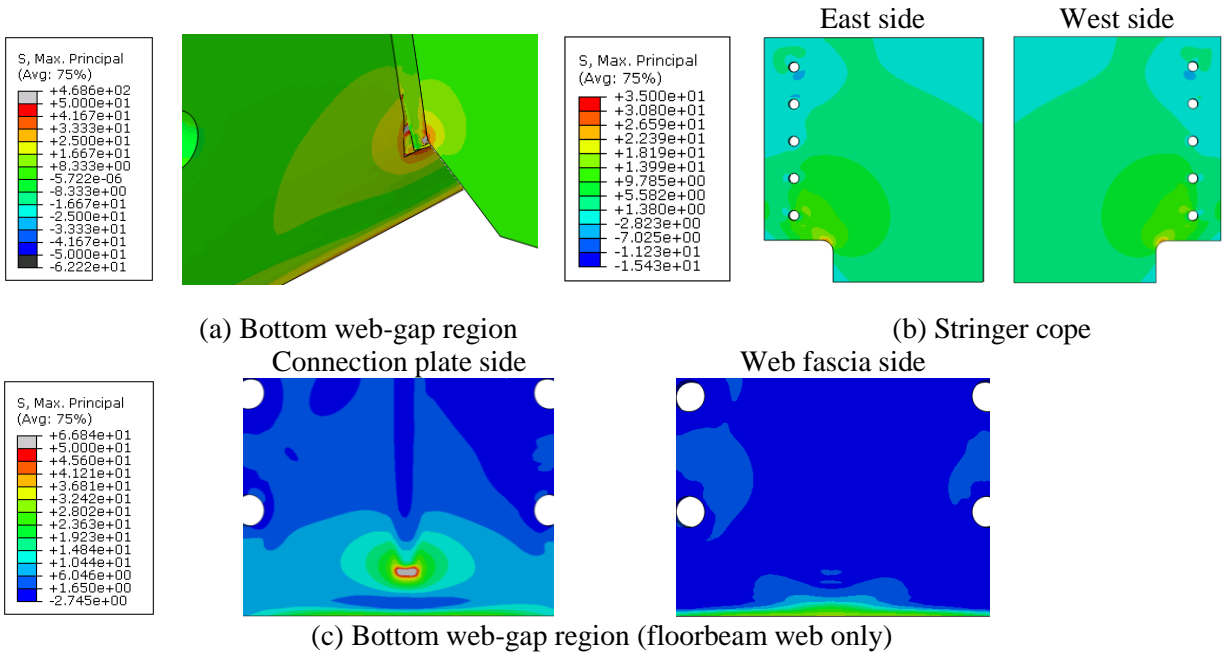


Figure 5-5: Simulation results for single-plate connection specimen FS1 Model 2

Model 3 – Trial 2 (Cracked, with Retrofit)

The crack geometries in Model 3 were the same as in Model 2, but Model 3 was simulated with the angles-with-plate retrofit installed, while Model 2 was not. The computed maximum principal

stresses for Model 3 are presented in Figure 5-6. The maximum and the minimum stress limits were set to match the stress limits in Figure 5-5 (Model 2) making the two results comparable.



* The limits of the color bar in Model 3 were the same as in Model 2

Figure 5-6: Simulation results for single-plate specimen FS1 Model 3

Compared with Model 2, in Model 3, stresses in the bottom web-gap region significantly decreased. For the stringer cope, stresses on the west side were clearly reduced. The stress distributions on the east and the west sides became more similar.

Maximum principal stresses were extracted from Path 1(a) and Path 2, as shown in Figure 5-3, to examine the distribution of stresses in the cracked region. The results are presented in Figure 5-7 and Figure 5-8 respectively.

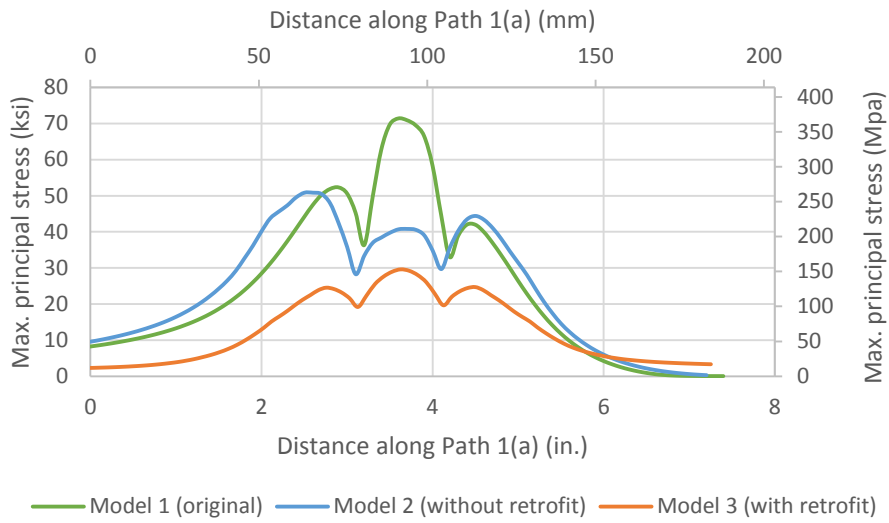


Figure 5-7: Stresses along Path 1(a) for single-plate connection FS1: Model 1, Model 2, and Model 3

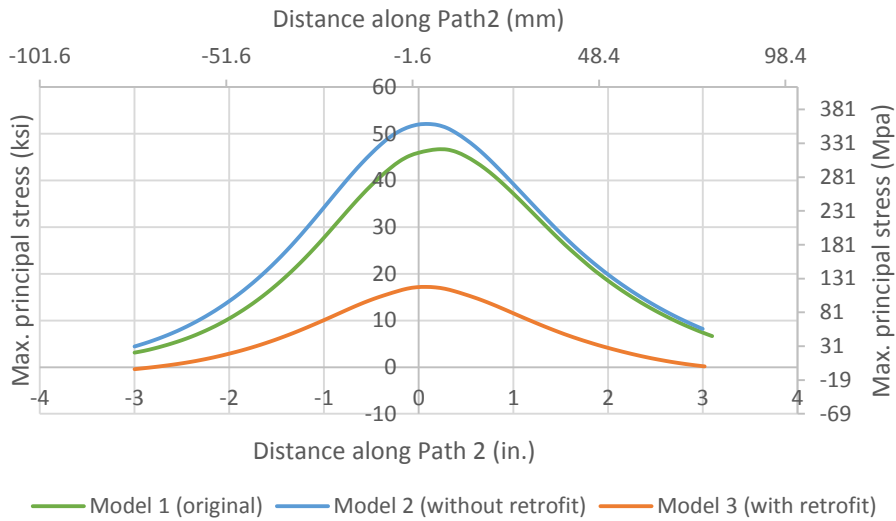


Figure 5-8: Stresses along Path 2 for single-plate connection FS1: Model 1, Model 2, and Model 3

For the early-stage fatigue damage, in which cracks had not yet propagated into the floorbeam web, the angles-with-plate retrofit was found to reduce stresses significantly. Stresses in the retrofitted condition were approximately 40% of the peak stress along Path 1(a) and 67% of the peak stress along Path 2.

5.2.2 Middle-Stage Fatigue Damage – Model 4 and Model 5

In Model 4 and Model 5, cracking was modeled as having propagated into the floorbeam web and had grown horizontally, corresponding to the end of Trial 3 and Trial 4, respectively. The cracks were simulated using the extended finite element method (XFEM), and the crack geometries were the same in the two models. The angles-with-plate retrofit was simulated in Model 5 but not in Model 4.

Model 4 – The End of Trial 3 (Cracked, without Retrofit)

Figure 5-9 presents the simulation results for Model 4.

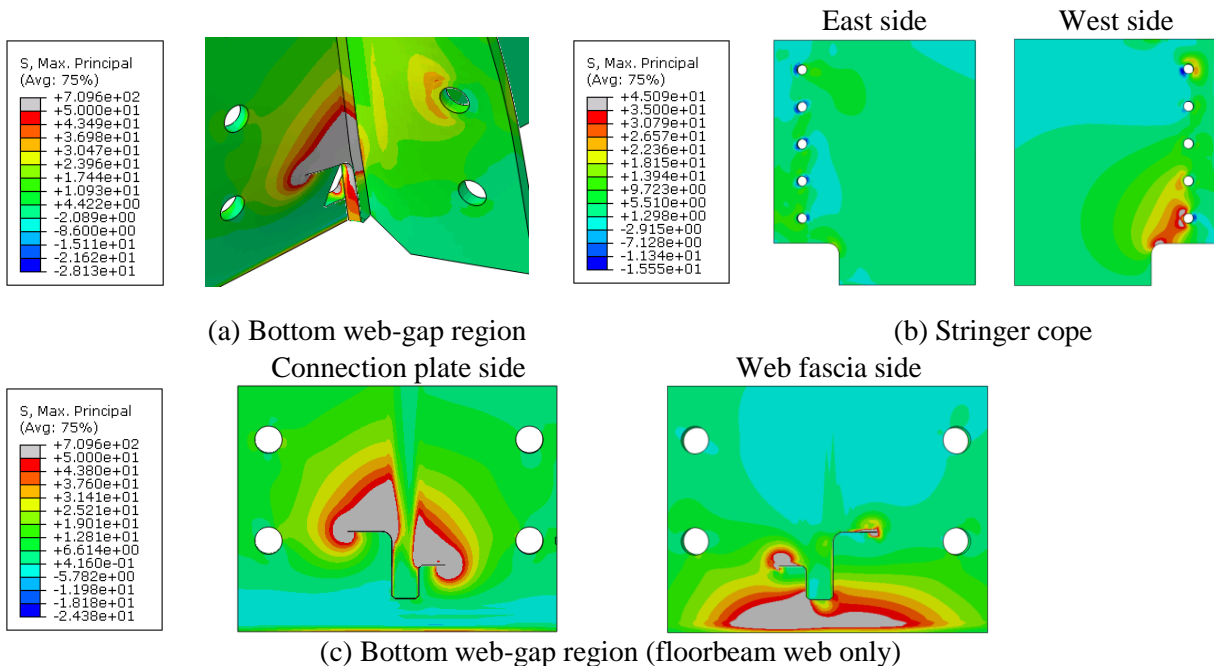


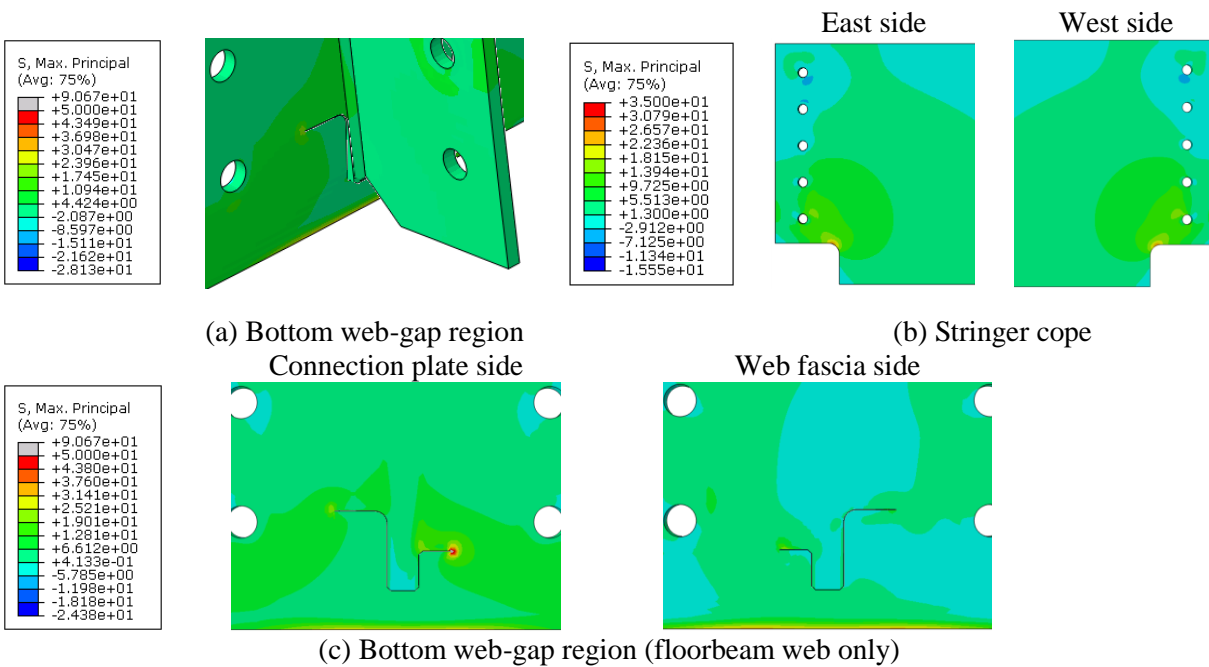
Figure 5-9: Simulation results for single-plate connection Specimen FS1: Model 4

Stresses on the connection plate side were concentrated at the crack tips and the regions above the horizontal cracks. On the web fascia side, stresses in the region near the bottom flange markedly increased compared to Model 1 and Model 2, in which the fatigue cracks had not propagated into the floorbeam web. Stresses in the stringer cope region were similar to those observed in Model 1

and Model 2. The development of cracks on the floorbeam web did not have a significant effect on stresses in the stringer cope regions.

Model 5 – Trial 4 (Cracked, with Retrofit)

Computed results for Model 5 are presented in Figure 5-10. Model 5 was assigned the same crack geometries as Model 4, and the angles-with-plate retrofit was simulated.



* The limits of the color bar in Model 5 were the same as in the Model 4

Figure 5-10: Simulation results for single-plate connection specimen FS1: Model 5

Comparing the results for Model 5 with Model 4, the angles-with-plate retrofit significantly reduced stresses on both sides of the floorbeam web. Stresses on the west side of the stringer cope decreased, and the stress distributions on the east and the west sides became more similar to each other.

Stresses were extracted along Path 1(b) and Path 2, as shown in Table 5-3. The results are presented in Figure 5-11 and Figure 5-12.

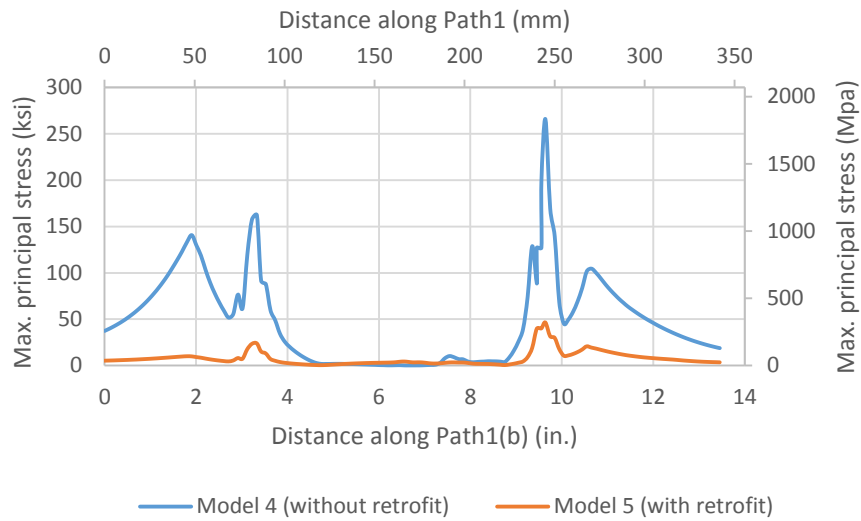


Figure 5-11: Stresses along Path 1(b) for single-plate connection specimen FS1 Model 4 and Model 5

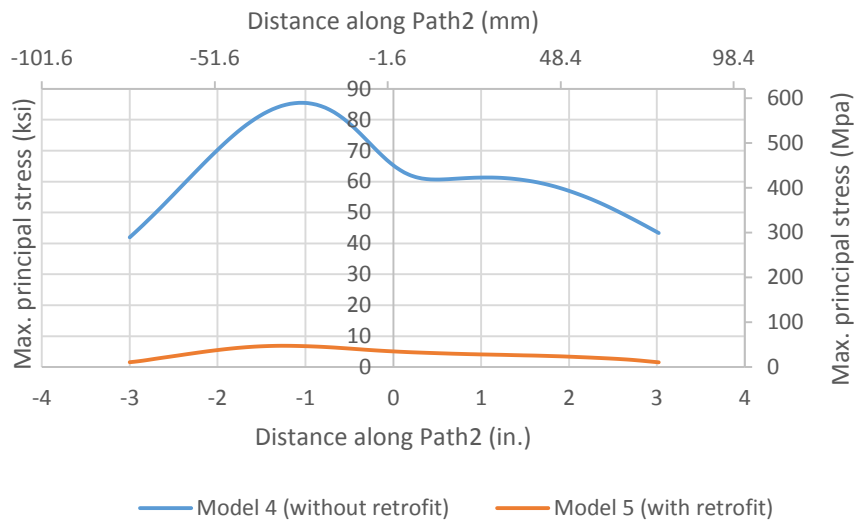


Figure 5-12: Stresses along Path 2 for single-plate connection specimen FS1 Model 4 and Model 5

Peak stresses along Path 1(b) and Path 2 reduced 85% and 92%, respectively, after retrofitting.

5.2.3 Late-Stage Fatigue Damage – Model 6 and Model 7

The cracks created within Model 6 simulated the actual cracks in the physical specimen at the end of Trial 5, as shown in Table 5-1. Compared with the previous models, an important difference in Model 6 is that a 2.7 in. crack was simulated as a through-thickness crack at the toe of the weld connecting the floorbeam web and the bottom flange.

Figure 5-13 shows the computed results for Model 6.

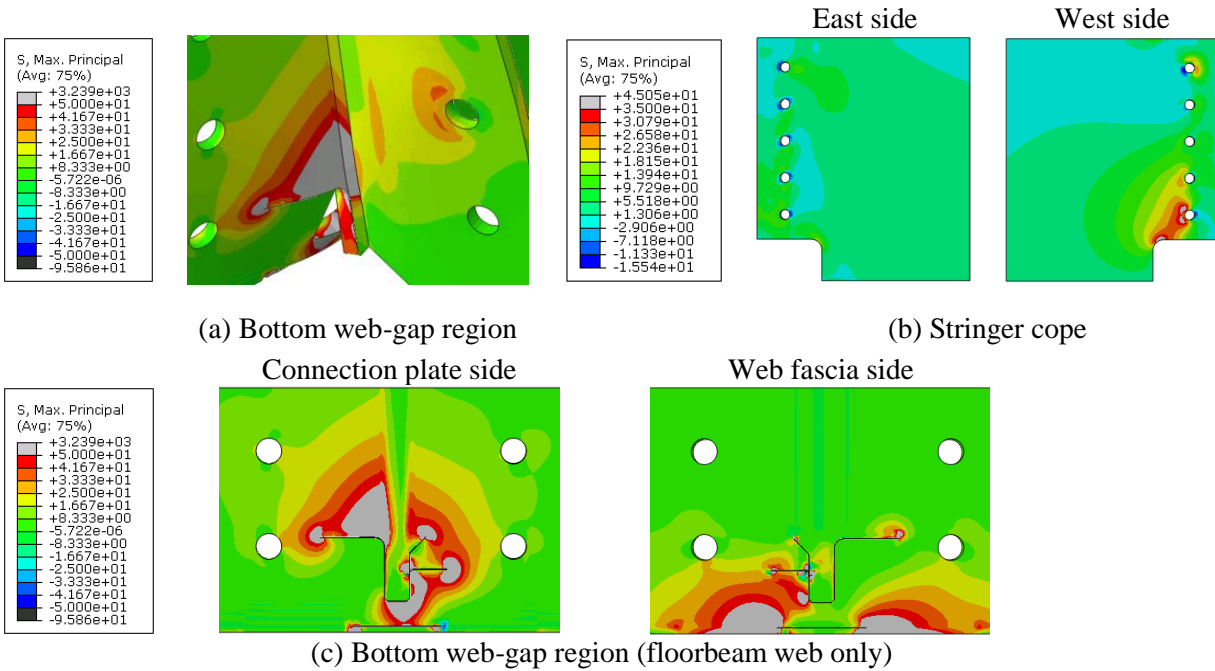
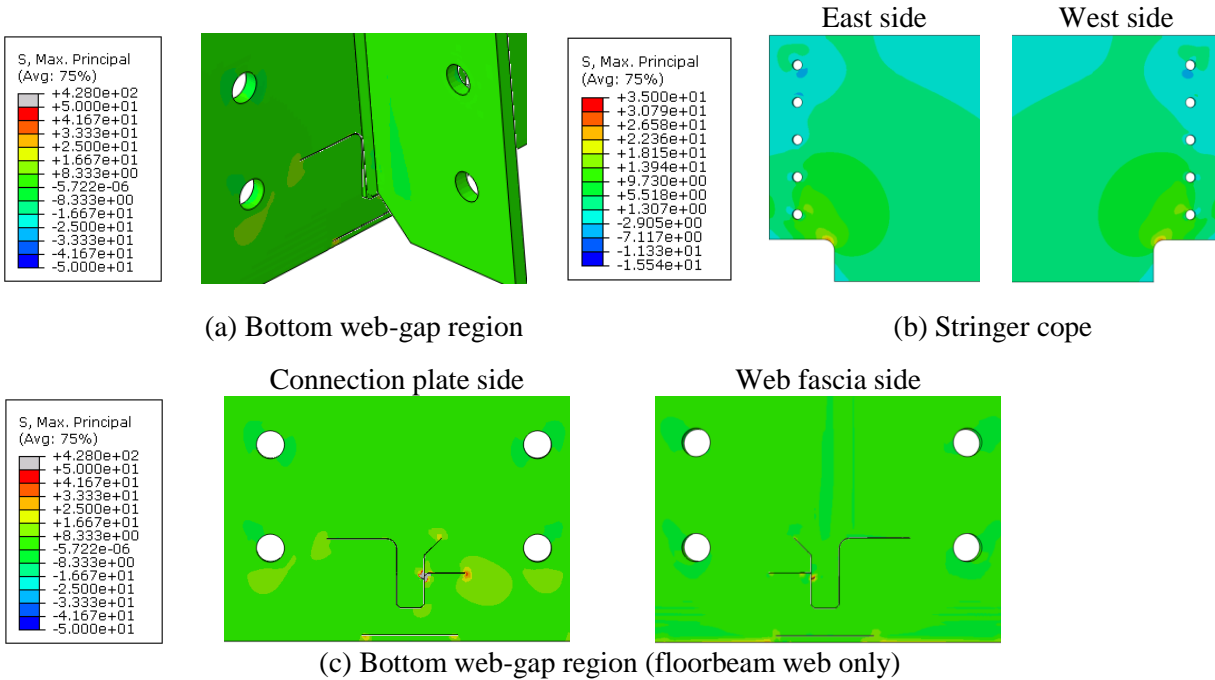


Figure 5-13: Simulation results for single-plate connection specimen FS1: Model 6

The angles-with-plate retrofit was simulated in Model 7, in which the crack geometries were the same as in Model 6. As shown in Figure 5-14, the stresses that were concentrated in the damaged regions in Model 6 were significantly less in Model 7.



* The limits of the color bar in Model 7 were the same as in the Model 6
Figure 5-14: Simulation results for single-plate connection specimen FS1: Model 7

Figure 5-15 and 5-16 present the stresses along Path 1(c) and Path 2 for Model 6 and Model 7. The peak stresses along the two paths were reduced 81% and 90%, respectively, by the retrofit.

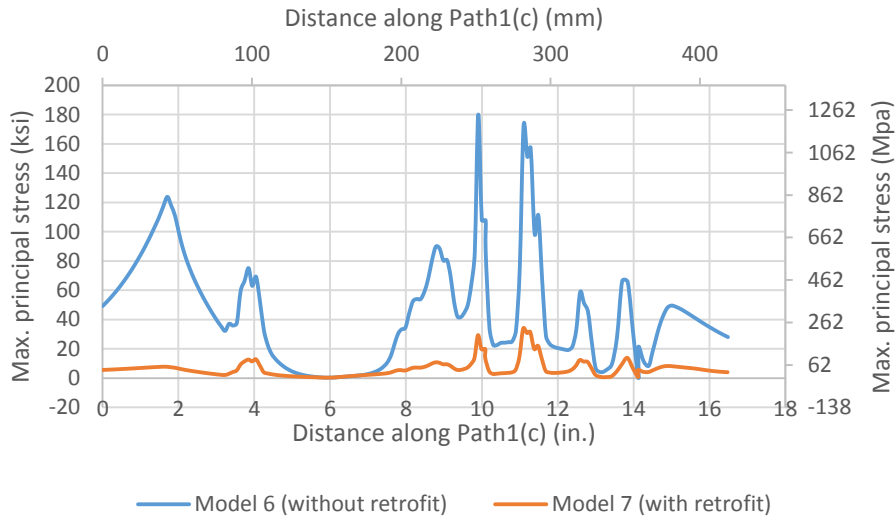


Figure 5-15: Stresses along Path 1(c) for single-plate connection specimen FS1 Model 6 and Model 7

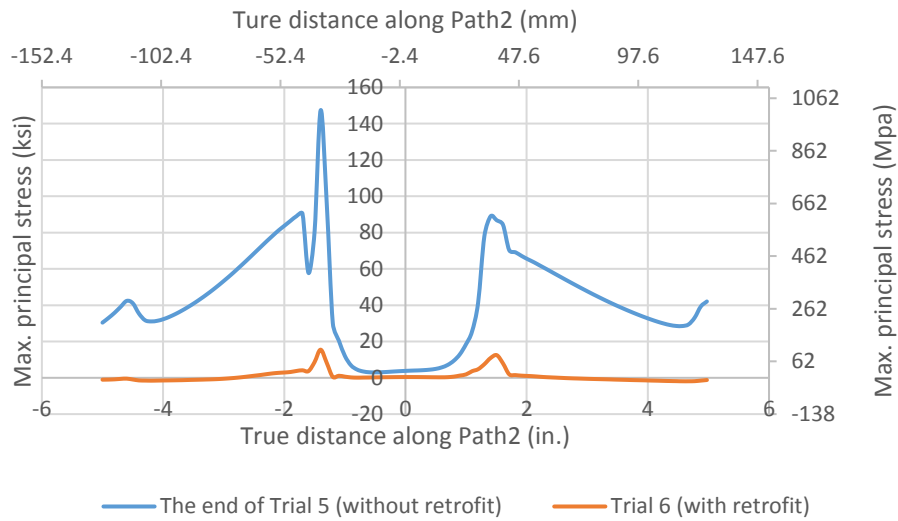


Figure 5-16: Stresses along Path 2 for single-plate connection specimen FS1 Model 6 and Model 7

The angles-with-plate retrofit was able to effectively reduce the stresses along Path 1((a), (b), (c)) and Path 2. The efficacy of the angles-with-plate retrofit in repairing different stages of crack propagation is summarized in Table 5-3.

Table 5-3: Summary of the efficacy of the angles-with-plate retrofit in the computer simulations for specimen FS1

	Model 2	Model 3	Model 4	Model 5	Model 6	Model 7
Crack propagation stage	Early stage		Middle stage		Late stage	
Crack discription	Cracks initiated at the end of the floorbeam web – connection plate weld		Cracks propagated into floorbeam web and grew horizontally		Cracks initiated at the floorbeam web – bottom flange weld and grew along it	
Retrofit (Y/N)	N	Y	N	Y	N	Y
Peak stress reduced along Path 1 ((a), (b), (c)) after retrofiting	40% reduction with respect to Model 2		85% reduction with respect to Model 4		81% reduction with respect to Model 6	
Peak stress reduced along Path 2 after retrofiting	67% reduction with respect to Model 2		92% reduction with respect to Model 4		90% reduction with respect to Model 6	

It is worth mentioning that before the crack initiated at the weld connecting the floorbeam web and the bottom flange, the stresses along Path 2 increased as the cracks on the floorbeam web propagated, as shown in Figure 5-17. This may lead to, or at least speed up the cracking of the floorbeam web to bottom flange weld. As presented in Table 5-3, the angles-with-plate retrofit was found to reduce 67% of the peak stress along Path 2 in Model 2 and 92% in Model 4, indicating

that the retrofit is also useful for preventing initiation of the crack on the weld connecting the floorbeam web and the bottom flange.

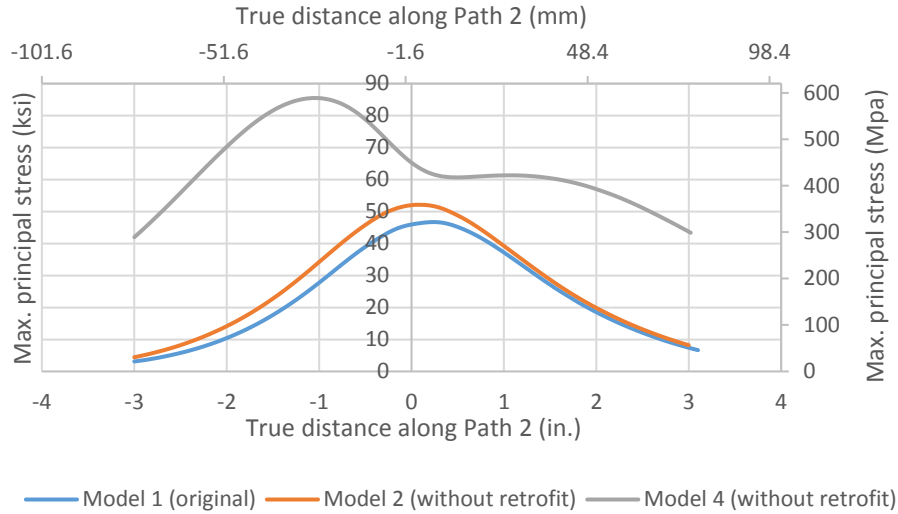
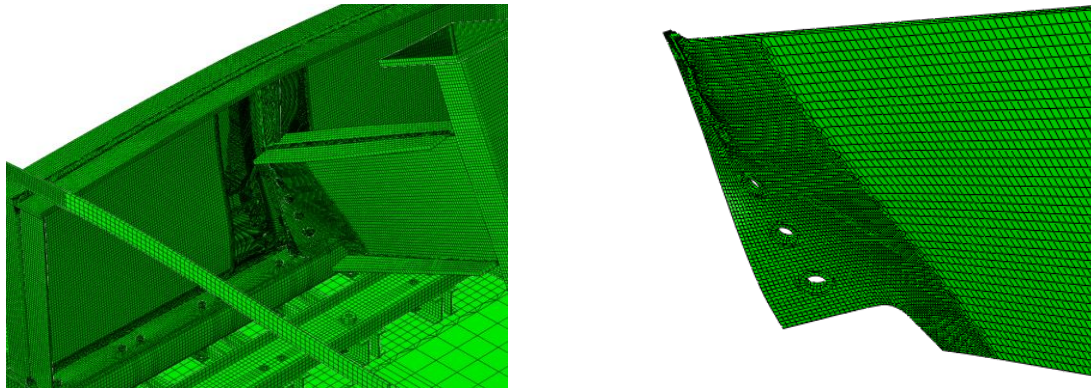


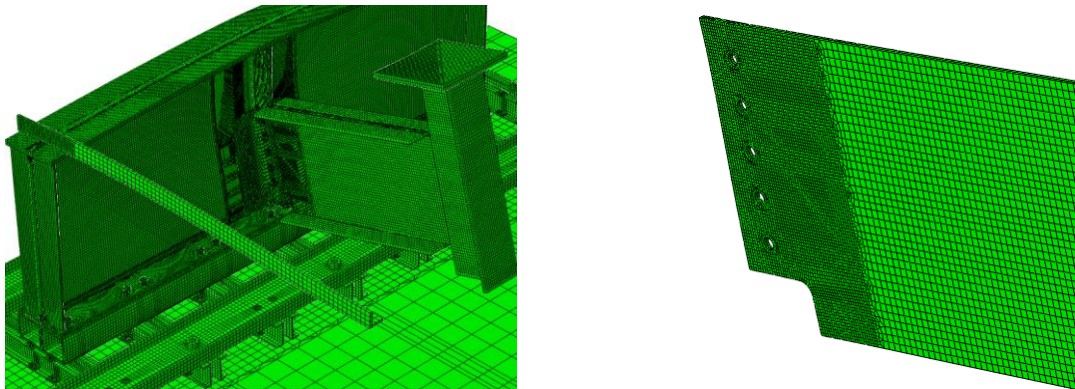
Figure 5-17: Comparison of stresses along Path 2 in Model 1, Model 2, and Model 4

While there were stress concentrations evident at the stringer cope, they were much lower-magnitude than stresses in the web-gap region of the floorbeam. As mentioned in the above sections, when the retrofit was not present the stress distributions on the west and east sides of the stringer web were different. Stresses on the west side were larger than the east. However, after retrofitting, stresses on the west side decreased to match the east, thus the stress distributions on the two sides became more similar.

This phenomenon can best be explained by examining the deformation of the connection plate and the stringer web connected to it, as shown in Figure 5-18.



(a) Model4 – the end of Trial 3 (without retrofit) deformation (magnified 50 times)



(b) Model5 – Trial 4 (with retrofit) deformation (magnified 50 times)

Figure 5-18: Deformation of the stringer web in single-plate connection models

As shown in Figure 5-18(a), the stringer web is subject to a twisting mode under the actuator load, due to the single-plate connection scheme. After retrofitting, the twisting was significantly reduced. This explained the change of the stresses around the stringer cope.

6. Comparison between Computer Simulation and Physical Test Results of Single-Plate Connection (FS1)

As presented in Figure 4-4, strain gages were attached in the area of the web-gap region and the stringer cope on the physical test specimen FS1. The comparison between the stresses measured by strain gages and the stresses extracted from computer models are presented from Figure 6-1 to Figure 6-7.

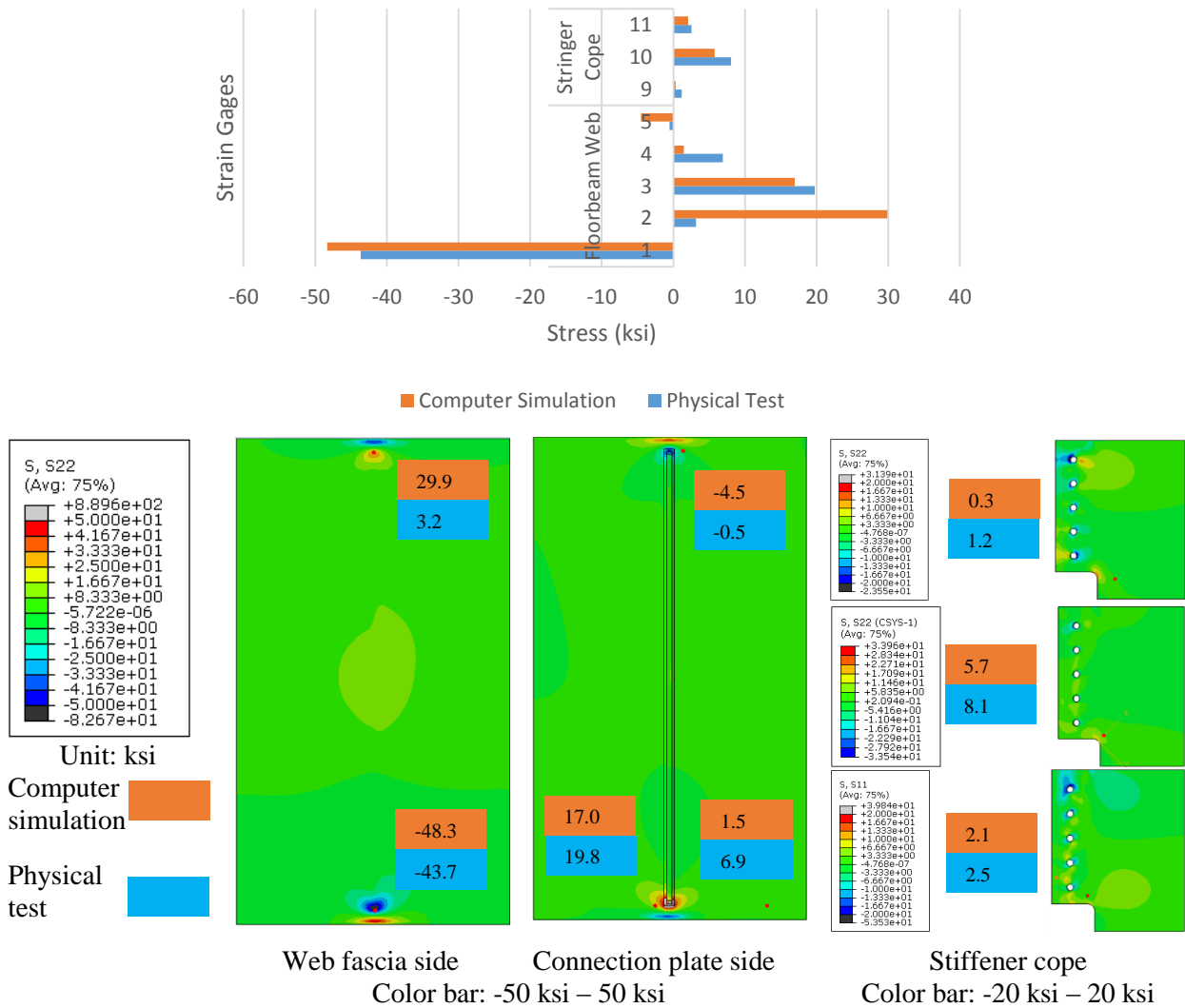
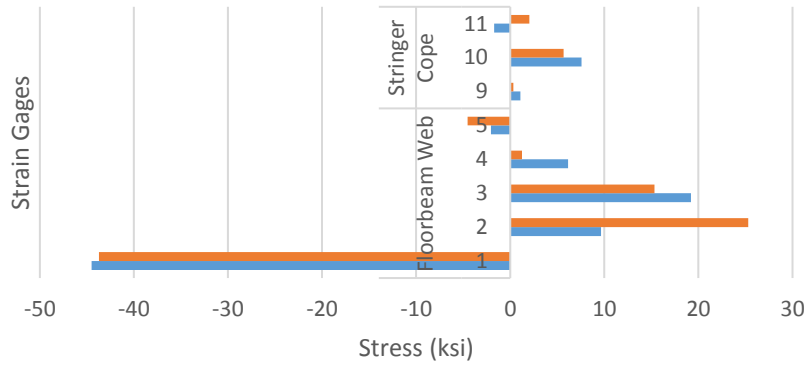


Figure 6-1: Comparison of stresses between FEA results and physical test measurements: Model 1 – The beginning of Trial 1 (without retrofit)



Computer Simulation Physical Test

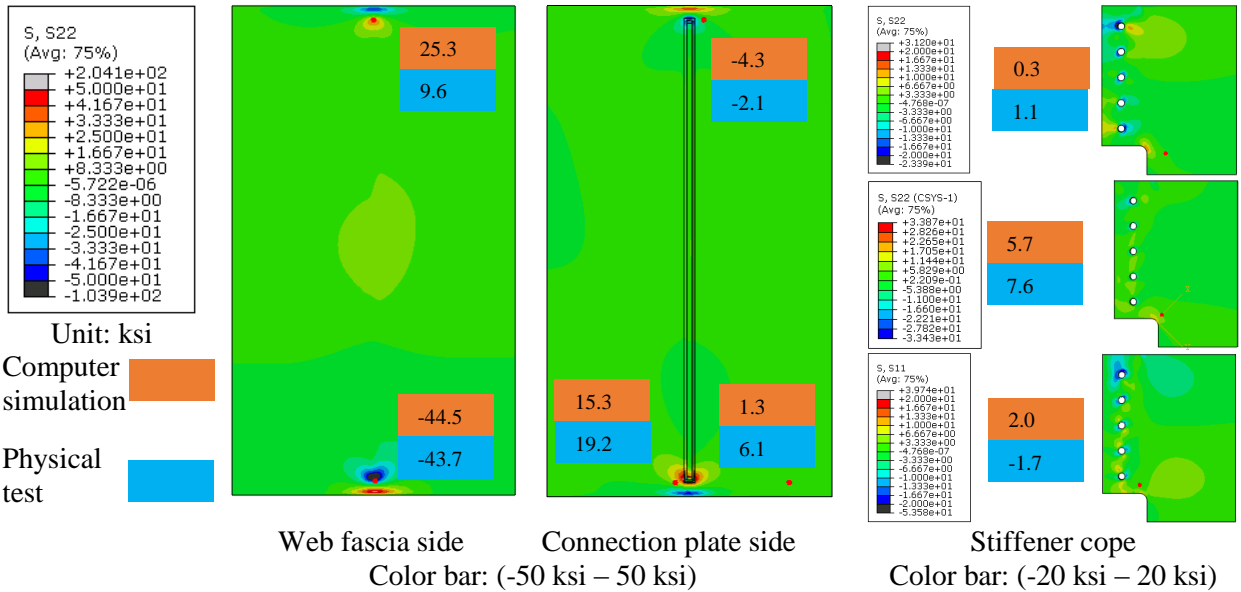
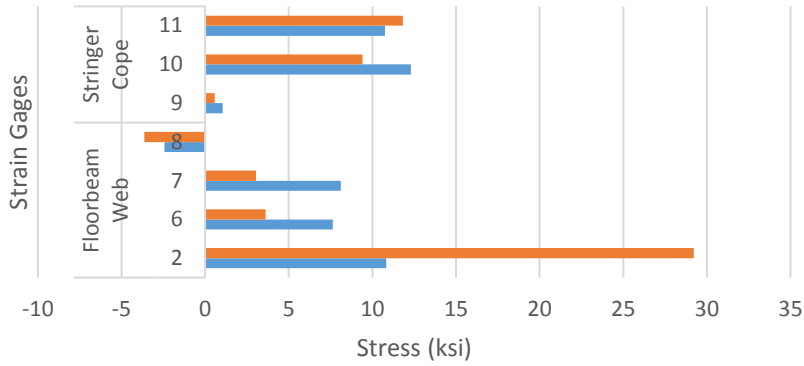
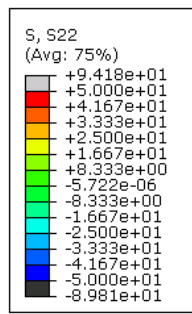


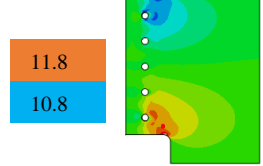
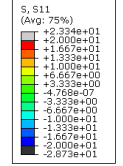
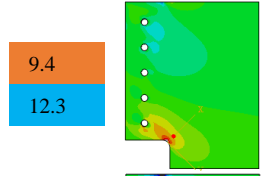
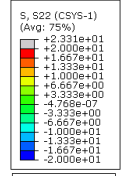
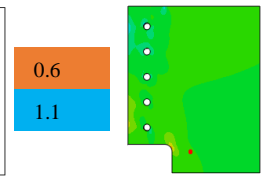
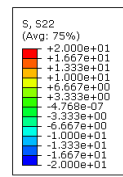
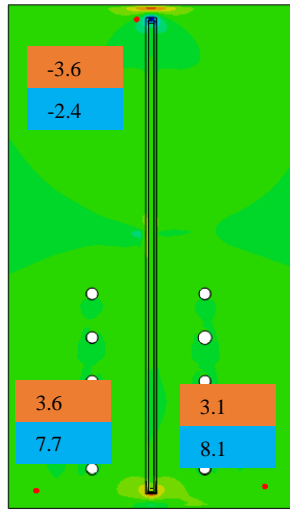
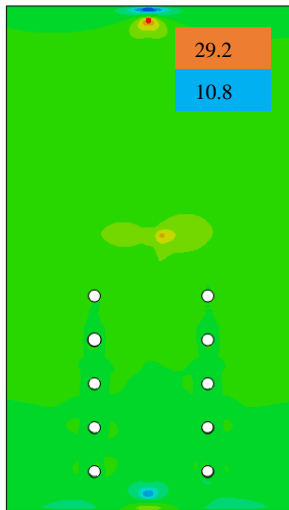
Figure 6-2: Comparison of stresses between FEA results and physical test measurements: Model 2 - The end of Trial 1 (without retrofit)



Computer Simulation Physical Test



Unit: ksi
 Computer simulation
 Physical test



Web fascia side

Connection plate side

Stiffener cope

Color bar: -50 ksi – 50 ksi

Color bar: -20 ksi – 20 ksi

Figure 6-3: Comparison of stresses between FEA results and physical test measurements: Model 3 - Trial 2 (with retrofit)

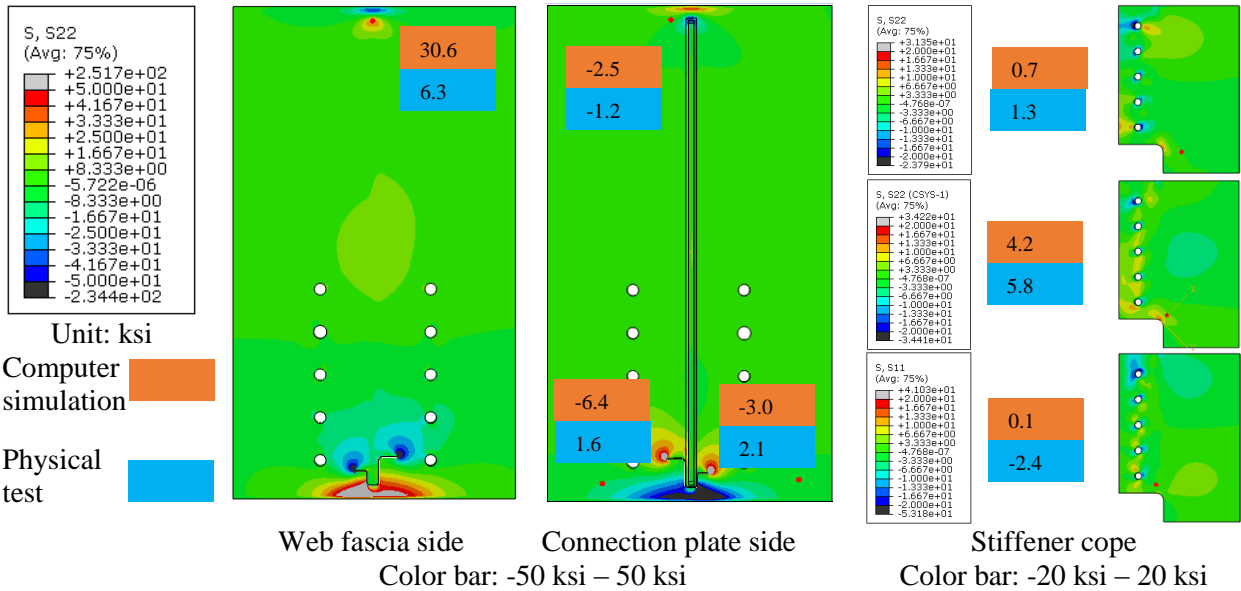
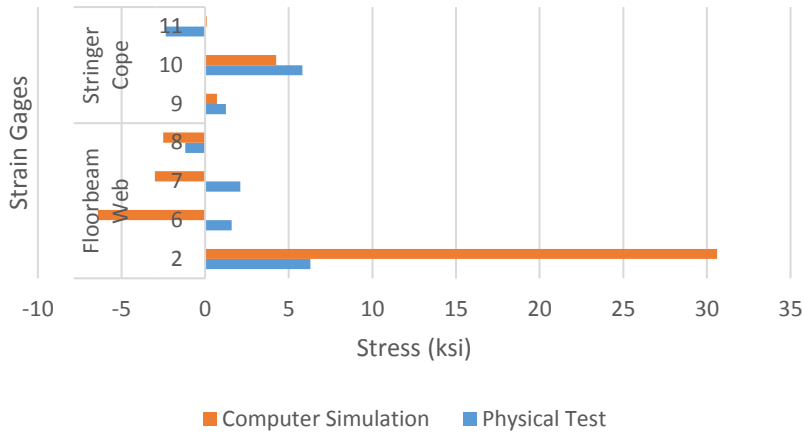
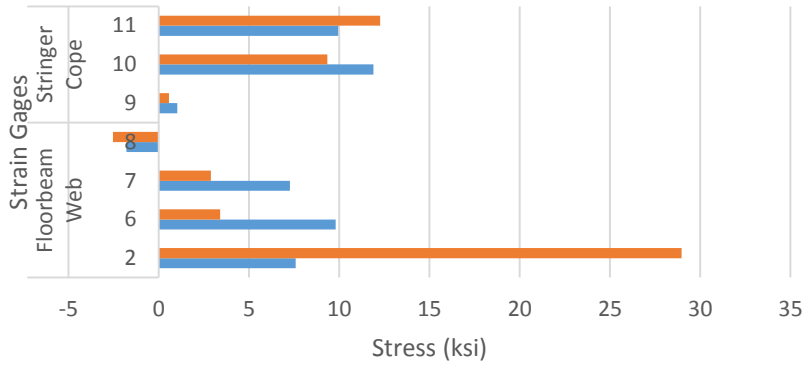
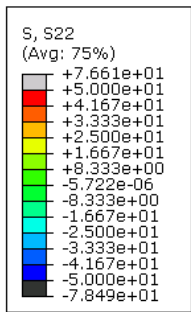


Figure 6-4: Comparison of stresses between FEA results and physical test measurements: Model 4 - The end of Trial 3 (without retrofit)



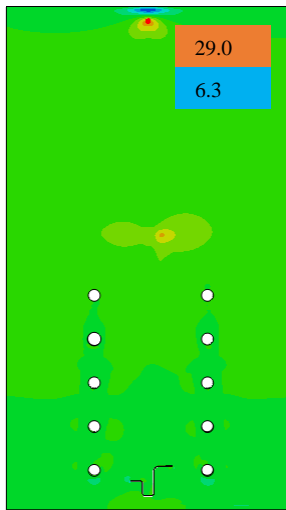
Computer Simulation Physical Test



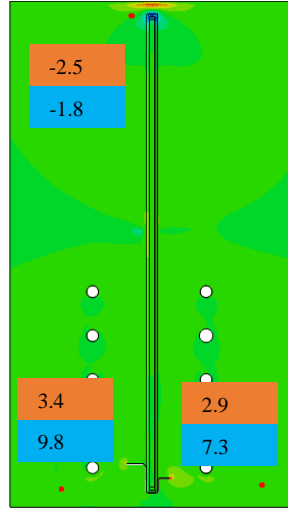
Unit: ksi

Computer simulation

Physical test

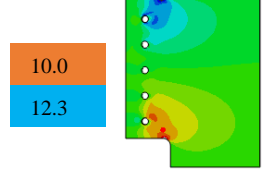
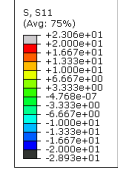
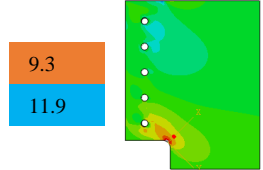
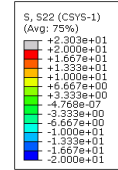
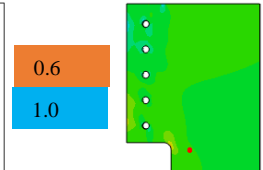
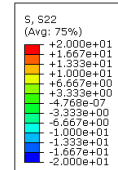


Web fascia side



Connection plate side

Color bar: -50 ksi – 50 ksi



Stiffener cope

Color bar: -20 ksi – 20 ksi

Figure 6-5: Comparison of stresses between FEA results and physical test measurements: Model 5 - Trial 4 (with retrofit)

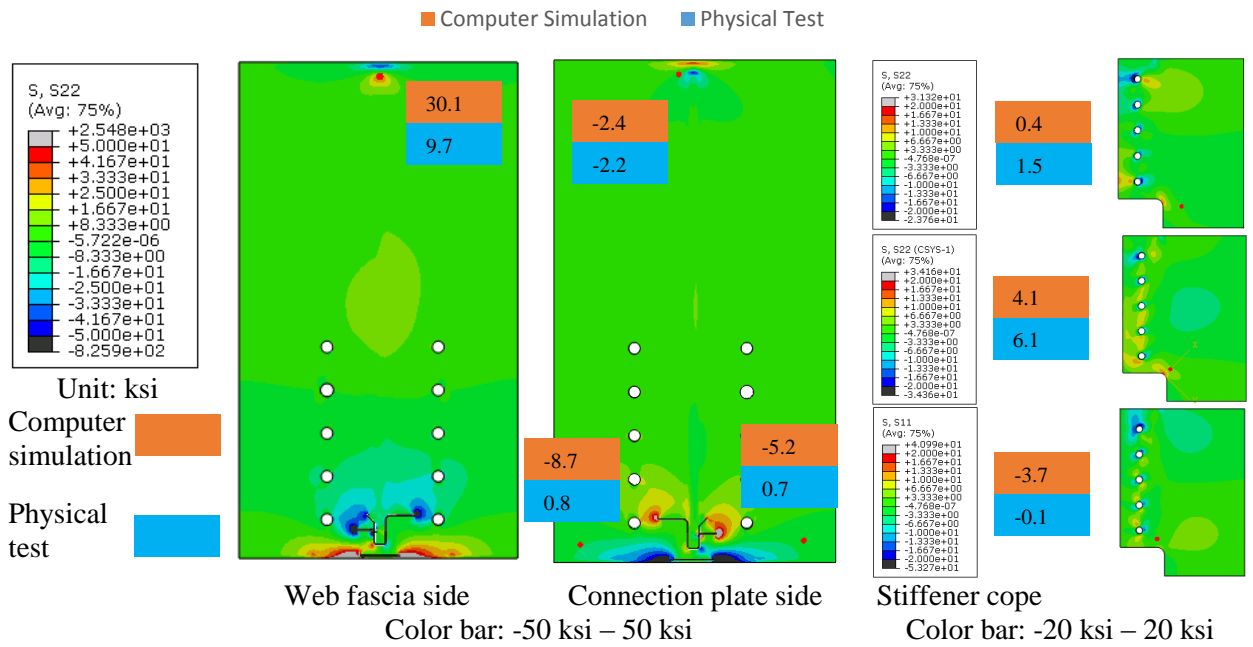
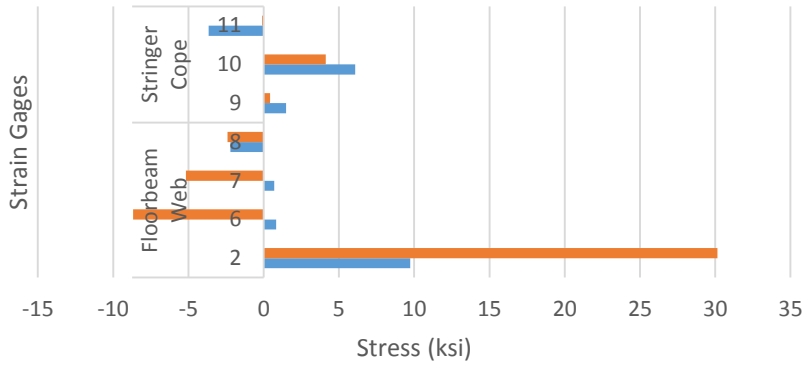


Figure 6-6: Comparison of stresses between FEA results and physical test measurements: Model 6 - The end of Trial 5 (without retrofit)

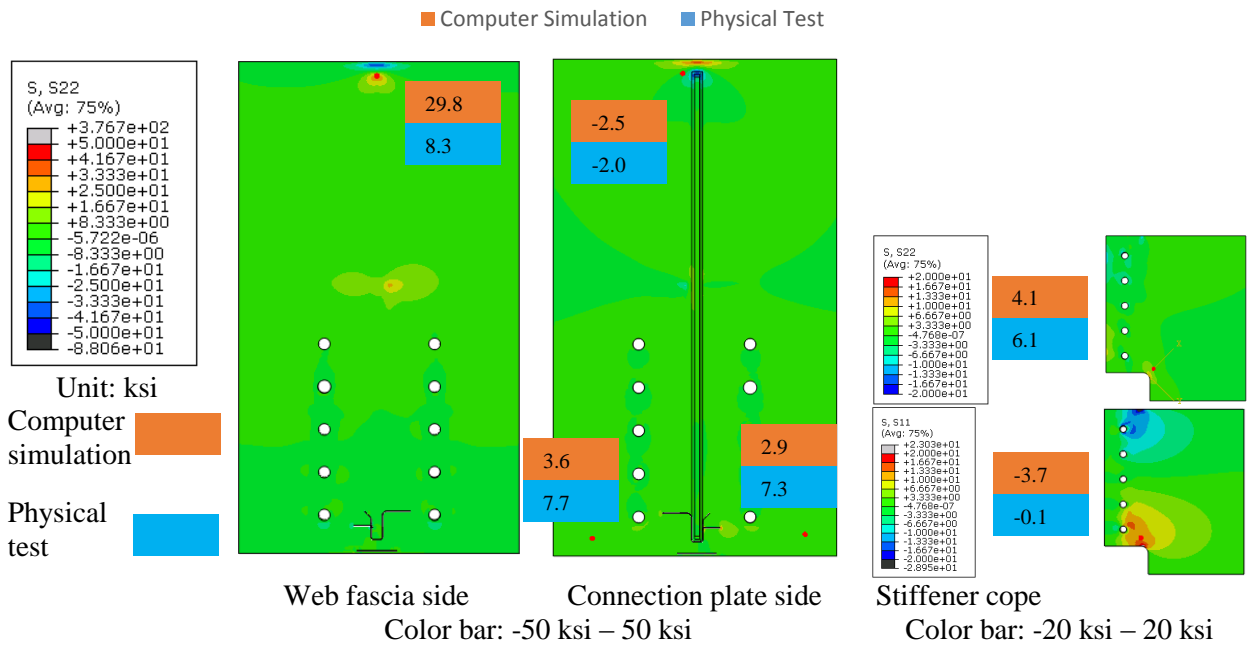
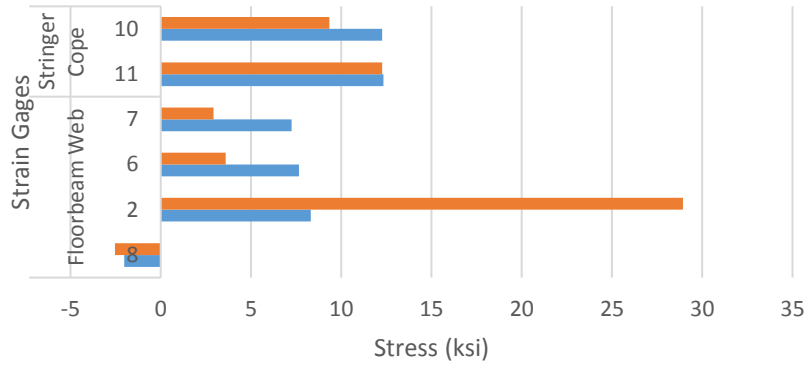
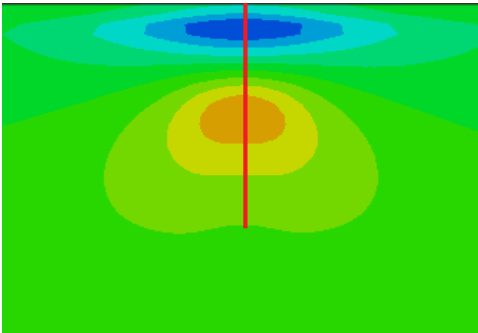


Figure 6-7: Comparison of stresses between FEA results and physical test measurements: Model 7 – Trial 6 (with retrofit)

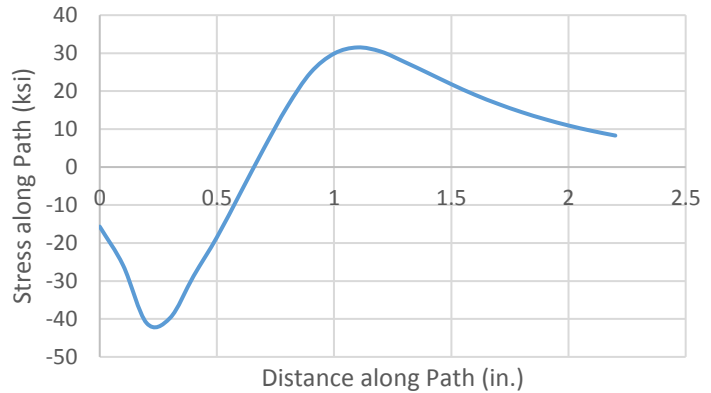
As presented in Figure 6-1 and Figure 6-2, the stresses at the bottom web-gap on the fascia side obtained from the computer simulations and the physical tests agreed well. However, the stresses in the upper web-gap region obtained from the computer simulations were much larger than those measured in the physical tests.

The web-gap regions were the locations where large stress concentrations occurred. Figure 6-8 shows the stresses extracted along the paths defined in the top and the bottom web-gap regions.

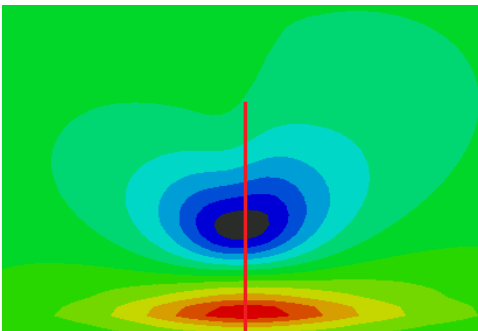
In the top web-gap region, the stresses varied from -40 ksi to 30 ksi over a length of approximately 0.7 in. In the bottom web-gap region, the stresses varied from -50 ksi to 60 ksi over half an inch. It is very difficult to accurately measure stresses within regions with such an extreme stress gradient.



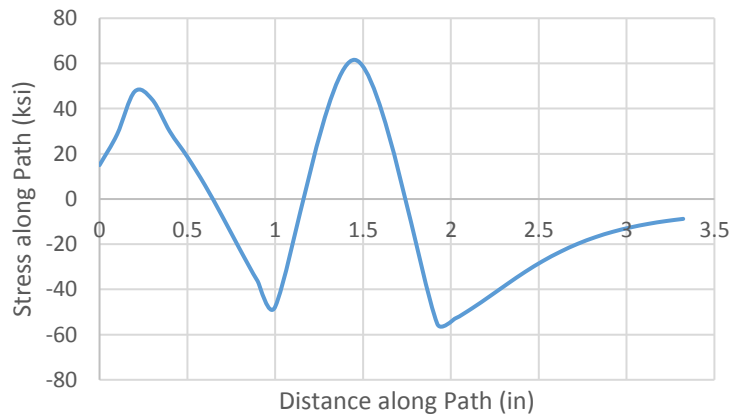
(a) Path of the top web-gap (Model 1)



(b) Stresses along the path of the top web-gap (Model 1)



(c) Path of the bottom web-gap (Model 1)



(d) Stresses along the path of the bottom web-gap (Model 1)

Figure 6-8: Stresses extracted along the paths defined in the web-gap regions

In Model 1, Model 2, Model 3, Model 5, and Model 7, stresses extracted from the computer models agreed well with the stresses obtained from the corresponding physical tests. However, for Model 4 and Model 6, the comparison was not as expected.

Model 4 and Model 6 were established to resemble the specimen at the end of Trial 3 and Trial 5. Retrofits were not applied in these models. The cracks in these models were created using the

extended finite element method (XFEM). When applying the XFEM technique, the cracks were defined as 3D shells with widths same as the thickness of the floorbeam web. That is to say, the cracks created in the models cut through the thickness of the floorbeam web.

Crack distributions through the thickness of the floorbeam web were very complicated and were not measured in the physical tests. When creating the crack in the models, the longest crack pattern in each trial was chosen, and was created as one that cut through the thickness of the floorbeam web. That simplified the crack modeling process, and also modeled the worst-case scenario for the crack placement. However, because of this, the cracks in the models created more serious stress demands than their corresponding physical tests. In Trial 3 of the physical test on Specimen FS1, the cracks grew into the floorbeam web, but only part of the crack extended through the web thickness. In Trial 5, the horizontal floorbeam web-to-flange crack initiated. However, while it was 2.7 in. long on the web fascia side, only $\frac{1}{4}$ in. was measureable on the connection plate side.

On the connection plate side, stresses computed in the lower portion of the floorbeam web decreased with increasing crack length. This was the same behavior observed in the physical tests. Stresses computed from strain gage measurements located at the lower part of the floorbeam web (Strain Gages 6 and 7) also decreased as cracks propagated, as presented in Figure 4-18, but not as much as observed in the finite element models. In Trial 8 of the physical tests, in which severe cracks were present, stresses obtained from Strain Gages 6 and 7 became negative, indicating compressive stresses; this trend was the same as that observed in the finite element models.

7. Physical Test of Double-Angle Connection (FS2)

7.1 Test Introduction

A photograph of the stringer-to-floorbeam specimen with double-angle connection (Specimen FS2) is provided in Figure 7-1. The specimen setup was very similar to the single-plate connection (Specimen FS1) introduced in Chapter 3. The only difference was in this test the stringer and the floorbeam were connected by two bolted steel angles, while in the single-plate connection test the stringer was bolted to a connection plate that was in turn welded to the floorbeam web. As will be discussed, retrofits were not used on this specimen because no visible cracking was ever detected.



Figure 7-1: Photograph of the double-angle connection specimen

7.1.1 Specimen Dimensions

The dimensions of the east connection angle are shown in Figure 7-2. The west connection angle is a mirror image of the east.

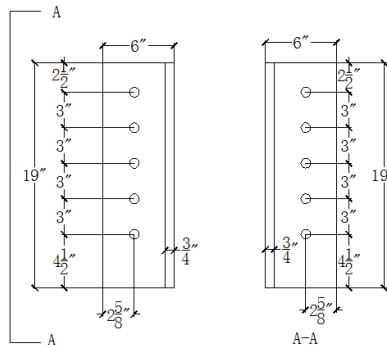


Figure 7-2: East connection angle dimensions in specimen FS2

The west connection angle is a mirror image of the east angle.

The stringer used in the double-angle connection specimen was a W 21×73. Its dimensions are presented in Figure 7-3.

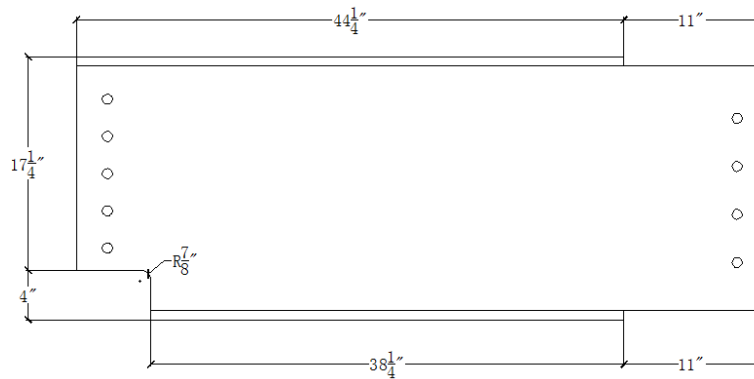


Figure 7-3: Stringer dimensions for the specimen utilizing a double-angle connection

Except for the connection elements and the stringer, all the other members in this test were the same as used in the single-plate connection test introduced in Chapter 3, thus are not repeated here. All steel members were Gr. A992.

7.1.2 Instrumentation

Cracks have been reported in the past as occurring in the cope areas of stringers in existing bridges (Roeder 2001; Al-Emrani 2005; Haghani 2012), and have also been detected near the fillet of the connection angles (Al-Emrani 2005; Haghani 2012). In riveted steel bridges, there were cracks observed in the rivets connecting the angle legs to the floorbeam web (Al-Emrani 2005; Haghani 2012). In this test, the double angle used to connect the stringer and the floorbeam was thicker than the commonly-used size, and A325 bolts were used instead of rivets. Therefore, the location considered to be most susceptible to fatigue cracking was the cope area of the stringer.

As shown in Figure 7-4, four strain gages were placed around the stringer cope. Strain gages were also attached to the both sides of the floorbeam web (Figure 7-5). The displacement of the actuator was measured using a string potentiometer and recorded during periodic monotonic tests.

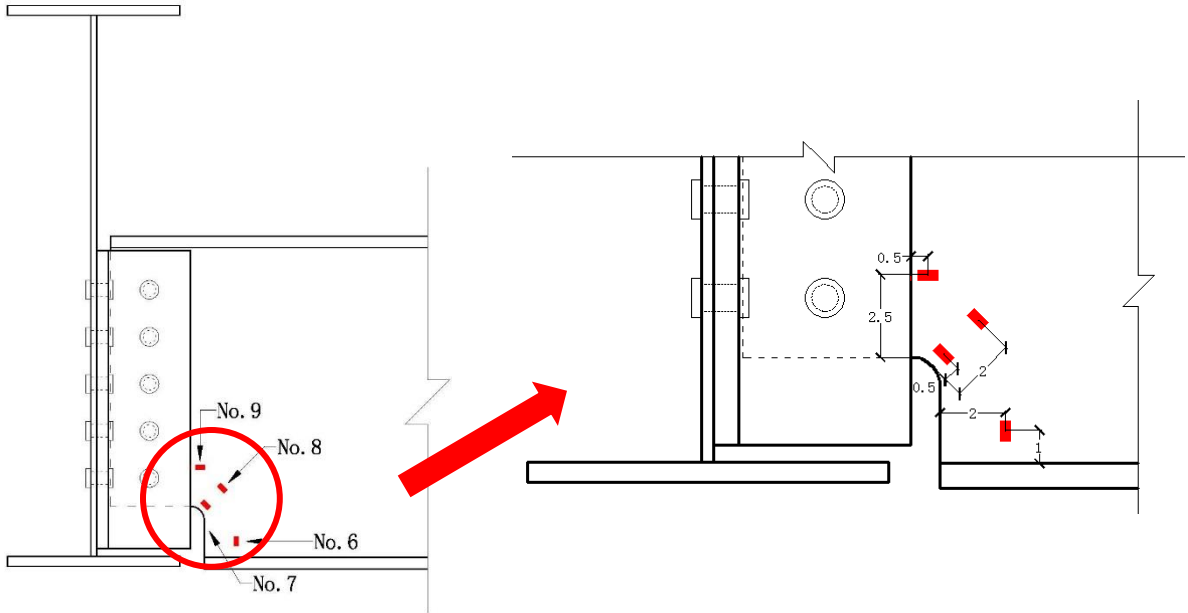


Figure 7-4: Strain gage placements of double-angle connection (specimen FS2) at stringer cope

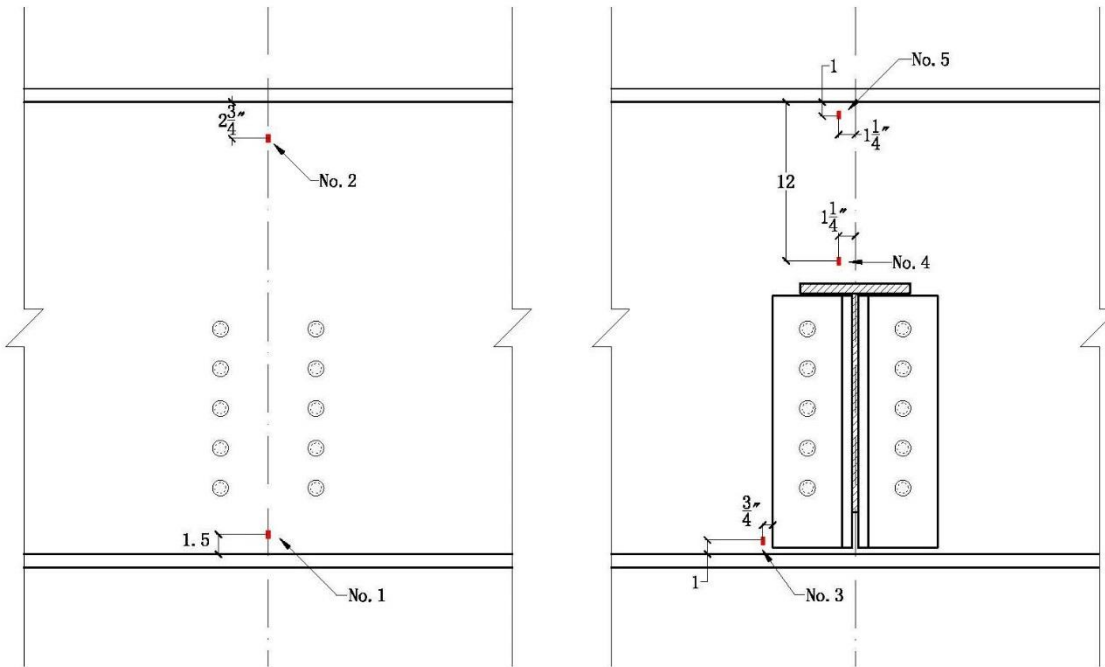


Figure 7-5: Strain gage placements of double-angle connection (specimen FS2) at floorbeam web

7.1.3 Test Procedure

A summary of the double-angle connection test (FS2) is provided in Table 7-1. Three support configurations were used in the test.

In the first configuration, the actuator pulled up on the stringer end of the specimen to provide a cyclic load of 3-5 kip. The specimen response was found to be very flexible; 3-5 kip was the largest load range for which the actuator load was able to maintain a smooth sinusoidal wave.

A second boundary condition configuration was used after 950,000 cycles were applied to the specimen in the first configuration. The bracing angles at the ends of the top flange on the floorbeam were removed to study the performance in the connection with a larger floorbeam web deformation.

After 350,000 cycles into the second configuration, a third test configuration was applied. The bracing angles was reinstalled, and a roller was placed underneath the center of the stringer bottom flange. The actuator pushed down to provide cyclic loads from -1 to -8 kip. The third configuration was applied because the specimen as previously configured was too flexible to sustain a load range larger than 3-5 kip. The researchers were interested in investigating the effects of high shear on the specimen's fatigue performance. While it was recognized that the roller should be located as close as possible to the stringer cope to generate a large shear load, the channels on the floor interfered with this, thus the closest position available for the roller support was at midspan of the stringer bottom flange. 400,000 cycles were applied in Configuration 3.

Table 7-1: Three configurations used in double-angle connection test (FS2)

Test	Configuration	Introduction	Number of cycles	Load range
2	1	With bracing angles, actuator pulled up	950,000	3 kip to 5 kip
2	2	Without bracing angles, actuator pulled up	350,000	3 kip to 5 kip
2	3	With bracing angles, roller under the stringer, actuator pushed down	400,000	-1 kip to -8 kip

Load Frequency: 2 Hz

A monotonic test was conducted every 50,000 cycles for the purpose of recording instrumentation readings. In Configuration 1 and Configuration 2, the actuator force was slowly increased from 0 to 6 kip. In Configuration 3, the actuator pushed down to load the specimen from 0 to -10 kip. The specimen was regularly examined to inspect for fatigue cracks.

7.2 Test Result

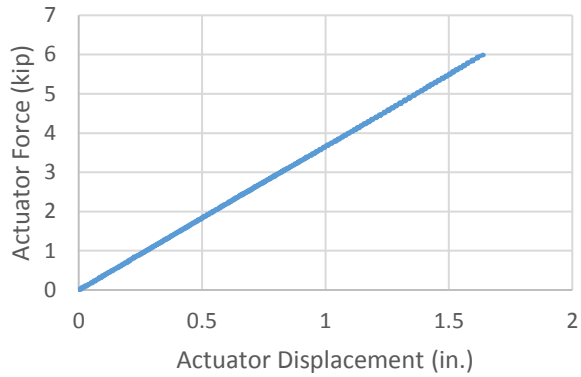
In the first and second configurations, the specimen was cycled from 3 - 5 kip. This was the largest load range that could be applied to allow the cyclic load provided in a smooth sinusoidal wave, since the floorbeam web became too flexible after buckling. The specimen was examined regularly for cracking, but no cracks were observed as developing under any of the three configurations.

7.2.1 Actuator Displacement

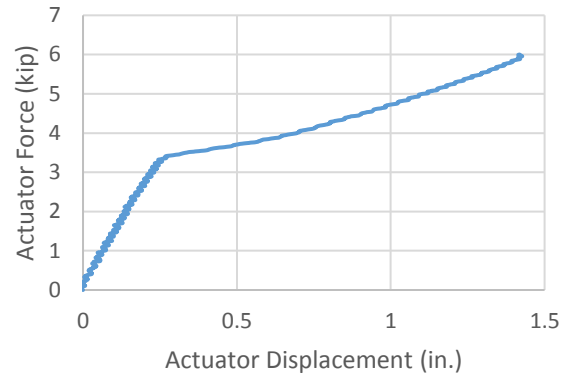
Configuration 1

As shown in Figure 7-6(a), the first time specimen FS2 was loaded, the relationship between actuator force and actuator displacement was linear. However, the linear relationship only appeared this first time. The buckled relationship appeared in the next monotonic test after 50,000 cycles, and appeared for all the other monotonic tests in performed Configuration 1.

The buckling behavior corresponded with approximately 3 kip actuator force and 0.2 in. of actuator displacement, as presented in Figure 7-6(b). The curve consisted of two parts. One was a straight line before buckling behavior appeared. The other was a slightly curved line that presented after buckling. The stiffness of the connection significantly decreased when buckling occurred. Figure 7-7 presents the actuator displacement with respect to the number of applied cycles.



(a) 0 cycle into Configuration 1



(b) 700,000 cycles into Configuration 1

Figure 7-6: Actuator displacement vs. actuator force in Configuration 1

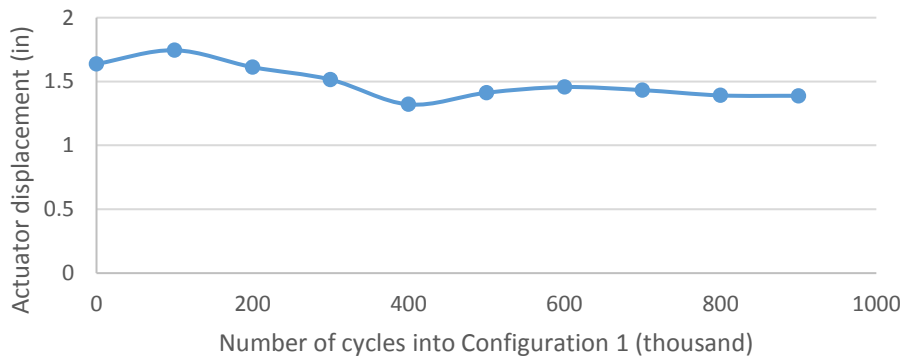


Figure 7-7: Actuator displacement at 6 kip actuator force for Configuration 1

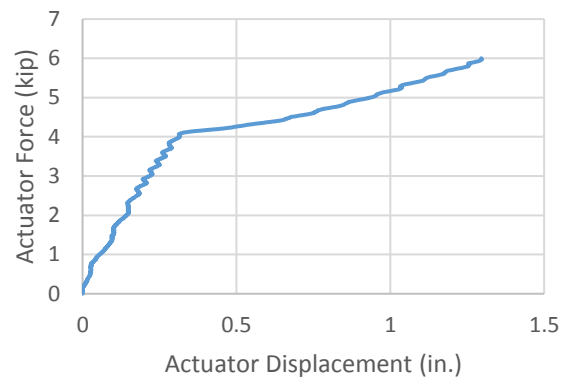
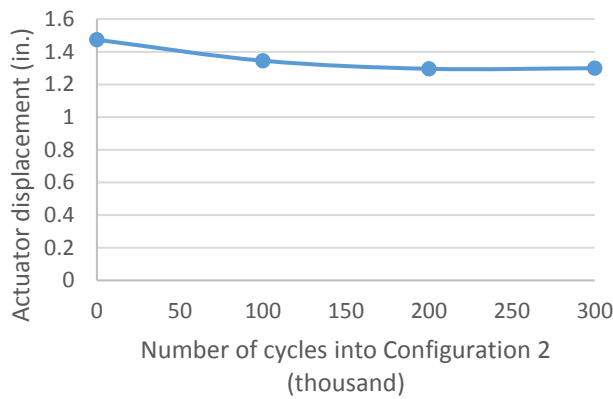
Configuration 2

Figure 7-8 presents the actuator displacement in Configuration 2. 950,000 cycles were applied on the specimen in Configuration 1, but no fatigue crack was observed. Therefore, the two restraining angles at the ends of floorbeam top flange were removed to generate larger deformations in the specimen. However, as shown in Figure 7-8, removing the restraining angles did not increase the actuator displacement.

Buckling behavior was also observed in this configuration. It is presented in the force–displacement curve in Figure 7-8(b). The floorbeam web buckled under approximately 4 kip of actuator force and 0.3 in. actuator displacement, while in Configuration 1 it buckled at

approximately 3 kip of actuator force and 0.2 in. actuator displacement. The buckling load in Configuration 2 was higher than in Configuration 1.

This explained why removing the restraining angles did not increase the actuator displacement. Removing the restraining angles did decrease the spring stiffness of the connection before buckling. The spring stiffness of Configuration 1 was approximately 15 kip/in, while as in Configuration 2 it was approximately 13 kip/in. However, removing the restraining angles also delayed buckling, thus it did not increase the actuator displacement.



(a) Actuator displacement at 6kip for Configuration 2

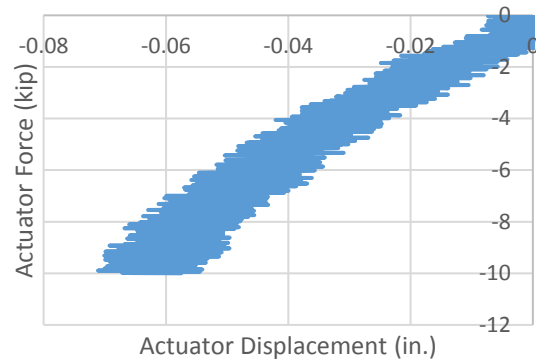
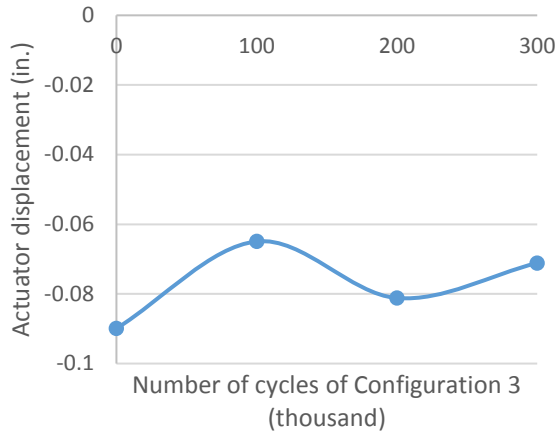
(b) 200,000 cycles into Configuration 2

Figure 7-8: Actuator displacement in Configuration 2

Configuration 3

Since no fatigue cracking was detected in the previous two configurations, the researchers were interested in whether inducing a larger shear force would induce fatigue cracking. A roller was placed underneath the stringer bottom flange at midspan of the stringer in Configuration 3.

As shown in Figure 7-9, the actuator displacement was very small in this configuration. The displacement of the actuator was susceptible to electronic noise (Figure 7-9(b)) due to the small measurement range.



(a) Actuator displacement at -10 kip in Configuration 3

(b) 300,000 cycles into Configuration 3

Figure 7-9: Actuator displacement in Configuration 3

7.2.2 Stress

Configuration 1

Figure 7-10 presents stresses computed from strain gage measurements at 0 cycles of Configuration 1 with respect to both actuator force and actuator displacement. As discussed in the previous section, buckling was not observed in the initial Configuration 1 measurements. Stresses at 0 cycle were also special; except for the stress computed from Strain Gage 1, which was located at the center of the bottom of the floorbeam web fascia side, all other stresses were proportional to both the actuator force and the actuator displacement.

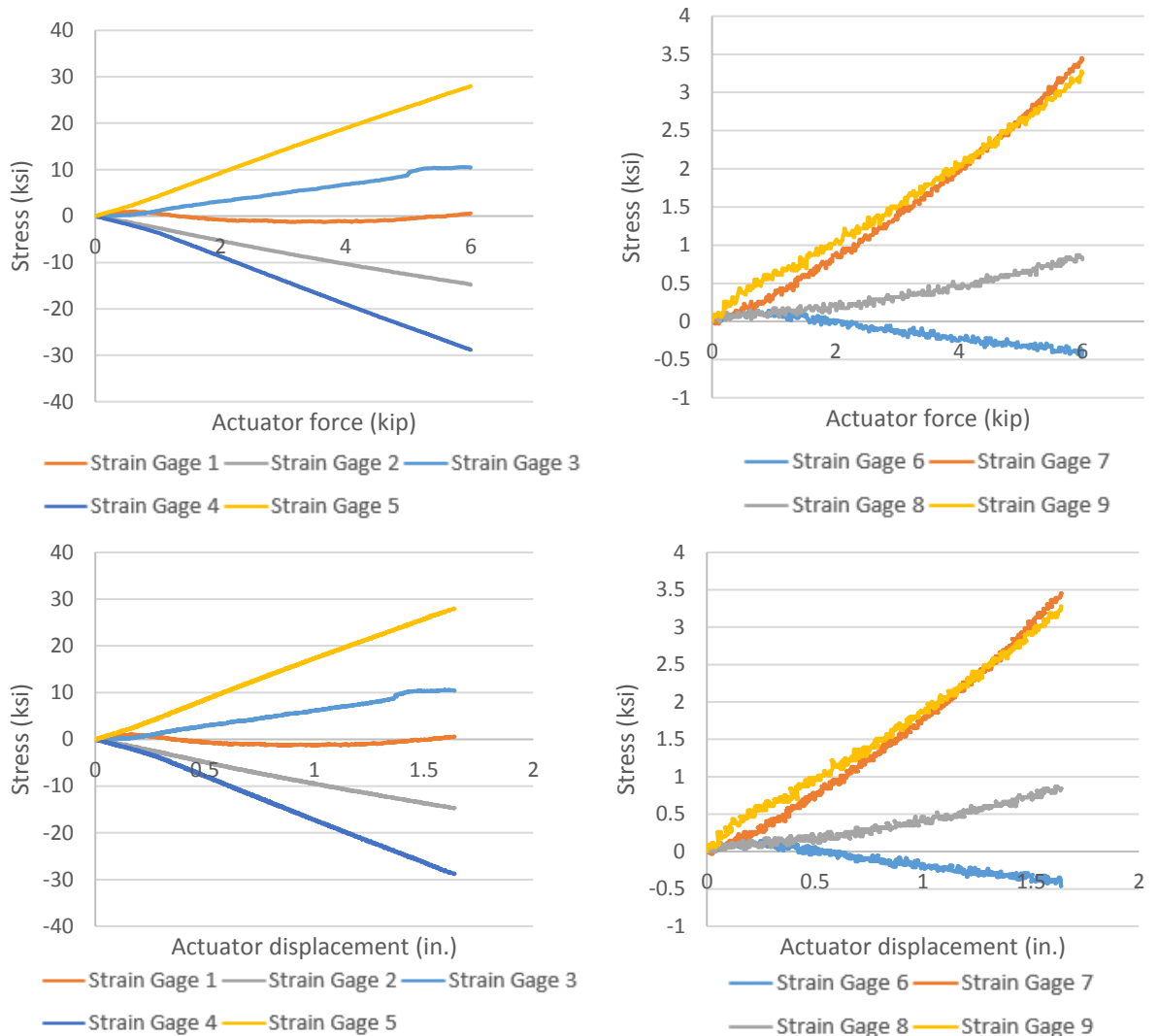


Figure 7-10: Stresses at 0 Cycle of Configuration 1

Except for the monotonic test performed at 0 cycles into Configuration 1, all other monotonic tests revealed the buckling behavior, as shown in Figure 7-11. After buckling, the slopes of the stress-force relationships changed significantly for both the floorbeam web and the stringer cope. In the stress-displacement curves for the floorbeam web, the buckling behavior is observable through the stresses in the lower region of the floorbeam web (Strain Gages 1 and 3), while the stresses in the middle and upper region (Strain Gages 2, 4, and 5) were proportional to the actuator displacement.

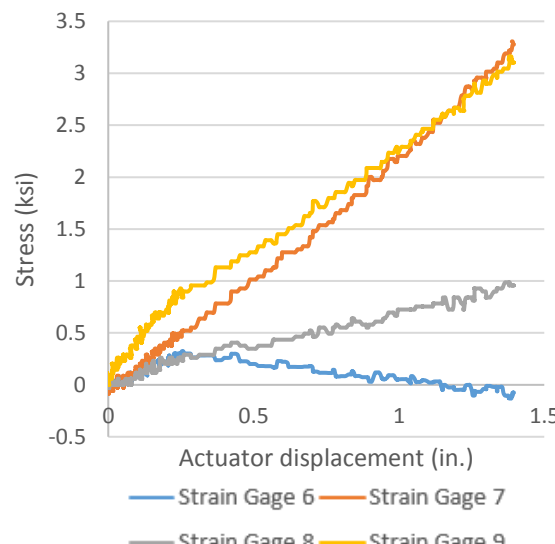
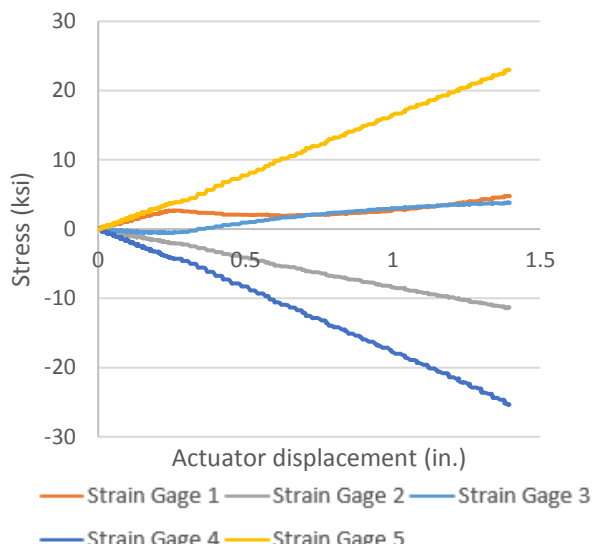
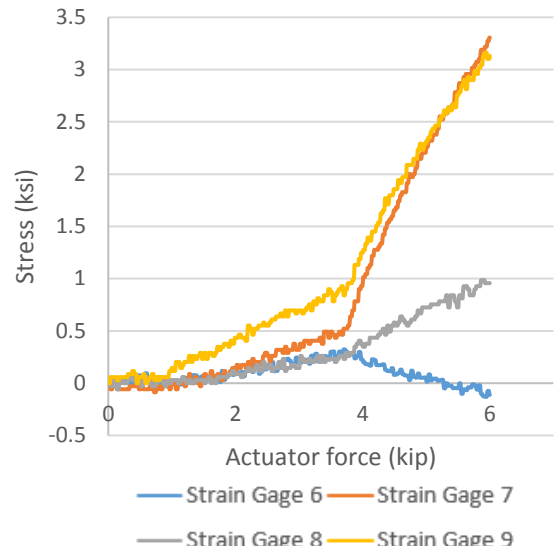
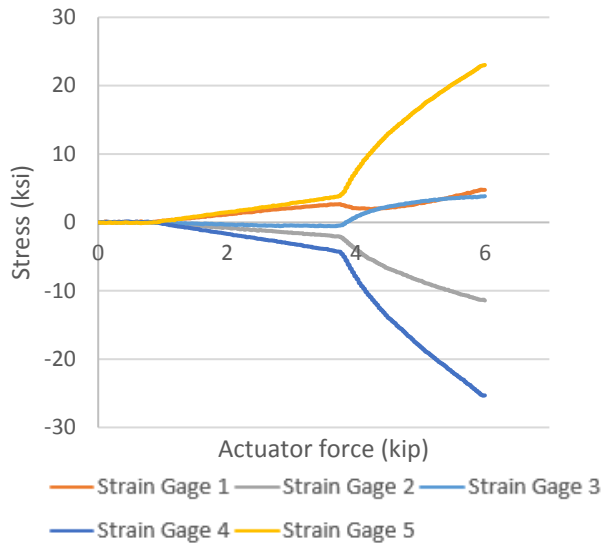


Figure 7-11: Stresses at 800,000 cycles of Configuration 1

Configuration 2

As presented in Figure 7-12, the stresses in Configuration 2 had the same characteristic as in Configuration 1. The only difference was that the onset of buckling in Configuration 2 was delayed to 4 kip of actuator force and 0.3 in. actuator displacement.

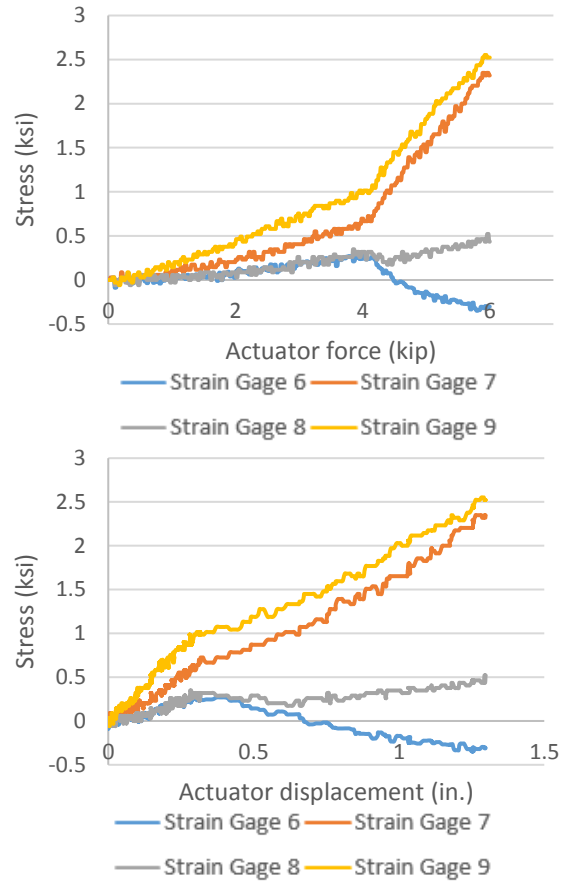
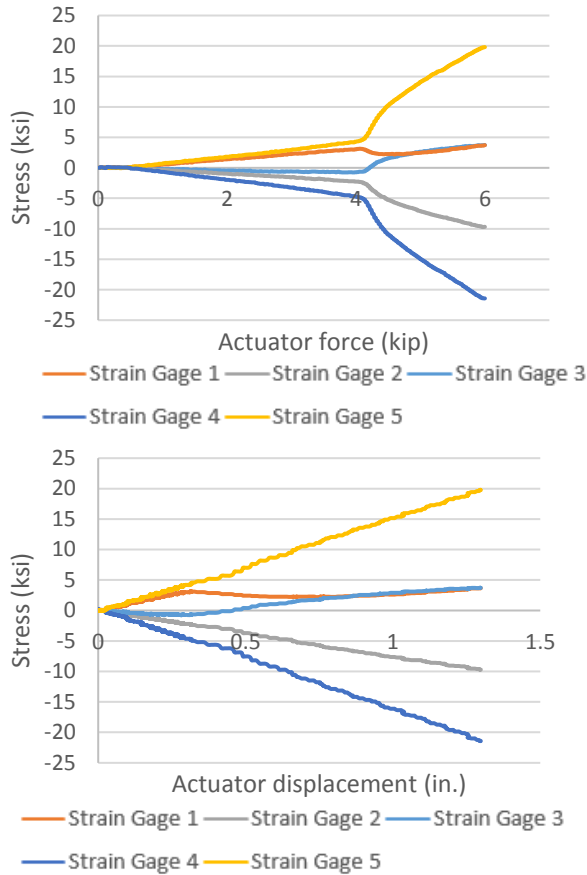


Figure 7-12: Stress at 200,000 cycles of Configuration 2

Configuration 3

As shown in Figure 7-13, in Configuration 3, stresses on the floorbeam web were very small.

Stresses on the stringer cope were also relatively low-magnitude.

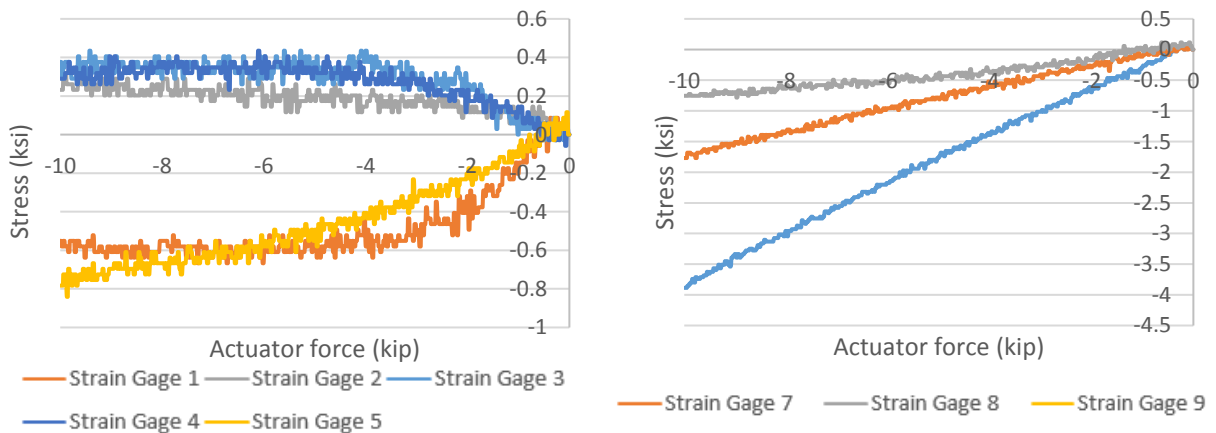


Figure 7-13: Stress at 100,000 cycles of Configuration 3

8. Computer Simulation of Double-Angle Connection (FS2)

Three computer models were created using commercially available finite element analysis software Abaqus V6.12 to resemble the physical test setups of Configuration 1 and Configuration 3 as faithfully as possible. The models also included a virtual set-up with a shorter floorbeam web to represent a more general scenario.

8.1 Model for Physical Test FS2 Configuration 1

8.1.1 Introduction

As presented in Figure 8-1 and Table 8-1, a model was established to faithfully represent the physical test setup used in Configuration 1. Identical modeling methodologies were used for these models as for the models created for specimen FS1, and thus are not repeated here. A 6 kip upward force was applied as a uniformly distributed surface load on the actuator plate.

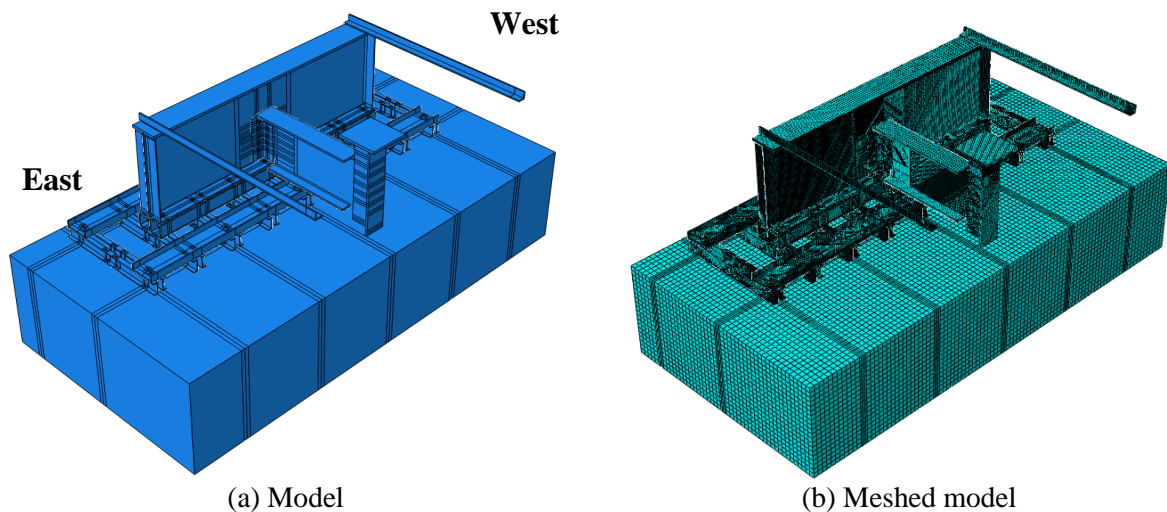
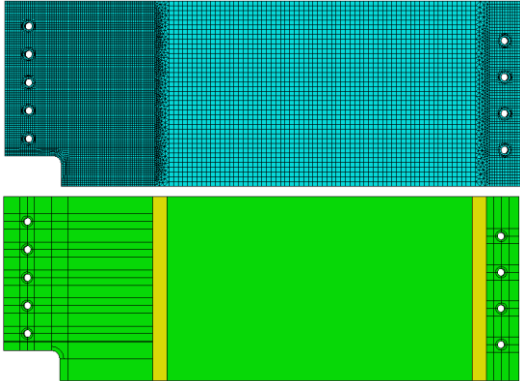
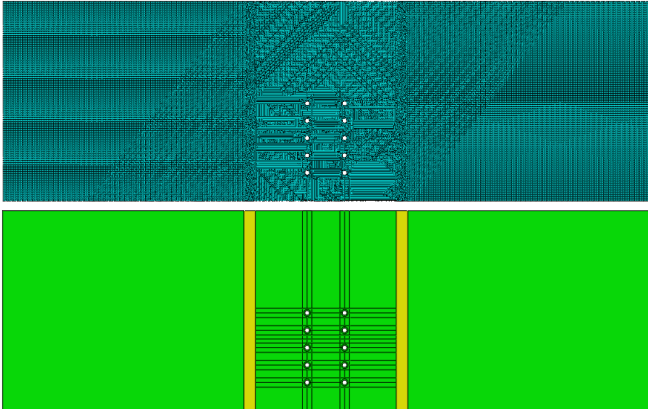
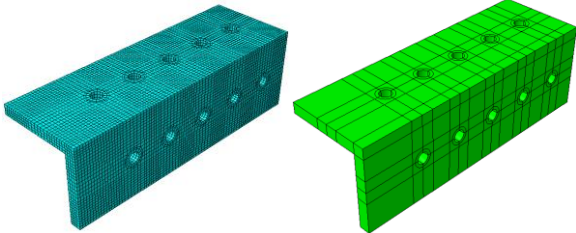
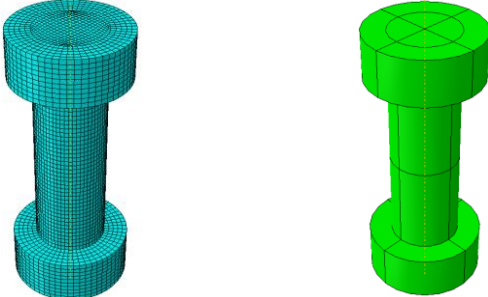



Figure 8-1: Finite element model for double-angle connection test FS2

Table 8-1: Element size and mesh technique for important parts in double-angle connection models

Part	Element size (in.)	Meshed part and partition technique
Stringer web	0.2 for the region near stringer cope 0.5 for the other region	
Floorbeam web	0.1 for the region near the center line 0.2 for the other region	
Connection angle	0.2	
Bolt	0.05 Except the super bolts used to connect the specimen to the floor 0.5 for the bolts connecting the floor	
Floorbeam web to bottom flange weld	0.1	

8.1.2 Simulation Results

The computed model for Specimen FS2, Configuration 1 is presented in Figure 8-2. Figure 8-3 to Figure 8-8 present the computed results for different parts of the model.

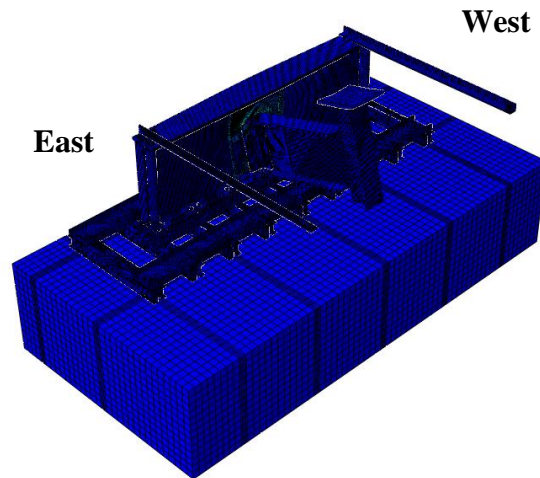


Figure 8-2: Computed model for double-angle connection test FS2, Configuration 1

Bolts

The connection elements used in this test were A325 bolts. They were not considered to be susceptible to fatigue problem. However, many aging stringer-to-floorbeam connections are riveted. In a study performed by AL-Emrani (AL-Emrani 2005), fatigue failure in rivets connecting the angle leg and the floorbeam web occurred in each of the three specimens tested.

The bolts connecting the angles and the floorbeam web carried both shear forces and moments. Figure 8-3 presents the computed maximum principal stresses in the modeled bolts. The stresses tended to concentrate near the junction of the shank and the head, especially for the top and bottom rows of bolts.

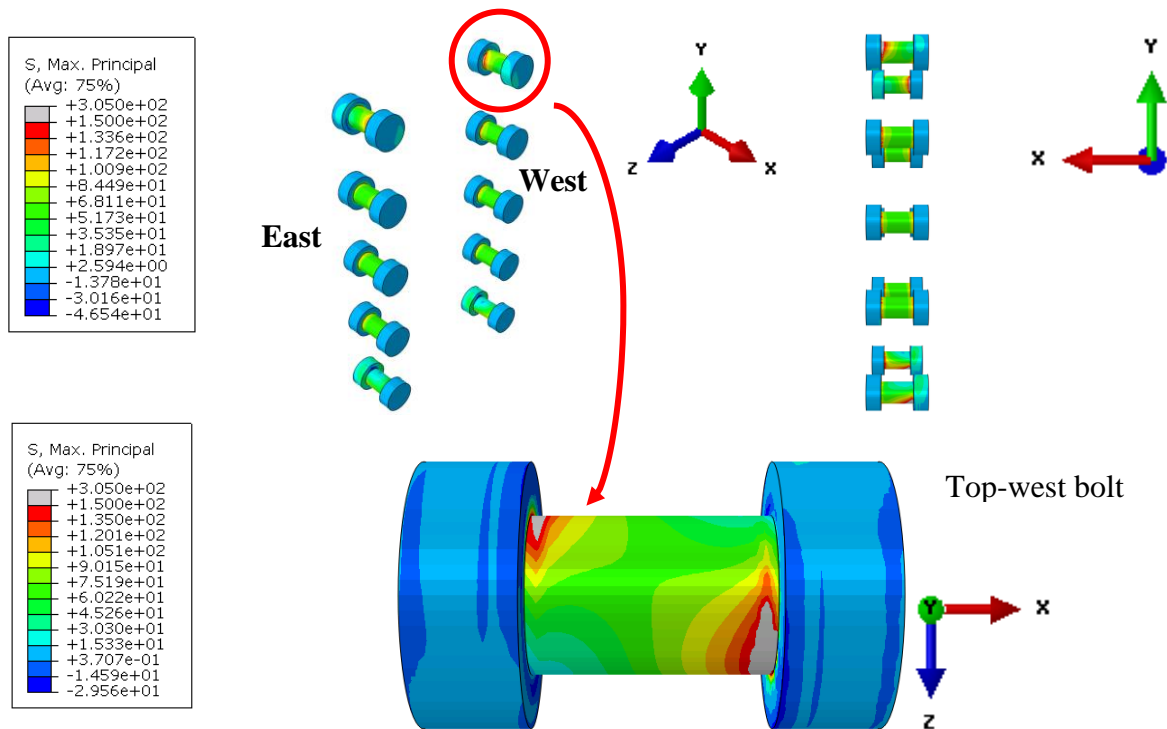


Figure 8-3: Maximum principal stresses of bolts connecting angle and floorbeam web for the model of double-angle connection test FS2, Configuration 1

The simulation results agreed with AL-Emrani's finding (AL-Emrani 2005). In his test, most of the cracks in the rivets were initiated at the junction of the bolt shank and head.

As shown in Figure 8-4, for the bolts connecting the angle leg and the stringer, stresses also concentrated at the junction of the shank and head, but stress magnitudes were approximately half that occurring in the bolts connecting the angle leg and the floorbeam web. Moreover, the stress distributions on the stringer–angle bolts and the floorbeam–angle bolts were very different. The stresses in the stringer angle bolts were distributed uniformly along the perimeter of the shank, while the floorbeam–angle bolts had an antisymmetric stress distribution. Moreover, all the bolts connecting the stringer had similar stresses, while the stresses of floorbeam–angle bolts were different along the height of the angle. The stresses of the bolts in the top row and the bottom row were much larger than the rows in the middle.

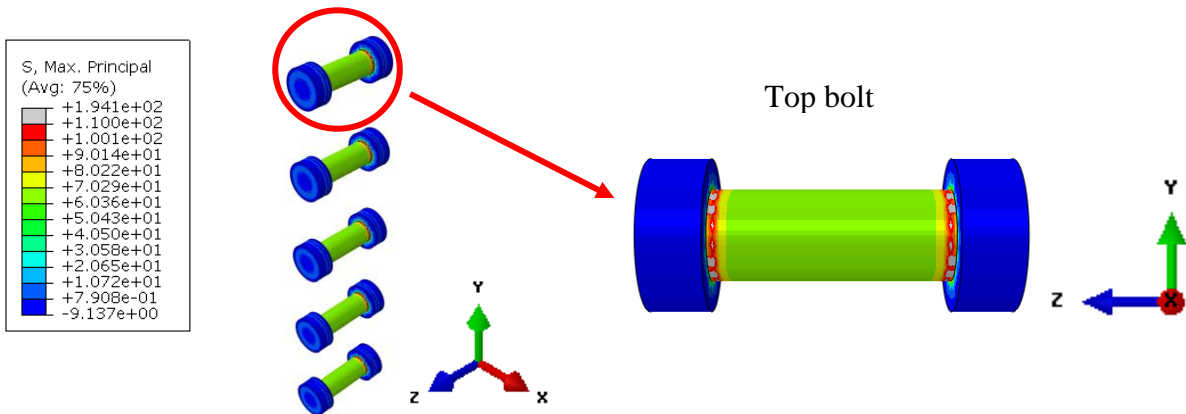


Figure 8-4: Max principal stresses in bolts connecting angle and stringer for the model of double-angle connection Test FS2, Configuration 1

Connection Angles

Figure 8-5 shows the maximum principal stress distribution for the west connection angle. Two locations showed concentrated stresses: the lower part of the angle fillet, and the top bolt hole on the angle leg connecting the floorbeam web. The system was tested upside down, so the corresponding locations on a connection angle in a real bridge are the upper part of the angle fillet and the bottom bolt hole on the leg connecting the floorbeam.

It is worth mentioning that the thickness of the connection angle used in this test was larger than the angle thickness commonly used in existing bridges, so the connection angles were not anticipated to be susceptible to fatigue problem in this test.

However, fatigue cracks on connection angles have been detected in existing bridges. Most of such cracks have been found in the top part of the angle fillet. AL-Emrani (2005) found that most of the cracks on the connection angles initiated at the location close to the angle fillet at the top row of the rivets. The simulation also showed stresses concentrated at the angle fillet. However, the simulations also indicated that the stresses at the top bolt hole of the angle leg connecting the floorbeam were three times larger than the stress at the angle fillet; this has not previously been reported as a location sensitive to fatigue.

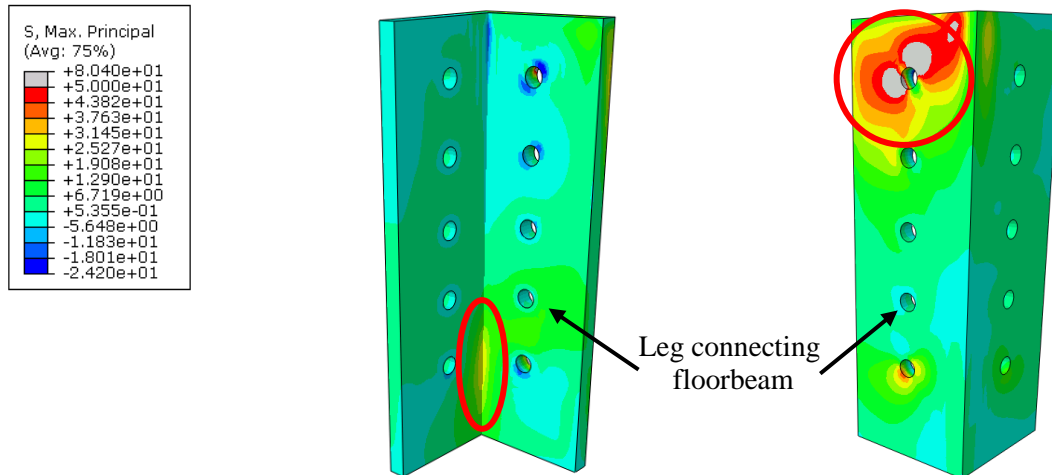


Figure 8-5: Maximum principal stresses of west connection angle for the model of double-angle connection Test FS2, Configuration 1

Floorbeam Web

As shown in Figure 8-6, the top edge of the connection plate was pushed into the floorbeam web from the connection plate side as the actuator moved upwards, generating compressive stresses on the connection plate side and tension stresses on the fascia side of the floorbeam web. The bottom edge of the connection plate, in contrast, was being pulled away from pulling the floorbeam web such that the bottom row of the bolts produced compressive stresses on the web fascia side and tension stresses on the connection angle side.

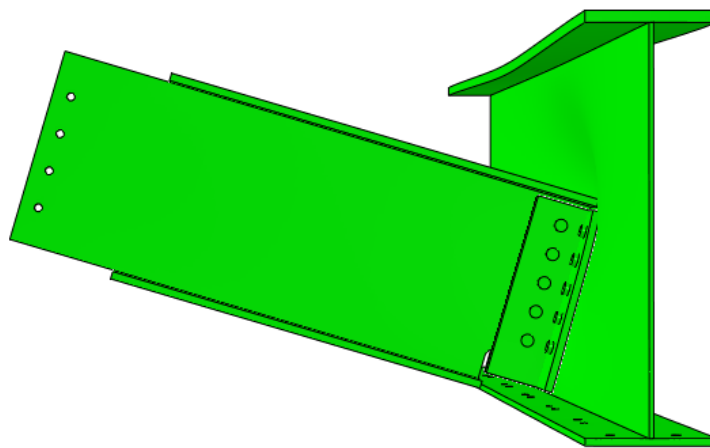


Figure 8-6: Floorbeam web and connection angle deformation for the model of double-angle connection Test FS2, Configuration 1 (Deformation is magnified 3.5 times.)

This behavior resulted in tension stresses concentrating in the top edge of the connection angle on the web fascia side and the bottom row of the bolts on the connection angle side. The compressive stresses, in contrast, concentrated at the top edge of the connection angle on the connection angle side and the bottom row of the bolts on the web fascia side.

As presented in Figure 8-7, the simulation results showed a large area of the floorbeam web exceeded the steel yielding limit, but there has been no suggestion in the literature indicating that floorbeam webs with double-angle connections are particularly susceptible to fatigue. Rather, fatigue cracks have usually been reported at connection angles, rivets, and stringer cope regions.

The maximum stresses in the double-angle connection model were one order of magnitude less than in the simulation of the single-plate connection.

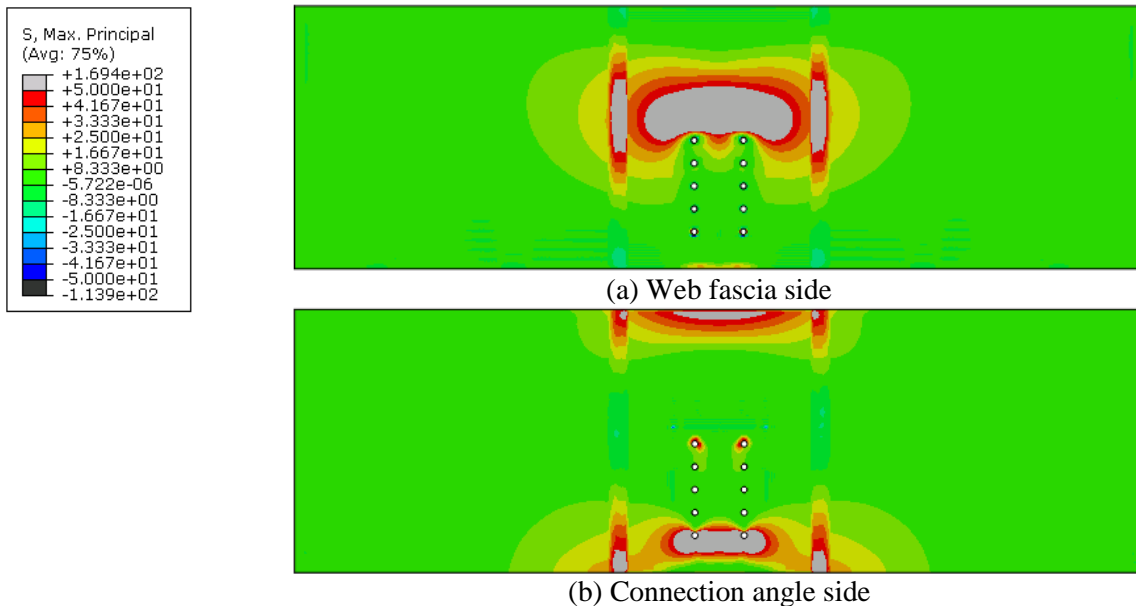


Figure 8-7: Maximum principal stresses of floorbeam web for the model of double-angle connection Test FS2, Configuration 1

Stringer Cope

Although the stringer cope region was anticipated to be fatigue-prone, the physical test did not reveal any cope cracking. The computed results (Figure 8-8) indicated that stresses in the stringer

cope region were smaller than other parts of the connection. The cope stresses were one order of magnitude less than the stresses on the floorbeam web, and were a quarter of the stresses on the connection angles, which were intentionally built to be thicker than commonly-used connection angles.

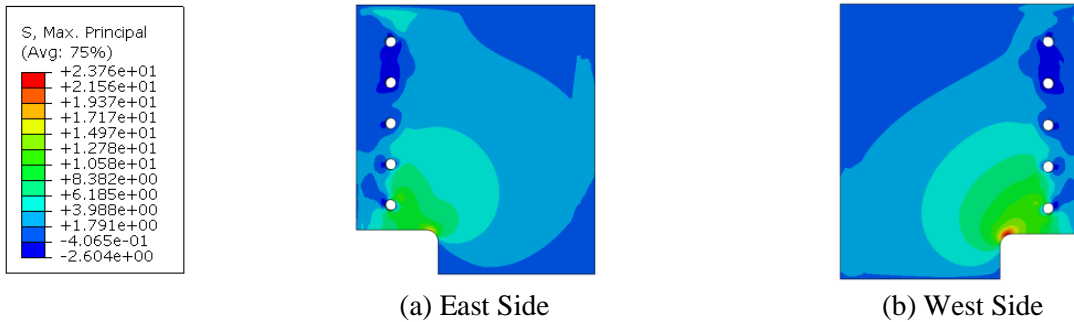


Figure 8-8: Maximum principal stresses of stringer cope for the model of double-angle connection Test FS2, Configuration 1

8.2 Model for Physical Test FS2 Configuration 3

8.2.1 Introduction

In the physical test, the original test setup was too flexible to sustain a large enough load range to produce fatigue cracking. The largest load range that could be applied in a smooth sinusoidal shape was only 3-5 kip. After applying 950,000 cycles in Configuration 1 and 350,000 cycles in Configuration 2, the specimen still did not develop any fatigue cracking. Because of this rather surprising behavior, the researchers wanted to investigate the performance of the specimen under increased shear loads.

The companion model to the physical test that included a roller placed underneath the center of the stringer was created (Figure 8-9) using Abaqus. An actuator load of 10 kip was applied downward as a uniformly distributed surface load on the actuator plate. The other details were the same as for the model introduced in Section 8.1.1.

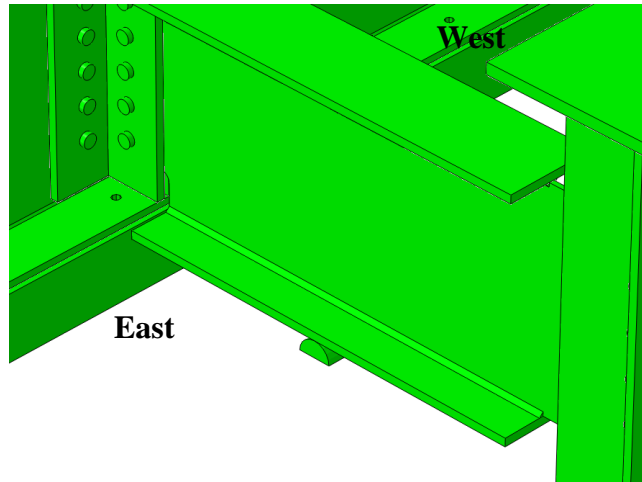


Figure 8-9: Finite element model for double-angle connection, Specimen FS2, Configuration 3

8.2.2 Simulation Results

The stresses obtained from this model were low-magnitude in the floorbeam web, stringer, and connection angles. Figure 8-10 to Figure 8-14 present the maximum principal stresses for bolts, connection angles, stringer cope, and floorbeam web.

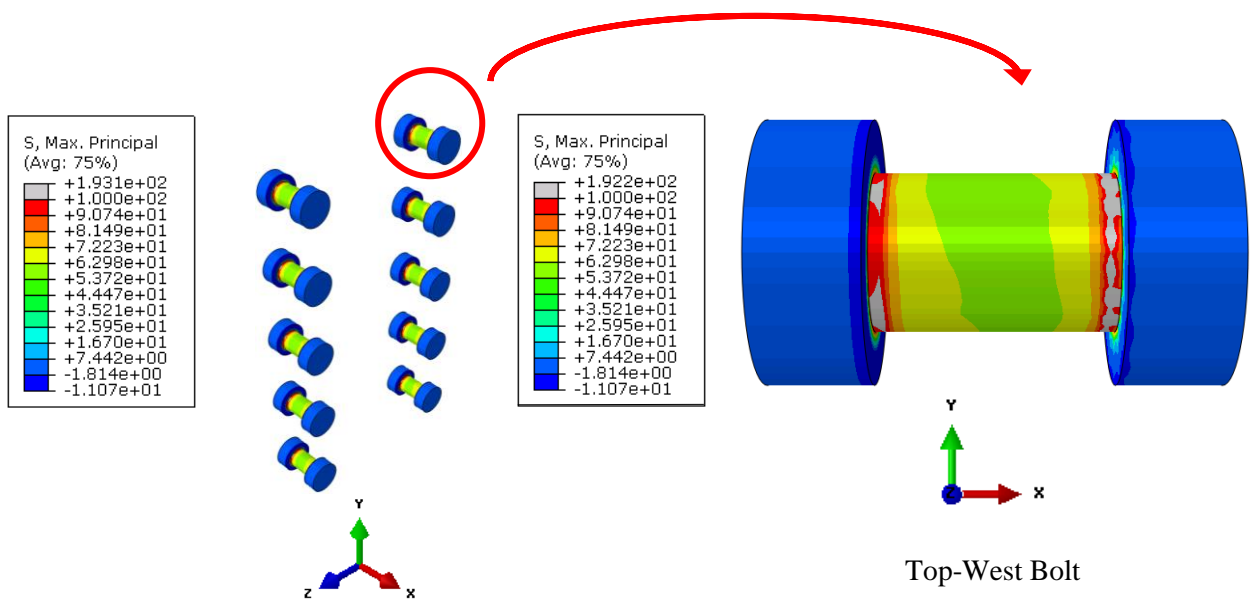


Figure 8-10: Maximum principal stresses of bolts connecting angle and floorbeam web for the model of double-angle connection test FS2, Configuration 3

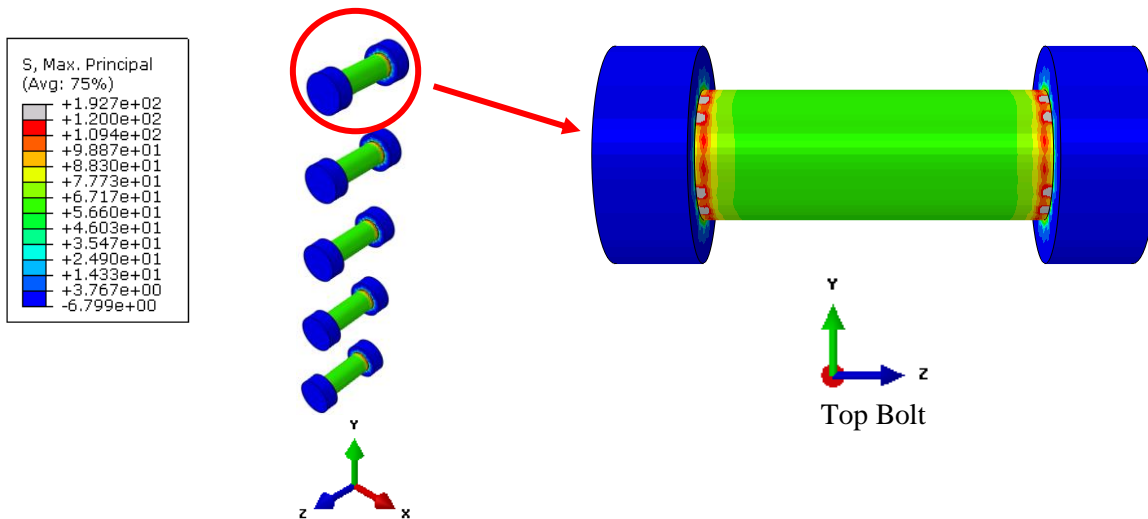


Figure 8-11: Maximum principal stresses of bolts connecting angle and stringer web for the model of double-angle connection test, Specimen FS2, Configuration 3

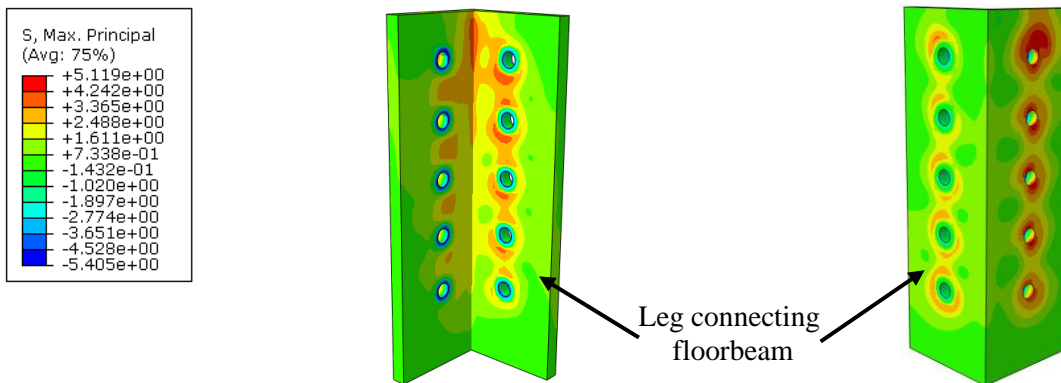


Figure 8-12: Maximum principal stresses of west connection angle for the model of double-angle connection test, Specimen FS2, Configuration 3

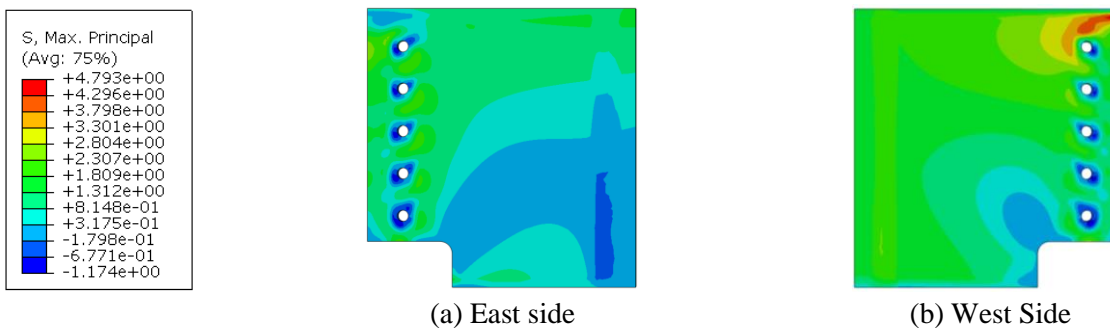


Figure 8-13: Maximum principal stresses of stringer cope for the model of double-angle connection test, Specimen FS2, Configuration 3

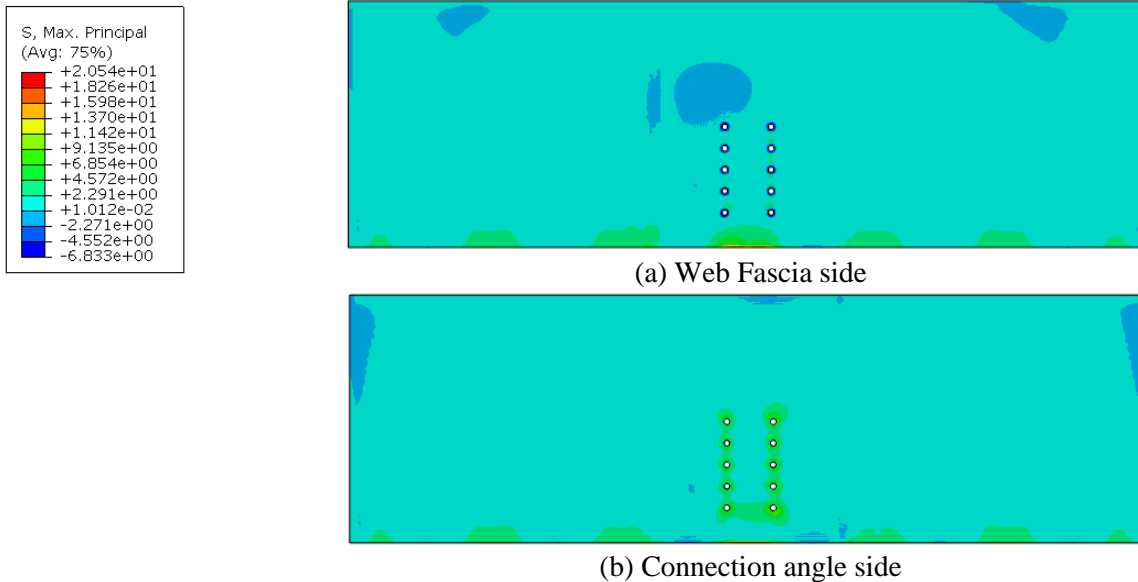


Figure 8-14: Maximum principal stresses of floorbeam web for the model of double-angle connection test, Specimen FS2, Configuration 3

8.3 Model for Virtual Specimen with Shorter Floorbeam Web

8.3.1 Introduction

The depths of the floorbeam and the stringer simulated in the previous models were 36 in. and 21.2 in., respectively. The ratio of the floorbeam-to-stringer depth in this test was larger than the ratio generally used in existing bridges. To consider the implications of a connection with a smaller floorbeam-to-stringer depth ratio, a model with a shorter floorbeam web depth was created, as shown in Figure 8-15.

The depth of the floorbeam web was shortened to 25.5 in., providing a total floorbeam depth of 27 in. All the other details were the same as for the Configuration 1 model, which is discussed in Section 8.1.1.

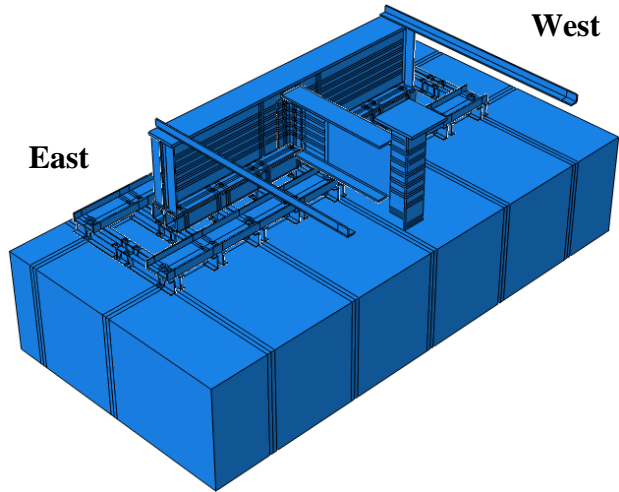


Figure 8-15: Finite element model for double-angle connection with shorter floorbeam web

8.3.2 Simulation Results

The stress distribution in the model with a shorter floorbeam web was very similar to the model created for Configuration 1. The stresses in the stinger cope region were nearly unchanged. The stresses on the bolts, floorbeam web, and connection angles were slightly smaller.

Figure 8-16 to Figure 8-20 present the maximum principal stresses for the bolts, connection angles, floorbeam web, and stringer cope.

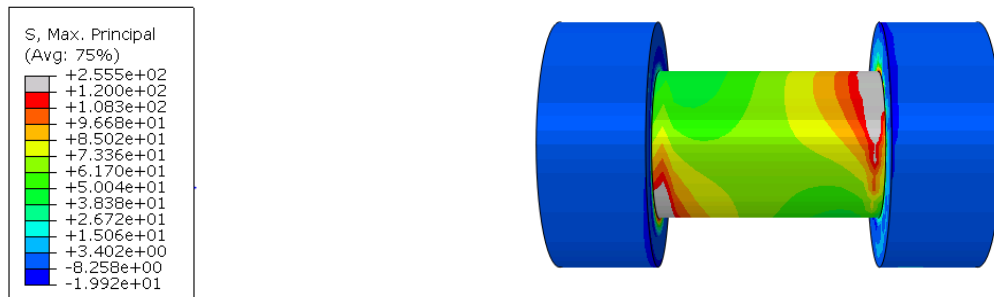


Figure 8-16: Maximum principal stresses of top west bolt connecting angle and floorbeam web for model of double-angle connection with shorter floorbeam web

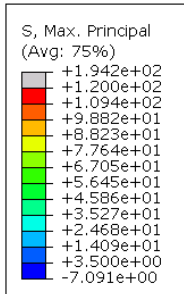


Figure 8-17: Maximum principal stresses of top bolt connecting angle and stringer web for model of double-angle connection with shorter floorbeam web

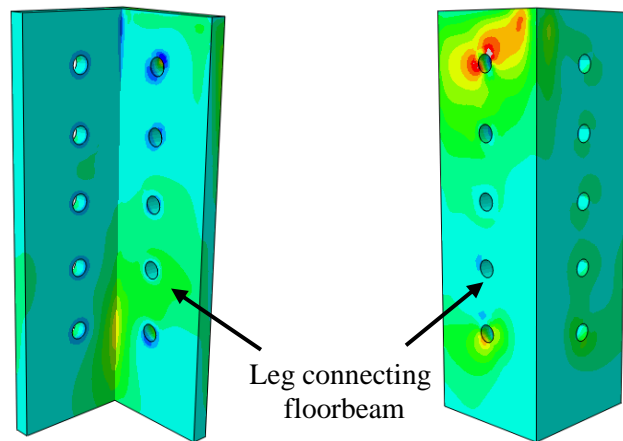
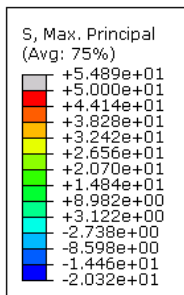
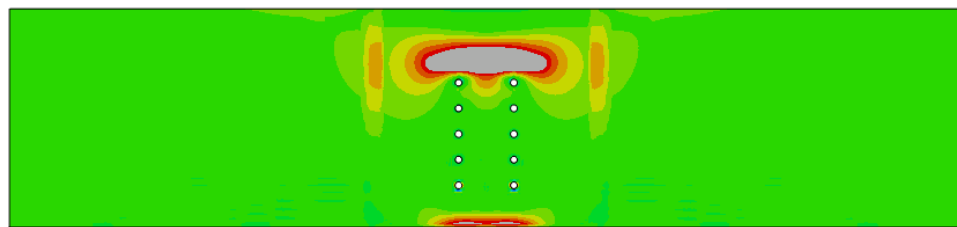
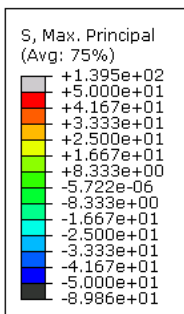
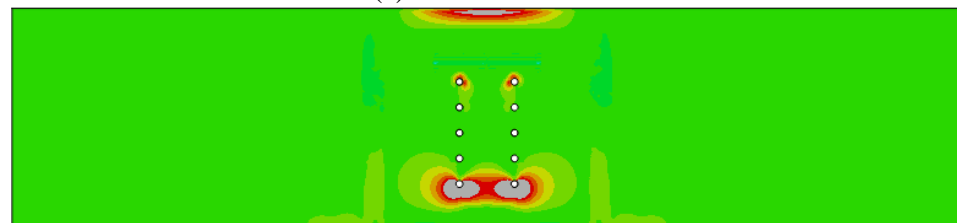


Figure 8-18: Maximum principal stresses of west connection angle for model of double-angle connection with shorter floorbeam web



(a) Web fascia side



(b) Connection angle side

Figure 8-19: Maximum principal stresses of floorbeam web for model of double-angle connection with shorter floorbeam web

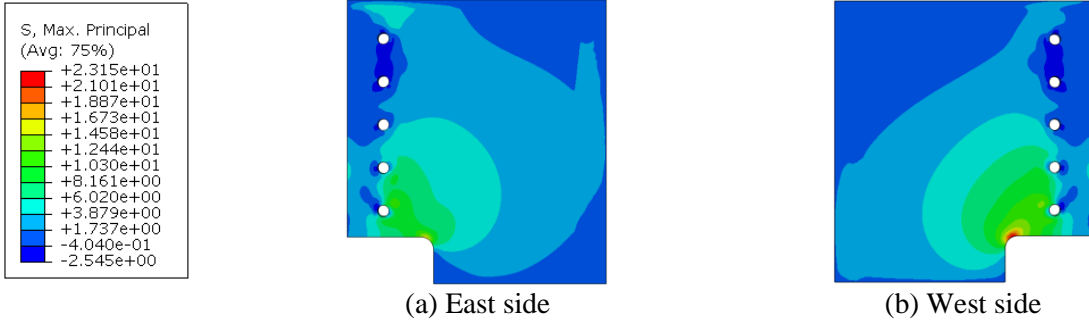


Figure 8-20: Maximum principal stresses of stringer cope for model of double-angle connection with shorter floorbeam web

The simulation results indicated that reducing the floorbeam-to-stringer depth ratio did not significantly increase stress demands in the connection. Therefore, fatigue may not be a concern in this geometry as well.

9. Comparison between Computer Simulation and Physical Test Results for Double-Angle Connection (FS2)

A comparison of the finite element analysis results and the physical test results is provided in this section. As shown in Figure 7-4 and Figure 7-5, strain gages were attached to the floorbeam web and the stringer web to compute stresses in the physical test. The stresses computed from the computer simulations were extracted from the same locations as the strain gage locations.

9.1 Configuration 1

Figure 9-1 presents the values of the stresses computed from strain gage measurements and the stresses extracted from the computer simulation for Configuration 1.

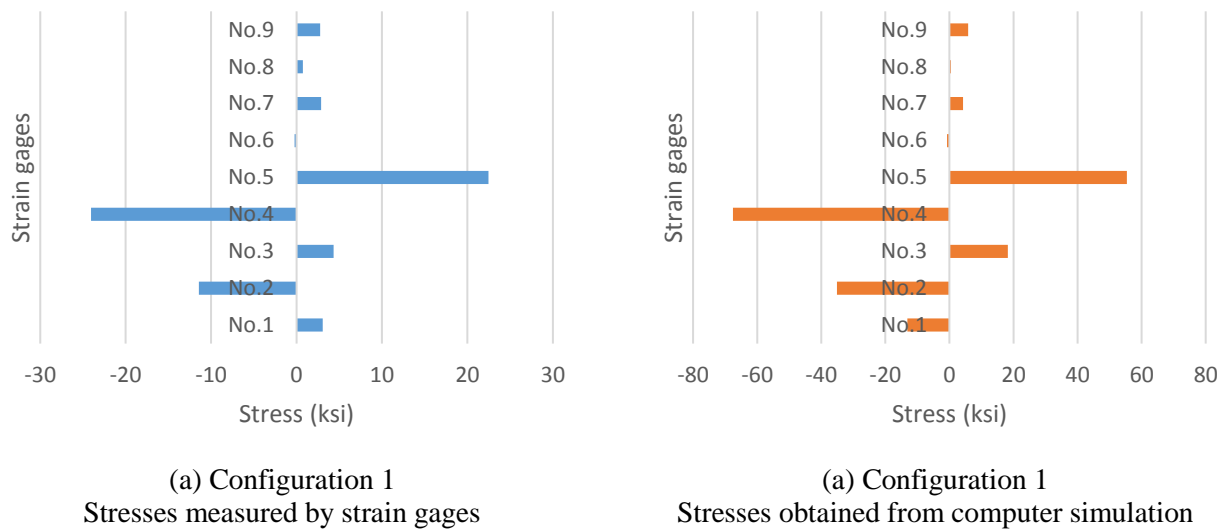


Figure 9-1: Comparison of computer simulation results and physical test results for double-angle connection, Specimen FS2 Configuration 1

Most of the stresses obtained from the computer simulations were much larger than the stresses computed from the strain gages. However, the two results produced similar stress distributions except for Strain Gage 1. This results indicated that the stress distribution obtained from computer simulation was reliable.

Stresses obtained from the physical test and the computer simulation are presented on the stress contour plots in Figure 9-2.

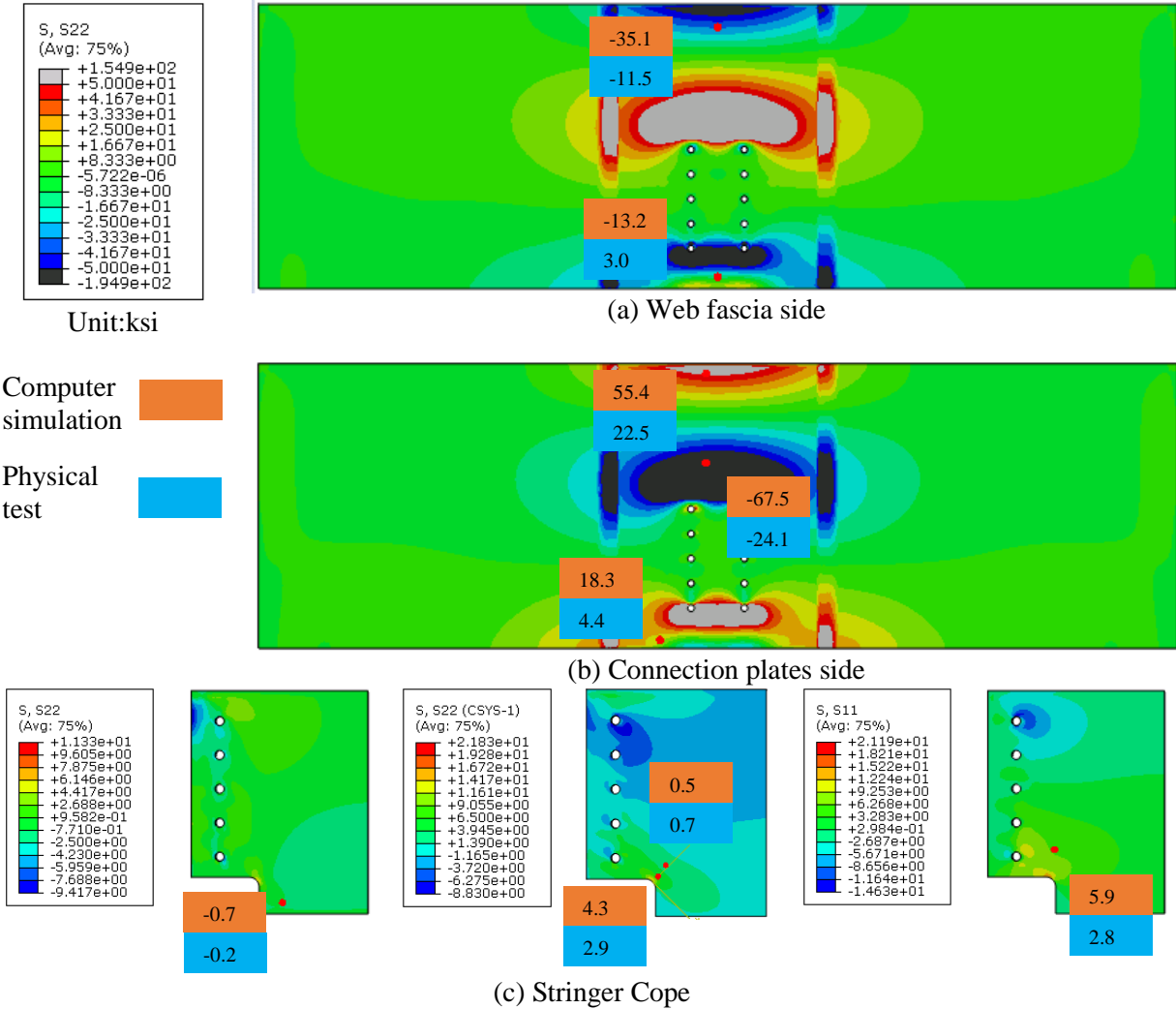
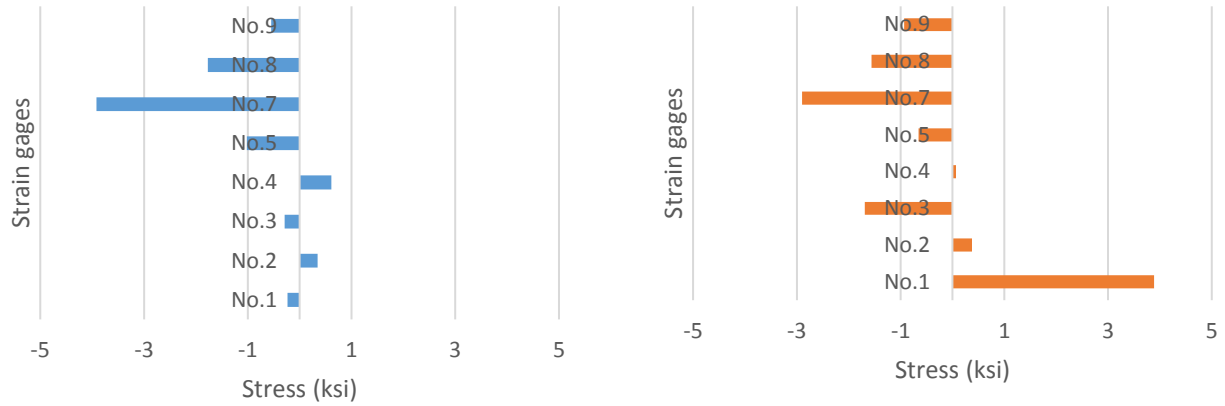


Figure 9-2: Comparison of computer simulation results and physical test results for double-angle connection, Specimen FS2, Configuration 1

9.2 Configuration 3

A comparison of stresses from the computer simulation results and the physical test results is provided in Figure 9-3 and Figure 9-4.



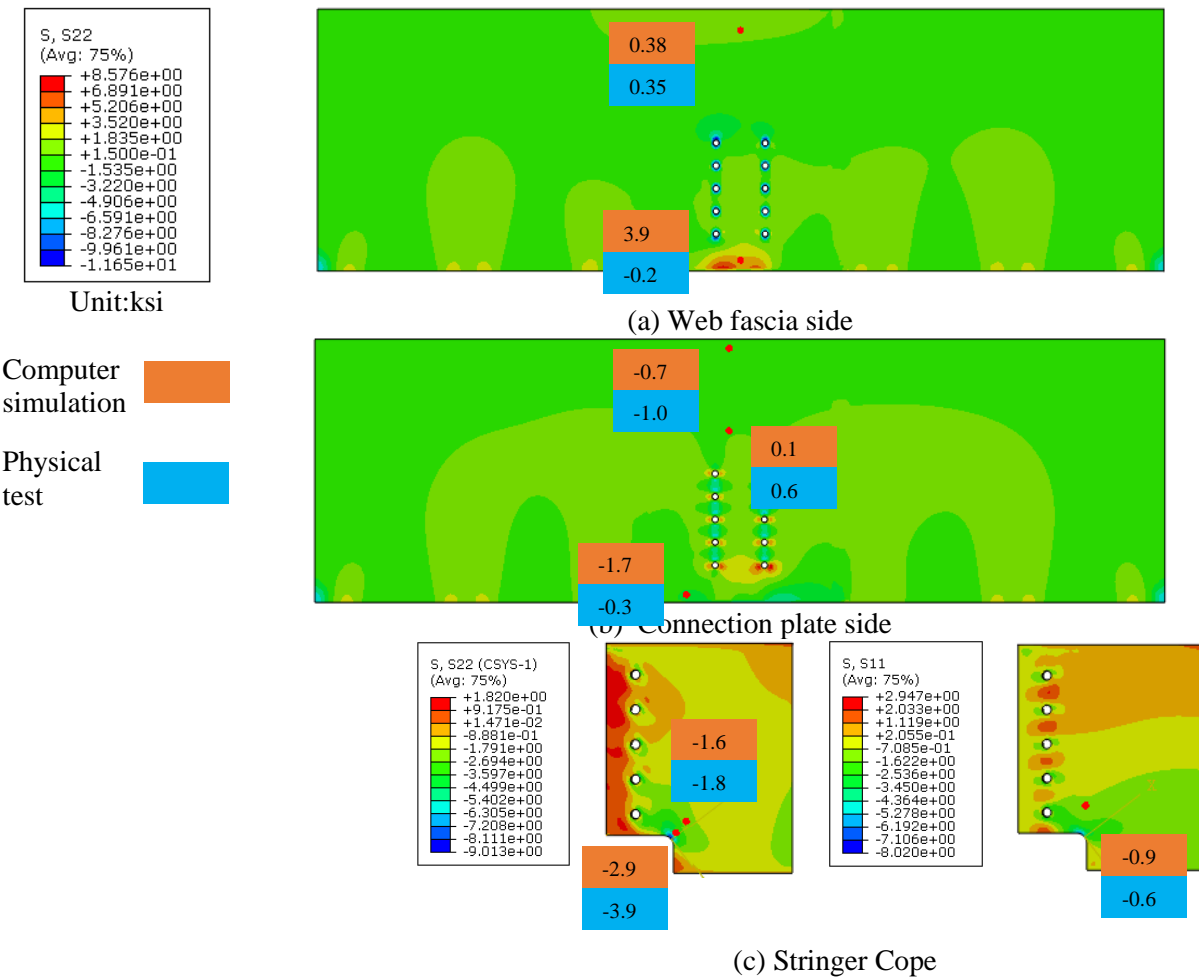
(a) Configuration 1

Stresses measured by strain gages

(b) Configuration 1

Stresses obtained from computer simulation

Figure 9-3: Comparison of computer simulation results and physical test results for double-angle connection Specimen FS2, Configuration 3



(c) Stringer Cope

Figure 9-4: Comparison of computer simulation results and physical test results for double-angle connection Specimen FS2, Configuration 3

Results obtained from both the test and simulation indicated small stress demands. The simulation and test results corresponded well in general. With such low stress demands, it is perhaps not too surprising that fatigue cracks were not able to develop in the specimen. In an effort to produce greater shear in the specimen, a roller was added to the setup under the stringer. The results indicated that this change was less likely to produce fatigue problems in the double-angle connection.

10. Discussion and Conclusion

10.1 Comparison between Single-Plate Connection (FS1) and Double-Angle Connection (FS2)

The difference in spring stiffness between the two connections was not very different until the floorbeam web buckled in the double-angle connection test. However, the spring stiffness of the double-angle connection significantly decreased after the buckling. The double-angle connection in the post-buckling stage was much more flexible than the single-plate connection.

Based on the results of the finite element analysis, the stress concentration produced by the single-plate connection was much larger than that produced by the double-angle connection. Under the same 6 kip actuator load, the peak stress observed in the single-plate connection model was one order of magnitude larger than in the double-angle connection.

For both of the two connections, no fatigue cracking was detected in the stringer cope regions. The strain gage readings and the computer simulations indicated that stresses there were very low.

In this study, the single-plate connection was found to be more sensitive to fatigue than the double-angle connection. The bottom web-gap region was the most vulnerable region. The double-angle connection did not exhibit any localized region with such a high stress concentration. However, the result was only for the specific setup used in this test. For a riveted double-angle connection or a connection with thinner angles, it is conceivable that fatigue issues may occur at the rivets or the angles.

10.2 The Mechanism of Fatigue in Web-Gap Region and Stringer Cope Area

Although fatigue cracks that may develop in the web-gap region and the stringer cope area are induced by relative displacement between adjacent members, the two are actually driven by different mechanisms.

For the web-gap region, cracks are induced by the combined effects of: large localized deformations in the web-gap region; stress concentration at the junction of floorbeam web, weld, and connection plate; and the presence of initial flaws that naturally come with the weld. In repairing a damaged web-gap region, the ultimate goal is to reduce the stresses in front of the cracks, which may be achieved by decreasing the web-gap deformation by reducing or removing the driving force, providing additional load path, redistributing the driving force, or increasing the length of the web-gap by repositioning the connection.

For cracking in a stringer cope, although it may still be categorized as distortion-induced fatigue, the mechanism is more similar to traditional in-plane fatigue. In this case, cracking is induced by the stringer end moment coupled with the presence of the stress concentration at the stringer cope.

The physical test and the corresponding computer simulations all indicated that the stringer cope was less likely to initiate fatigue crack than the web gap region. In a report by Roeder (2001), the author also mentioned that it was difficult to generate a crack in the stringer cope. However, the cracking of stringer copes was still reported in existing bridges. This discrepancy is worthy of further consideration.

Roeder (2001) posited that the behavior of a stringer cope in an existing bridge is more similar to the behavior of a notched specimen than the carefully flame-cut specimens in lab tests. Figure 10-1 presents a comparison of the specimen FS1 stringer cope and a cope in an existing bridge near Topeka, Kansas.



(a) Stringer cope of an existing bridge



(b) Stringer cope of the lab specimen

Figure 10-1: Comparison between stringer cope of an existing bridge and the lab specimen

The author here agrees with Roeder (2001). Figure 10-1(a) shows a stringer cope in an existing bridge, and it indeed appears to be a more severe detail than that tested in the lab. This means that the fabrication method used in these aging bridges may be an important matter that influenced the result. In addition to the potential for fatigue cracking created by workmanship, the flame-cutting process can leave a region of hardened and brittle material adjacent to the cut (Mertz 2012), which may also play a role in fatigue cracking.

Roeder (2001) also mentioned in his report that the surface condition might be another issue. During the long service life of an aging bridge, its surfaces may be much coarser than a new lab specimen. Initial flaws are not important for the rate of crack propagation, but they are a major factor affecting the crack initiation life of the detail.

10.3 Suggestions for Using the Angles-with-Plate Retrofit to Repair Stringer to Floorbeam Connections

In this study, the angles-with-plate retrofit was found to effectively stop the development of fatigue cracks in the web-gap region of the single-plate connection. However, in practice, increasing the connection stiffness may result in increasing the stringer end moment, therefore, raising the possibility of cracking in the stringer cope.

Moreover, cracks in stringer cope areas were reported in existing bridges even though tests usually indicated that those details were not particularly sensitive to fatigue. With retrofits, it is conceivable that the increased stringer end moment may cause or speed up crack initiation in an uncracked stringer cope.

When retrofitting the floorbeam web-gap, the stringer cope should be carefully evaluated and treated if necessary. If necessary, the stringer cope should be ground to smooth the radius and the surface. After the treatment, the stringer cope should be repainted to prevent corrosion. An alternative approach is to increase the cross-section of the stringer cope. This could be achieved by bolting doubler plates or by extending the leg of the angle used in retrofitting the web-gap to cover the stringer cope.

10.4 Conclusion

Physical tests were performed on a single-plate and a double-angle stringer-to-floorbeam connections to study their performance under distortion-induced fatigue. A series of finite element models was created using Abaqus v6.12 to capture the geometry and the physical properties of the test set-ups. The results indicate that the angles-with-plate retrofit can effectively repair distortion-induced fatigue damage in web-gap regions.

10.4.1 Single-Plate Connection (FS1)

- Cracks initiated and propagated in the bottom floorbeam web-gap region. The cracks first initiated at the end of the connection plate-to-floorbeam web weld, grew vertically along the weld, and then horizontally into the web. The floorbeam web-to-bottom flange weld crack appeared later. No cracking was detected anywhere else, including the stringer cope region.

- Cracks on the floorbeam web grew slowly and steadily after they were detected. The growth rate did not significantly increase as the cracks grew longer. The growth rate for Crack 1 in Trial 1 was 8.3 in. per million cycles, and the fastest crack growth in Trial 8 occurred at Crack 8, with a growth rate of 14.6 in. per million cycles. However, the floorbeam web-to-bottom flange weld crack propagated very quickly once it was detected. The growth rate for this crack was 40.6 in. per million cycles. Without a retrofit in place, the specimen soon reached a critical level.
- The angles-with-plate retrofit successfully stopped the development of cracks up to:
 - 3 in. long floorbeam web-to-bottom flange weld crack, and
 - Cracks distributed in a 3 in. × 2 in. (width × height) area in the bottom web-gap region

Moreover, the angles-with-plate retrofit effectively halted all crack propagation under the increased load range, under which the displacement of the retrofitted connection was the same as the displacement of the unretrofitted connection under the original load range.

- The bottom flange-to-web weld crack had already become a long crack when it was detected. However, the width of the crack was so small that it was very difficult to detect the crack earlier.
- Without the retrofit, the strain gages located at the lower part of the floorbeam web on the connection plate side (Strain Gages 6 and 7) indicated that region was losing its load-carrying capability as the cracks propagated in the floorbeam web and on the weld connecting the floorbeam web and the bottom flange. The two strain gages (Strain Gages 6 and 7) were very sensitive to crack growth. Stresses in this region could be used to detect cracks and monitor structural health.

- The stresses in the regions near the junction of the floorbeam and the stringer were very complex, and not easily determinable by applying simple structural mechanics principles.
- The retrofit provided an additional load path for the web-gap, and therefore reduced stresses in the damaged region. The computer simulations indicated that the retrofit was able to reduce peak stresses along the cracks that developed on the web by 80% and by 90% along the crack at the web-to-flange weld. It also mitigated the distortion of the stringer cope, thus reduced the stresses in the cope area. However, the stresses in the stringer cope region were low enough such that fatigue cracks were less likely to initiate there.

10.4.2 Double-Angle Connection (FS2)

- Three configurations were applied in the test, but none of them resulted in fatigue cracking in the connection. The stringer cope region was anticipated to be sensitive to fatigue in the test, but the physical tests and the computer simulations indicated that stresses at the cope were very low, and thus fatigue problems were unlikely to occur.
- The stresses and deformations obtained from the shear-only configuration (Configuration 3) were extremely low magnitude, indicating that the connection was also not very susceptible to fatigue under this loading condition.

In the physical tests, the angles-with-plate retrofit successfully stopped fatigue crack propagations in the bottom web-gap region of the single-plate stringer-to-floorbeam connection. The finite element analysis results indicated that stresses in the bottom web-gap regions were significantly reduced after retrofitting. Both the physical test and the finite element analyses indicated that the bolted double-angle stringer-to-floorbeam connection is less prone to distortion-induced fatigue damage than the single-plate connection. The stringer cope regions were expected to be sensitive

to fatigue, however, no fatigue cracks were detected in these regions in the tests and stresses were found to be low in both of the physical test and the finite element analysis.

10.5 Suggestions for Future Research

In evaluating the effectiveness of a distortion-induced fatigue retrofit, most research has been performed on component tests, small-scale tests, or using numerical analysis. The studies on the performance of these retrofits in large-scale tests or existing bridges are very limited.

Ever since distortion-induced fatigue problems have been apparent, engineers have realized that a “shear connection” cannot be treated as a true pin. The name “semi-rigid connection” is more accurate. However, few studies have been performed aimed at studying the properties of these connections under moments, and there is a lack of quantitative equations to determine their properties.

The following are several suggestions for future research:

- More field tests are needed to understand the distortion-induced fatigue performance of existing floorbeam-stringer bridges. Data needed includes stress ranges, local deformations, relative displacements between adjacent members, spring stiffness of connections, and stringer end moments.
- More large-scale tests or tests on real bridge components are needed to evaluate the performance of retrofits.
- More studies are needed to optimize the angles-with-plate retrofit and provide guidance in choosing the proper retrofit configuration and dimensions.
- More studies are needed to quantitatively determine the bending properties of semi-rigid connections, and their use in analyzing distortion-induced fatigue problems.

- Specific rules are needed to guide the process of repairing and evaluating distortion-induced fatigue.

References

- Alemdar, F., Nagati, D., Matamoros, A., Bennett, C., and Rolfe, S. (2014). "Repairing Distortion-Induced Fatigue Cracks in Steel Bridge Girders Using Angles-with-Plate Retrofit Technique. I: Physical Simulations." *J. Struct. Eng.*, 10.1061/(ASCE)ST.1943-541X.0000876, 04014003.
- Alemdar, F., Overman, T., Matamoros, A., Bennett, C., and Rolfe, S. (2014). "Repairing Distortion-Induced Fatigue Cracks in Steel Bridge Girders Using Angles-with-Plate Retrofit Technique. II: Computer Simulations." *J. Struct. Eng.*, 10.1061/(ASCE)ST.1943-541X.0000874, 04014004.
- Al-Emrani, M. (2005). "Fatigue Performance of Stringer-to-Floor-Beam Connections in Riveted Railway Bridges." *J. Bridge Eng.*, 10.1061/(ASCE)1084-0702(2005)10:2(179), 179-185.
- Bennett, C., Matamoros, A., Barrett-Gonzalez, R., Rolfe, S. (2014). "TPF-5(189): Enhancement of Welded Steel Bridge Girders Susceptible to Distortion-Induced Fatigue." Structural Engineering and Engineering Materials SM Report No. 106, University of Kansas, Lawrence, KS.
- Dexter, R. J., Ocel, J. M. (2013). "Manual for Repair and Retrofit of Fatigue Cracks in Steel Bridges." Draft Report to Federal Highway Administration No. FHWA-IF-13-020, University of Minnesota, Minneapolis, MN.
- Fisher, J. W., Jian, J., Wagner, D. C., and Yen, B. T. (1990). "Distortion-induced fatigue cracking in steel bridges." *NCHRP Rep. 336*, Transportation Research Board, Washington, D.C.
- Haghani, R., Al-Emrani, M., Heshmati, M. (2012). "Fatigue-Prone Details in Steel Bridges." *Buildings*, 2(4), 456-476.
- Hartman, A., Bennett, C., Matamoros, A., Rolfe, S. (2013). "Innovative retrofit technique for distortion-induced fatigue cracks in steel girder web gaps." *Bridge Structures*, 9, 57-71.
- Liu, H. (2015). "A Finite-Element-Based Approach to Modeling Cracking & Repairs for Distortion-Induced Fatigue in Steel Bridges." Ph.D. Dissertation, University of Kansas, Lawrence, KS.
- Mertz, D. (2012). "Steel Bridge Design Handbook: Design for Fatigue." Technical Report to U.S. Department of Transportation Federal Highway Administration No. FHWA-IF-12-052-Vol.12, HDR Engineering, Inc., Pittsburgh, PA.
- Roeder, C. W., MacRae, G. A., Kalogiros, A. Y., Leland, A. (2001). "Fatigue Cracking of Riveted, Coped, Stringer-to-Floorbeam Connections". Final Report to Washington State Department of Transportation No. WA-RD 494.1, University of Washington, Seattle, Washington.
- Wipf, T. J., Greimann, L. F., Khalil A. H., and Wood, D. (1998). "Preventing Cracking at Diaphragm/Plate Girder Connections in Steel Bridges." Iowa DOT Project HR-393, Center for Transportation Research and Education, Iowa State University, Ames, IA.

Wipf, T. J., Greimann, L. F., Wood, D. L., Phares, B. M. and Tarries, D. (2003). "Retrofit Methods for Distorsion Cracking Problems in Plate Girder Bridges." Iowa DOT Project TR-436, Center for Transportation Research and Education, Iowa State University, Ames, IA.

PART II:

**APPLICATION OF ANGLES-WITH-PLATE RETROFIT FOR REPAIRING
DISTORTION-INDUCED FATIGUE DAMAGE IN SKEWED GIRDER TO
CROSS-FRAME CONNECTIONS**

1. Introduction

1.1 Background

Distortion-induced fatigue is a serious problem faced by many aging bridges, caused by secondary stresses not accounted for in the original design. Secondary stresses are thought to cause approximately 90% of fatigue damage in steel bridges (Connor and Fisher 2005). For example, bolted or riveted girder to cross-frame connections were only designed to transfer shear force. However, although the connections allow generally large rotations, they are not 100% free to rotate. As shown in Figure 1-1, when live loads produce relative displacement between adjacent girders, fatigue moments are generated and produce secondary stresses at the connections. Usually, the fatigue moments are not large-magnitude, but for fatigue-sensitive details, even small load ranges may lead to cracking.

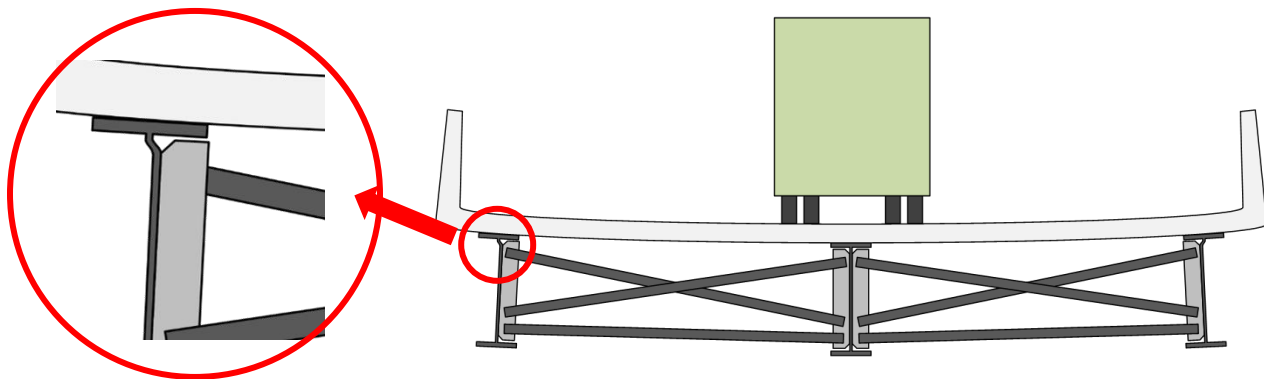


Figure 1-1: Out-of-plane deformation induced by relative displacement between adjacent members caused by living load (Hartman and Hassel, 2010)

The web-gap region is a detail that is highly sensitive to distortion-induced fatigue. Figure 1-2 depicts a web-gap region formed by a girder web, a flange and a cropped stiffener functioning as a connection plate. The cropped ends of the stiffeners were designed to avoid the intersection of two welds. In 1985, the AASHTO bridge design specification instituted the requirement that a connection plate must be connected to both of the flanges. However, in numerous bridges built

prior to 1985, connection was not provided between stiffeners and flanges, because engineers believed that doing so was a good practice to prevent cracking in flanges. This practice produced a very flexible web-gap region in which highly localized bending was able to occur under the rotation of the cross-frame.

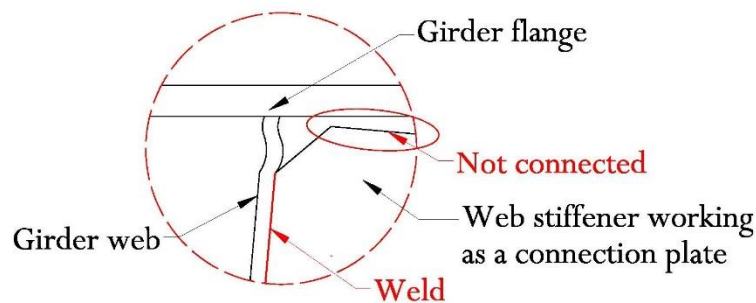


Figure 1-2: Distortion in a web-gap region

Many retrofit methods have been developed to repair distortion-induced fatigue damage. They can be generally be divided into two categories: softening methods and stiffening methods. Softening methods include diaphragm or cross-frame removal, bolt/rivet removal, bolt loosening, connection plate shortening, and drilling a large hole (>3 in.) in the web gap region (Dexter and Ocel 2013). These methods are aimed at reducing the connection stiffness such that less moment is generated in the web gap. Stiffening methods, however, increase connection stiffness by providing positive attachments, such that alternative load paths are provided and stresses at damaged details are reduced.

Many studies have been aimed at developing new stiffening techniques, but bolting is generally accepted as the best connection method to guarantee the efficacy of the attachments. Traditionally, attachments are provided between the flange and the stiffener, but to do so, the concrete deck must be removed to drill bolt holes through the steel flanges when cracking is in the top web-gap. The difficulty involved with removing the concrete deck gives rise to the need to develop an alternative

method (Bennett et al. 2014). The angles-with-plate retrofit is a stiffening method that does not require removing the concrete deck.

Developed at the University of Kansas, the angles-with-plates retrofit has shown its potential in repairing straight girder to cross-frame connections (Alemdar et al. 2014a, 2014b; Hartman et al. 2013; Bennett et al. 2014). As shown in Figure 1-3, the angles-with-plate retrofit provides connection between the stiffener and the girder web, instead of connecting the flange and the stiffener. The retrofit consists two steel angles and a backing plate for an exterior connection, and four angles for an interior connection. The angles connect the stiffener to the girder web, while the backing plate distributes the load across a broad area of the web, such that stresses are no longer concentrated in a small region.



(a) Angle



(b) Backing plate

Figure 1-3: Angles-with-plate retrofit (Alemdar et al. 2014a; 2014b)

The good performance of the angles-with-plate retrofit on straight girder to cross-frame connections is one of the motivations for investigating its performance in skewed connections.

Connections in skewed bridges are thought to be more sensitive to distortion-induced fatigue than non-skewed bridges (Fisher and Mertz 1984). In a skewed bridge, with a layout such that cross-frames are placed perpendicular to the girder web, each cross-frame is connecting two different positions along the span. Therefore, the relative displacement between the two positions that the

cross-frame is connecting is usually larger than in a non-skewed bridge. When a layout is used such that bracing is placed parallel to the skew angle (a skewed connection), distortion-induced fatigue is thought to be less of a concern (Hassel et al. 2013), since in this layout the cross-frame is connecting the same span points. The AASHTO Bridge Design Specification [2013] requires that for a bridge with a skew angle larger than 20 degrees, cross-frames must be provided perpendicular to the girder web (AASHTO 2013), due to concerns regarding cross-frame flexibility and the effectiveness of live load distribution. However, some states still allow the use of skewed connections beyond this limit (Hassel et al. 2013).

1.2 Objectives and Scope

This study consists of two parts. Part one included physical tests conducted on 20-degree and 40-degree skewed girder to cross-frame connection subassemblies. Part two presents the results from a series of computer models created using the commercially-available finite element analysis software Abaqus V6.13.

The computer simulations are described in the companion report *Computer Simulations of Retrofitting Skewed Steel Bridges for Distortion-Induced Fatigue* authored by Yaqin Chen, in which the simulation results for the web-gap regions are presented.

The report here describes the physical tests, presents a comparison of the physical test results and the computer simulation results, and includes a discussion of the influence of the angles-with-plate retrofit on stresses on the cross-frame gusset plate.

The objective of this study was aimed at evaluating the efficacy of the angles-with-plate retrofit for repairing fatigue damage in web-gap regions of skewed girder to cross-frame connections, as well as to generate a better understanding of the distortion-induced fatigue performance of skewed girder to cross-frame connections.

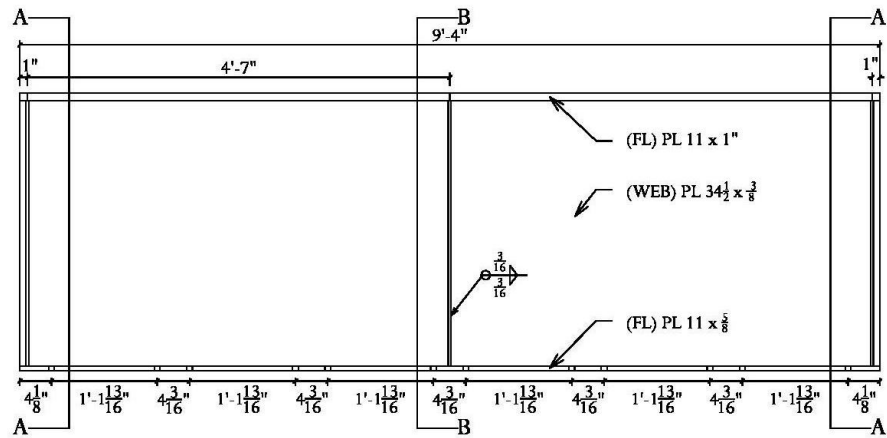
2. Physical Test of the 20-Degree Skewed Girder to Cross-Frame Connection – Test Introduction

2.1 Description of the 20-Degree Skewed Girder to Cross-Frame Specimen

The test specimen consisted of a built-up steel girder and a 20-degree skewed cross-frame. The specimen layout is shown in Figure 2-1. The built-up girder was 9 ft long, 36 in. tall, with a $34\frac{1}{2}$ in. \times $\frac{3}{8}$ in. web, a 11 in. \times 1 in. top flange and a 11 in. \times $\frac{5}{8}$ in. bottom flange. The specimen included a $34\frac{3}{8}$ in. \times 5 in. \times $\frac{3}{8}$ in. transverse stiffener functioning as a connection plate with $1\frac{1}{4}$ in. cropped ends. The stiffener was welded to the centerline of the girder web, but no connection was provided between the connection plate and the girder flanges, such that web gaps were created near the top and bottom flanges.

Four stiffeners were welded to both flanges and the web at the ends of the girder. Both ends of the top flange of the girder were restrained from lateral movement by two angles. The bottom flange of the girder was fixed to the laboratory strong floor by bolting to a tie system of post-tensioned C 5 \times 9 and C10 \times 30 channels. Therefore, the specimen was tested upside-down, with the flange attached to the laboratory floor simulating a top flange connected to a laterally-stiff bridge deck.

ELEVATION



SECTION A-A

SECTION B-B

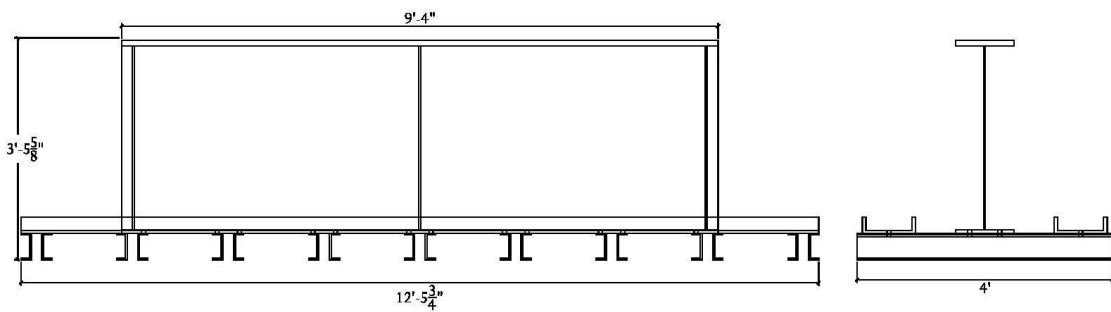
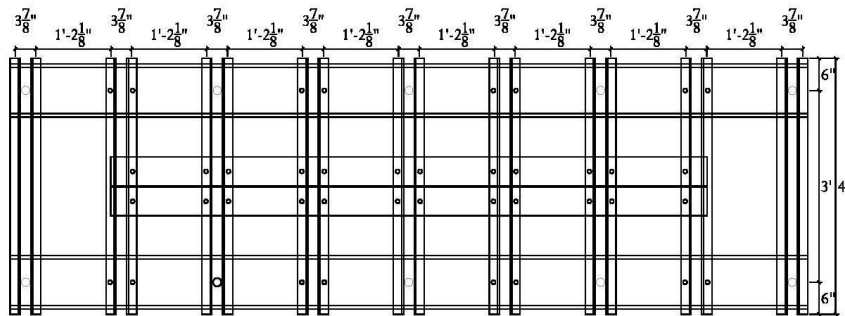
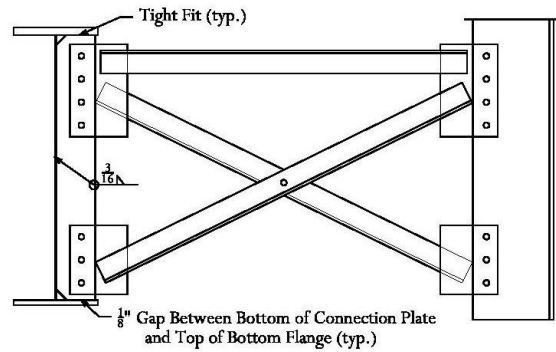
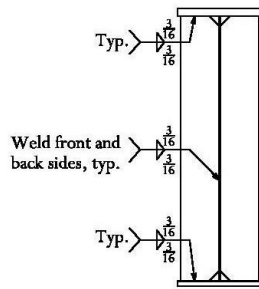


Figure 2-1: Specimen layout

In a real bridge system, the top flange of a girder is restrained by a bridge deck, but this situation is difficult to establish in a component test. By fixing the bottom flange to the laboratory floor, the displacement of the bottom flange was fully restrained, and the influence of in-plane bending was eliminated. Although this kind of component test is different from the in-plane and out-of-plane deformation that occurs in a real bridge, computer simulations performed for the previous girder to cross-frame tests at the University of Kansas showed that the stress distribution in the component test was similar to that of a real bridge (Alemdar et al. 2014a; 2014b).

A 20-degree skewed cross-frame was bolted to the connection plate at the mid-length point of the girder. The details of the cross-frame are presented in Figure 2-2. The far end of the cross-frame was bolted to a WT section, which was then connected to a servo-hydraulic actuator. In the test, the actuator applied upwards cyclic loading to simulate the effect of passing traffic. Lateral movement of the actuator was restrained by two pairs of rollers.

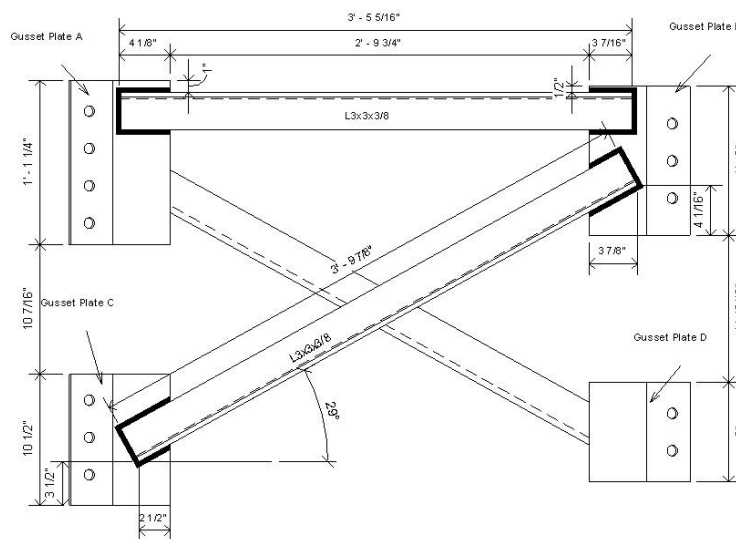


Figure 2-2: Dimensions of the 20-degree skewed cross-frame

The stiffened angles-with-plate retrofit was used in the test; it consisted of two stiffened angles and one backing plate. Figure 2-3 presents the dimension of the retrofit. Photographs of the specimen and retrofit are shown in Figure 2-4.

The bolted connections were made using $\frac{3}{4}$ in. A325-SC bolts. All welds in the tests were $\frac{3}{16}$ in. fillet welds.

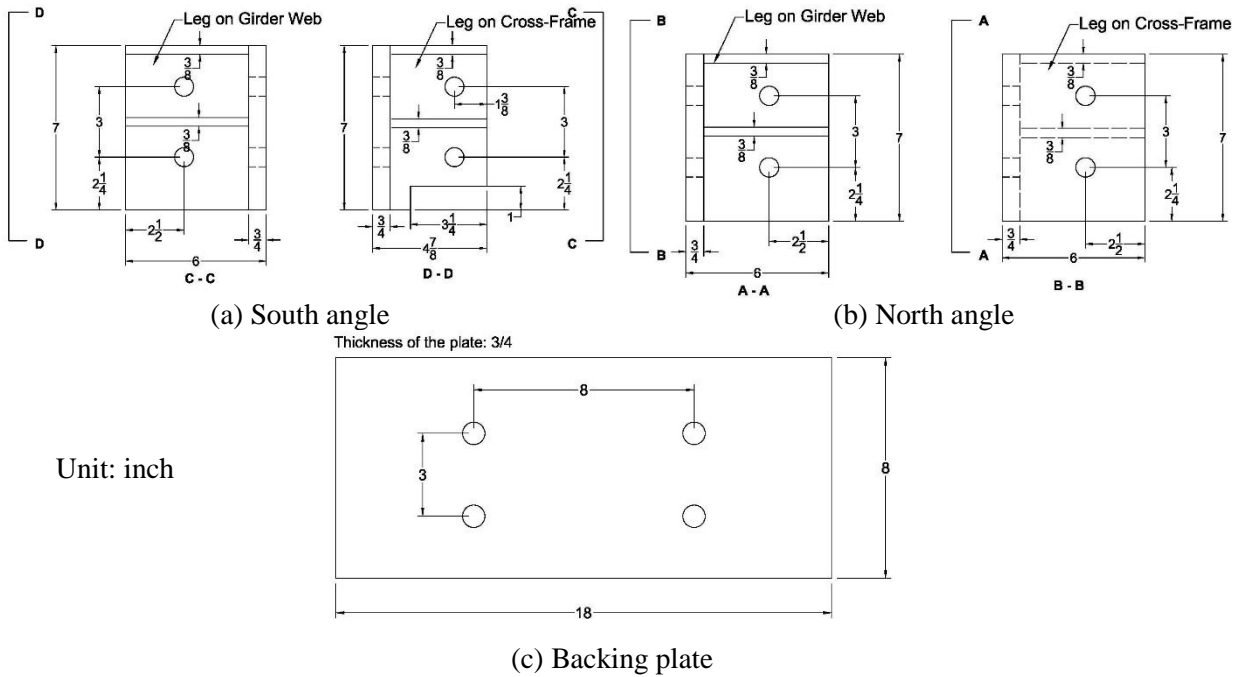


Figure 2-3: Angles-with-plate retrofit dimensions

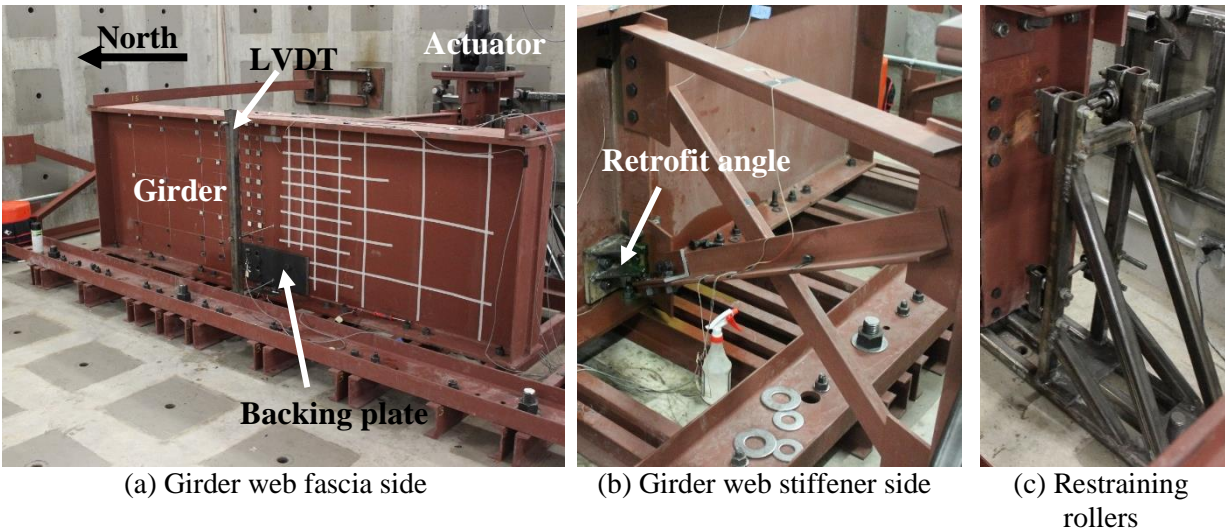


Figure 2-4: Photographs of 20-degree skewed specimen and retrofit

2.2 Instrumentation

Actuator displacements were measured using the integrated LVDT and actuator force data was recorded simultaneously via a load cell.

Strain gages were attached to the specimen at regions susceptible to fatigue problems as detected through finite element analysis and existing literature. In this test, the primary susceptible region was the bottom web-gap.

Three LVDTs (Linear Variable Differential Transformers) were attached at different depths on the girder web at mid-span to measure out-of-plane deformations.

Strain gage readings, LVDT readings, actuator displacement and actuator force were recorded while performing monotonic tests. Schematic drawings showing the LVDT and strain gage placements are presented in Figure 2-5.

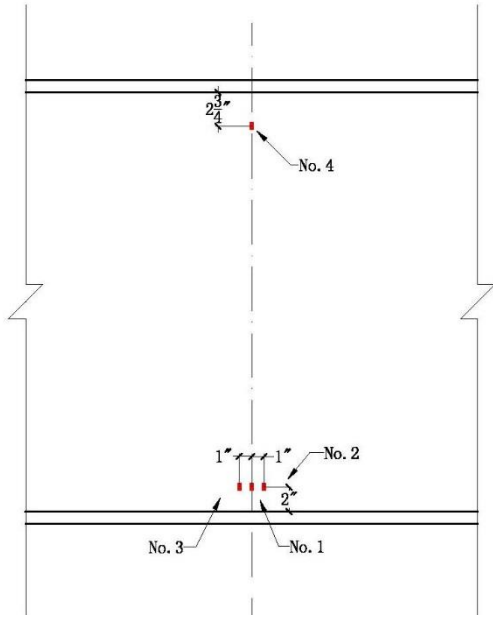
Rotations of the girder web were measured using an array of mirrors attached to the girder web and a laser pointer. Figure 2-6 shows the placement of the mirrors. During the test, the mirrors reflected the laser on a wall opposite to the girder web, such that the movement of the web was magnified and could be recorded. The rotation of the web at the location of each mirror was calculated from the displacement of the reflected light, as shown in Figure 2-7.

When θ is small, $\tan\theta \approx \theta$

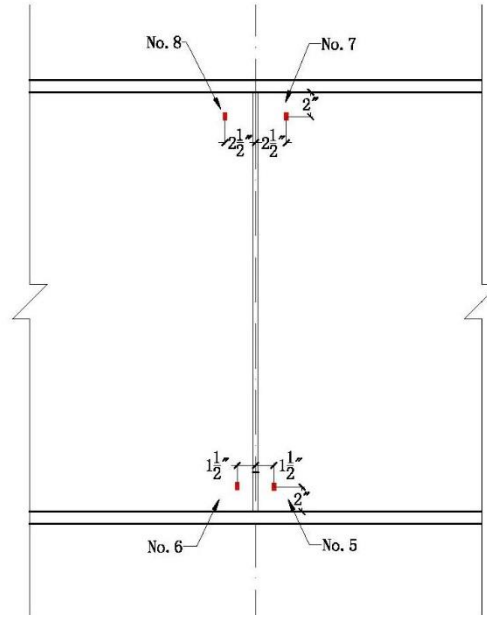
$$\tan\theta_1 = \theta_1 = \frac{\Delta_1}{L}, \quad \tan\theta_2 = \theta_2 = \frac{\Delta_2}{L}$$

$$\theta = \theta_1 - \theta_2 = \frac{\Delta_1 - \Delta_2}{L} = \frac{\Delta}{L}$$

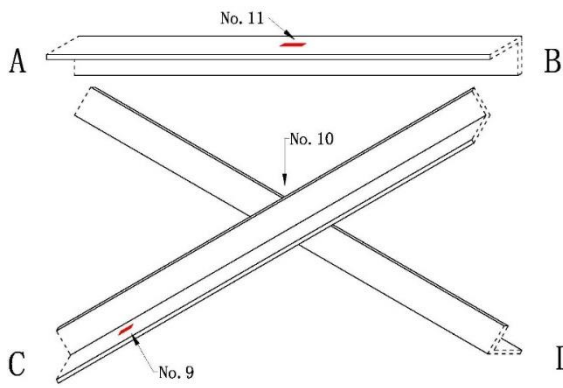
$$\text{Mirror Rotation } \alpha = \frac{\theta}{2} = \frac{\Delta}{2L} \quad (\text{Equation 2-1})$$



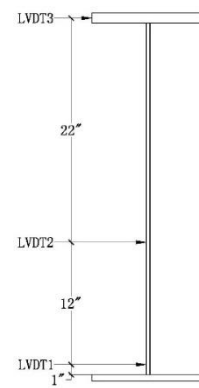
(a) Strain gages on girder web fascia side



(b) Strain gages on girder web stiffener side



(c) Strain gages on cross-frame



(d) LVDTs

Figure 2-5: Strain gage and LVDT placements for 20-degree skewed specimen

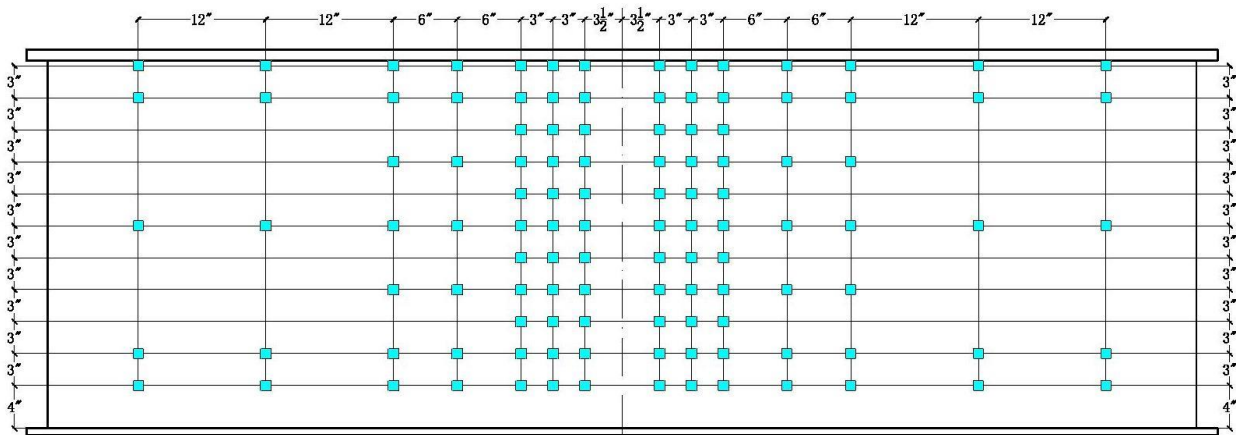


Figure 2-6: Mirror array for the 20-degree skewed specimen

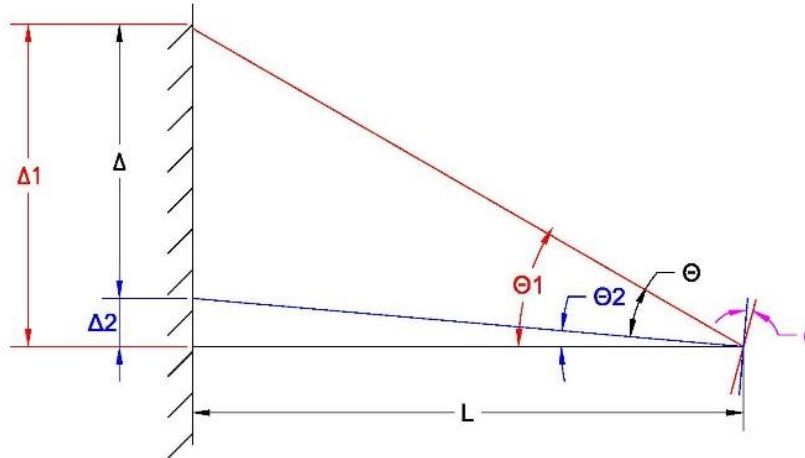


Figure 2-7: Girder web rotation computations, using measured displacement of reflected laser light

2.3 Test Procedure

A summary of the test trials performed on the 20-degree skewed girder to cross-frame specimen is presented in Table 2-1.

Table 2-1: Test summary of 20-degree skewed specimen

Trial	Retrofit status	Number of cycles	Total cycles
Trial 20-1	Unretrofitted	16,504	16,504
Trial 20-2	Retrofitted	1,200,000	1,216,504
Trial 20-3	Unretrofitted	20,000	1,236,504

Load range: 0.5-6.2 kip

Load frequency: 2 Hz

In the test, the actuator provided a cyclic load range of 0.5 kip - 6.2 kip, applied upward, with a sinusoidal wave shape. The specimen was examined at regular intervals for cracking using dye penetrant.

The test consisted of three trials. In Trial 20-1, the specimen was cycled without retrofit to initiate cracks. Trial 20-2 was aimed at testing the efficacy of the angles-with-plate retrofit. In this trial, the retrofit was installed at the bottom web-gap when crack length reached 1¼ in. on the north side of the stiffener and ¼ in. on the south side of the stiffener. The girder was loaded monotonically every 25,000 cycles by slowly increasing the actuator force from 0 - 6 kip while recording actuator force, actuator displacement, LVDT data, and strain gage data (these loadings are referred to as

“monotonic tests”). The retrofit was removed every 100,000 cycles to measure crack lengths at the web-gap, and then reinstalled. 1,200,000 cycles were applied in Trial 20-2. In Trial 20-3, the retrofit was removed and the cracks were allowed to grow freely.

Measurements were taken using the mirror array in both the retrofitted and unretrofitted conditions to evaluate the efficacy of the retrofit.

3. Physical Test of 20-Degree Skewed Girder to Cross-Frame Connection – Test Results

3.1 Crack Initiation and Propagation

3.1.1 Cracks at Girder Bottom Web-Gap

Cracks were observed in the bottom web-gap region 16,504 cycles into Trial 20-1. They grew vertically along the girder web-stiffener weld. When the cracks were detected, they were 1¼ in. on the north side of the stiffener and ¼ in. on the south side of the stiffener. The north side was the side that the skewed cross-frame formed an obtuse angle with the girder web.

The angles-with-plate retrofit was installed immediately after cracks were observed. In Trial 20-2, the retrofit was removed to examine the cracks every 100,000 cycles. The crack propagation rate was slowed dramatically with the retrofit in place. After 1,200,000 cycles had been applied in Trial 20-2, the cracks had grown to approximately 1.6 in. on the north side of the stiffener and 1 in. on the south side of the stiffener, as shown in Figure 3-1.

In Trial 20-3, the retrofit was removed, and the cracks were allowed to grow freely. The crack propagation rate increased again, and the crack lengths reached 4¼ in. on the north side and 2.8 in. on the south side over just 20,000 cycles.

Throughout the test, cracks propagated vertically along both weld lines connecting the girder web and the stiffener, but never propagated into the girder web.

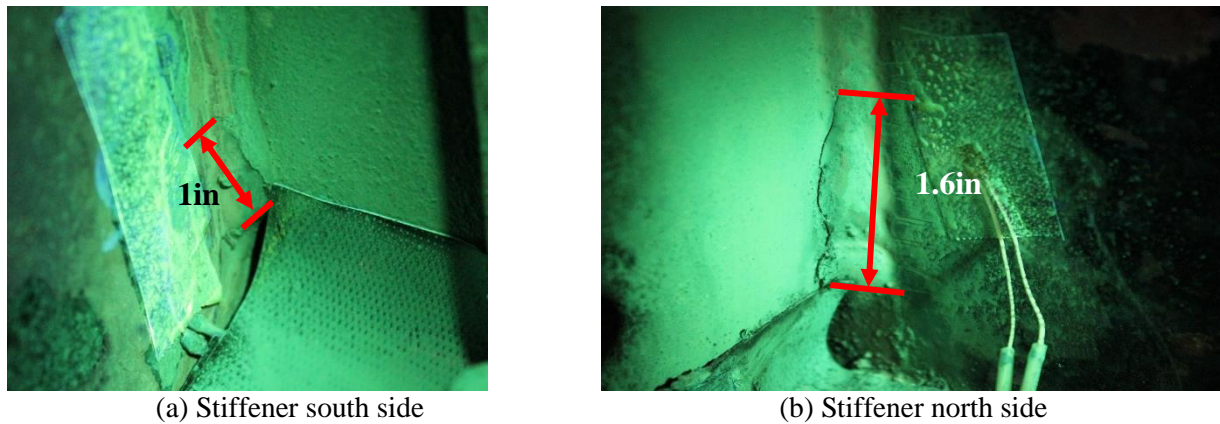
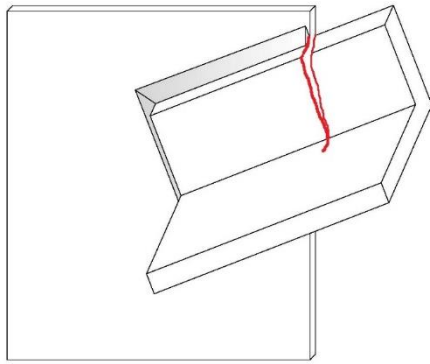


Figure 3-1: Cracks at bottom web-gap for 20-degree skewed specimen 1,200,000 cycles into Trial 20-2

3.1.2 Cracks on Cross-Frame

The cross-frame was not considered to be sensitive to fatigue since cross-frame cracking has rarely been reported. However, unexpected, the cross-frame failed four times in Trial 20-2.

697,000 cycles into Trial 20-2, the actuator displacement interlock was triggered. After inspecting, a crack was observed at the junction of the cross-frame angle and the bottom gusset plate. As presented in Figure 3-2, when it was observed, the crack had already cut through the vertical leg of the angle. The exact time of the crack initiation was unknown. However, initiation occurred near this cycle count since the girder had been inspected just 22,000 cycles earlier and the crack was not observed. After the crack was detected, a steel angle was bolted as a retrofit on the damaged cross-frame, as shown in Figure 3-2. However, it was not able to provide enough stiffness and was not able to stop the crack growth. The crack cut through the remaining cross-frame angle in less than 100,000 cycles.



The angle bolted to repair the crack on the cross-frame

Figure 3-2: Crack on 20-degree skewed cross-frame 697,000 cycles into Trial 20-2 and the steel angle bolted to repair it

775,000 cycles into Trial 20-2, a large crack was observed on the bottom gusset plate of the cross-frame (Figure 3-3). It grew along the cross-frame angle-to-gusset plate weld.

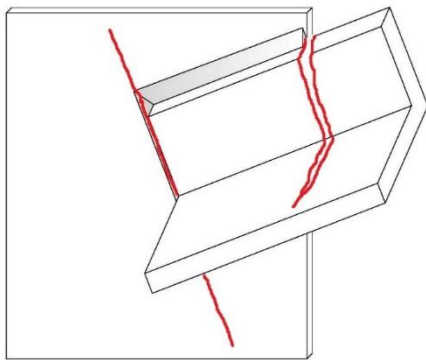


Figure 3-3: Cracks on 20-degree skewed cross-frame 775,000 cycles into Trial 2

A plate was then attached to the cracked gusset plate so that test could continue. At 875,000 cycles into Trial 20-2, a bolt on the steel angle used to repair the crack on the cross-frame failed in shear, as shown in Figure 3-4. When it was noticed, the bolt had already failed entirely. The crack on the gusset plate continued growing and extended beyond the attached plate. The test continued after replacing the bolt and plate. However, after 22,000 cycles (897,000 cycles into Trial 2), the bolt failed at the same location.



Figure 3-4: Shear failure of the bolt connecting the steel angle and cross-frame

As presented in Figure 3-5, a decision was made to weld the cracks on the cross-frame as well as to bolt the angle and the plate, and more bolts were added on the cross-frame retrofit angle. The test continued, and no more problems occurred on the cross-frame for the remainder of the test.

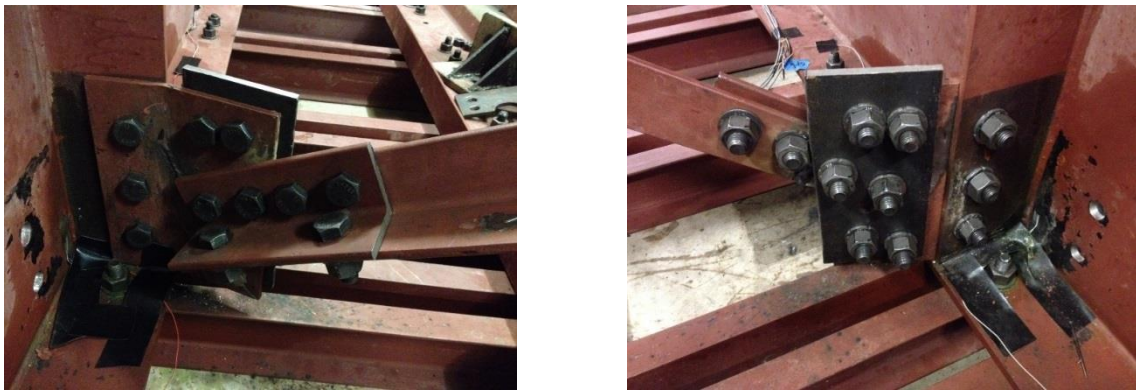


Figure 3-5: Cross-frame after re-welding and repair

3.1.3 Bottom Web-Gap Crack Growth

Figure 3-6 depicts the propagation of the bottom web-gap crack versus the number of applied cycles. In the retrofitted trial, the growth rates were extremely small compared with the rates in the unretrofitted trials. In the unretrofitted trials, the crack growth rates in the south bottom and north bottom web-gap regions were 58.2 and 106.2 in. per million cycles, respectively, while in the retrofitted trials, the crack growth rates were only 0.6 and 0.3 in. per one million cycles.

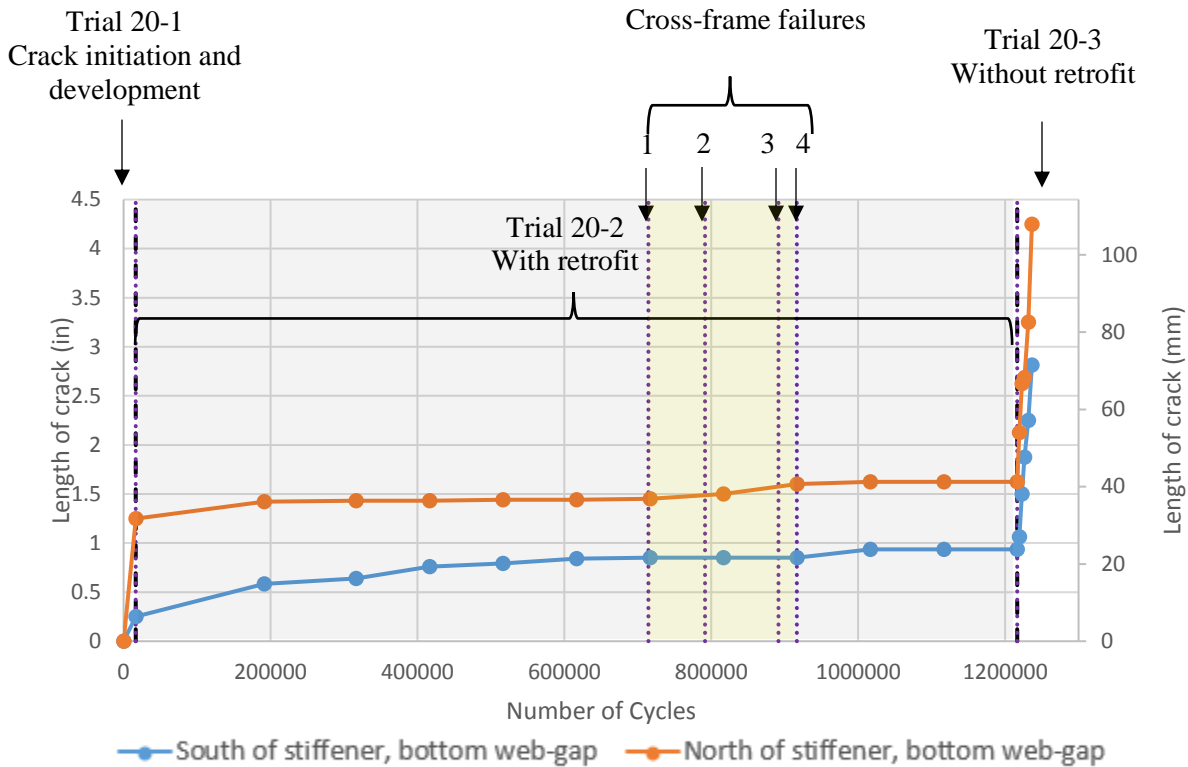


Figure 3-6: Crack propagation vs. number of applied cycles for 20-degree skewed specimen

Explained below, the notations 1, 2, 3, and 4 in Figure 3-6 correspond to the four failures of the cross-frame.

- 1: A crack was observed at the junction of the cross-frame angle and the bottom gusset plate. A steel angle was bolted on the cross-frame in attempting to repair the damage.
- 2: A large crack was observed on the gusset plate of the cross-frame along the weld connecting the cross-frame angle to the gusset plate. A plate was then bolted to the gusset plate to strengthen it.
- 3: The bolt used to repair the damaged cross-frame angle cracked by shear. The broken bolt was replaced with a new one.

4: The bolt used to repair the damaged cross-frame failed again. A decision was made to weld the cracks on the cross-frame as well as to bolt the angle and the plate. More bolts were added to strengthen the connection.

3.2 Actuator Displacement

The actuator displacement was examined because of possible insights into the relative flexibility of the specimen with and without the angles-with-plate retrofit installed, including potential indication of softening of the connection as cracks initiated and propagated.

Figure 3-7 presents actuator displacement versus the number of cycles for the test of the 20-deg. skewed specimen.

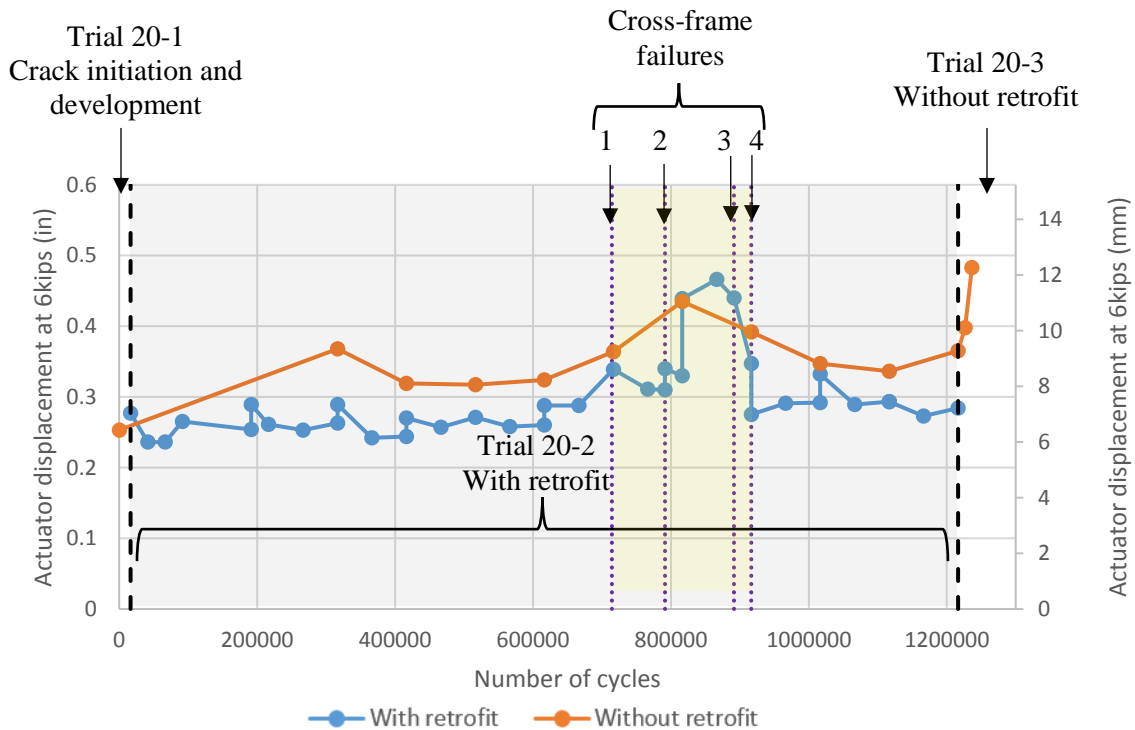


Figure 3-7: Actuator displacement at 6 kip of actuator force for the 20-degree skewed specimen

Ignoring the period in which the cross-frame was broken, the retrofit increased the connection stiffness approximately 26.4%, on average.

The actuator displacement increased and become abnormal during the period in which the cross-frame was broken. The angle and the plate bolted on the cross-frame was not able to provide enough stiffness, thus the behavior of the damaged cross-frame governed the actuator displacement. This phenomenon ended after the cracks on the cross-frame were welded.

In Trial 20-3, the growth of cracks in the web-gap region led to an increase in the actuator displacement. The connection stiffness decreased 24.8% over 20,000 cycles. Compared to the beginning of the test, the connection stiffness decreased approximately 47.6%.

3.3 Stress

Figure 3-8 and Figure 3-9 present the strain gage readings at 6 kip of actuator force. The strain gage data were recorded during the intermittent monotonic tests. In Trial 20-2, the retrofit was removed every 100,000 cycles to examine the crack length. At that time, the readings made without the retrofit in place were recorded. The strain gages were fragile, especially those underneath the retrofit. That is why only a few of the gages on the lower part of the girder web were available for measurement after retrofitting.

Stresses on the upper part of the girder web (strain gages 4, 7, 8) were insensitive to the retrofit status and crack growth. However, stresses on the lower part of the specimen (strain gages 1, 2, 3, 5, 6) were very sensitive to the retrofit. When the retrofit was not attached, the length of cracks significantly influenced the stresses in the lower region. They changed dramatically with respect to the number of cycles. In Trial 20-3, while the specimen was cycled without the retrofit installed, the stresses in the lower region changed significantly. Even the stresses obtained from strain gages 9 and 10, which were located on the cross-frame, were clearly affected by the growth of cracks.

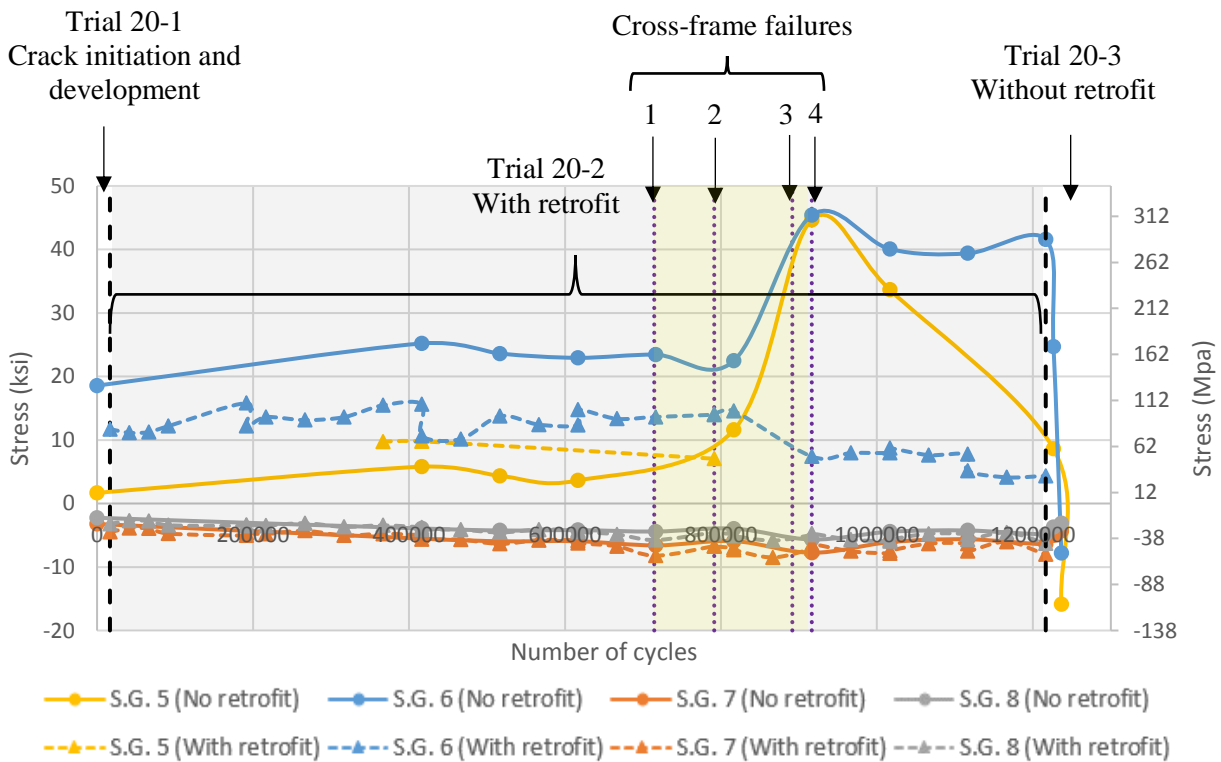
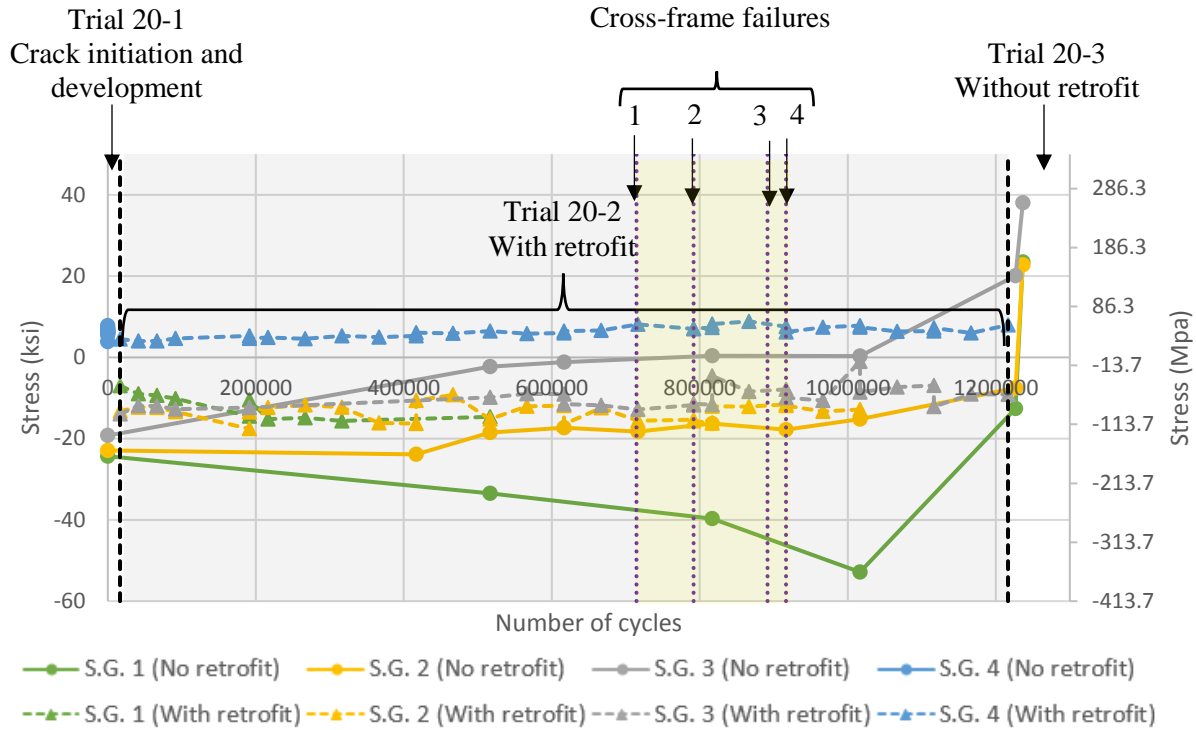


Figure 3-8: Stresses computed from strain gages placed on girder web at 6 kip actuator force for 20-degree skewed specimen

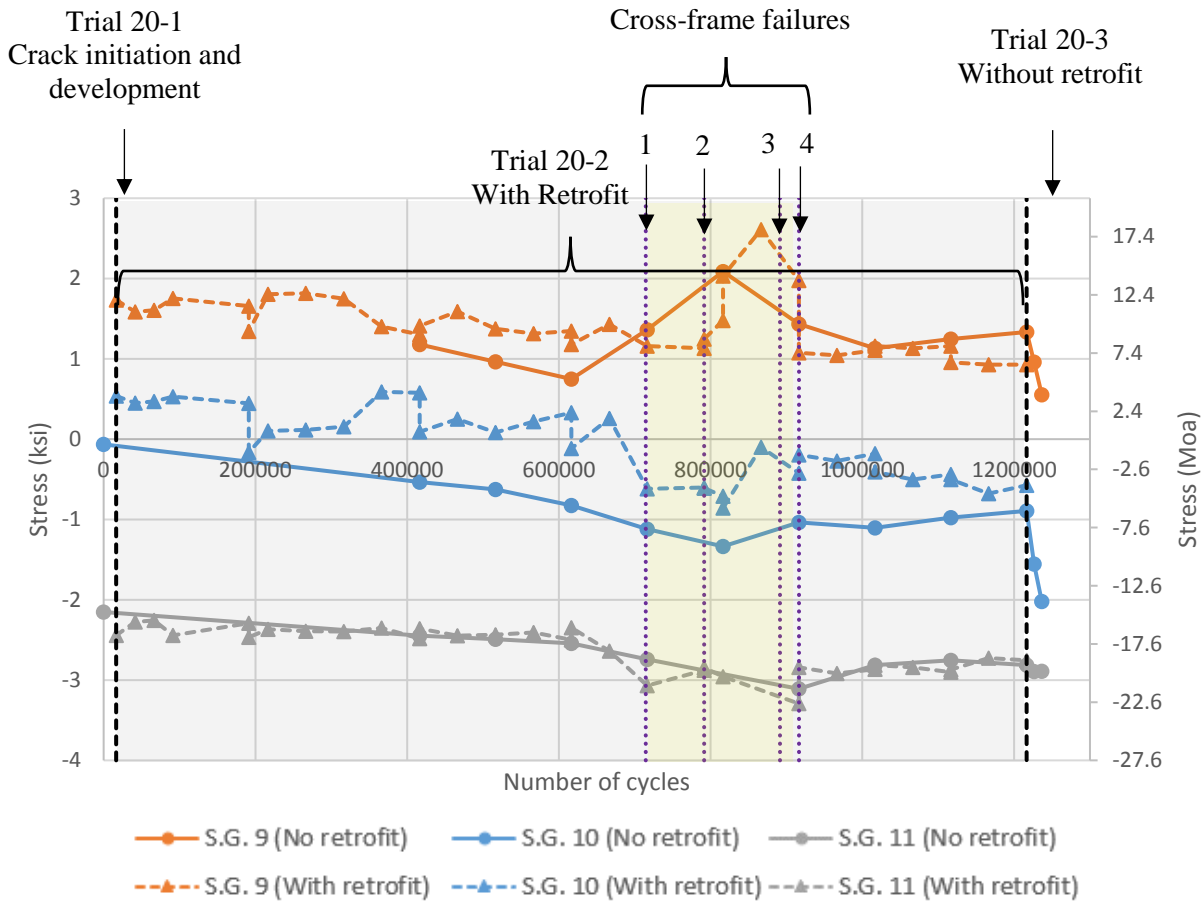


Figure 3-9: Stresses measured by strain gages placed on cross-frame at 6 kip actuator force for 20-degree skewed specimen

3.4 LVDT

The LVDT placements are shown in Figure 2-5. Figure 3-10 shows that the retrofit significantly reduced local deformations in the web-gap region. LVDT 1, located 1 in. above the bottom flange, showed a 94% decrease in out-of-plane deformations after retrofitting.

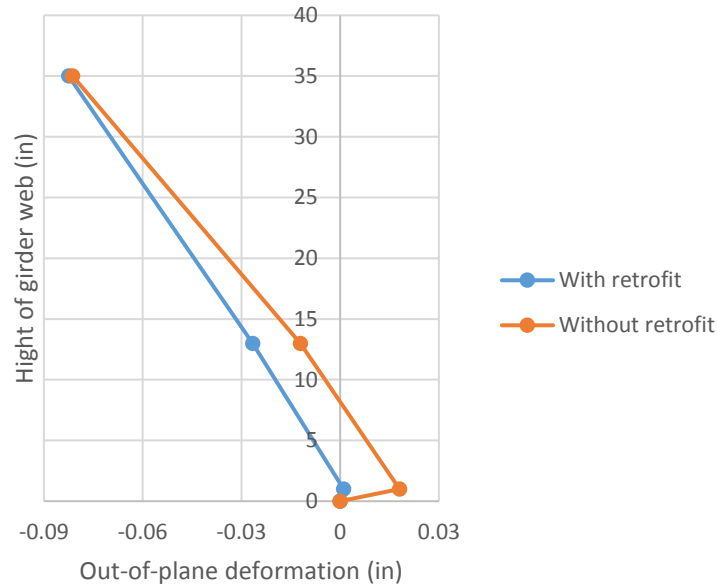


Figure 3-10: LVDT readings for 6 kip of actuator force for 20-degree skewed specimen

3.5 Mirror Array Measurements

The results presented in this section were calculated from the data gathered at the end of Trial 20-2 (with retrofit) and the beginning of Trial 20-3 (without retrofit).

3.5.1 Girder Web Rotation

As discussed in Section 2.2, the girder web rotation can be calculated using Equation 2-1:

$$\alpha = \frac{\Delta}{2L} \quad \text{(Equation 2-1)}$$

Where:

α = Girder web rotation angle

Δ = Distance of laser point movement on the measurement wall

L = Distance from the mirror to the measurement wall

Created using Matlab 2014a, the contour plots of the rotations about Y-axis and X-axis are presented in Figure 3-11 and Figure 3-12, respectively. In these figures, the rectangular borders

correspond to the edges of the girder web. Data were not recorded in the blank areas of the figures. Data were not recorded near the girder ends since it was not a region of high interest. Data in the regions near the bottom of the girder web could not be measured, as the steel channels connecting the specimen to the floor interfered with the laser sight-line.

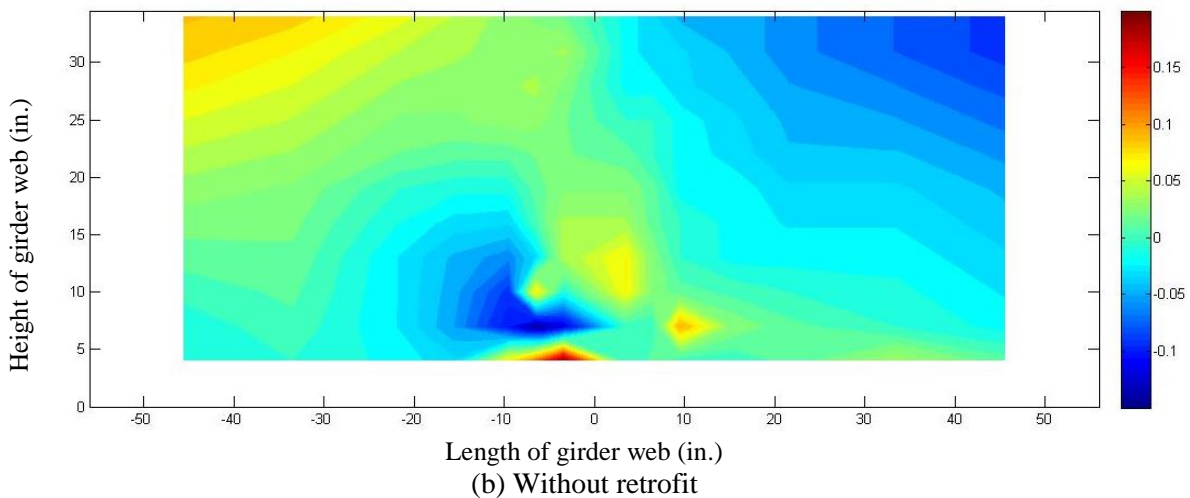
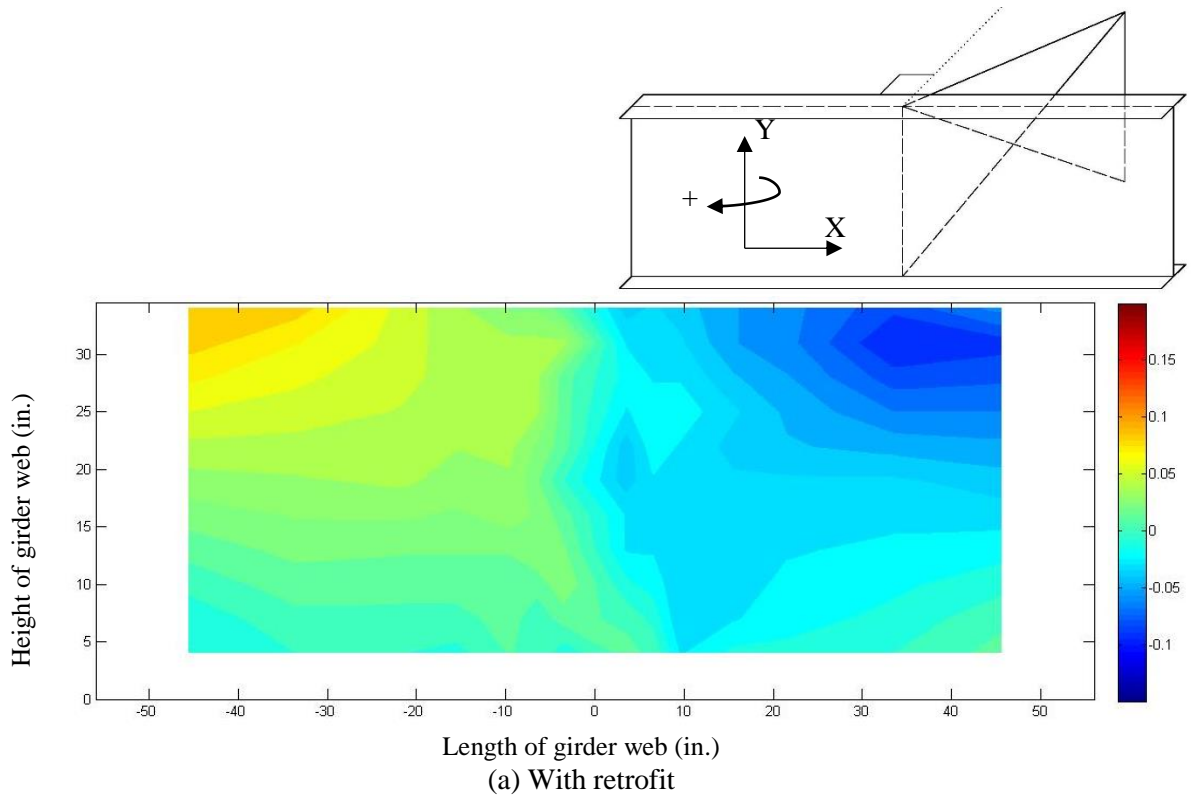


Figure 3-11: Y-axis rotations (degree) of the girder web for 20-degree skewed specimen under 6 kip of actuator force, computed from the mirror array measurements

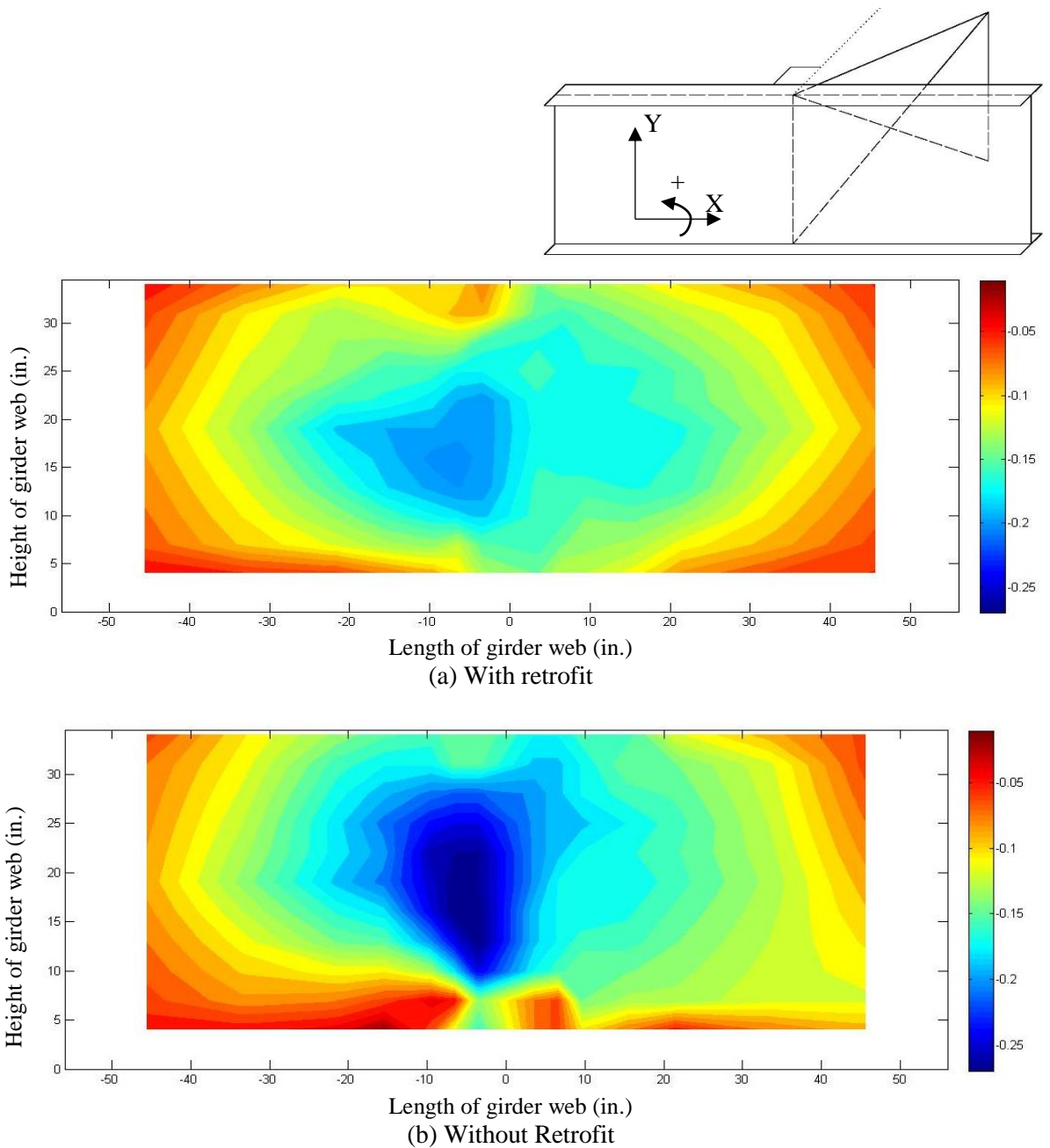


Figure 3-12: X-axis rotations (degree) of the girder web for 20-degree skewed specimen under 6 kip of actuator force, computed from the mirror array measurements

3.5.2 Approximated Stress Calculated from Girder Web Rotation

A method for calculating girder web stresses from girder web rotations was described by Bonet (2014). As depicted in Figure 3-13, assuming that stress and deformation are zero at the center

layer of the girder web thickness, then stress at the surface of the girder web can be derived as the following:

$$\sigma = \varepsilon \cdot E = \frac{\Delta d}{d} \cdot E = \frac{R \cdot \Delta\alpha - r \cdot \Delta\alpha}{d} \cdot E = \frac{\Delta\alpha}{d} \cdot (R - r) \cdot E = \frac{\Delta\alpha}{d} \cdot \frac{t}{2} \cdot E \quad (\text{Equation 3-1})$$

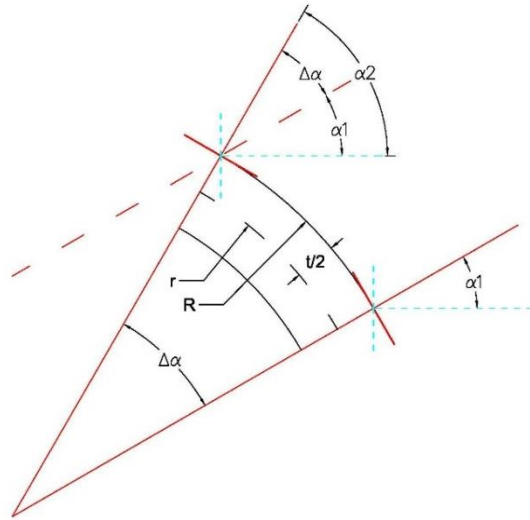


Figure 3-13: Calculate approximated girder web stresses from girder web rotation

Then approximated stresses can be expressed as:

$$\sigma = \frac{\Delta\alpha}{d} \cdot \frac{t}{2} \cdot E \quad (\text{Equation 3-2})$$

σ = Stress

t = Thickness of girder web

$\Delta\alpha$ = Rotation angle difference between two mirrors

E = Elastic modulus of steel

d = Distance between two mirrors

For calculating stresses in the X and Y directions, Equation 3-3 and Equation 3-4 were used:

$$\sigma_x = \frac{\Delta\alpha_y}{d_x} \cdot \frac{t}{2} \cdot E \quad (\text{Equation 3-3})$$

$$\sigma_y = \frac{\Delta\alpha_x}{d_y} \cdot \frac{t}{2} \cdot E \quad (\text{Equation 3-4})$$

Equation 3-2 was derived by assuming the center layer of the web thickness was the neutral layer where deformations and stresses were zero (pure bending). Any stresses caused by axial elongations in the X and Y directions and rotations about the Z-axis (in-plane bending) were neglected (Figure 3-14). In this test, the bottom flange of the girder was restrained by the lab floor so that rotations about the Z-axis were largely eliminated, and since loads were only applied on the far end of the cross-frame, elongations in the X and Y directions of the girder web were negligible. The method described is reasonable for estimating the stress distribution for this specific test setup. However, it may not be applicable in some other cases.

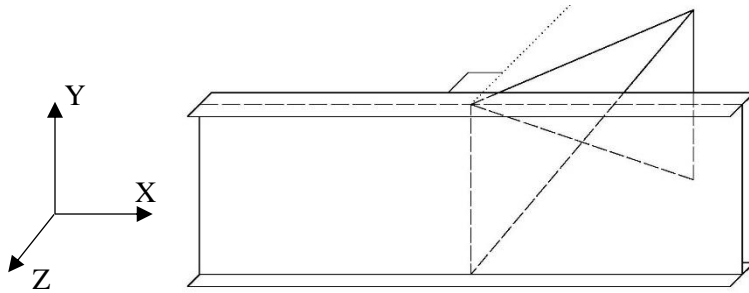


Figure 3-14: Specimen coordinate system

The approximated stresses in X and Y direction are presented in Figure 3-15 and Figure 3-16. The coordinate origin of the calculated stress was set as the center of the two mirrors. The contour plots were created using Matlab 2014a.

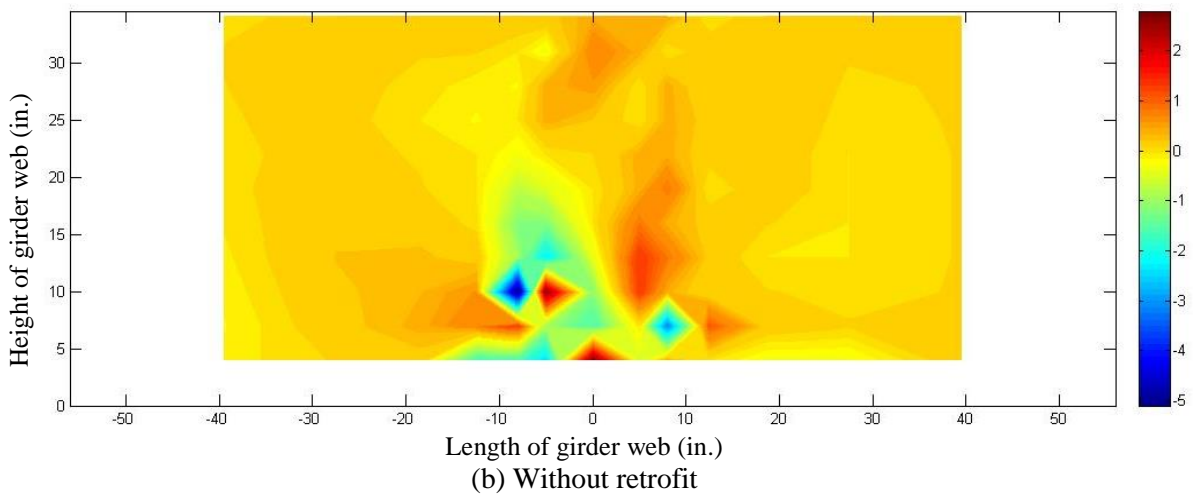
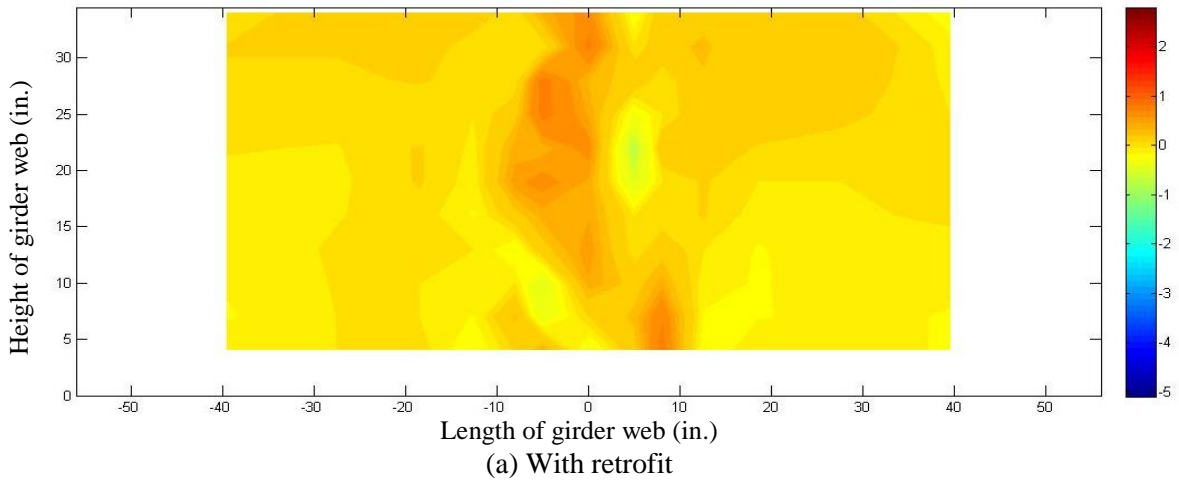
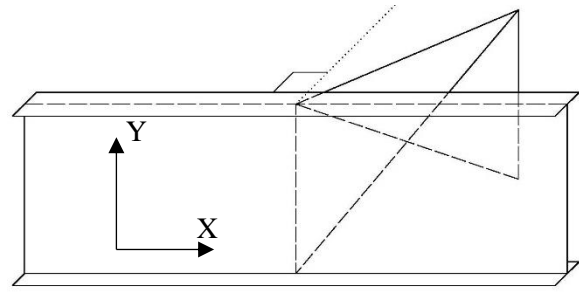


Figure 3-15: Approximated stress (ksi) in the girder web in X direction for 20-degree skewed specimen under 6 kip of actuator force, computed from the mirror array measurements

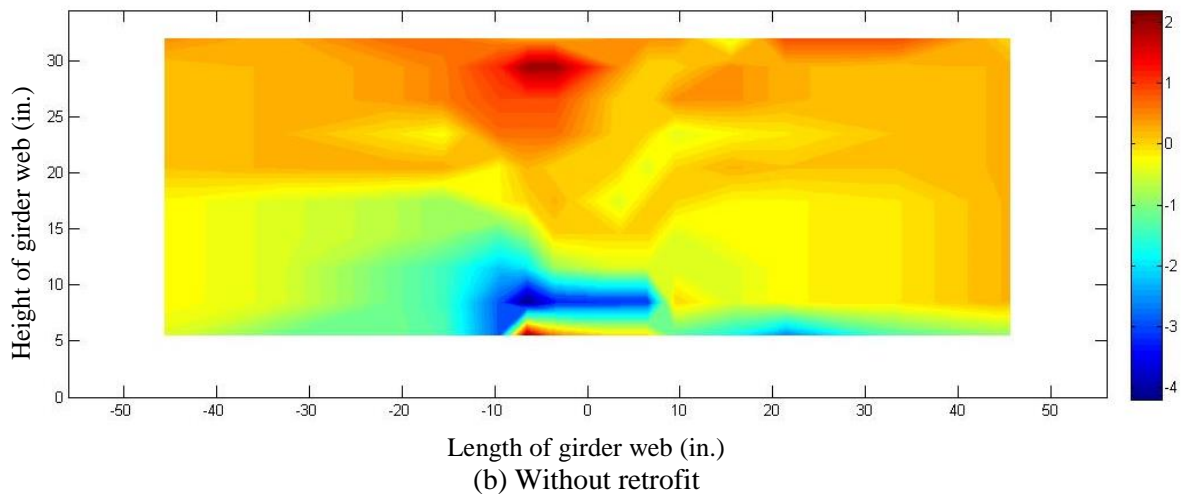
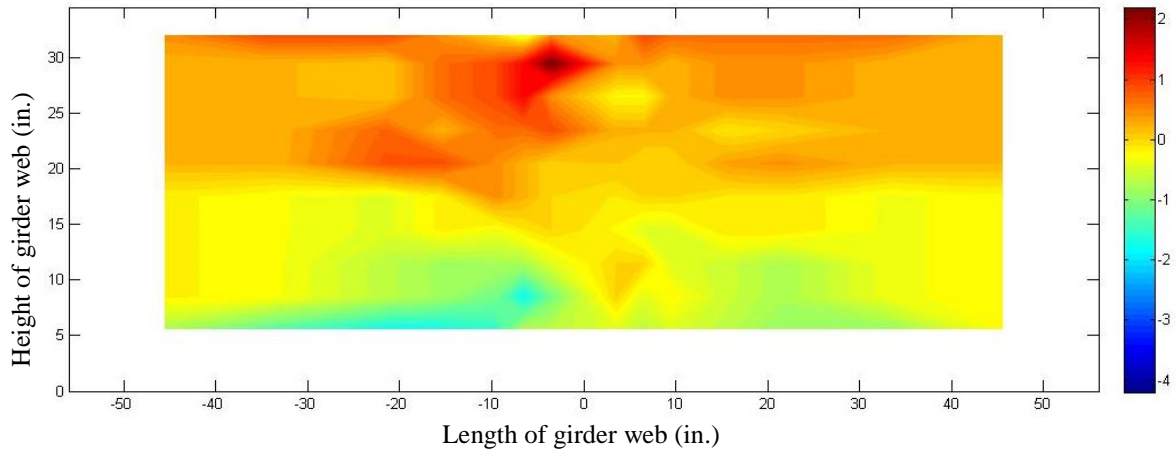
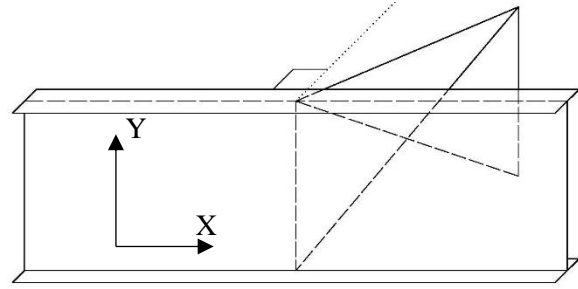


Figure 3-16: Approximated stress (ksi) in Y direction of the girder web for 20-degree skewed specimen under 6 kip of actuator force, computed from the mirror array measurements

After retrofitting, the maximum tension stress in the X direction decreased 68%, and the maximum compression stress in the X direction was reduced 87%, based on computations from the mirror array measurements.

In the Y direction, the maximum compression stress was reduced 58%, but the maximum tension stress remained nearly the same. The larger magnitude stresses in Y direction were distributed at the top part of the girder web, therefore were not affected by the retrofit which was installed at the bottom web-gap. This finding is consistent with the strain gages measurement discussed in Section 3.3.

Since the retrofit was aimed at repairing the bottom web-gap, it might not be reasonable to analyze the results of the whole girder web. If only considering the results for the region underneath the retrofit, in the X direction, the maximum tension stress and maximum compression stress were reduced 68% and 89% respectively. In the Y direction, the maximum tension stress was reduced 99% and the maximum compression stress decreased 58%.

The results indicated that the retrofit was very effective in reducing local stresses in the damaged web-gap region.

4. Physical Test of the 40-Degree Skewed Girder to Cross-Frame Connection –Introduction

4.1 Description of the 40-Degree Skewed Girder to Cross-Frame Specimen

The cross-frame of the specimen described in this section was skewed 40-degree from the position perpendicular to the girder web. This was the only difference between the 40-degree skewed specimen and the 20-degree skewed specimen. Other specimen details have already been introduced in Section 2.1, thus are not presented in this section.

The dimensions of the 40-degree skewed cross-frame are presented in Figure 4-1.

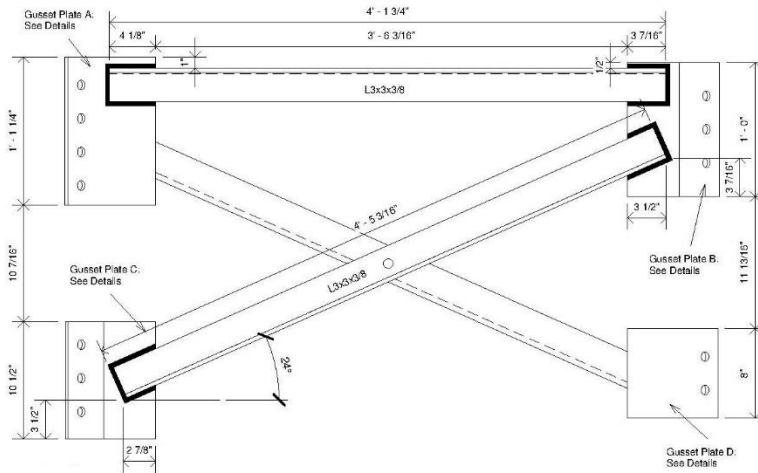
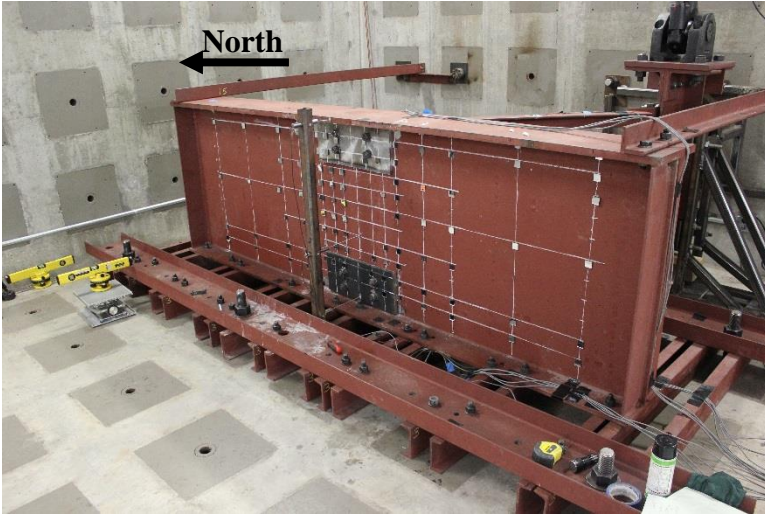
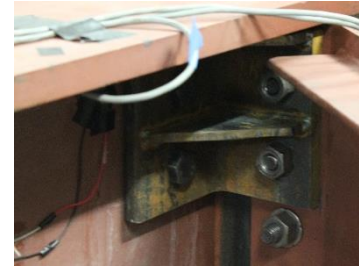


Figure 4-1: Dimensions of 40-degree skewed cross-frame

In this test, the angles-with-plate retrofits were installed on both the top and the bottom web-gap, since cracks were found in both of the two regions. The angles-with-plate retrofit used in this test had the same dimensions as the retrofit used in the 20-degree skewed test. Figure 4-2 presents the photographs of the 40-degree skewed specimen and test set-up.



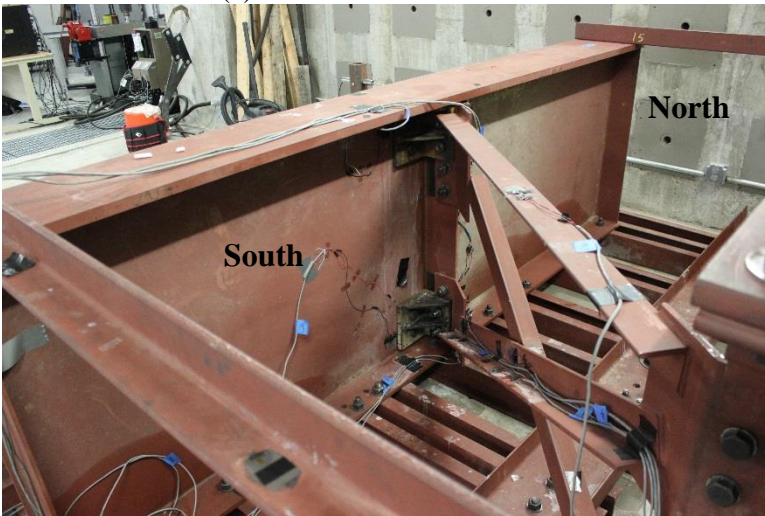
(a) Girder web fascia side



(c) Retrofit angle at top web-gap



(d) Retrofit angle at bottom web-gap



(b) Girder web stiffener side



(e) WT section and restraining rollers

Figure 4-2: Photographs of 40-degree skewed specimen with angles-with-plate retrofit installed

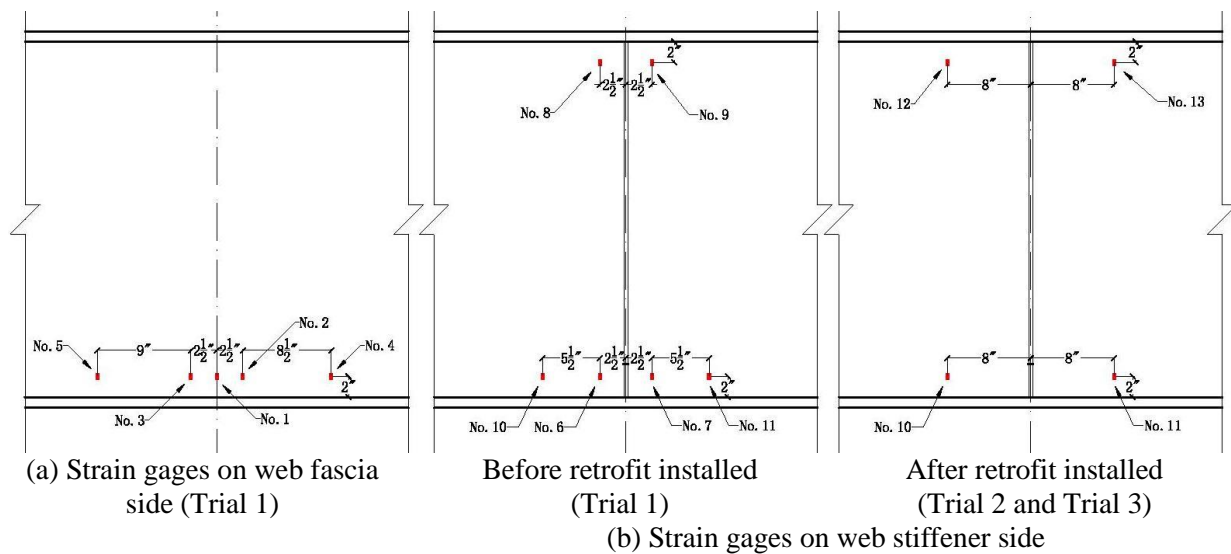
4.2 Instrumentation

Actuator displacement and load cell readings were collected in the test of the 40-degree skewed system, as for the 20-degree skewed system.

Strain gages were attached to the specimen at regions known to be susceptible to fatigue problems (bottom web-gap), to indicate the influence of the crack propagation on the stresses, and to verify the reliability of the finite element models by comparing with the stresses extracted from the models. Unlike the 20-degree skewed test, in this test, the strain gages behind the retrofit angles

and the plates were abandoned after installing retrofit, as the strain gages were so delicate that most were broken after retrofit application.

Four LVDTs (Linear Variable Differential Transformers) were attached to the centerline of the girder web to measure out-of-plane deformations. Strain gage readings, LVDT readings, actuator displacement, and actuator force were recorded while performing monotonic tests. The LVDT and strain gage placements are presented in Figure 4-3.



*Strain gages No.1 – No.9 were abandoned after retrofit installed.

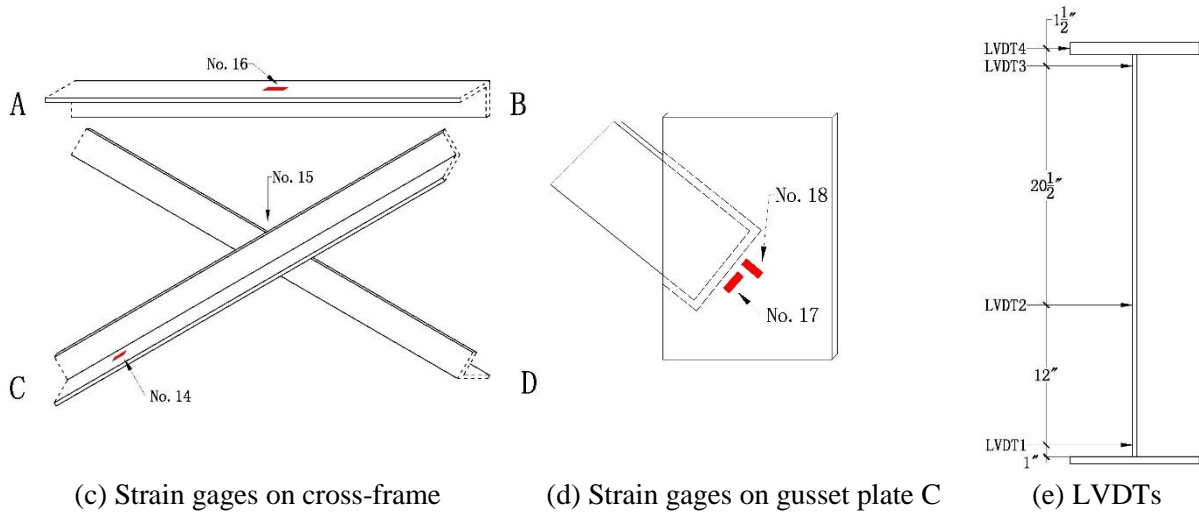


Figure 4-3: Instrumentation of the 40-degree skewed specimen

Section 2.2 described the mirror array and procedures used to calculate rotations and approximated stresses in the girder web. The procedures were also performed for the 40-degree skewed specimen. Figure 4-4 shows the placement of the mirror array. The layout was slightly different from that used in the 20-degree skewed test. A column of mirrors was added at the centerline of the girder web in this test, while there was no mirror placed at the girder web centerline on the 20-degree skewed specimen.

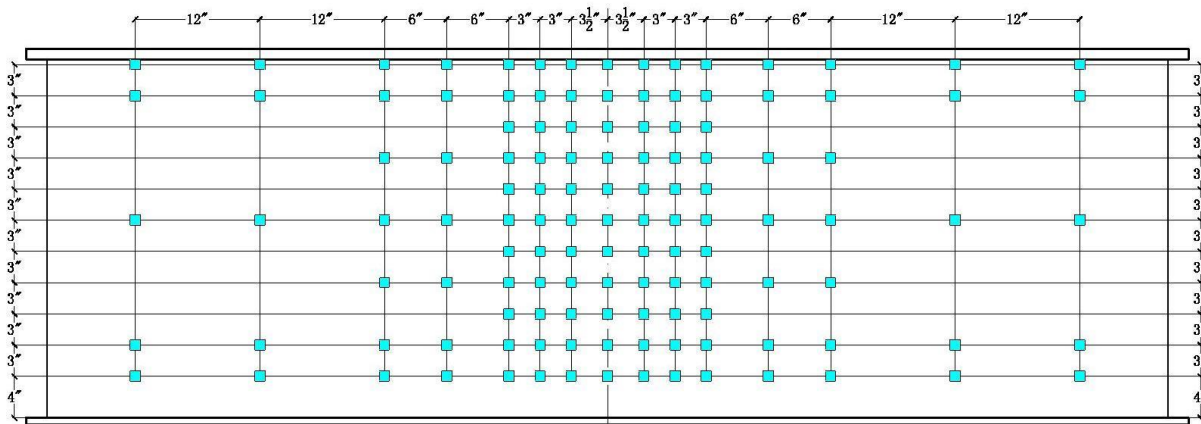


Figure 4-4: Mirror placements for 40-degree skewed specimen

4.3 Test Procedure

Upward cyclic loading of 0-2.3 kip was provided at a frequency of 2 Hz on the 40-degree skewed specimen. In the undamaged state, this load range generated an actuator displacement range of 0-0.27 in., which was the same as the displacement range of the undamaged 20-degree specimen, as shown in Figure 4-5.

The cyclic load applied on the 20-degree specimen was 0.5-6.2 kip. Load ranges are often selected to be the invariants. However, in this study, the 40-degree specimen was much more flexible than the 20-degree specimen. Applying the same load range would have generated an unreasonably large displacement range in the 40-degree specimen.

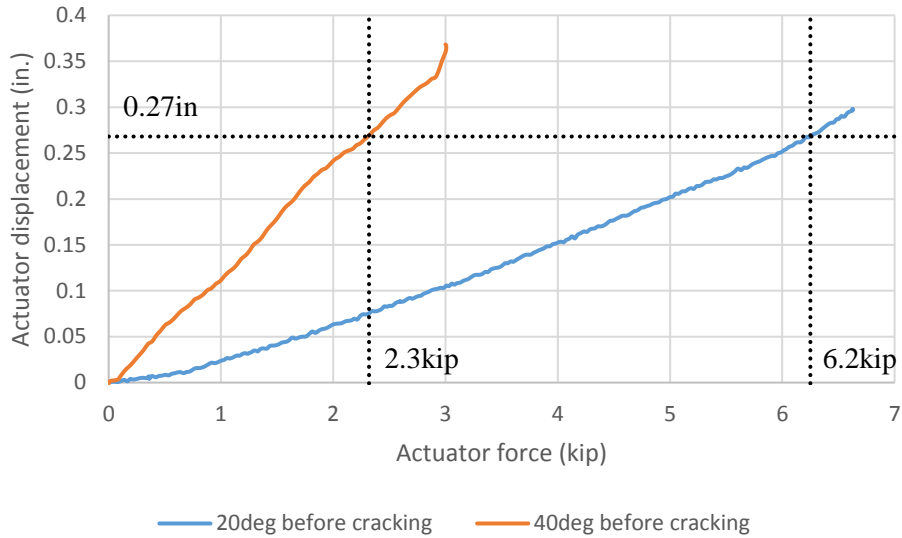


Figure 4-5: Actuator displacement vs. actuator force before specimen cracking for 20-degree specimen and 40-degree specimen

The specimen was regularly inspected to detect and measure cracks, using dye penetrant.

Three trials were conducted in this test. In Trial 40-1, the specimen was cycled without retrofit to initiate cracks. The angles-with-plate retrofits were installed when the cracks grew to the length shown in Figure 5-1. In Trial 40-2, the specimen was cycled with the angles-with-plate retrofit installed to test the efficacy of the retrofit. Monotonic tests were conducted every 25,000 cycles, during which the actuator load was slowly increased from 0 - 2.5 kip while recording instrumentation data. The retrofit was removed at regular intervals to inspect the cracks. In Trial 40-3, the retrofits were removed to study the fatigue performance of the specimen without retrofit.

A summary of the test is presented in Table 4-1.

Table 4-1: Test summary of 40-degree skewed specimen

Trial	Retrofit status	Number of cycles	Total cycles
Trial 40-1	Unretrofitted	313,000	313,000
Trial 40-2	Retrofitted	1,200,000	1,513,000
Trial 40-3	Unretrofitted	1,200,000	2,713,000

Load range: 0-2.3 kip

Load frequency: 2 Hz

5. Physical Test of 40-Degree Skewed Girder to Cross-Frame Connection – Result

5.1 Crack Initiation and Propagation

Since the girder bottom flange was restrained to the laboratory floor while the top flange was allowed to move, the bottom web-gap region was expected to be more sensitive to fatigue than the top web-gap region. However, a 3/8 in. crack (North top 1) was first observed at the north side of the top web-gap region, 17,520 cycles into Trial 40-1 (north was the side for which the cross-frame and the girder web formed an obtuse angle, as shown in Figure 4-2). The crack initiated at the top end of the weld connecting the girder web and the stiffener, and grew vertically downward along the weld.

50,000 cycles into Trial 40-1, a 1/4 in. crack (North bottom 1) was observed on the north side of the bottom web-gap region. It initiated at the bottom end of the girder web to stiffener weld, and grew vertically upward along the weld.

215,000 cycles into Trial 40-1, a 3/16 in. crack (South top 1) was detected at the top end of the girder web to stiffener weld, on the south side of the top web-gap region. In the south bottom web-gap region, the researchers observed some discontinuous spots shining under the fluctuating load that implied crack initiation (South bottom 1). But, the crack was so small at this point that it was very difficult to measure its length. It is worth mentioning that this crack did not initiate at the bottom end of the weld, which rarely happens in the distortion-induced fatigue tests of web-gap regions.

The angles-with-plate retrofits were installed in both the top and the bottom web-gap regions 313,000 cycles into Trial 40-1. Figure 5-1 presents a schematic drawing showing the crack lengths when the retrofits were installed.

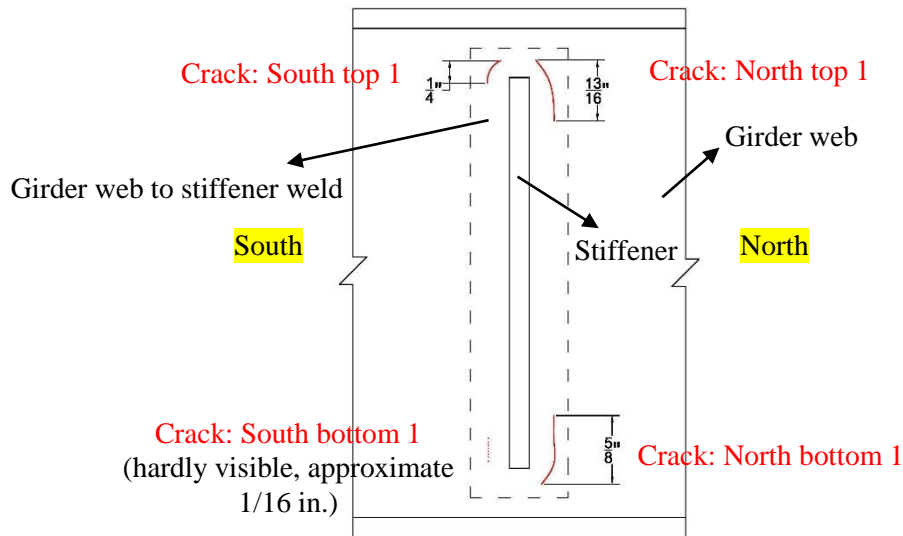


Figure 5-1: Cracks present in 40-degree skewed specimen 313,000 cycles into Trial 40-1 (schematic)

In Trial 40-2, the specimen was cycled with the angles-with-pate retrofit installed. 1,200,000 cycles were applied on the specimen in this trial. The retrofit was removed several times to inspect the cracks, and no visible crack propagation was observed.

The retrofit was removed to allow the cracks propagate freely in Trial 40-3, and 1,200,000 cycles were applied. In Trial 40-3, the cracks grew slowly and remained thin for the majority of the cycles. The crack widths did not noticeably increase until 1,050,000 cycles into Trial 40-3.

A $\frac{1}{4}$ in. crack (South top 2) was observed on the south side of the top portion of the stiffener 435,000 cycles into Trial 40-3. Most of the fatigue cracks reported in web-gap regions initiated at the end of the weld connecting the girder web and the stiffener, growing along the weld and then propagating into the girder web and growing horizontally. Cracking of the stiffener was an unexpected occurrence.

786,000 cycles into Trial 40-3, another $\frac{1}{16}$ in. crack (South top 3) was observed on the south side of the top part of the stiffener. After another 145,000 cycles, a new $\frac{3}{4}$ in. crack (South top 4) was observed in the same region.

931,000 cycles into Trial 40-3, a $\frac{1}{2}$ in. crack (North bottom 2) was detected at the north bottom end of the girder web to stiffener weld. The cracks propagated into the girder web 1,050,000 cycles into Trial 40-3. A schematic drawing showing the distribution of the cracks 1,150,000 cycles into Trial 40-3 is presented in Figure 5-2.

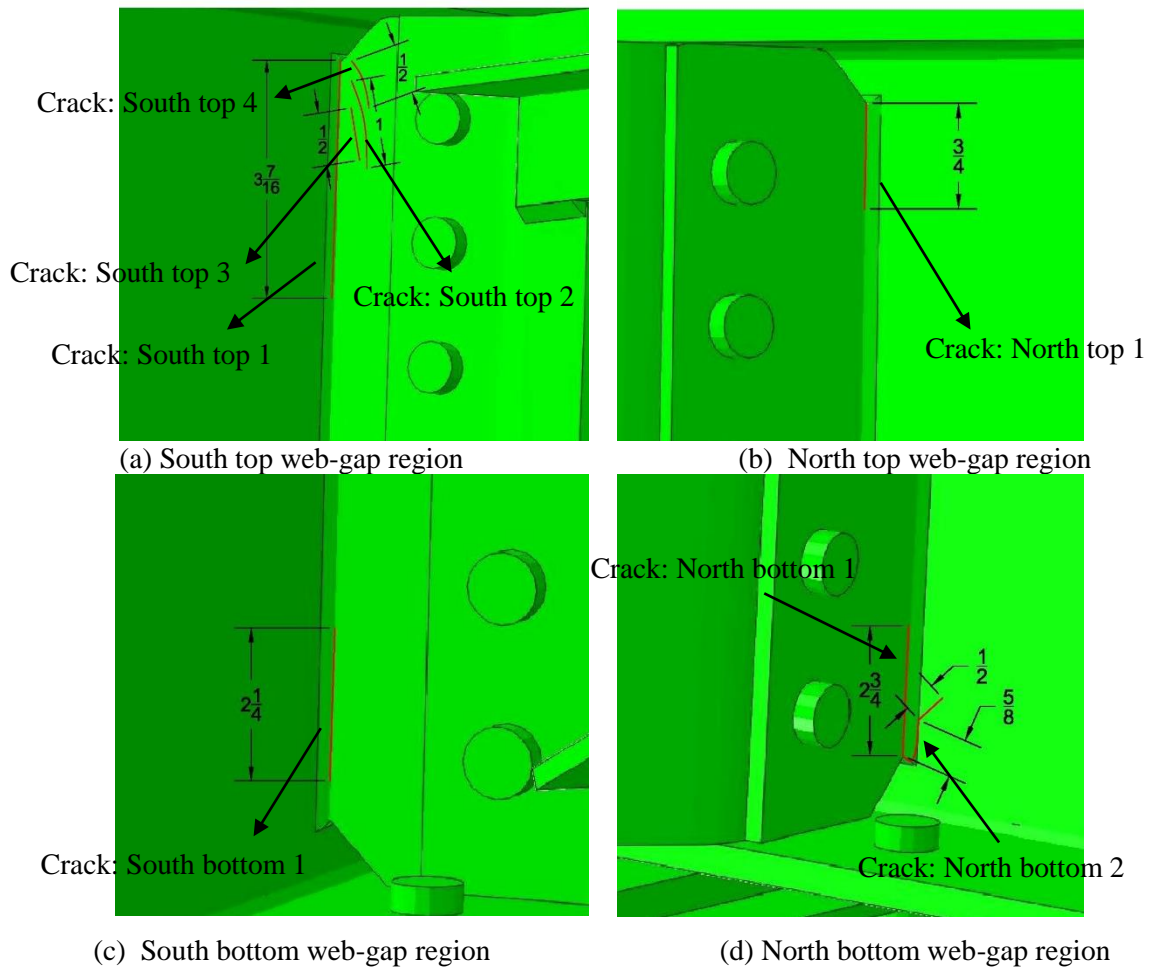


Figure 5-2: Cracks of 40-degree skewed specimen 1,150,000 cycles into Trial 40-3 (schematic drawing)

Photographs of the fatigue cracks 1,150,000 cycles into Trial 40-3 are presented in Figure 5-3. Cracks are shown as white lines in the photographs.

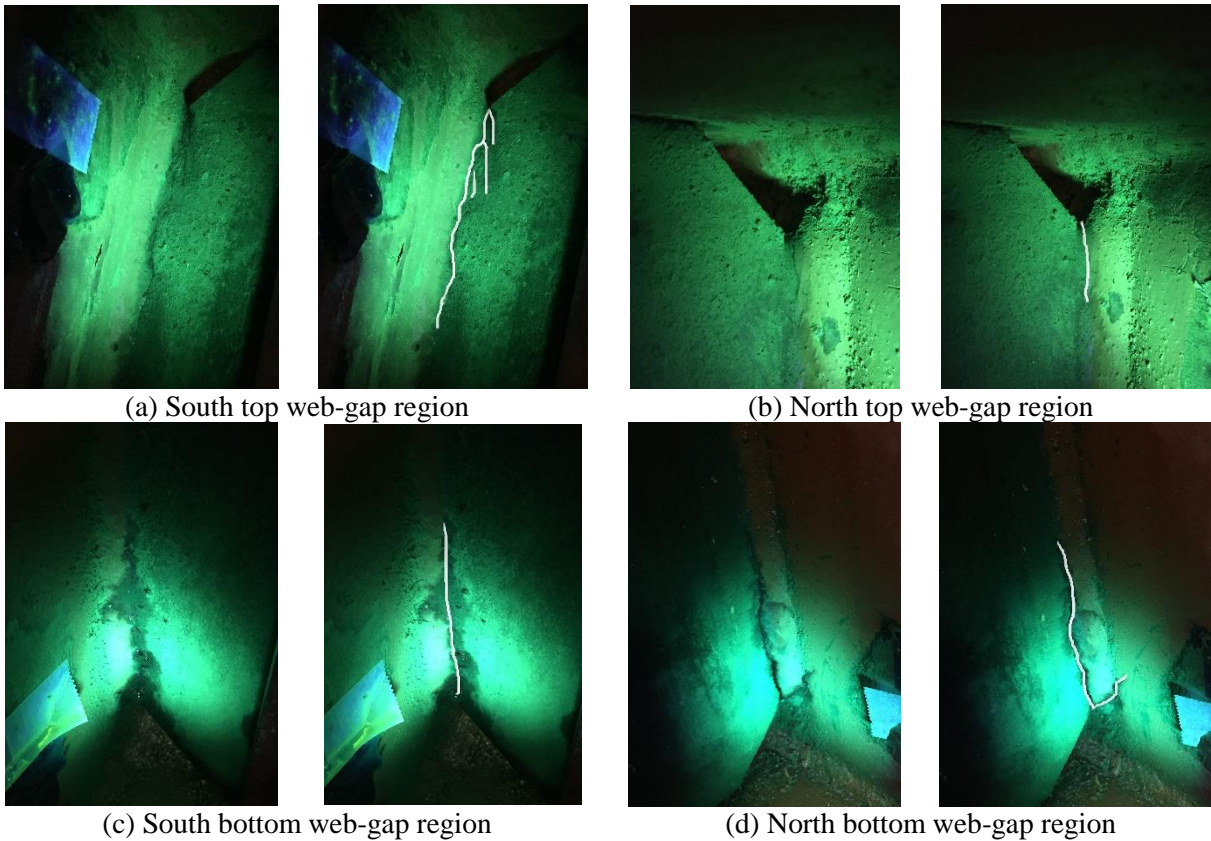


Figure 5-3: Cracks of 40-degree skewed specimen 1,150,000 cycles into Trial 40-3

The cracks on the stiffener (Crack: South Top 2, 3, 4, as notated in Figure 5-2) were surface cracks and were very thin. As shown in Figure 5-4, which presents the crack initiation and propagation with respect to the number of applied cycles, propagation of the cracks on the stiffener (Crack: South Top 2, 3, 4, as notated in Figure 5-2) tended to pause after their initiation.

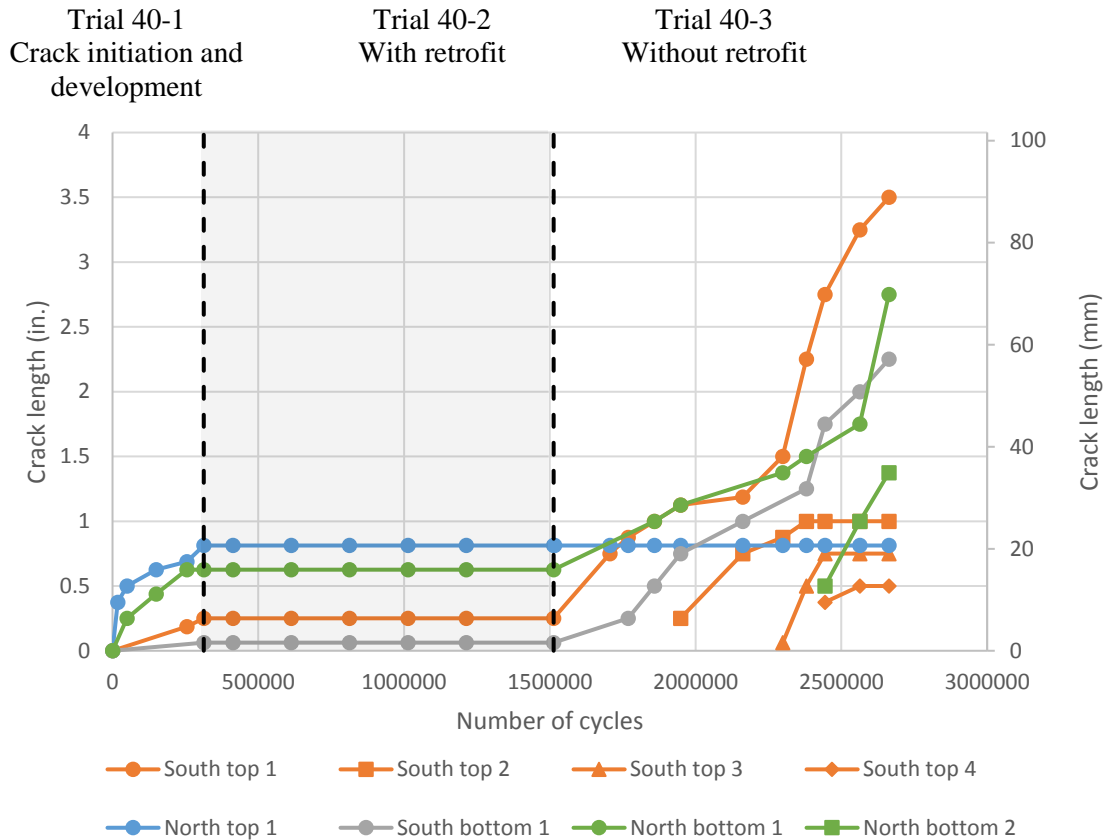


Figure 5-4: Crack propagation vs. number of applied cycles for 40-degree skewed specimen

5.2 Actuator Displacement

Figure 5-5 presents actuator displacement at 2.5 kip of actuator force with respect to the number of applied cycles. The angles-with-plate retrofits were installed on both the top and the bottom web-gap at the beginning of Trial 40-2. After installing the retrofit, the actuator displacement decreased about 50%. In Trial 40-3, the retrofits were removed, and cracks were allowed to propagate freely. At the end of the test, the connection stiffness had decreased approximately 20% as compared with the beginning of the test.



Figure 5-5: Actuator displacement vs. number of applied cycles at 2.5 kip of actuator force for the 40-degree skewed specimen

5.3 Stress

The strain gage placements are given in Figure 4-3. Figure 5-6 presents the stresses computed from strain gages 1 - 5, which were located in the bottom web-gap region on the fascia side of the girder web. The measurements were taken at the beginning of Trial 40-1. The applied actuator load was 2.5 kip. As expected, large stress gradients existed in the web-gap region, and an unsymmetrical result was observed due to the skewed angle of the connection.

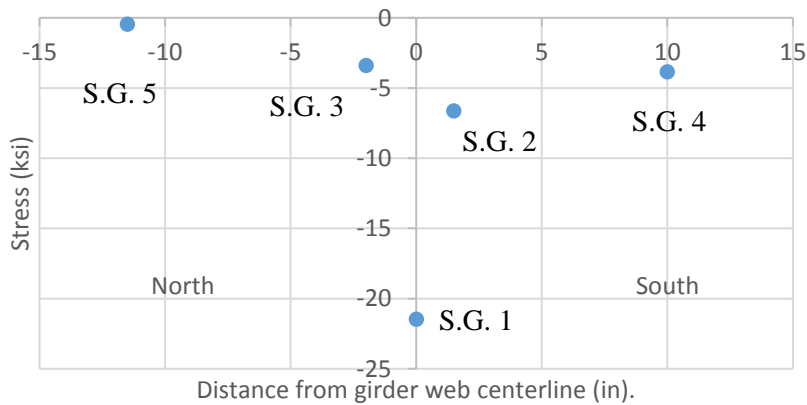


Figure 5-6: Stresses computed from strain gages 1 to 5 at the beginning of Trial 40-1 for the 40-degree skewed specimen under 2.5 kip of actuator force

As presented in Section 3.1.2, during the test of the 20-degree skewed specimen, the gusset plate cracked in Trial 20-2, in which the specimen was cycled with the angles-with-plate retrofit installed. Cracking of the gusset plate was unexpected, and there was a concern that it might be the retrofit that caused the gusset plate to crack. Unfortunately, this question was not able to be answered in the physical test since in the 20-degree skewed specimen no instrumentation was applied on the gusset plate.

As shown in Figure 4-3, in the test of the 40-degree skewed specimen, strain gages 17 and 18 were attached to the bottom gusset plate to measure the change of the stresses due to installing the angles-with-plate retrofit. Figure 5-7 presents the stresses measured by the two strain gages.

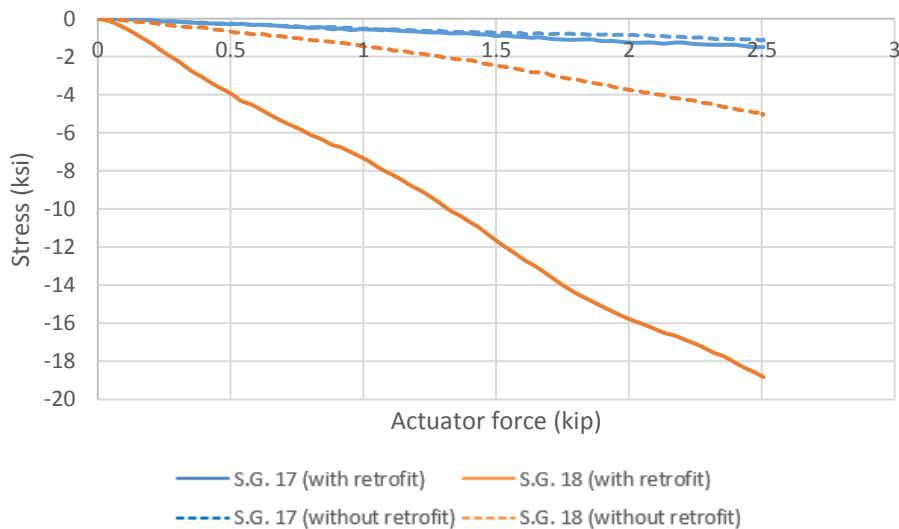


Figure 5-7: Stresses measured by strain gages 17 and 18 placed on the bottom gusset plate for the 40-degree skewed specimen

Strain gage 17 and 18 were placed parallel and vertical to the weld connecting the cross-frame angle and the gusset plate respectively. As shown in Figure 5-7, stresses computed using strain gage 17, which was placed parallel to the weld, were not significantly influenced by the retrofit states. However, the stresses computed from strain gage 18, which was placed vertically with respect to the weld, did not increase, but significantly decreased after installing the retrofit.

A similar phenomenon may have also occurred in the 20-degree skewed specimen. The gusset plate cracking may not have occurred because the retrofit was installed, but because the applied load range was very large.

Figure 5-8 presents the stresses computed from strain gages 10, 11, 12, and 13 located on the connection plate side of the girder web, as shown in Figure 4-3. These strain gages were placed outside the retrofit angles. They were not effective in indicating the crack initiation and propagation since the stresses were insensitive to crack growth.

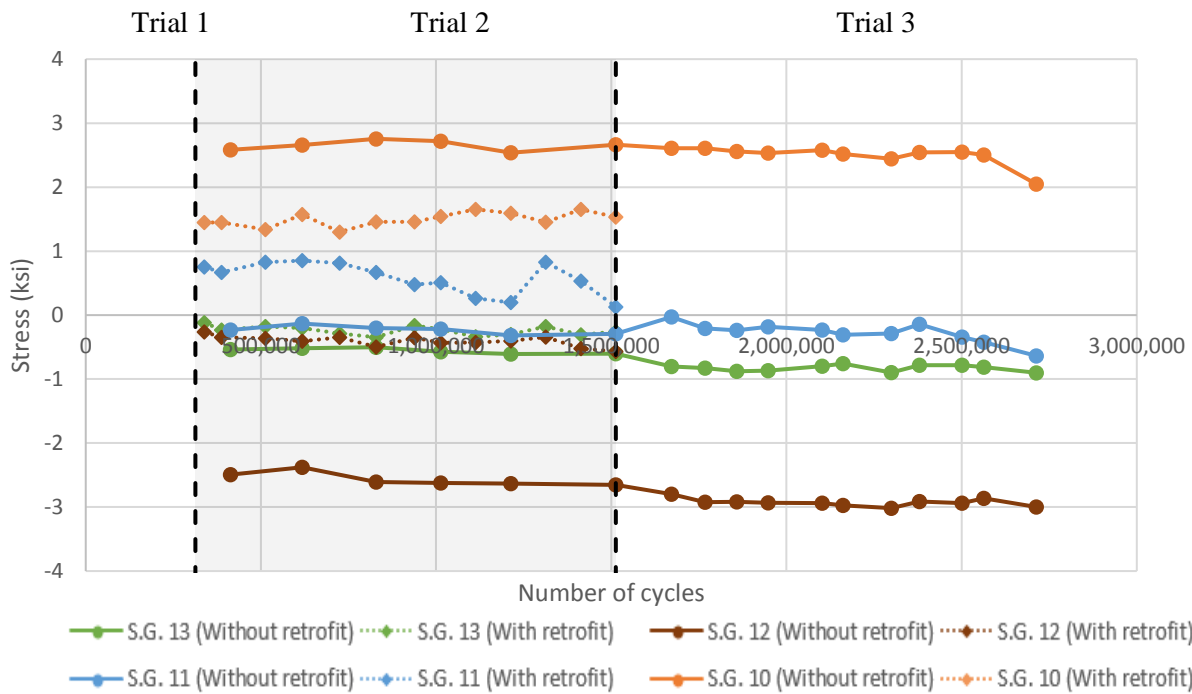


Figure 5-8: Stresses computed from strain gages 10, 11, 12, 13 vs. number of applied cycles for the 40-degree skewed specimen under 2.5 kip of acutator force

Stresses computed from strain gages located on the cross-frame are presented in Figure 5-9. The stress magnitudes decreased after the retrofit was installed. The stresses were insensitive to the initiation and propagation of fatigue cracks in the web-gap region.

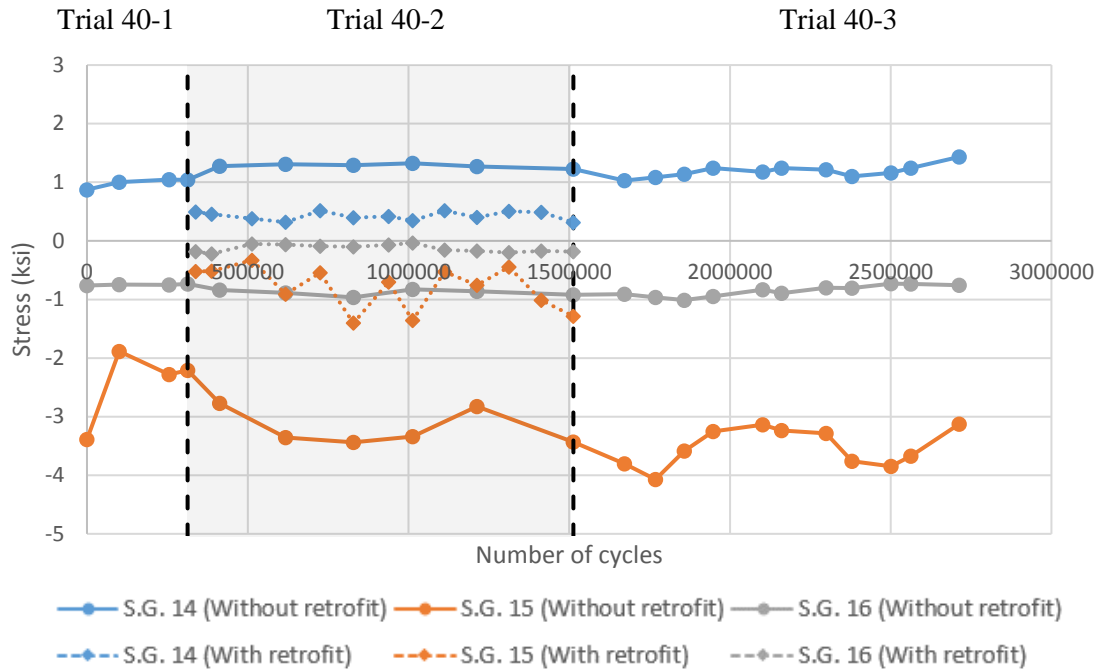


Figure 5-9: Stresses measured by strain gage 9, 10, 11 vs. number of applied cycles for the 40-degree skewed specimen under 2.5 kip of actuator force

5.4 LVDT

Figure 5-10 presents measurements from the LVDTs for the 40-degree skewed specimen. The placements of the LVDTs are presented in Figure 4-3.

After retrofitting, the relative out-of-plane deformation at the bottom web-gap (the difference between LVDT1 and the bottom flange) was reduced 98.4%; the relative out-of-plane deformation at the top web-gap (the difference between LVDT3 and LVDT4) was reduced 75.9%.

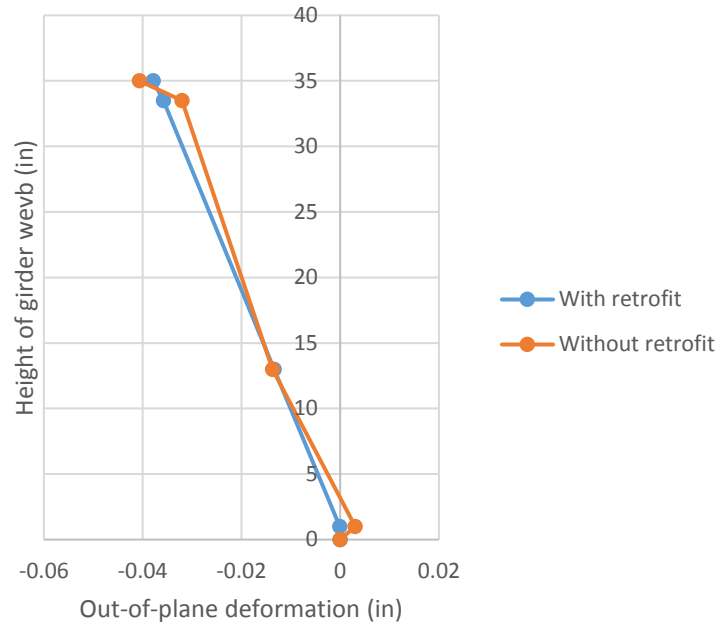


Figure 5-10: LVDT measurements for 2.5 kip of actuator force for the 40-degree skewed specimen

5.5 Mirror Array Measurements

The results presented in this section were calculated from the data gathered at the end of Trial 40-1 (without retrofit) and the beginning of Trial 40-2 (with retrofit).

5.5.1 Girder Web Rotation

The contour plots for rotations about the girder's Y-axis and X-axis are presented in Figure 5-11 and Figure 5-12, respectively.

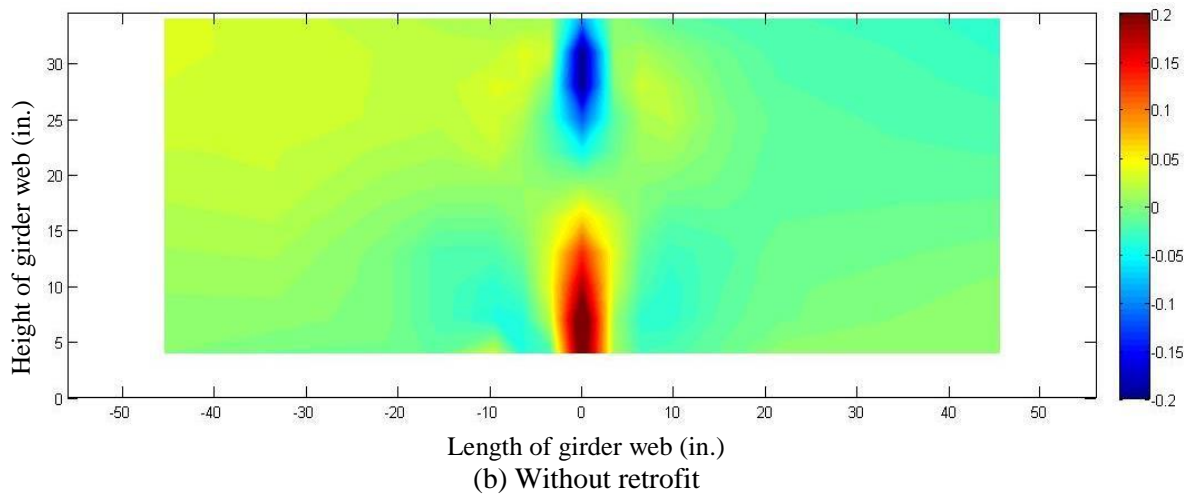
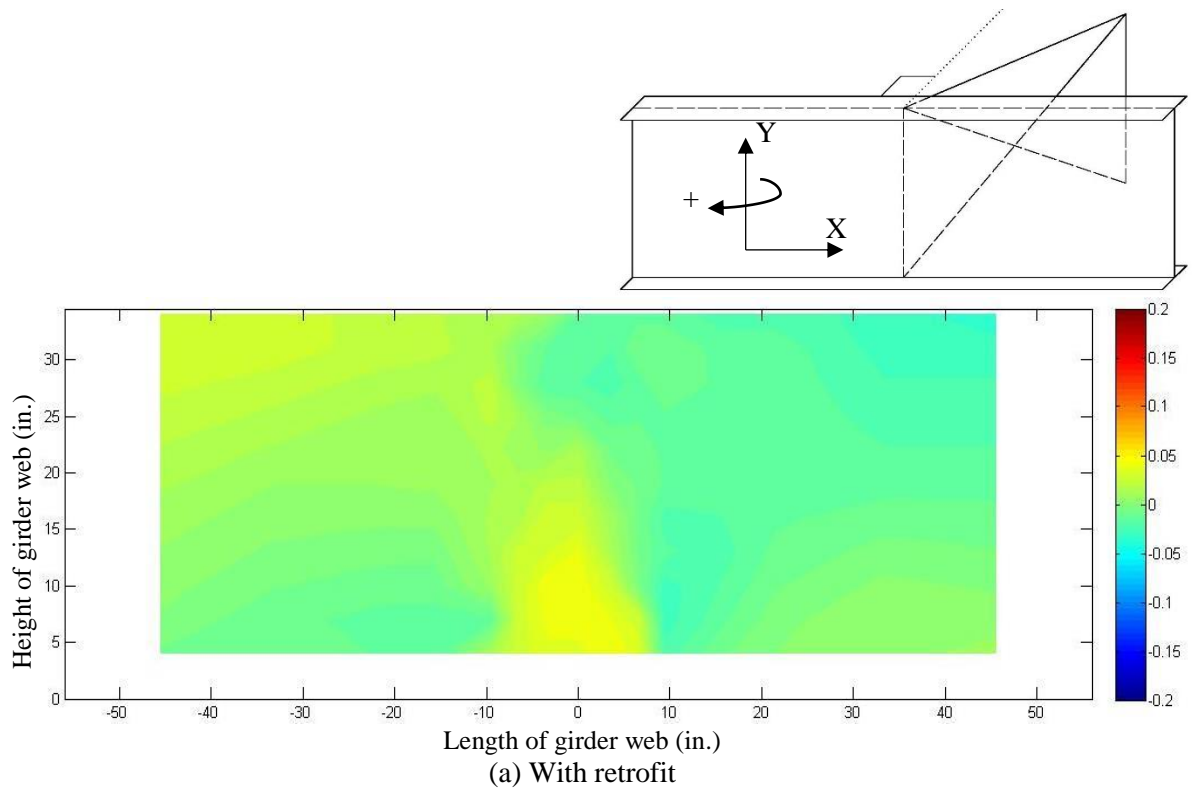


Figure 5-11: Y-axis rotations (degree) of the girder web computed from mirror array measurements for 40-degree skewed specimen under 2.5 kip of actuator force

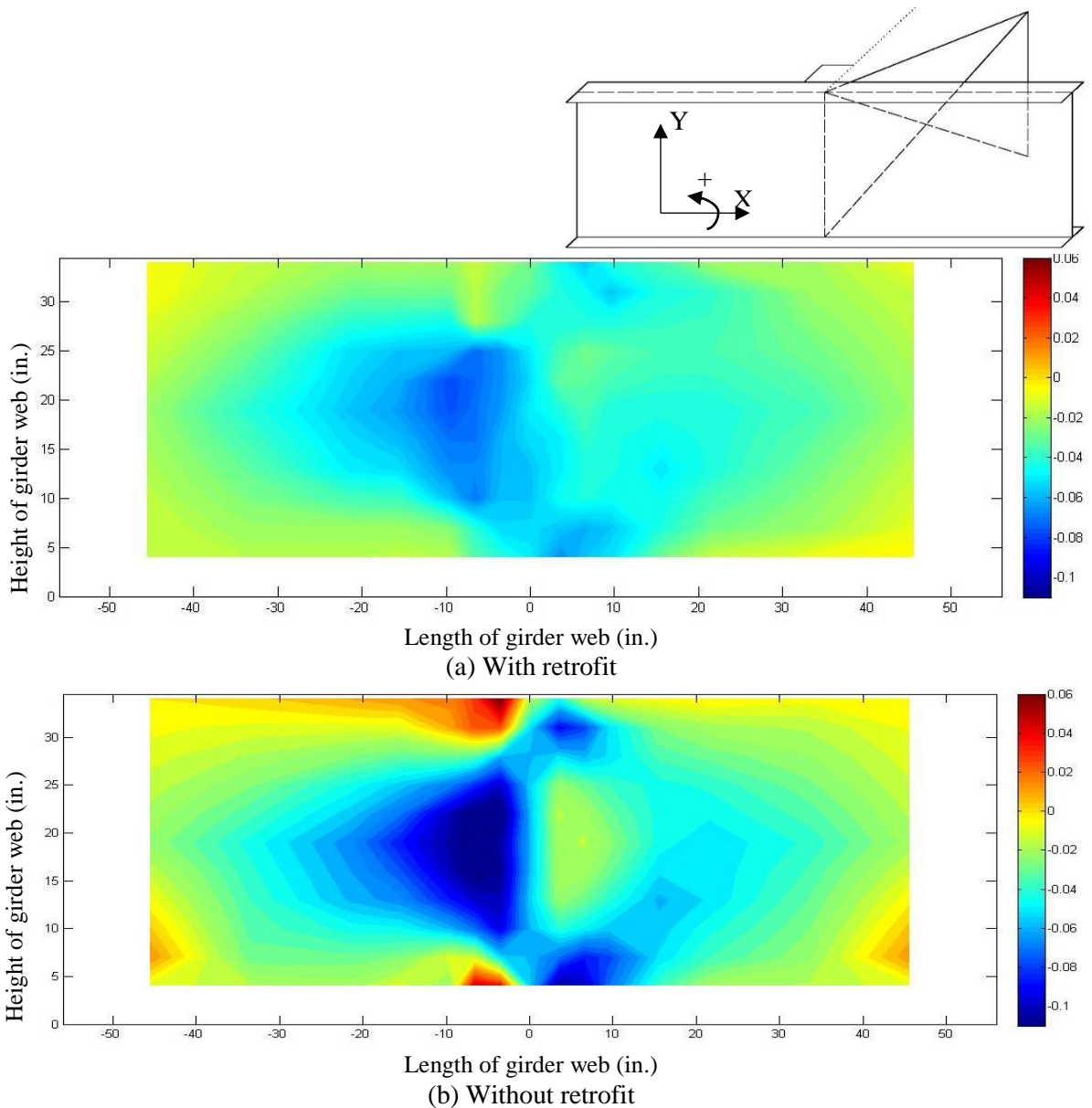


Figure 5-12: X-axis rotations (degree) of the girder web computed from mirror array measurements for 40-degree skewed specimen under 2.5 kip actuator force

Deformations in the girder web were significantly reduced after the angles-with-plate retrofit was installed. The effect was especially remarkable in reducing localized Y-axis rotations near the top and bottom web-gap regions. For the Y-axis rotations, the maximum positive and negative values decreased 83% and 83% respectively. For the X-axis rotations, the maximum positive value reduced 100% (there was no positive X-axis rotation after retrofiting). The maximum negative value reduced 32%.

5.5.2 Approximated Stresses Calculated from Girder Web Rotation

The stress contour plots in X and Y directions derived from the mirror array measurements are presented in Figure 5-13 and Figure 5-14 respectively, using the same procedure described in Section 3.5.2.

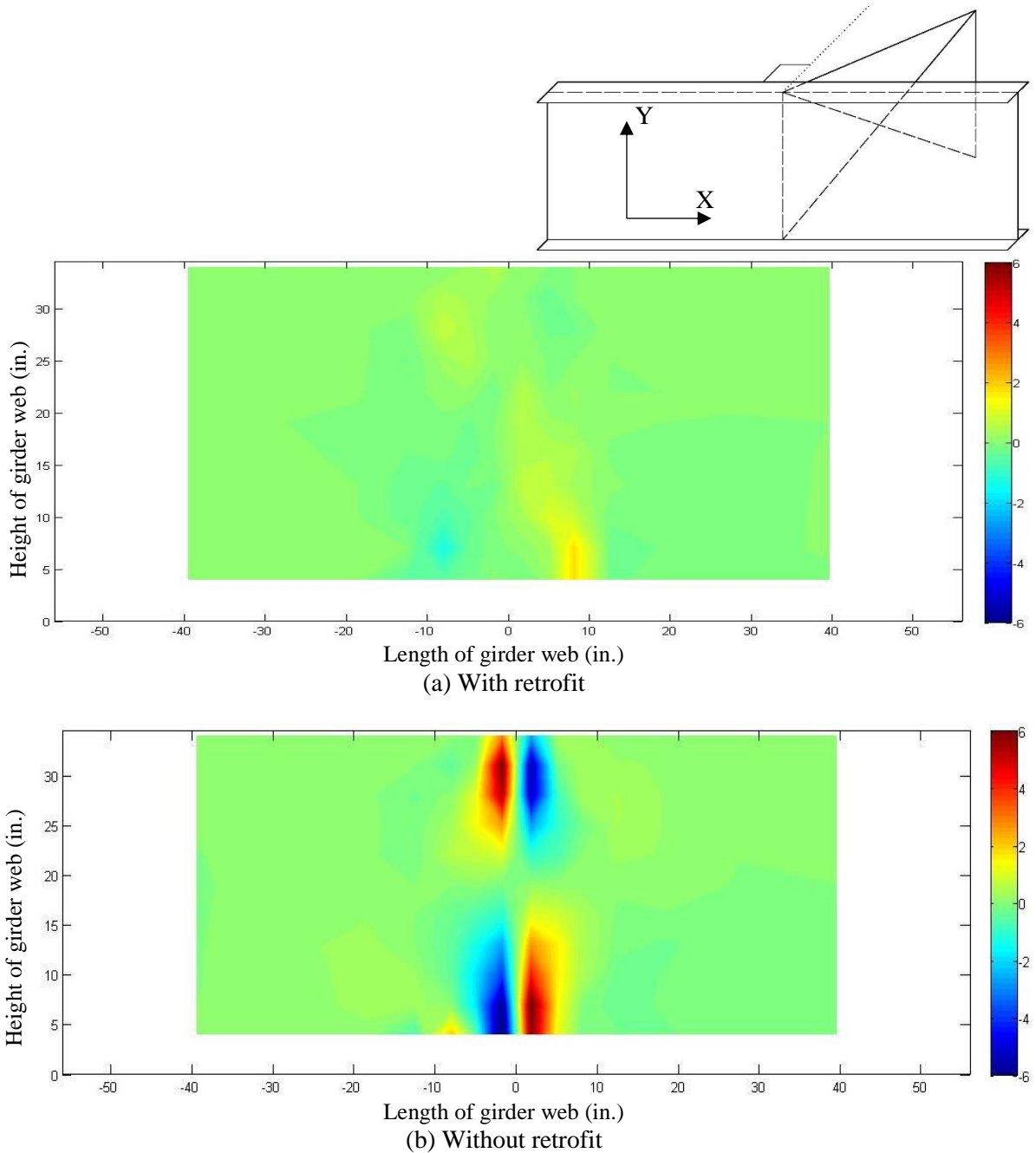


Figure 5-13: Approximated stress (ksi) in X direction of the girder web for 40-degree skewed specimen under 2.5 kip of actuator force from mirror array measurements

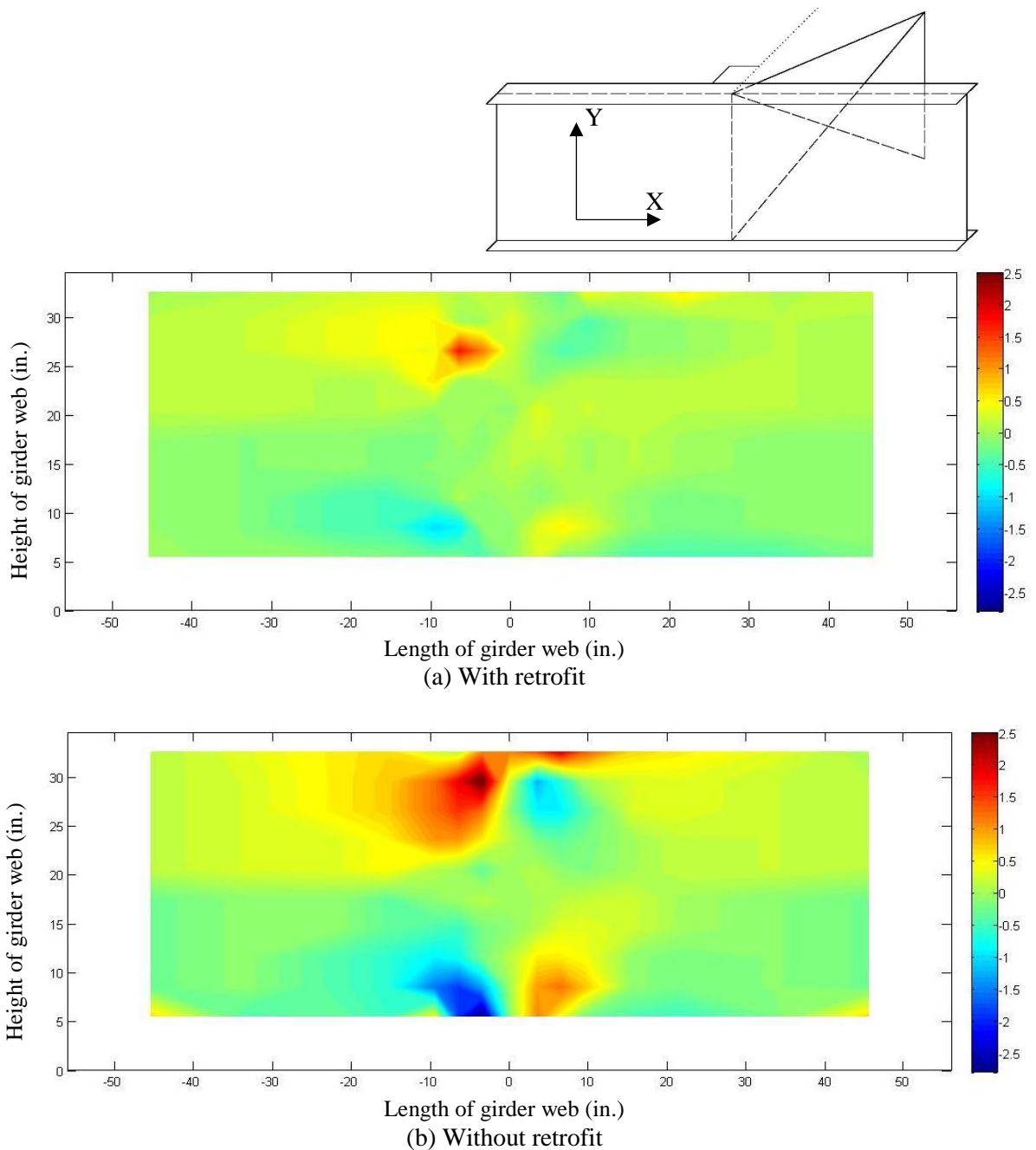


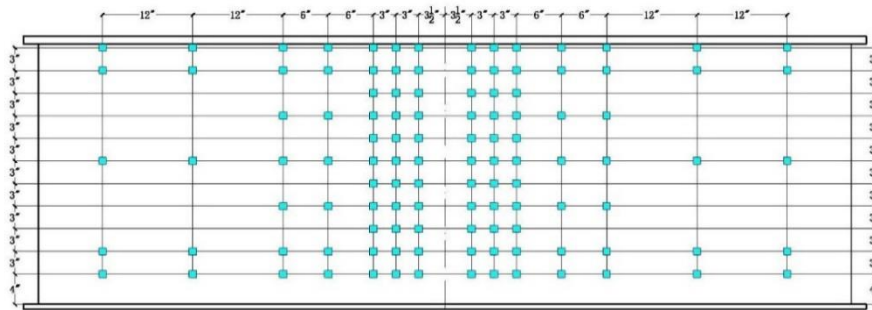
Figure 5-14: Approximated stress (ksi) in Y direction in the girder web for 40-degree skewed specimen under 2.5 kip of actuator force from mirror array measurements

In reducing localized stresses in the top and bottom web-gap regions, the effect of the angles-with-plate retrofit was very significant. For the approximated stresses in X direction, the maximum tension stress reduced 72% and the maximum compression stress reduced 81%. For the

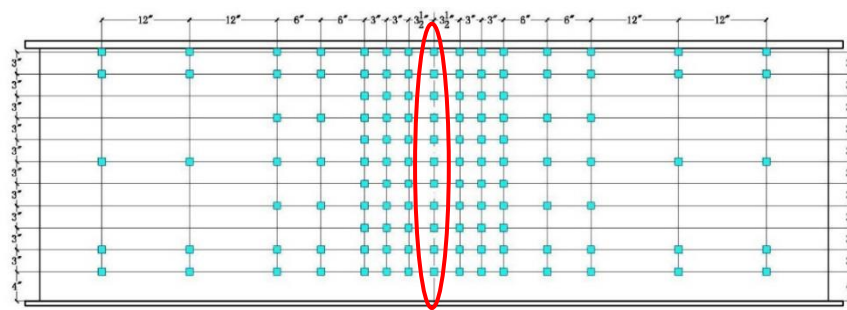
approximated stresses in Y direction, the maximum tension stress and maximum compression stress reduced 37% and 65%, respectively.

5.5.3 Influence of the Center Mirror Column on the Rotation and Approximated Stress Contour Plots

The center mirror column was added when testing the 40-degree skewed specimen (there were no mirrors included at the girder web centerline in the test of the 20-degree skewed specimen). Therefore, the rotation values at the girder web centerline were not recorded in the 20-degree skewed test. Figure 5-15 presents a comparison of the mirror placements for the two tests. The red ellipse indicates the center mirror column.



(a) Mirror placements for the 20-degree skewed specimen



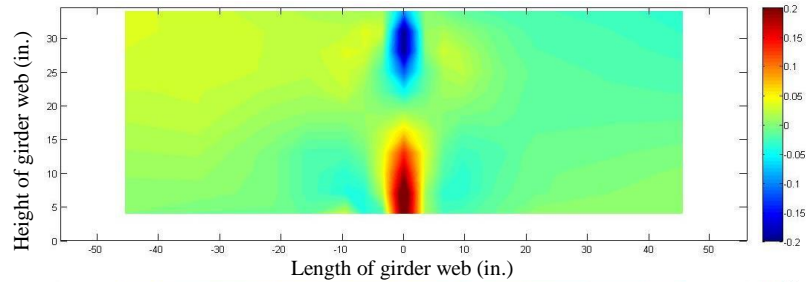
(b) Mirror placements for the 40-degree skewed specimen

Figure 5-15: Mirror array configurations for 20-degree and 40-degree skewed specimens

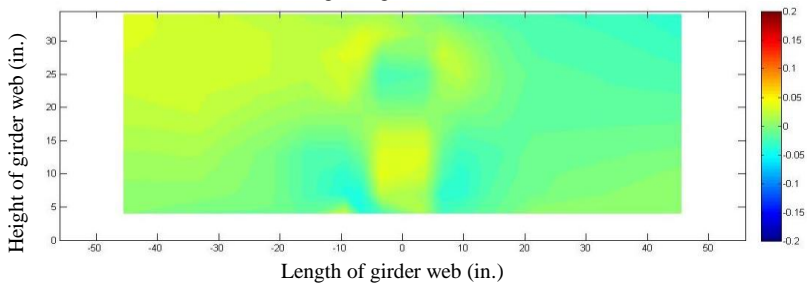
The influence of the center mirror column on the rotation and approximated stress contour plots are discussed in this section. Figure 5-16 and Figure 5-17 present the results of the 40-degree specimen when angles-with-plate retrofit was not installed. The title “with center mirror column”,

means in the presented figures, rotation values of the girder web centerline were used in calculating and plotting, while the title “without center mirror column” means those values were not used.

With center mirror column

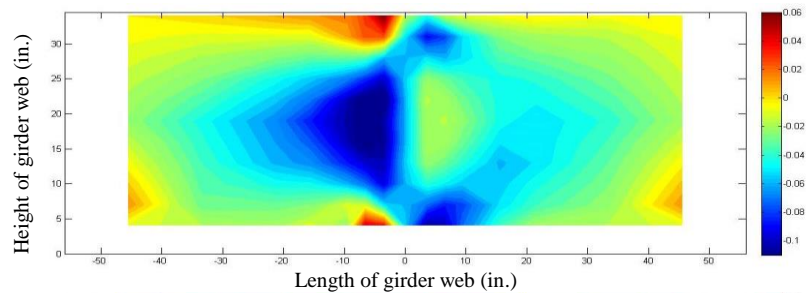


Without center mirror column

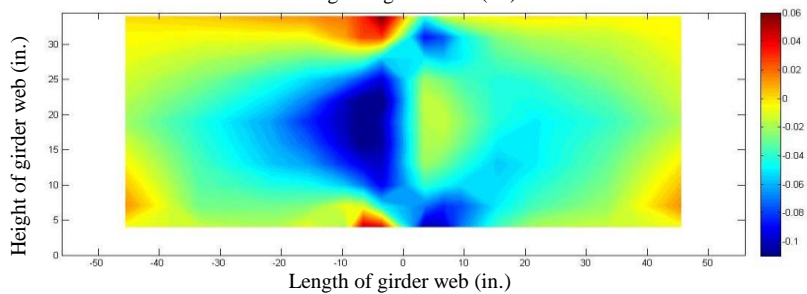


(a) Rotation about Y-Axis (Applied Actuator Force: 2.5 kip; Unit: degree)

With center mirror column



Without center mirror column



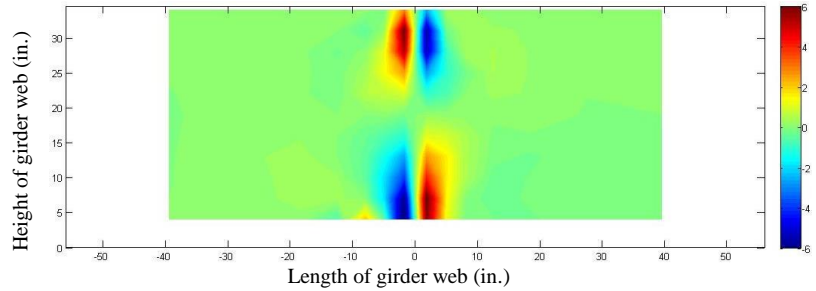
(b) Rotation about X-Axis (Applied Actuator Force: 2.5 kip; Unit: degree)

Figure 5-16: Influence of center mirror column on rotation plots for 40-degree skewed specimen

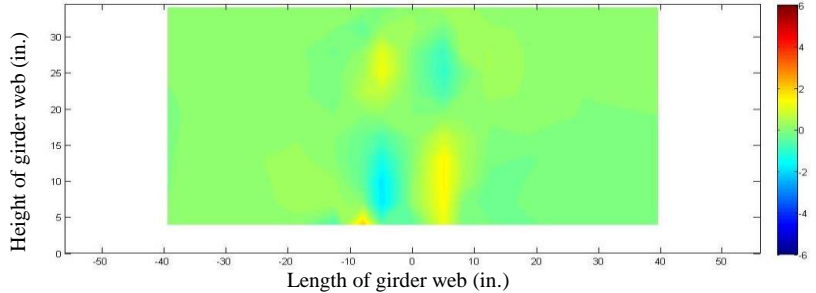
Ignoring the rotation values of the girder web centerline hardly affects the X-axis rotation contour plot. However, its influence on the Y-axis rotation contour plot is significant. The localized deformations near the top and bottom web-gap regions did not appear when the rotation values of

the girder centerline were not accounted for. The same phenomenon likely exists for the 20-degree skewed specimen, in which the rotation values at the girder centerline were not recorded. The X-axis rotation contour plot of the 20-degree skewed specimen may still be reliable, but the contour plot of the Y-axis rotation likely did not represent some important characteristics.

With center mirror column

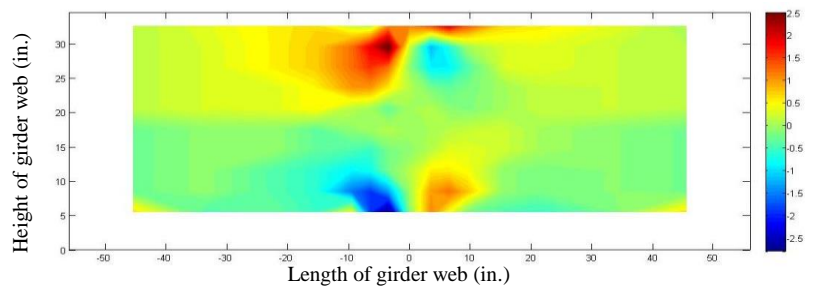


Without center mirror column

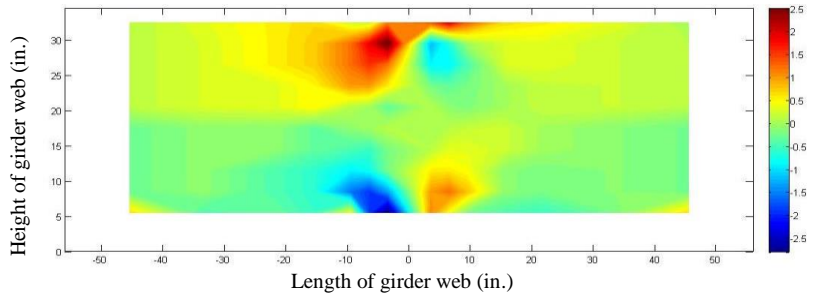


(a) Approximated Stresses in X Direction (Applied Actuator Force: 2.5 kip; Unit: ksi)

With center mirror column



Without center mirror column



(b) Approximated Stresses in Y Direction (Applied Actuator Force: 2.5 kip; Unit: ksi)

Figure 5-17: Influence of center mirror column on plots of approximated stresses for 40-degree skewed specimen

In the contour plot showing the X-axis approximated stresses, the calculated stresses near the web-gap region significantly decreased when the rotation values of the girder web centerline were not used in the calculation, while the approximated stresses in Y direction were hardly affected. This result was predictable since the approximated stresses in X direction were calculated from the Y-axis rotations. Ignoring the rotation values of the girder web centerline resulted in losing the characteristics of the localized Y-axis rotations. Therefore, the calculated x-axis stresses at the web-gap regions were much smaller. For the test of the 20-degree specimen, since the rotation values at the girder web centerline were not recorded, the X-axis approximated stresses in the web-gap regions may be much smaller than reality, but the approximated stresses in Y direction are expected to still be reliable.

6. Comparison of Physical Tests and Computer Simulations

A series of computer models were created using the commercially-available finite element analysis software Abaqus V6.13. The models were created to simulate the physical test specimens as faithfully as possible. The finite element analysis indicated that the peak maximum principal stress along a predefined node path decreased 56% and 66% after retrofitting in the 20-degree and 40-degree skewed models respectively (Chen 2015). The details of the computer simulations are presented in the companion report *Computer Simulations of Retrofitting Skewed Steel Bridges for Distortion-Induced Fatigue* (Chen 2015). A comparison of the physical test results and the computer simulation results are provided in this section.

It is worth mentioning that in the companion report (Chen 2015), an actuator load of 6 kip was simulated for all of the models. Since the applied actuator loads in the monotonic loading of the physical test for the 40-degree skewed specimen were only 2.5 kip, in this section, 2.5 kip actuator

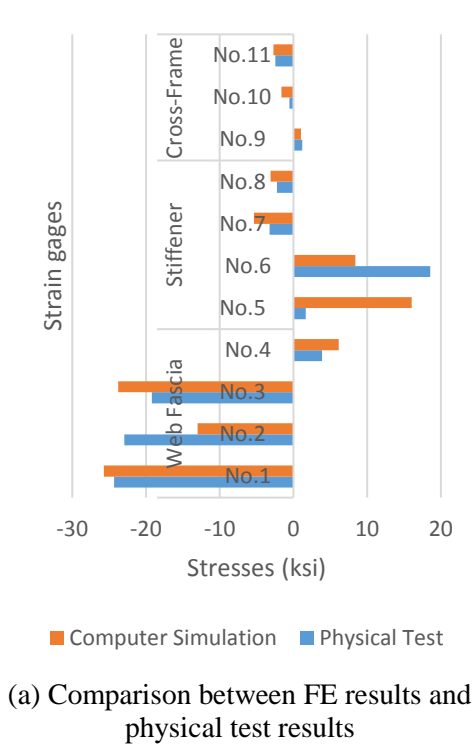
load was applied in the computer models for the 40-degree skewed specimen, making the physical test results and the computer simulation results comparable.

6.1 Stresses Computed from Strain Gages

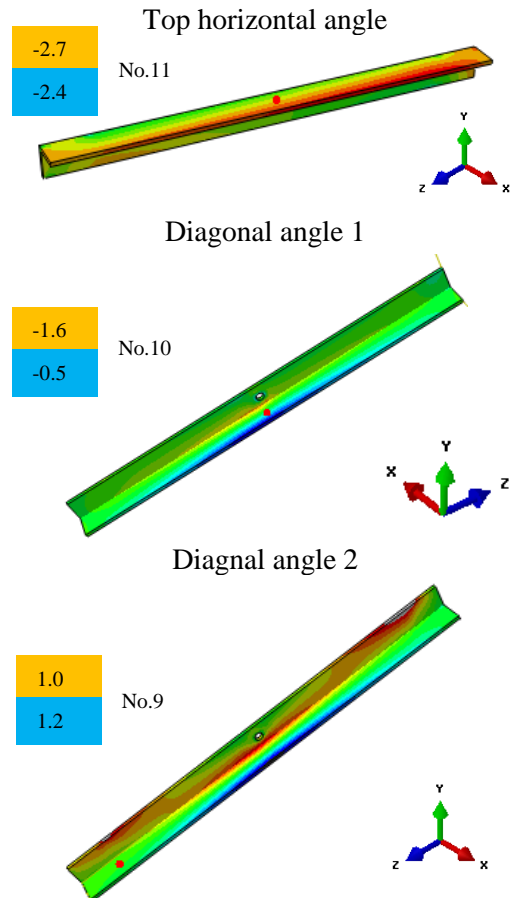
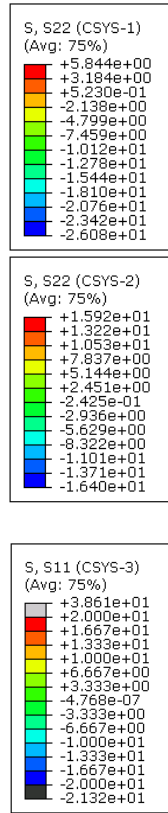
A comparison between the stresses computed from strain gages and the stresses extracted from the computer simulations is made in this section. Some measured stresses exhibited a relatively large difference compare with their corresponding computer simulation results, especially for those in the regions where large stress gradients existed, for example, strain gages 5 and 6 in Figure 6-1, and strain gage 1 in Figure 6-3. In those regions, a small offset in the strain gage position could result in very different stresses. However, in general, the physical test results and the computer simulation results matched very well.

6.1.1 20-Degree Skewed Girder to Cross-Frame Specimen

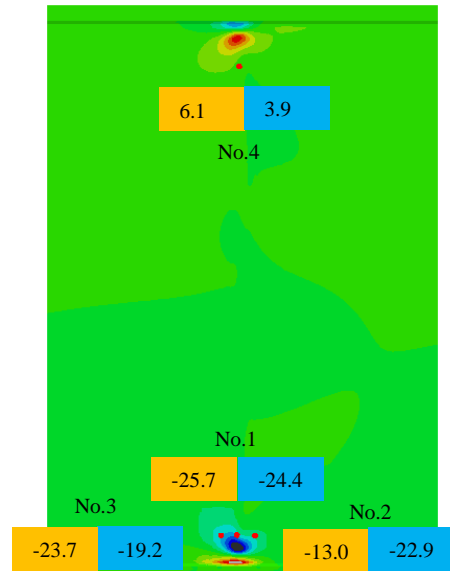
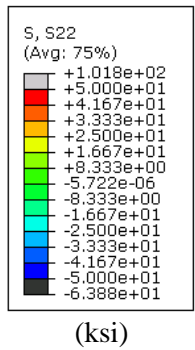
A comparison of stresses between the physical tests and the computer models is presented in the following figures (Figure 6-1 and Figure 6-2). Stresses computed from strain gages are shown in blue, while stresses extracted from computer models are shown in orange.



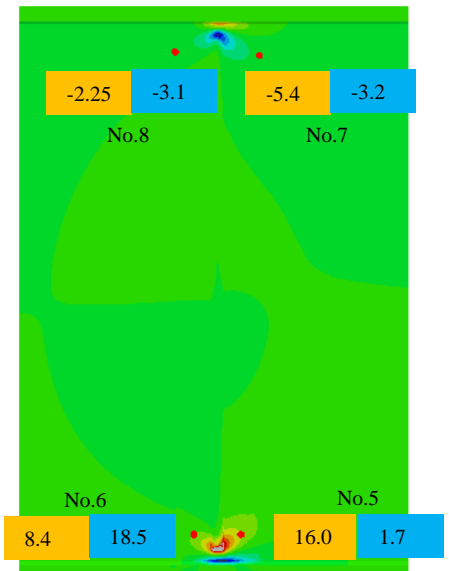
(a) Comparison between FE results and physical test results



(b) Stress on Cross-frame (ksi)



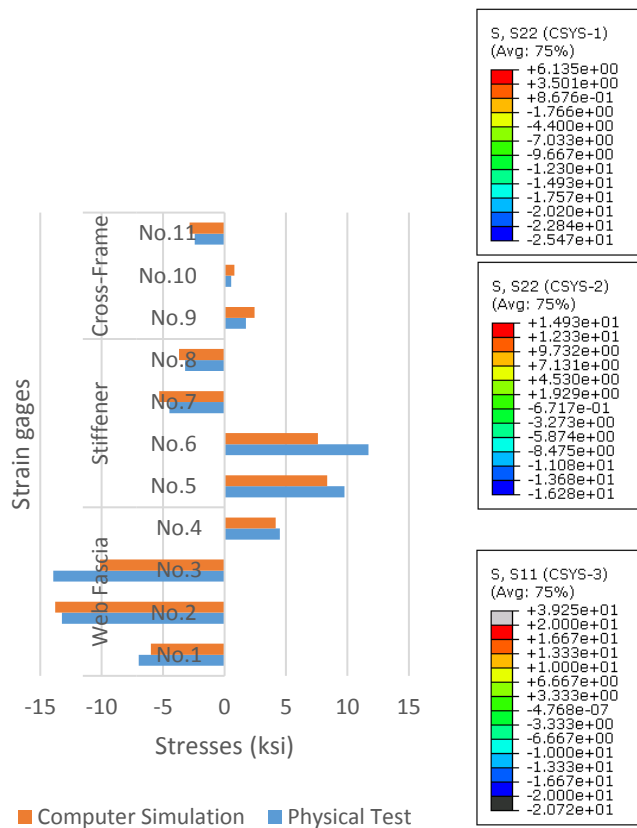
(c) Stress on girder web fascia side (ksi)



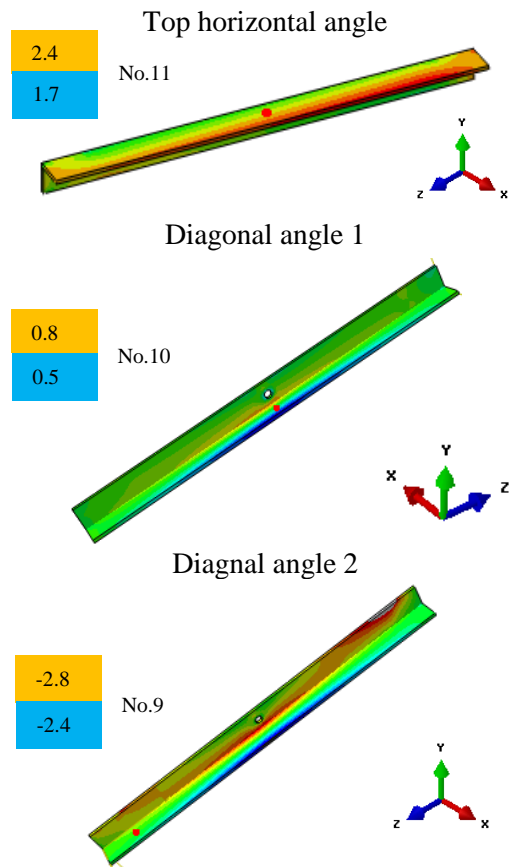
(d) Stress on girder web stiffener side (ksi)

*Stresses are shown in the same direction as their corresponding strain gages

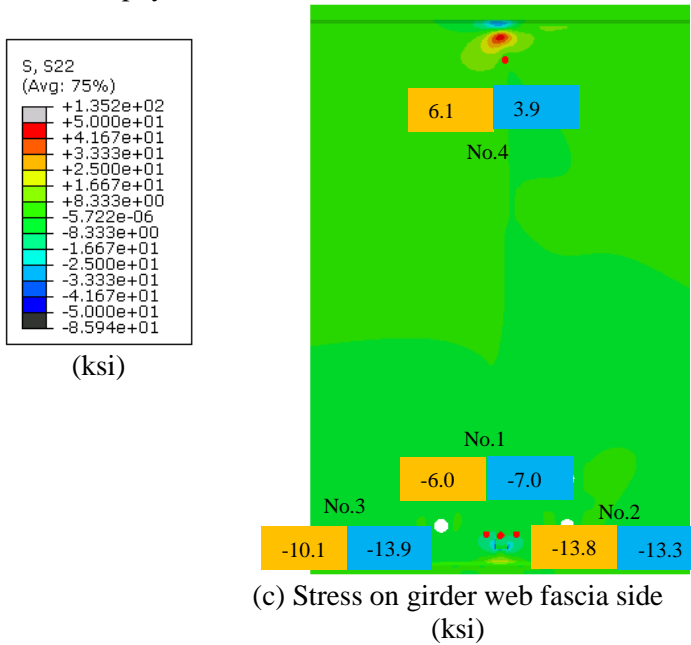
Figure 6-1: Comparison between FE results and physical test results for 20-degree skewed specimen without retrofit installed, under 6 kip of actuator force



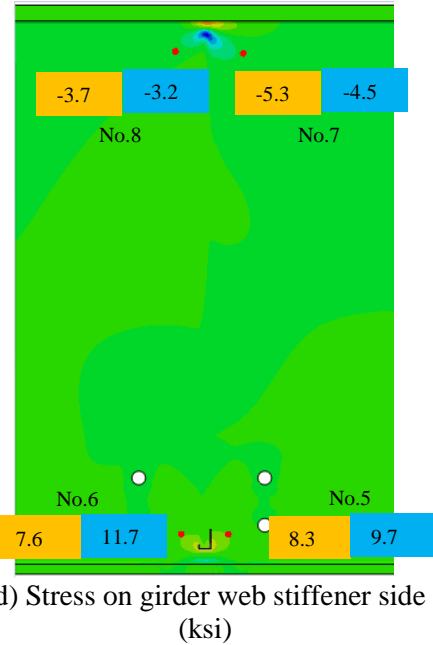
(a) Comparison between FE results and physical test results



(b) Stress on Cross-frame (ksi)



(c) Stress on girder web fascia side (ksi)



(d) Stress on girder web stiffener side (ksi)

*Stresses are shown in the same direction as their corresponding strain gages

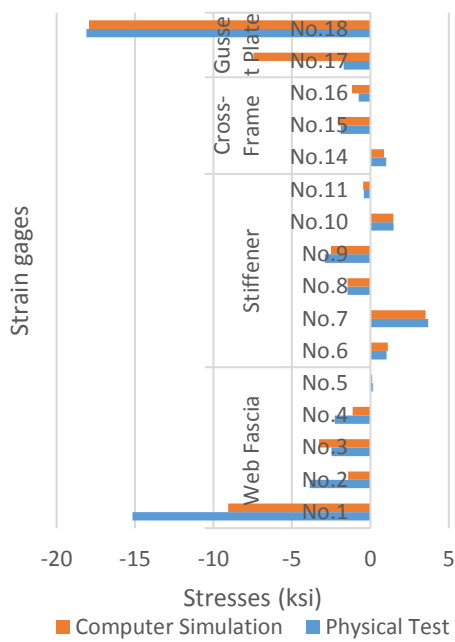
Figure 6-2: Comparison between FE results and physical test results for 20-degree skewed specimen with retrofit installed, under 6 kip of actuator force

6.1.2 40-Degree Skewed Girder to Cross-Frame Specimen

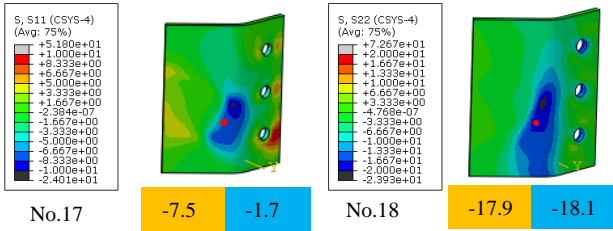
The strain gage placements used in the 40-degree skewed specimen are presented in Figure 4-3.

Figure 6-3 presents a comparison in stresses between the physical test and the computer simulation.

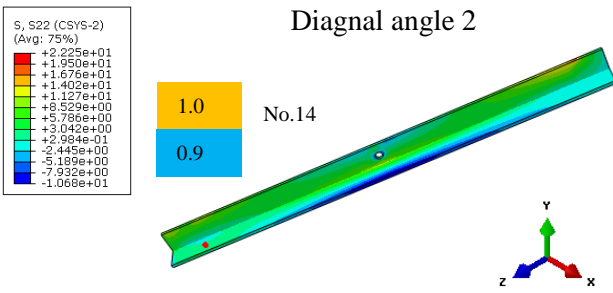
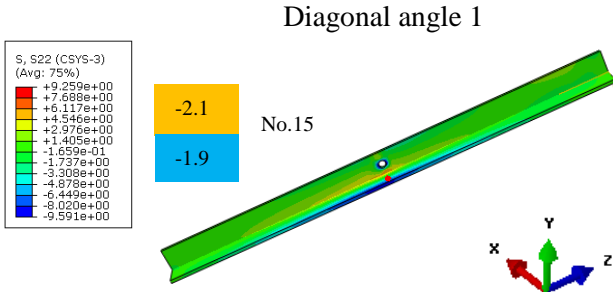
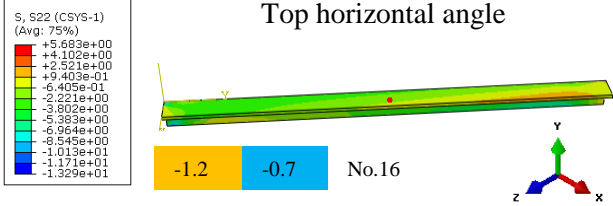
Only results for the case without the retrofit installed is presented in this section, because there was no corresponding computer model for the case with retrofit installed. Retrofits were installed in both the top and the bottom web-gap regions in the physical test of the 40-degree skewed specimen because cracks were observed in both of the two regions. However, only the bottom web-gap regions were retrofitted in the computer models since the cracking of the top web-gap region was unexpected.



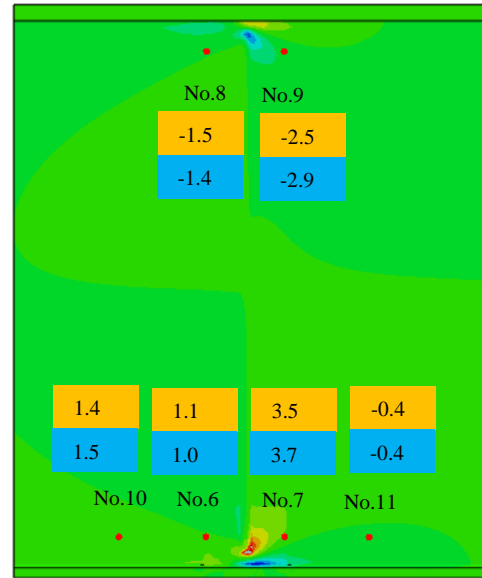
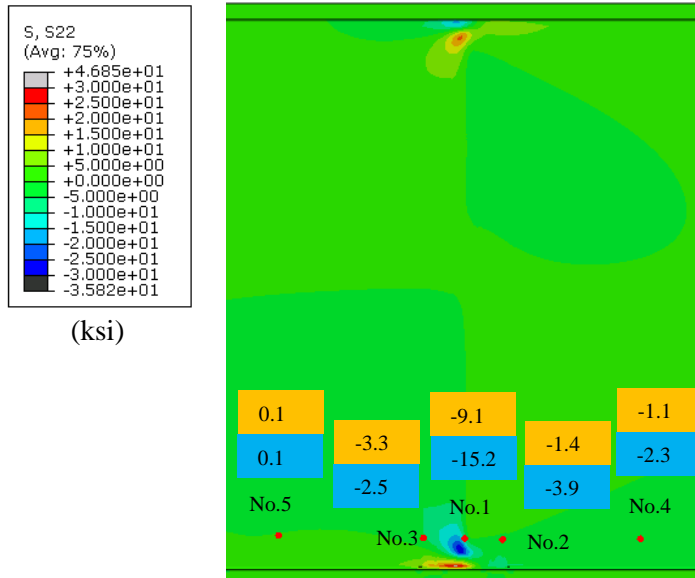
(a) Comparison between FE results and physical test results



(b) Stresses on bottom gusset plate (ksi)



(c) Stress on Cross-frame (ksi)



(d) Stresses on girder web fascia side (ksi) (e) Stresses on girder web stiffener side (ksi)

*Stresses are shown in the same direction as their corresponding strain gages

Figure 6-3: Comparison between FE results and physical test results for the 40-degree skewed specimen without retrofit installed under 2.5 kip of actuator force

6.2 Stresses Approximated from Girder Web Rotations

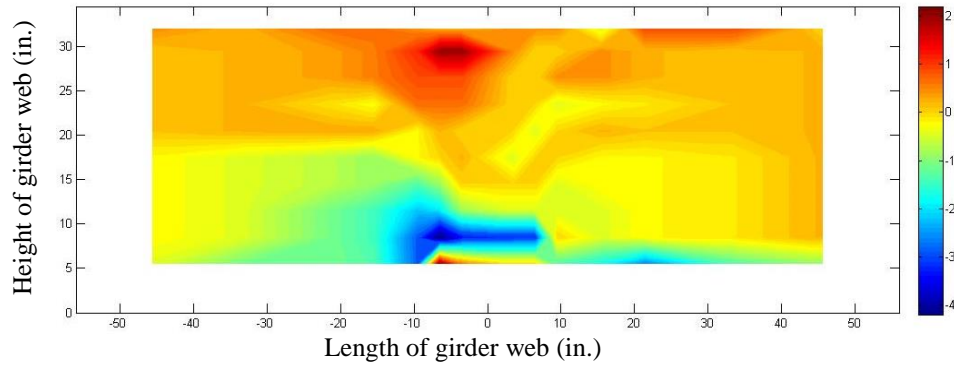
The approximated stresses were calculated from the girder web rotations obtained from the mirror array measurements, and were presented as contour plots in Section 3.5.2 and Section 5.5.2. A comparison between the stresses approximated from the girder web rotations and the stresses obtained in the computer simulations is given in this section. The edges of the girder web have been presented as the rectangular border in the following figures. In the approximated stresses contour plots, data in some regions were not available and are shown as blank. Therefore, blank areas were intentionally left in the computer simulation results to make the two results comparable.

6.2.1 20-Degree Skewed Girder to Cross-Frame Specimen

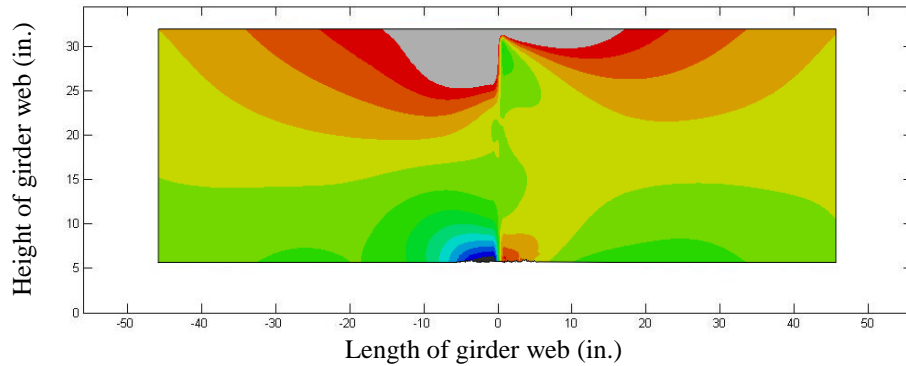
Figure 6-4 and Figure 6-5 provide a comparison between the stresses approximated from the girder web rotations and the stresses obtained in the computer simulations for the 20-degree skewed specimen. The two results matched well on the distribution of the stresses in Y direction. However, the stress distributions in X direction did not compare well.

The mismatch for stresses in X direction can be explained by the missing center mirror column in the 20-degree test. Mirrors were not placed at the centerline of the 20-degree skewed specimen. As discussed, for the results of the 40-degree skewed specimen, neglecting the rotation values of the center mirror column resulted in losing characteristics of the stress distribution in the X direction, while the approximated stresses in Y direction were not significantly affected. The center mirror column may influence the approximated stresses of the 20-degree skewed specimen in the same way as it affected the 40-degree skewed specimen.

Stresses approximated from girder web rotations

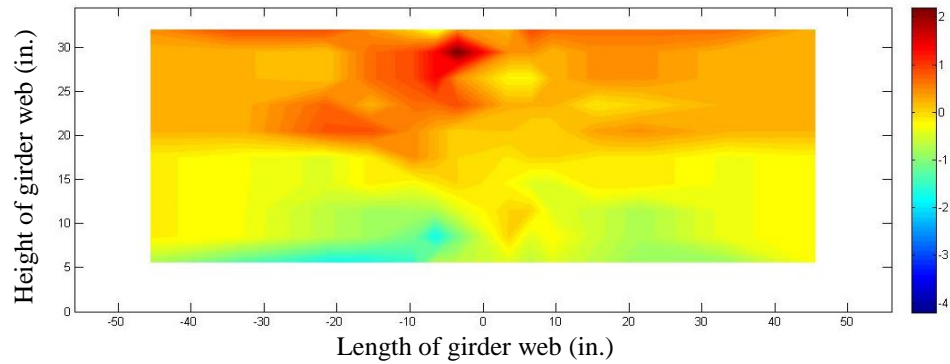


Stresses obtained in computer simulations

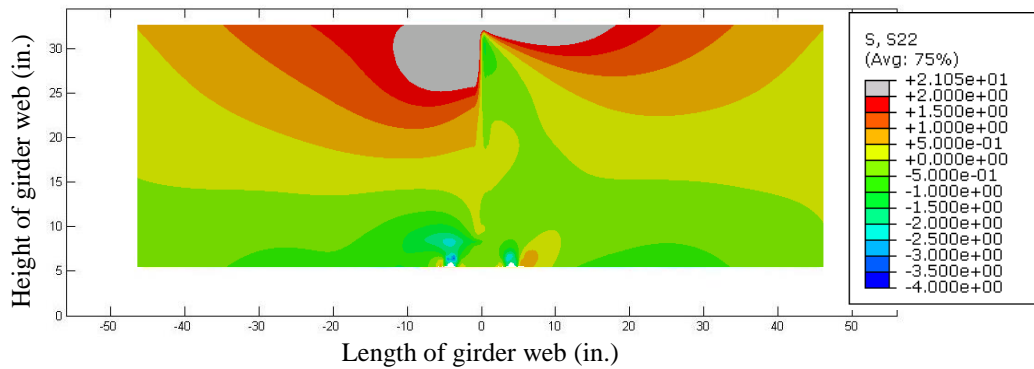


(a) Stresses in Y direction - without retrofit installed (applied actuator force: 6 kip; unit: ksi)

Stresses approximated from girder web rotations



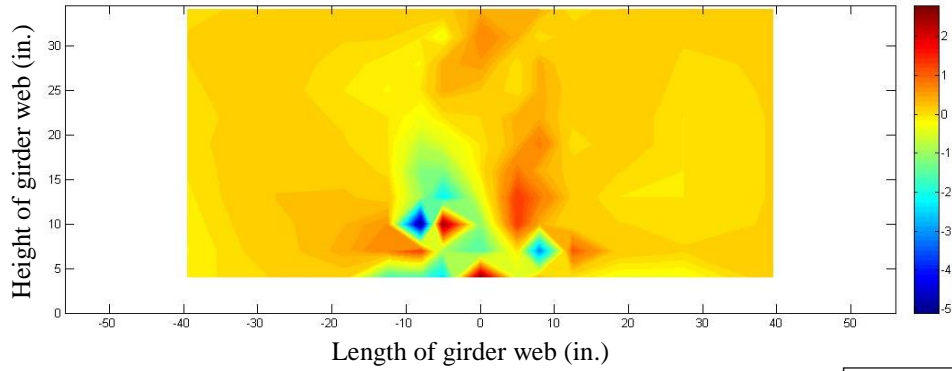
Stresses obtained in computer simulations



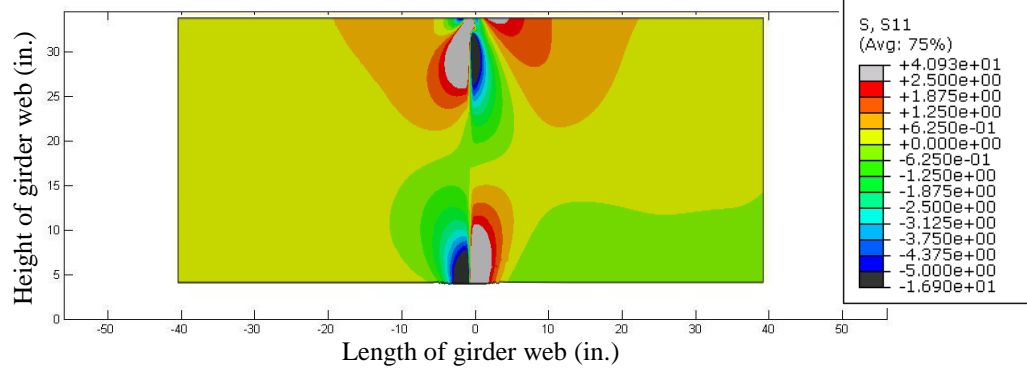
(b) Stresses in Y direction - with retrofit installed (applied actuator force: 6 kip; unit: ksi)

Figure 6-4: Comparison between stresses in Y direction calculated from girder web rotations and obtained from computer simulations for 20-degree skewed specimen

Stresses approximated from girder web rotations

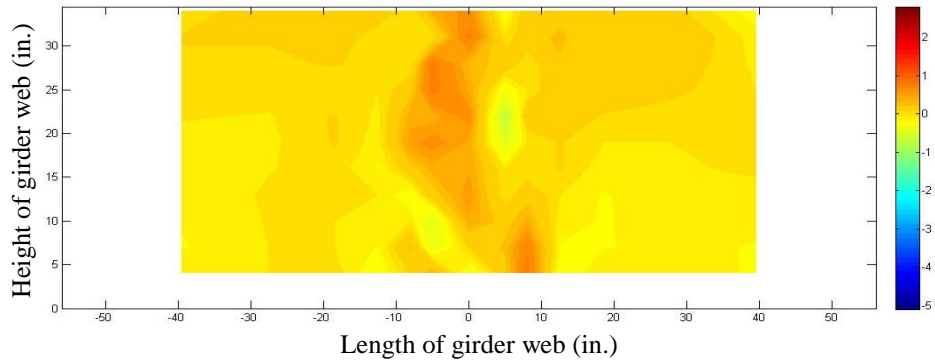


Stresses obtained in computer simulations

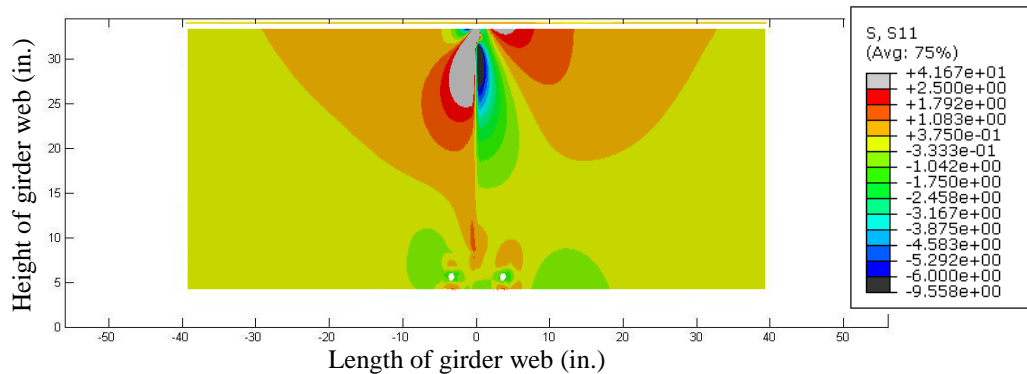


(a) Stresses in X direction - without retrofit installed (applied actuator force: 6 kip; unit: ksi)

Stresses approximated from girder web rotations



Stresses obtained in computer simulations



(b) Stresses in X direction - with retrofit installed (applied actuator force: 6 kip; unit: ksi)

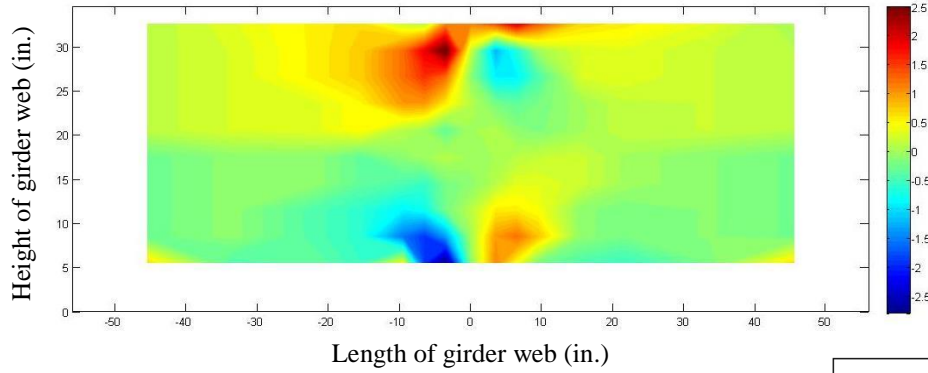
Figure 6-5: Comparison between stresses in X direction calculated from girder web rotations and obtained from computer simulations for 20-degree skewed specimen

6.2.2 40-Degree Skewed Girder to Cross-Frame Specimen

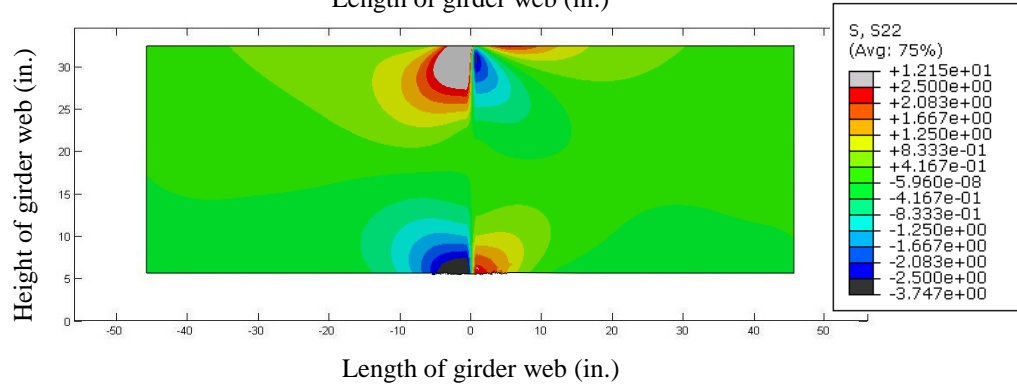
A comparison between stresses approximated from girder web rotations and the stresses derived from the computer simulations for the 40-degree skewed specimen is given in Figure 6-6.

Only the case without the retrofit installed is presented since there was no corresponding retrofitted model available, as discussed in Section 6.1.2. As shown in the following figure, the physical test results and the computer simulation results matched each other well. The stress distributions were almost identical.

Stresses approximated from girder web rotations

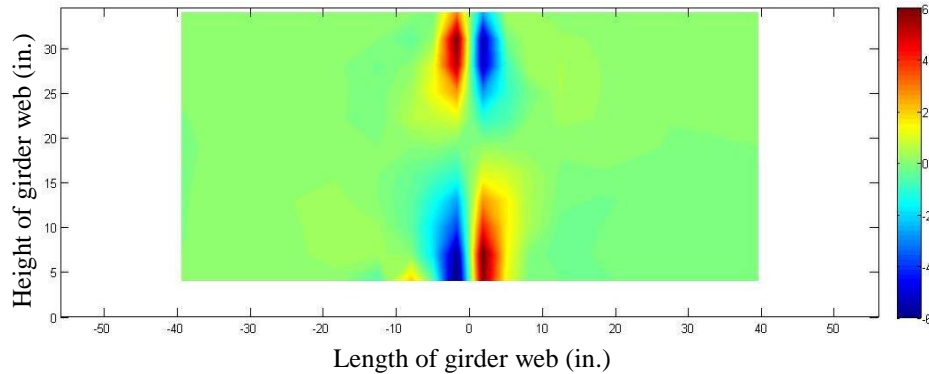


Stresses obtained in computer simulations

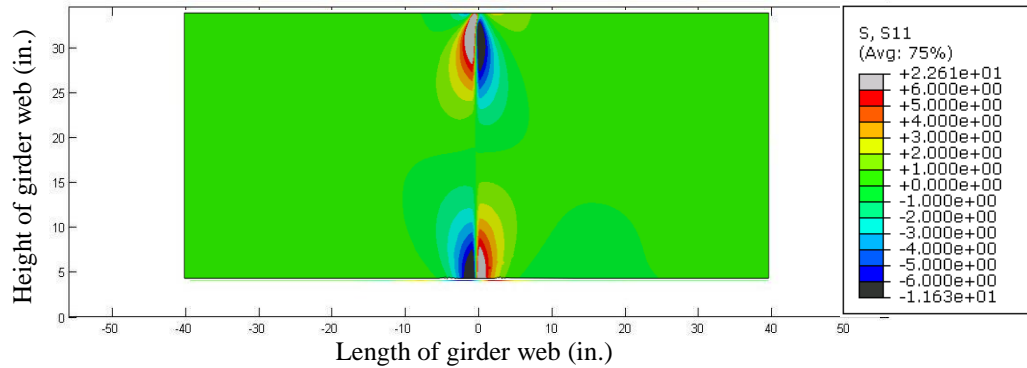


(a) Stresses in Y Direction - Without Retrofit Installed (Applied Actuator Force: 2.5 kip; Unit: ksi)

Stresses approximated from girder web rotations



Stresses obtained in computer simulations



(b) Stresses in X Direction – Without Retrofit Installed (Applied Actuator Force: 2.5 kip; Unit: ksi)

Figure 6-6: Comparison between stresses calculated from girder web rotations and stresses obtained from computer simulations for 40-degree skewed specimen without retrofit installed

7. Influence of Angles-with-Plate Retrofit on Cross-Frame Gusset Plate Stresses

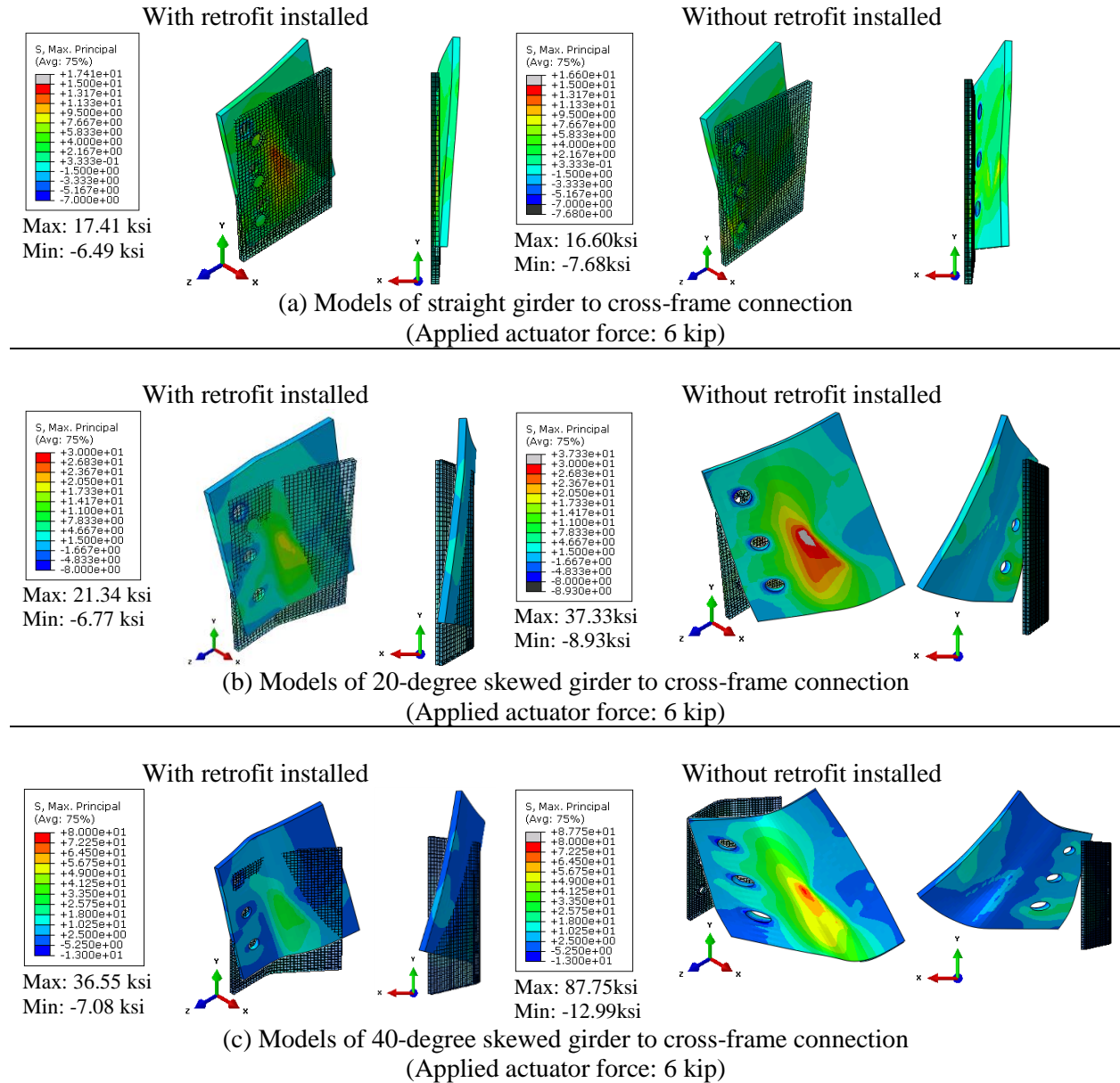
As described in section 3.1.2, in the test of the 20-degree skewed specimen, the cross-frame gusset plate cracked while the angles-with-plate retrofit was in place. This caught the researchers' attention. Was it the retrofit that increased the stress demands at the gusset plate, leading to cracking?

The question was unanswerable from the results of the physical test of the 20-degree skewed specimen, since no instrumentation was applied on the gusset plate in that test. In the test of the 40-degree skewed specimen, as described in Section 5.3, two strain gages were attached on the gusset plate. Their results indicated that after installing the angles-with-plate retrofit, the stresses on the gusset plate did not increase, but significantly decreased.

Figure 7-1 presents a comparison of the gusset plate stresses with and without the angles-with-plate retrofit installed from the computer simulations. Under the same actuator loads, the maximum principal stresses on the gusset plate increased as the connection became skewed. After retrofitting, it was only in the straight connection that the gusset plate stresses increased a little bit (less than 5%). In the 20-degree skewed and the 40-degree skewed connections, the maximum principal stresses on the gusset plate decreased 42.8% and 58.3%.

The deformation scale factors are 50× for all of the models presented in Figure 7-1. The colored shapes present the deformed gusset plates, and the shadows indicate the undeformed shapes. Without the retrofit installed, the distortion of the gusset plate became more severe as the skew angle increased. After retrofitting, the gusset plate deformation decreased due to the stiffness of the attached angles, thus resulting in the stress reduction. Both the computer simulations and the

strain gages used in the physical test indicated that the angles-with-plate retrofit is unlikely to be the reason the gusset plate cracked in the 20-degree skewed specimen.



*¹ The colored shapes present the deformed shapes. The shadows present the undeformed shapes. The deformation scale factors are 50× for all of the models.

*² Only the bottom web-gap regions were retrofitted in the computer simulations. (However, in the physical test of the 40-degree skewed specimen, retrofits were attached on both the bottom and the top web-gap regions.)

*³ 6 kip actuator loads were simulated in the computer simulations. (However, in the physical test of the 40-degree skewed specimen, the applied actuator loads were 2.5 kip.)

Figure 7-1: Comparison of gusset plate stresses with and without angles-with-plate retrofit installed

8. Conclusions

In this study, fatigue tests were performed on 20-degree and 40-degree skewed girder to cross-frame subassemblies to evaluate the effectiveness of a newly-developed retrofit technique, called the angles-with-plate retrofit, in mitigating distortion-induced fatigue damages in web-gap regions. A series of companion finite element analyses are available in a companion report (Chen 2015). A comparison of the physical test results and the finite element analysis results are provided in this report. The following conclusions can be drawn from this study,

- 1. For the skewed girder to cross-frame connections tested in this study, the angles-with-plate retrofits were very effective in stopping crack initiation and propagation, reducing localized deformations in the web gap regions, and reducing stresses in the web-gap regions.**

Crack initiation and propagation in the test of the 40-degree skewed specimen was halted after installing the angles-with-plate retrofits. For the 20-degree skewed specimen, although the propagation of the cracks did not fully stop with the retrofit installed, crack growth slowed significantly in the retrofitted trial. In the unretrofitted trials, the crack growth rates in the south bottom and north bottom web-gap regions were 58.2 and 106.2 inches per one million cycles respectively, while in the retrofitted trials, the crack growth rates were only 0.6 and 0.3 inches per one million cycles. The efficacy of the retrofit was quite good.

For the 20-degree skewed specimen, deformations in the bottom web-gap region were reduced 94% after installing the retrofit. For the 40-degree skewed specimen, after installing the retrofits, deformations in the bottom and the top web-gap regions decreased 98.4% and 75.9%, respectively.

The approximated stresses in the web-gap regions calculated from the measured rotation values significantly decreased after installing the angles-with-plate retrofits. For the 20-degree skewed specimen, after installing the retrofit, the maximum tension and compression stresses in the bottom web-gap region decreased 68% and 89% in the X-direction. In the Y-direction, the maximum tension and compression stresses decreased 99% and 58%, respectively. For the 40-degree skewed specimen, after installing the retrofits, the maximum tension and compression stresses were reduced 72% and 81% in the X-direction, and were reduced 37% and 65% in the Y-direction.

- 2. Fatigue cracks were found in the bottom web-gap region in the 20-degree skewed specimen, and both the bottom and the top web-gap regions in the 40-degree skewed specimen.**

Since the bottom flange was restrained, the bottom web-gap region was expected to be more sensitive to fatigue than the top. Fatigue cracks were found in the bottom web-gap regions in both of the tests as expected, but the top web-gap region also cracked in the test of the 40-degree skewed specimen.

- 3. During cyclic loading, fatigue cracks on the 40-degree skewed specimen remained very thin in width but grew in length for most of the cycles in the unretrofitted condition.**

The cracks on the 40-degree skewed specimen grew to more than 3 in. long, but remained very thin until 1,050,000 cycles into Trial 3. After that, the cracks at the bottom web-gap region suddenly became wider and deeper over just 100,000 cycles. In a real bridge structure, these types of cracks would be very difficult to detect until the crack widths increased sufficiently.

- 4. The gusset plate cracking that occurred in the test of the 20-degree skewed specimen indicated that the angles-with-plate repaired the web gap detail sufficiently such that a “lesser” fatigue detail suffered cracking.**

The bottom gusset plate of the 20-degree skewed specimen cracked with the angles-with-plate retrofit in place. The stresses measured from the strain gages attached on the 40-degree specimen and the computer simulation results all indicated that for the skewed connections, the stresses on the gusset plates did not increase, but decreased after installing the retrofits.

- 5. The strain gages attached close to the cracked web-gap could be effective tools to indicate crack propagation.**

Attached close to the cracked web-gap, the strain gages applied in the test of the 20-degree skewed specimen were sensitive to the growth of cracks. However, the strain gages placed on the 40-degree skewed specimen were insensitive to crack propagation. It may be because the strain gages were placed too far away from the web-gap in that test.

- 6. The physical test results and the computer simulation results agreed well**

The stresses measured by the strain gages attached on the physical specimen agreed well with the stresses extracted from the computer simulations. The stress contour plots obtained from the mirror array measurements and the computer simulations were almost identical. The comparison indicated that the results obtained in the computer simulations, which are presented in the companion report *Computer Simulations of Retrofitting Skewed Steel Bridges for Distortion-Induced Fatigue* (Chen 2015), should be reliable.

The angles-with-plate retrofit successfully halted crack propagation in both the 20-degree and the 40-degree skewed cross-frame to girder connection subassemblies. The localized deformations

and stresses in the web-gap regions were also significantly reduced after retrofitting. A comparison of the physical test results and the finite element analysis results (Chen 2015) indicated that the two agree well with each other. Therefore, the finite element analysis provided in the companion report (Chen 2015), which showed that after retrofitting the peak maximum principle stresses reduced 56% and 66% in the 20-degree and 40-degree models respectively, should be reliable. The results of this study indicate that the angles-with-plate retrofit effectively mitigated distortion-induced fatigue damage in the web-gap region of skewed bridge girders, and therefore is a promising retrofit technique for such repairs.

Reference

- AASHTO (2013). "LRFD Bridge Design Specifications, 6th Ed." American Association of State Highway and Transportation Officials, Washington, D.C.
- Alemdar, F., Nagati, D., Matamoros, A., Bennett, C., and Rolfe, S. (2014). "Repairing Distortion-Induced Fatigue Cracks in Steel Bridge Girders Using Angles-with-Plate Retrofit Technique. I: Physical Simulations." *J. Struct. Eng.*, 10.1061/(ASCE)ST.1943-541X.0000876, 04014003.
- Alemdar, F., Overman, T., Matamoros, A., Bennett, C., and Rolfe, S. (2014). "Repairing Distortion-Induced Fatigue Cracks in Steel Bridge Girders Using Angles-with-Plate Retrofit Technique. II: Computer Simulations." *J. Struct. Eng.*, 10.1061/(ASCE)ST.1943-541X.0000874, 04014004.
- Bennett, C., Matamoros, A., Barrett-Gonzalez, R., Rolfe, S. (2014). "TPF-5(189): Enhancement of Welded Steel Bridge Girders Susceptible to Distortion-Induced Fatigue." *Structural Engineering and Engineering Materials SM Report No. 106*, University of Kansas, Lawrence, KS.
- Bonet, E. (2014). "Utilizing Fiber-Reinforced Polymers to Retrofit Steel Bridge Girders Damaged by Fatigue Loading." *Master's Thesis*, University of Kansas, Lawrence, KS.
- Connor, R. and Fisher, J. (2005) *Identifying Effective and Ineffective Retrofits for Fatigue Cracking in Steel Bridges using Field Instrumentation*. Structures Congress 2005: pp. 1-9.
- Chen, Y. (2015). "Retrofitting Skewed Steel Bridges for Distortion-induced Fatigue," Unpublished manuscript.
- Dexter, R. J., Ocel, J. M. (2013). "Manual for Repair and Retrofit of Fatigue Cracks in Steel Bridges." *Draft Report to Federal Highway Administration No. FHWA-IF-13-020*, University of Minnesota, Minneapolis, MN.

- Fisher, J. W. and Mertz, D. R. (1984). "Fatigue and Fracture in Steel Bridges." The Conference on Bridges, Pittsburgh, PA, 10-21.
- Hartman, A. S. (2013). "Analytical and Experimental Investigation for Distortion-Induced Fatigue in Steel Bridges." Ph.D. Dissertation, University of Kansas, Lawrence, KS.
- Hassel, H., Bennett, C., Matamoros, A., and Rolfe, S. (2013). "Parametric Analysis of Cross-Frame Layout on Distortion-Induced Fatigue in Skewed Steel Bridges." J. Bridge Eng., 10.1061/(ASCE)BE.1943-5592.0000388, 601-611.